The University of Nottingham
UNITED KINGDOM · CHINA · MALAYSIA

DEVELOPMENT AND ASSESSMENT OF A FAST PYROLYSIS REACTOR FOR BIO-OIL, SYNGAS AND BIO-CHAR PRODUCTION FROM BIOMASS RESIDUES

MD ABDUR RAZZAQUE, BSc.

Thesis submitted to the University of Nottingham for the degree of Doctor of Philosophy

July 2016

ABSTRACT

Design, development and assessment of a Fluidized Bed Reactor (FBR) is a very complex process, where enormous empirical correlations; charts and graphs; lot of parameters, assumptions, unit operations are involved, straight forward design equations and design data are limited, and generally the operation of the system requires many adjustments. The improved design of FBR with high coefficient of performance (COP), low energy consumption, high yield and environmentally friendly (low emission) is the target. The scope of the study is to design and fabrication of a lab scale fluidized bed fast pyrolysis system with throughput capacity of 1 kg of dry biomass per hour which includes a bubbling fluidized bed reactor, 2 cyclone separators in series, 4 condensers in series operating between temperatures of 600-300; 300-200; 200-125 and 125-40°C to selectively condense alkanes, phenols, aromatics, indene, methyl-indene, benzene, toluene, methyl–naphthalene, esters, acids, alcohols, ketones; 2 heaters (1 pre- and 1 primary), an auger feeder with hopper and controller, blowers and rig structure. A 3-D simulation was performed to facilitate the mounting of different unit operations, instruments and control panels with sufficient maintenance and manoeuvring accessibilities yet compact structure with low structural footprints.

The rig is having the dimensions of 2204X2750X1100mm (L x H x W) and suitable for batch operation to produce about 650 gm bio-oil, 150 gm non-condensable and 200 gm bio-char from 1kg of dry biomass pyrolysis. The rig is manually operated, however the data acquisition and logging systems are digital and has provision of scrubbing exhaust gas, and an online analyser has been installed to measure and monitor lower hydrocarbons including hydrogen concentrations and Lower Explosive Limit (LEL) in the exhaust gas. Four types of biomass such as Empty fruit bunch (EFB), Urban tree shavings (UTS), Saw dust Broga (SDB) and Saw dust Semenyih (SDS) were pre-treated with aqueous acidic (H_2SO_4) and alkaline (NaOH) solutions to find the percentage of solids extraction with varying liquid-solid ratios, acid/alkali concentrations, reaction temperatures and retention time. For pyrolysis operation, UTS was selected among the four biomass samples with a set of pre-treatment parameters (4.81 wt. % H_2SO_4, 15:1 liquid-solid ratio, 4hr retention time, 70°C, 100rpm agitation speed) that

maximizes bio-oil production. Pyrolysis in a batch tubular furnace at 600°C with nitrogen flowrate of 30 ml/min resulted in bio-oil yield of 39.43% and 27.67%, and char yield of 38.07% and 30.73% from raw and pre-treated UTS respectively. The semi-batch pyrolysis results were compared with biomass pyrolysis results from the batch pyrolysis rig operations. The catalytic upgrading of the bio-oil to liquid fuel in a batch reactor is ongoing research work.

The contribution of this research can be summarised as the successful design, fabrication, testing and operation of a Fluidized Bed System to produce fuel from biomass in batch pyrolysis. Characterization of the feedstock to get the optimum operation condition of the designed FBR to get the best yield out of the system and evaluation of the performance characteristics (Mass and Energy Balance) of the system. Characterization of the products (bio-oil, bio-char and syngas) following standard methods having results comparable with literature.

LIST OF PUBLICATIONS

1. **Poster presentation I**: Razzaque, M.A., Kabir Kazi, F. and Abakr, Y. A. "Production of biofuel from agricultural residues via fast pyrolysis process and upgrading" Poster presented in Postgraduate Research Week, 2012, UNMC

2. **Poster presentation II**: Razzaque, M.A., El-Hassan, M.H.A., Abakr, Y.A. and Kabir Kazi, F. "A lab scale biomass pyrolysis process unit design and fabrication" Poster presented in Malaysia Aerospace Mission Workshop, KLTC, Kuala Lumpur, 18th March 2013.

3. **Paper I:** Kabir Kazi, F., Razzaque, M.A., El-Hassan, M.H.A. and Abakr, Y.A., "Design and fabrication of a bench-scale continuous fast pyrolysis rig" Presented in ICCE 2013, International Conference and Exhibition on Clean Energy, September 9-11, 2013, Ottawa, Ontario, Canada. Published in the proceedings of ICCE 2013, a publication of the International Academy of Energy, Minerals and Materials, 2190 Esprit Drive, Ottawa, Canada, K4A 4Z1

4. **Paper II:** Kabir Kazi, F., Razzaque, M.A., El-Hassan, M.H.A. and Abakr, Y.A., "Effect of aqueous pre-treatment on biomass pyrolysis to bio-oil" Presented in ICCE 2014, 3rd International Conference and Exhibition on Clean Energy, October 20-22, 2014, Quebec City, Canada. Published in the proceedings of ICCE 2013, a publication of the International Academy of Energy, Minerals and Materials, 2190 Esprit Drive, Ottawa, Canada, K4A 4Z1.

5 .**Paper III**: Mohammed, I.Y., Razzaque, M.A., Yusuf, S., Alshareef, I. and Kabir Kazi, F. "Aqueous pre-treatment of Napier Grass prior to Fast Pyrolysis", Paper accepted for presentation in ICCE 2014, 3rd International Conference & Exhibition on Clean Energy, October 20-22, 2014 ,Quebec city, Canada.

6. **Paper IV**: Mohammed, I.Y., Kabir, Kazi F, Yousif, A.A., Razzaque, M.A and Yusuf, S. "Novel method for the determination of water content and higher heating value of pyrolysis oil", BioRes., 10(2), 2681-2690.

DEDICATION

With gratitude and appreciation, this thesis is dedicated to my wife. Her love, support and understanding helped make this project possible.

DECLARATION

This is to certify that this thesis comprises of my original research work. Due acknowledgment has been made in the text to all the material used in the study. I also declare that this work has not been previously submitted for any other degree at The University of Nottingham Malaysia Campus or any other Institutions.

MD. ABDUR RAZZAQUE

ACKNOWLEDGMENTS

First and foremost, I express my deep gratitude to the Almighty Allah for the blessings and mercy showered on me to get through all the difficult time and giving me the best to complete the research work successfully and to write this thesis.

I would like to thank my supervisor Dr. Yousif Abdalla Abakr and my co-supervisors Dr. Feroz Kabir Kazi and Dr. Mohammad Khalid Siddiqui for their proper guidance without which this work would not be a possible one.

I would like to thank Mohammed Hassan Ahmed El-Hassan and Cheng Kei Vin for the SolidWorks and AutoCAd drawings of the rig and all the unit operations. I like to thank Isah Yakub Mohammed for his sincere cooperation in various stages of experiments.

I would like to thank the technical staffs of mechanical workshop and analytical unit of UNMC for their supports to furnish the fabrication works and the pyrolysis of biomass and analysis of bio-oil.

Last but not the least, thanks to my parents for their enthusiastic supports which encouraged me throughout my academic pursuits.

I would like to thank MOSTI for the financial support for this work through MOSTI project: 03-02-12-SF0113.

TABLE OF CONTENTS

LIST OF TABLES

LIST OF FIGURES

LIST OF SYMBOLS

A	heat transfer area (m^2)
A_r	Archimedes number (dimensionless)
A_t	tube cross-sectional area (m^2)
C_d	discharge coefficient (dimensionless)
C_D	drag coefficient (dimensionless)
C_p	specific heat capacity of condensing vapours (J/molK)
D	diameter of the bed (m)
D_c	cyclone body diameter (cm)
D_s	shell inner diameter (mm)
D_e	diameter of gas exit of cyclone (cm)
D_d	diameter of dust outlet of cyclone (cm)
d_i	tube inside diameter (mm)
d_e	shell side equivalent diameter (mm)
d_o	tube outer diameter (mm)
d_p	mean diameter of sand particle (μm)
d_p^*	dimensionless particle diameter (dimensionless)
d_m	particle size of binary mixture of sand and biomass (μm)
d_p	size of sand particles (μm)
d_{pc}	cut-point diameter (μm)
d_{pj}	characteristics diameter of the jth particle size range (μm)
d_b	size of biomass particles (μm)
d_{bo}	diameter of bubble bursting at bed surface (cm)
d_h	grid hole diameter (mm)
g	acceleration of gravity (m/sec^2)
G_f/G_{mf}	ratio of flow rate at operating velocity to flow rate at minimum fluidization velocity
H	total height of the reactor (m)
H_c	height of cyclone inlet (cm)
H_v	pressure drop in cyclone, expressed in number of velocity heads (nos.)
$(h_c)_v$	mean condensation coefficient (W/m^2K)
h_s	heat transfer coefficient for water (W/m^2K)
h_o	tube outside fluid film coefficient (W/m^2K)

h_i tube inside fluid film coefficient (W/m^2K)

h_{od} tube outside dirt coefficient (fouling factor) (W/m^2K)

j_H heat transfer factor(dimensionless)

j_f friction factor (dimensionless)

k_L thermal conductivity of condensed liquid (composite value) (W/m^2K)

k_w thermal conductivity of the tube wall material (W/mK)

L minimum bubbling bed height (m)

l_b baffle spacing (mm)

L_b expanded bed height (m)

L_{bc} length of cyclone body (cm)

L_c cyclone cone length (cm)

L_h hole pitch (mm)

l_{hc} height of the cover (mm)

L_{mf} height of bed at minimum fluidization of sand particles(m)

l_{or} spacing between adjacent holes in the distributor(mm)

m mass of bed material (kg)

m' coefficient of bed expansion ratio(dimensionless)

m_j percentage of mass of particles in the jth size range (%)

N number of grid holes (nos.)

N_d holes density (holes per unit area of the bed), ($nos./m^2$)

N_e number of effective turns (nos.)

N_p number of tube-side passes (nos.)

N_t no of tube bundle (nos.)

Pr Prandtl number (dimensionless)

p_t tube pitch length (mm)

Q volumetric flowrate of fluidizing gas at bed condition (m^3/sec)

Q_{Total} total heat load of the condenser (W)

Q_1 sensible heat of condensing vapour (from vapour inlet temperature of 600°C to boiling point of the individual molecules (W)

Q_2 latent heat of condensing vapour (W)

Q_3 sensible heat of condensed liquid from boiling point of the individual molecules to the condenser exit temperature (W)

Q_4 sensible heat released by non-condensable gas from vapour inlet temperature (600°C) to condenser exit temperature (W)

Re_{mf} Reynold's number at minimum fluidization velocity (dimensionless)

$Re_{p,mf}$ Particles Reynold's number at minimum fluidization velocity (dimensionless)

Re_p Particles Reynold's number (dimensionless)

r the bed expansion ratio(dimensionless)

S length of vortex finder (cm)

TDH transport disengaging height (m)

U overall heat transfer coefficient (W/m^2K)

U_{cf} minimum velocity for complete fluidization (m/sec)

U_{mf} minimum fluidization velocity (m/sec)

u^*_{max} maximum superficial gas velocity (dimensionless)

u_o superficial gas velocity at bed condition (m/sec)

U_{sc-1} superficial gas velocity for scenario -1 calculated for $d_{pavreage}$ (m/sec)

U_{sc-2} superficial gas velocity for scenario -2 calculated as U_{max} (m/sec)

U_{sc-3} superficial gas velocity for scenario -3 calculated as U_{inter} (m/sec)

U_{sc-4} superficial gas velocity for scenario -4 calculated as U_{min} (m sec)

U_t terminal velocity (m/sec)

U_{tr} transport velocity (m/sec)

u_t^* dimensionless gas velocity(dimensionless)

U_h velocity of gas through a single grid hole (m/sec)

V_i the inlet gas velocity through inlet duct (m/sec)

W weight of particles (kg)

W_c length of cyclone inlet (cm)

ε sand voidage at static condition (dimensionless)

ε_{mb} bed voidage at minimum bubbling estimated (dimensionless)

ε_{mf} bed voidage at minimum fluidization (dimensionless)

Δp_d pressure drop across the distributor (Pa)

ρ_f density of fluidizing gas (kg/m^3)

ρ_g density of fluidizing gas (kg/m^3)

ρ_L condensed liquid density (composite value)(kg/m^3)

ρ_v condensing vapour density (composite value)(kg/m^3)

Δp_b fluidized bed pressure drop (Pa)

Δp_{bmax} fluidized bed pressure maximum drop (Pa)

ΔP_t tube side pressure drop (Pa)

ΔP_s shell side pressure drop (Pa)

ρ_p density of sand particles (kg/m^3)

ρ_s density of sand particles (kg/m^3)

ρ_m density of binary mixture of sand and biomass (kg/m^3)

ω_p weight fraction of sand particles (dimensionless)

ω_b weight fraction of biomass particles (dimensionless)

ρ_b density of biomass particles (kg/m^3)

μ_g fluidizing gas viscosity at bed condition ($N.s/m^2$)

μ condensate viscosity (kg/m.sec)

μ_w water viscosity (kg/m.sec)

μ_L condensate viscosity (composite value) (kg/m.sec)

$ø_s$ sphericity of sand particles (dimensionless)

λ enthalpy of condensing vapour (kJ/mol)

ΔT_{lm} log mean temperature difference (°C)

Δt gas residence time (sec)

Γ_v vertical tube loading, condensed liquid per unit tube perimeter (kg/m.sec)

η_j particle collection efficiency (%)

η_o the overall collection efficiency (%)

NOMENCLATURE

ASTM	American Society for Testing and Materials
BFB	Bubbling Fluidized Bed
CFFRC	Crops for the Future Research Centre
CHNS/O	Carbon, Hydrogen, Nitrogen, Sulphur, Oxygen
db	dry basis
DOE	Design of Experiments
EDX	Energy Dispersive X-ray Spectroscopy
EFB	Empty Fruit Bunch
FESEM	Filed Emission Scanning Electron Microscopy
FT	Fischer-Tropsch
FTIR	Fourier Transform Infra-red
GCMS	Gas Chromatography Mass Spectrometry
HDO	Hydro Deoxygenation
HHV	Higher Heating Value
LAP	Laboratory Analytical Procedure
LEL	Lower Explosive Limit
mf	moisture free
MJ	Mega Joules
MMT	Million Metric Tons
MOSTI	Ministry of Science, Technology and Innovation
MSDS	Material Safety and Data Sheets
NG	Napier Grass
NIST	National Institute of Standards and Technology
NREL	National Renewable Energy Laboratory
PVC	Polyvinyl Chloride
USDA	United States Department of Agriculture
UNMC	University of Nottingham Malaysia campus
UTS	Urban Tree Shavings
SDB	Saw Dust Broga
SDS	Saw Dust Semenyih
SEM	Scanning Electron Microscopy
SOFC	Solid Oxide Fuel Cell
SS	Stainless Steel
TDH	Transport Disengaging Height
TTS	Taman Tasik Semenyih

CHAPTER 1: INTRODUCTION

1.1 Research background

Lignocellulosic biomass is an abundant and geographically diverse natural resource. In 2010, Malaysia produced nearly 80 million metric tons (MMT) of oil palm residues (National Biomass Strategy, 2020). In 2007, nearly 104.54 MMT of biomass was produced in Malaysia, of which 93 MMT from agricultural sector, 6 MMT from forest industries and 5 MMT from municipal solid waste (Mekhilef et al., 2011).

The depletion of fossil energy resources, global climate changes, and environmental pollution has made the renewable energy of growing interest. Among renewable resources, biomass is the only resource that can produce liquid fuel. Biomass has some good attributes: (i) it is renewable, and (ii) it is low in sulphur and nitrogen contents.

Biomass contains several minerals (Na, K, Mg, Ca, Fe, Cu, Cr, Zn, Si) collectively called ash. Some of these minerals particularly iron (Fe), copper (Cu) and chromium (Cr) enhance the bio-oil yield while the others such as sodium (Na), potassium (K), calcium (Ca), zinc (Zn), magnesium (Mg) and silicon (Si) retard the bio-oil yield while enhance char formation (Edye, 2014; Sadaka, 2014; Lou et al., 2013; Lin, 2012; Patwardhan et al., 2010; Fu et al., 2009; Varhegyi, 1988; Dobele, 2005). In biomass, typically 1.3 to 22.9% of ash is Fe, Cu and Cr, and the remaining 98.7 to 77.1% of minerals retard bio-oil yields (Patwardhan et al., 2010; Vassilev, 2010; Masia, 2007; Miller, 2007). The present research is also focused on the selective extraction of these retardant elements prior to the biomass pyrolysis and study the effect on the bio-oil yield by pyrolysis reactions. In the present research, aqueous pre-treatments (acidic, alkaline or neutral) are engaged, prior to pyrolysis, to preferentially extract minerals and extractives from the biomass. Aqueous acidic pre-treatments with the exception of nitric acid extract selectively Na^+, K^+, Mg^{2+}, Ca^{2+}, S and P (Bensah, 2013; Pittman Jr., et al., 2012; Scott et al., 2000). Aqueous alkaline pre-treatments, however, extract organics such as lignin, acetyl and other uranic acids (Moe, 2014; Harmsen et al., 2013; Agbor et al., 2011; Hendriks, 2009; Wayman et al., 2005). Neutral water alone (room temperature or elevated temperatures) can extract Na, K, Ca and Mg (Brown, 2014).

Biomass can be considered as an indirect form of solar energy and a renewable source of carbon as plants convert sunlight and CO_2 into stored chemical energy through photosynthesis (Nag and Manchikanti, 2008). Bioenergy (heat and electricity), liquid biofuels for transportation, chemicals, and other bio-based products can be found by the conversion of stored chemical energy in biomass. Therefore, a net reduction in greenhouse gas emissions which may impact global climate change, and provide other benefits such as reducing energy consumption from fossil sources can be earned through this utilization of biomass (Goodfrey, 2004).

Biochemical and thermochemical are two major commonly grouped technology platforms for the biomass conversion pathways which are in various stages of development. Opportunities exist to combine technologies into so-called "hybrid processes" as these platforms are not exclusive (Brown, 2007). The biochemical technologies like fermentation to produce alcohol fuels and anaerobic digestion to produce methane gas are outside the scope of this research and it will only focus on thermochemical conversion.

Direct liquefaction, pyrolysis, gasification and combustion are four main processes (in order of increasing temperature) for thermochemical conversion techniques which utilize heat to decompose biomass. Pyrolysis oil or bio-oil, a liquid product is produced by fast pyrolysis, a promising route for biomass conversion which is a thermochemical process (Bridgwater, 1999).

Fluidized beds are commonly used for solid-fluid reaction systems. The fluidized beds have many advantages: (i) uniform particle-fluid mixing with good heat and mass transfers, (ii) continuous operations, (iii) no moving parts, and (iv) high reaction rates due to enhance heat and mass transports.

Biomass pyrolysis, in fluidized bed reactor, follows complex and competitive reactions as it involves simultaneous change of chemical composition and physical states of the organic materials in biomass that exhibits series and/or parallel reactions (Brown, 2014a; Jared, 2009; Hoekstra et al., 2014). A pictorial reaction pathway based on (Brown, 2014a) for lignocellulosic biomass pyrolysis is shown in Figure 1-1.

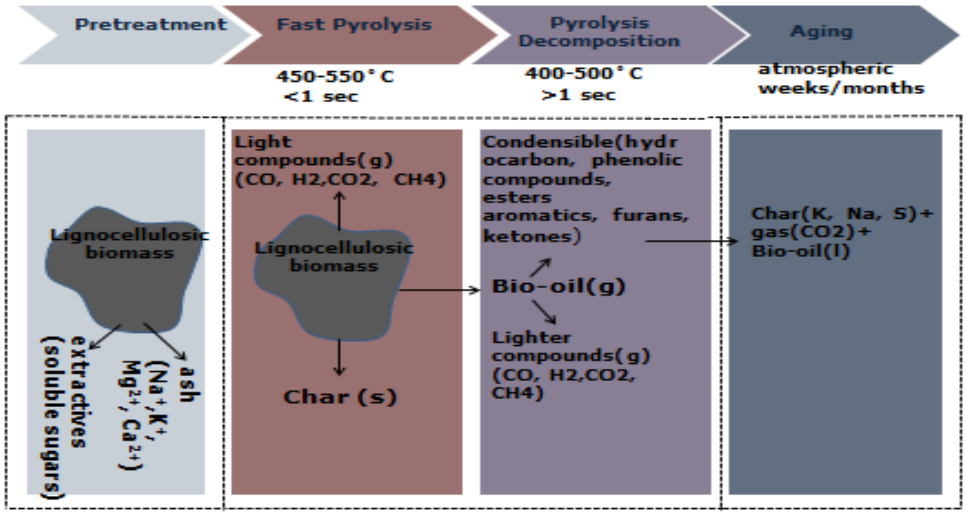

Figure 1-1: The representation of the reaction paths for biomass pyrolysis (Brown, 2014a).

Fast pyrolysis operates between temperatures of 450 to 700°C (in the absence of oxygen) thermally decomposes biomass into its molecular constituents in 0.5 to 5.0 seconds (Bridgwater, 2012; Boateng, 2007; Sadaka, 2006; Bridgwater and Peacocke, 2000; Demirbas, 2000; Bridgwater, 1999). The process is endothermic thus requires external heat to bring the biomass from ambient conditions to the reaction temperature regime (with a rapid heating rate of 10 to 200°C per second) and to provide heat of reactions to targeted bio-oil production. Typical heat energy requirement is 1.0 to 1.8 MJ/kg of dry biomass (Daugaard et al., 2003). Supplying of this heat to the biomass is critical for pyrolysis reactions selectivity and yield. If the biomass is slowly heated, secondary reactions occur and more chars are formed with expense of decreased bio-oil yields (Gronli et al., 2005). Rapid heating in a fast pyrolysis reactor typically occurs by means of a hot carrier gas or solid particulate heat carrier materials, or a heated reactor wall, or a combination of these (Bridgwater, 2007 and Diebold, 1999). Nitrogen being an inert gas is used as carrier gas in the present research. Depending on the reactor configuration, the mode of heat transfer to the reacting particles is dominated by conduction or by convection or by radiation; however each of these processes will contribute to some degree of heating.

The reaction temperature is also critical for fast pyrolysis and has effects on the product selectivity and yields. Higher level of char formations occur at temperatures less than 425°C and non-condensable gas production increases at temperatures above 600°C (Jared, 2009). Bio-oil yield is maximized at temperatures of 500°C ± 25°C with typical yield of 60 to 80% (with water content of 10 to 46%) of dry biomass feed (Bridgwater et al., 2012; Imam and Capareda, 2012; Pattiya and Suttibak, 2012). Variation of products with temperature from biomass pyrolysis is given in Figure 1-2 (Bridgwater 2012). As biomass is pyrolyzed, the reaction products evolve in the form of condensable vapour, tiny aerosol droplets, non-condensable gases and bio-char.

Crude pyrolysis liquid or bio-oil is dark brown and approximates to biomass in elemental composition. It is composed of a very complex mixture of oxygenated hydrocarbons with an appreciable amount of water from both the original moisture content in the biomass and reactions product. Solid char may also be present depending on the effectiveness of the solid particle separations in the downstream separations. The effect of pyrolysis temperature on pyrolysis reactions products yield from biomass feedstock is shown in Figure 1-2.

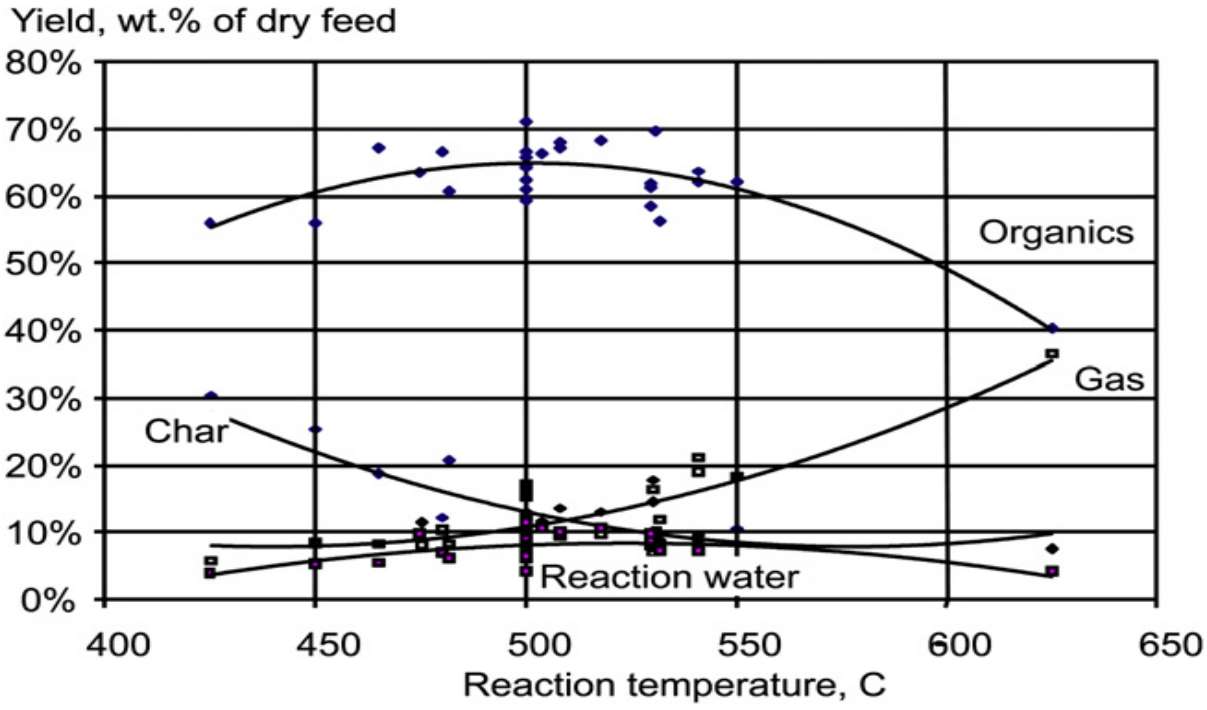

Figure 1-2: Effect of biomass pyrolysis temperatures on products yield (Bridgwater 2012).

1.2 Problem statement

Design, development and assessment of a Fluidized Bed Reactor (FBR) is a very complex process, where enormous empirical correlations; charts and graphs; lot of parameters and assumptions; lot of unit operations are involved, straight forward design equations and design data are limited, and generally the operation of the system requires many adjustments. The improved design of FBR with high coefficient of performance (COP), low energy consumption, high yield and environmentally friendly (low emission) is the target. This research targets to design a FBR to solve all the existing shortcomings. The FBR designed earlier for bench-scale operation with reactor characteristics (reactor dia. 3.4-30cm, reactor height 7.9-170cm, plenum dia. 3.4-30cm, plenum height 15-90cm, distributor hole nos. 1-4200, hole diameter 1-25mm, operation gas velocity 0.4-0.7m/sec, particle size 256-655μm) were found in literature (Escudero and Heindel 2011; Park et al., 2011; Patwardhan et al., 2011, Salehi et al., 2011, Drake 2011; Hoe et al., 2010; Ryu et al., 2010; William et al., 2010; Aho et al., 2008; Iowa State University; Vakshouri 2008; Fernandez 2008; Kumar et al., 2008; Boateng et al., 2007; Sadaka 2006; Yang 2003; Kunii and Levenspiel 1991).

1.3 Significance of study

There is no optimum design data available for FBR in the open literature. This study will enable us to determine the design parameters of a FBR to produce bio-oil, bio-char and syngas from lignocellulosic biomass. The research aims to optimize the operational parameters for FBR. Thus it will be a platform for future research to design FBR. It will also help to determine the pre-treatment parameters for biomass prior to pyrolysis for bio-oil yield and quality. The characterization of the pyrolysis products may draw attention to other new information.

1.4 Aim and objectives

The objectives of the present research are (i) to design and fabricate a lab scale continuous bubbling fluidized bed pyrolyzer rig with downstream cleaning and condensation unit operations, (ii) to define the conditioning and pre-treatment requirements of biomass for the pyrolysis reactions in the new reactor, (iii) to

characterize the feedstock, products and by-products, (iv) to assess the performance of the pyrolysis reactor and evaluate its yield for batch operation and (v) to estimate the energy efficiency of the designed FBR.

1.5 Research scope

In this research, a fluidized bed system is designed and fabricated to produce bio-oil, bio-char and syngas from biomass and to characterize the products. The design capacity of the FBR is 1kg/hr dry biomass. The types of biomass to be tested are Urban Tree Shavings (UTS), Empty Fruit Bunch (EFB), Saw-dust Semenyih (SDS) and Saw-dust Broga (SDB). The FBR with internal diameter of 82.80 mm and length of 1.83 m, the cyclone separators with body diameter and total length (body and cone length together) of 82.8 mm and 330 mm respectively and the condensers shell having 82.80 mm diameter and length of 410, 450, 550 and 700 mm respectively are designed. Each of these condensers is connected to liquid collectors with internal diameter and length of 82.80 and 220 mm respectively. The characterization of products, assessment of syngas and prototype is performed. Further improvement on the design is also suggested.

1.6 Thesis outline

This thesis consists of six remaining sections to systematically explain and support the research effort. The next section, Chapter 2, gives the detail design of a bubbling fluidized bed reactor including literature review is performed to determine the general state-of-the-art of the science and technology of biomass fast pyrolysis and review previous research efforts related to fluidized bed reactors. In Chapter 3, design and fabrication of unit operations are discussed. In Chapter 4, commissioning of the feeder system is given. Chapter 5 discusses the effect of pre-treatment on biomass pyrolysis. Chapter 6 focuses on pyrolysis and products characterization. Chapter 7 includes the conclusions of the research and recommendations for future work. Supplemental information is located in Appendices and is referred when necessary.

CHAPTER 2

DETAIL DESIGN OF A BUBBLING FLUIDIZED BED REACTOR

2.1 Overview

This chapter describes the main design of the research study which includes the detail design of a bubbling fluidized bed reactor with gas distributor and plenum chamber. The bubbling fluidized bed reactor and the subsequent items are designed based on the correlations, charts and graphs from the open literature. The design capacity of the Fluidized Bed Reactor (FBR) is 1kg/hr dry biomass.

2.2 Literature review on Fluidized bed reactor

Fluidization is a process through which a bed of solid particles is expanded into suspended mass of particles that assumes the shape of the containing vessel (Perry, 1999). The suspended solid particles are supported by the drag of upward-flowing gas. Fluidized beds provide nearly uniform temperature within the reactor system, high overall reaction effectiveness factors (due to small particle sizes and turbulence), and easy transfer of solids from fluidized bed reactor to downstream unit operations. Fluidized beds are used for coal combustion, ore reduction, and for other solid-gas reaction systems. Fluidized bed reactor often handles moderately large size particles (2 to 6 mm) in reaction system (Kunii and Levenspiel, 1991). Compared with fixed bed reactors, the pressure drop over a fluidized bed reactor is much smaller. However, fluidized bed has some disadvantages: difficult to maintain homogeneous phase, particle entrainment, particle attrition and reactor surface erosion (Geldart, 1986).

The behaviour of solid particles in fluidized bed depends largely on particle size distributions and particle-gas density differences. Geldart (1973) classified the fluidization behaviour of the solids, in gases, into four recognizable groups (Figure 2-1): (i) cohesive, where particles are small (<20 μm) and tend to stick together, thus becomes difficult to fluidize and back mixing is poor. This powder-like particle gives no

bubbles but makes channels and cracks. Bed expansion is low when channelling occurs but can be high when fluidized. This group of particle makes solid slugs but no spouting; (ii) aeratable, where particles are moderately large (30 to 100 μm) and tend to aerate easily. When these particles are fluidized, the bed expands substantially before bubble appears. Solid mixing is high with high gas back mixing. No spouting occurs except in

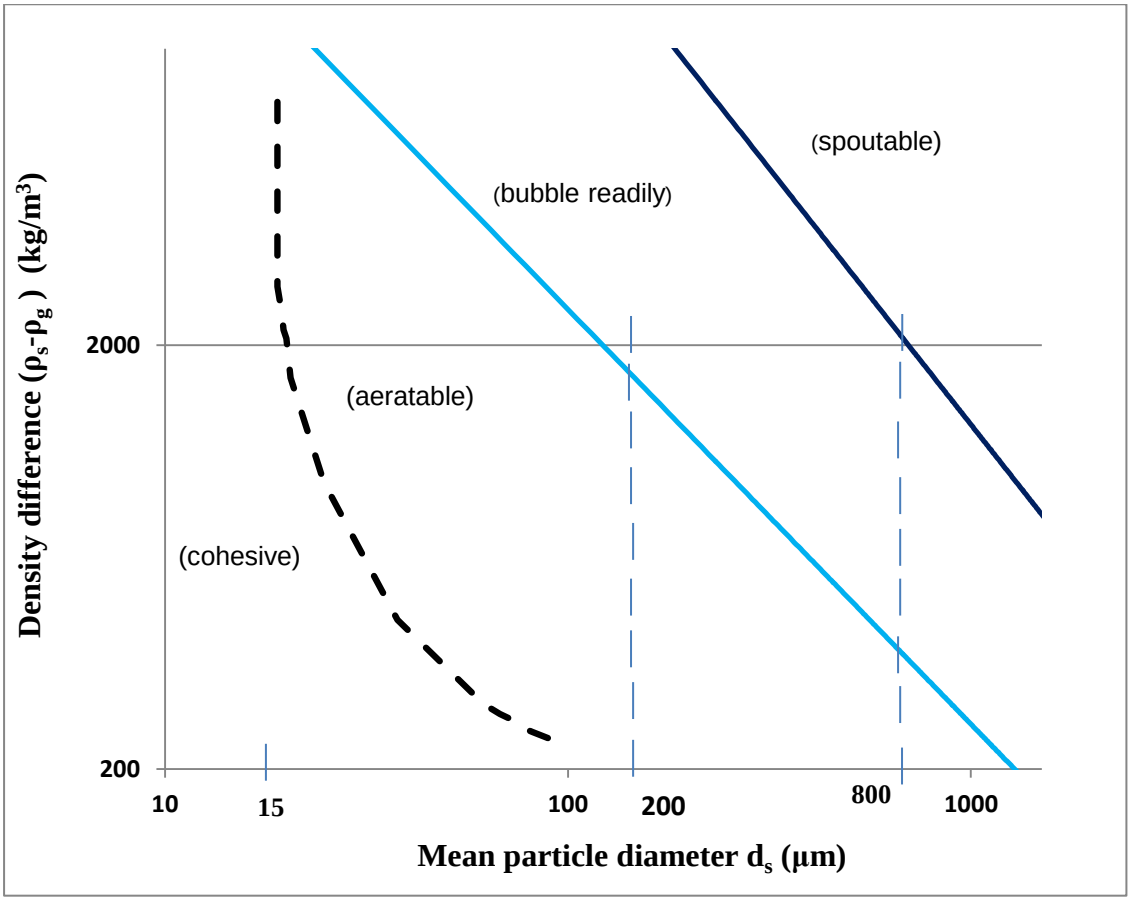

Figure 2-1: The Geldart's classification of particles (Geldart, 1986).

shallow beds. Thus a fluidized bed with this group of particles can be operated in both particulate and fluidization regimes (For aeratable powders, no bubbles will be observed, instead the bed expands homogeneously. The bubbles appear only when the gas velocity is increased beyond the minimum bubbling velocity, the fluidization velocity at which the bubbles are first observed, U_{mb}. The homogeneous expansion is also called particulate fluidization which occurs only in this group of powders for gas-solid systems) (Yang,

2003; Kunii and Levenspiel, 1991). In the bubbling fluidization regime, gas bubbles form and coalesce frequently as they move upward, although there exists a maximum stable bubble size of 3 to 10 cm (Kunii and Levenspiel, 1991; Geldart, 1986); (iii) in bubble readily regime, the particles are relatively large (40 to 500 μm) and tend to form bubbles at the minimum fluidization velocity (the inter particle forces are negligible and bubbles start to form at or only slightly above minimum fluidization velocity) (Geldart, 1986). The bed expansion, solid and gas back mixing is moderate. The bubble size increases with the bed height and it is roughly independent of the mean particle size. There is no maximum stable bubble size for this group (bubble size increases with both bed height and excess gas velocity i.e. (U_0-U_{mf}); coalescence is the predominant phenomenon and there is no evidence of a maximum bubble size, bubble sizes are independent of both mean particle size and size distribution) (Geldart, 1986) and (iv) in spoutable regime, particles are large *(*>1 mm) and tend to make channels, thus they form spouted beds when fluidized. The bed expansion, particles and gas back mixing is low for this group. Spouting occurs even in deep beds with this group of particles. Among all the scenarios the bubble readily group of particles is most suitable for gas-solid fluidization.

In a fluid bed, the gas passes upward through a bed of fine particles or sand (for biomass pyrolysis). When the gas flow-rate is low, the fluid merely percolates through the void spaces between stationary particles creating a fixed bed (Figure 2-2a). With increasing gas flow-rate, particles move apart and a few vibrate and move in restricted region making an expanded bed (Figure 2-2b). At a higher velocity, a point is reached where all the particles are just suspended by the upward-flowing gas, the frictional force counterbalances the weight of the particles, and the pressure drop through any section of the bed is about equal to the weight of fluid and particles in that section and the bed is considered to be fluidized and is referred to a bed at minimum fluidization (Figure 2-2b). With an increase in flow-rate beyond the minimum fluidization, large instabilities

with bubbling and channelling of gas occur. At higher flow-rates, agitation becomes more violent and the movement of solids becomes more vigorous. In addition, the bed does not expand much beyond its volume at minimum fluidization and such a bed is called a bubbling fluidized bed (Figure 2-2d).

In gas-solid systems, gas bubbles coalesce and grow as they rise, and in a deep bed of small diameter they may eventually become large and spread across the vessel. In the

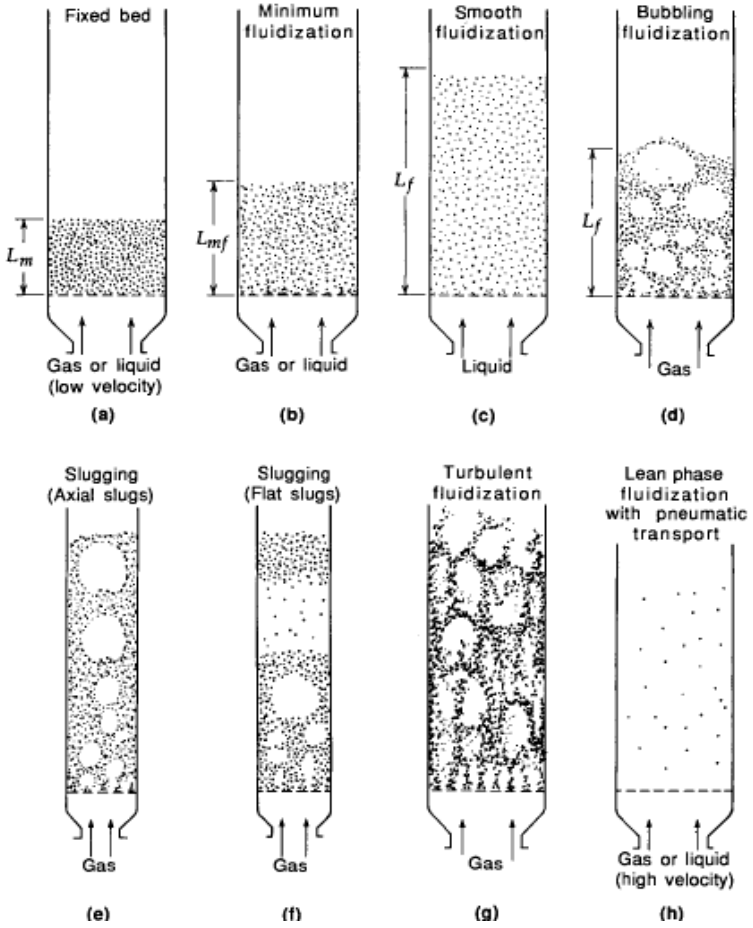

Figure 2-2: Various kinds of contacting of a batch of solids by fluid (Kunii and Levenspiel, 1991).

case of fine particles, they flow smoothly down by the wall around the rising void of gas which is called slugging (Figure 2-2e). For coarse particles, the portion of the bed above the bubble is pushed upward by the large gas bubbles. The particles rain down from the

slug and finally disintegrate. At about this time another slug forms, and this unstable oscillatory motion is repeated. This phenomenon is called flat slug (Figure 2-2f).

Turbulent fluidized bed forms when fine particles are fluidized at a sufficiently high gas flow-rate (above the terminal settling velocity), the upper surface of the bed disappears, entrainment becomes appreciable, and instead of bubbles, a turbulent motion of solids clusters and gas bubbles of various sizes and shapes occur (Figure 2-2g). With a further increase in gas velocity, solids escape the bed with the gas and the bed become dispersed (Figure 2-2h). Summary of different bed types, their characteristics and performance is given in Table 2-1.

The quality of fluidization depends on the physio-chemical characteristics of the particulate matter, particles size and distribution, particle-fluid density ratios, fluidized bed geometry, and fluid flow characteristics. Particles with wide size distribution can be fluidized in wide range of gas flow-rates, permitting flexible operations with deep, large beds.

On the contrary, beds of large uniformly sized particles often fluidize poorly, with bumping, spouting, and slugging, which may cause serious structural damage in large beds. The quality of fluidization of these beds can be improved by adding a small amount of fines to act as lubricant. Large particles fluidize in a much narrower range of gas flow-rates: hence, shallower beds must be used.

A second factor is the fluid-solid density ratio. Normally, liquid-solid systems fluidize homogeneously, whereas gas-solids exhibit heterogeneity. However, as mentioned earlier, one may have deviations from the norm with low-density particles in dense gas or high-density particles in low-density liquid. The fluidization quality is better when the bulk density of biomass is larger (Cui and Grace, 2007; Kunii and Levenspiel, 1991).

Bubbling Fluidized Bed (BFB) technology offers good performance in terms of efficiency,

Table 2-1: Comparison of types of contacting for reacting gas-solid systems (Kunii and Levenspiel, 1991).

Bed type	**Gas-solid Reaction**	**Temperature distribution**	**Particles**	**Pressure drop**	**Heat exchange**	**Conversion**
Fixed bed	Unsuited for continuous operations.	Large temperature gradients occur.	Must be fairly large and uniform.	Pressure drop is not a problem.	Insufficient heat exchange.	Close to 100% of the theoretical conversion is possible.
Bubbling and turbulent fluidized bed	Excellent in continuous operations.	Temperature is almost constant throughout.	Wide size distribution and much fines possible.	For deep beds pressure drop is high.	Efficient heat exchange.	For high conversion, staging or other special design is necessary.
Fast fluidized bed and concurrent pneumatic transport	Suitable for rapid reactions.	Temperature gradients in direction of solids flow.	Fine solids, top size governed by minimum transport velocity.	Low for fine particles, but can be considerable for larger particles.	Intermediate between fluidized and moving bed.	High conversion possible.

fuel flexibility and especially in regard to the installation and maintenance costs (Pena, 2011). BFB has advantages such as heat can be supplied externally to bed, good mass and heat transfer, less complex, requires small sized particles and easy to scale up. The Figure 2-3 below describes that BFB is a better choice as energy consumption is higher for circulating fluid bed (CFB) for the circulation of solids, particle attrition is more in CFB (Brown and Holmgren, 2014) . Also bubbling fluidized bed offers some more advantages such as; back mixing can be avoided; gas release during reaction can be handled easily and transportation of large quantities of solid as part of the reaction process can be handled easily, the mixing of the solid ensures that there are practically no temperature gradients in the bed (Subbu, 2011; Jakobsen, 2008; Kunii and Levenspiel, 1991). The bubbling fluidized bed is the best fit for its advantageous characteristics of fluidized beds and the existence of large bubbles for which the bed is very nonhomogeneous and the pressure drop across the bed oscillates in time making it a better choice (Thermopedia, 2014).

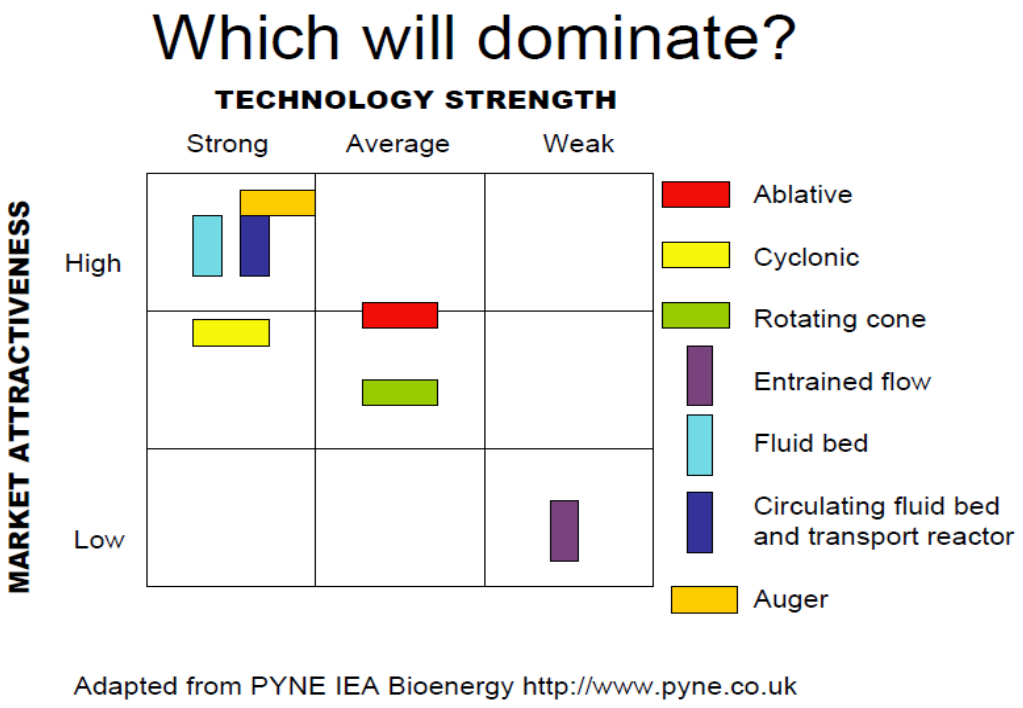

Figure 2-3: Comparison of different reactor types according to their market attractiveness (Brown and Holmgren, 2014).

In gas-solid fluidization, the distributor disperses the solids rapidly and prevents segregation and settling of solids that can cause variable temperature and rapid de-fluidization (Vakshouri, 2008). Schematic diagram of a bubbling fluidized bed reactor is given in Figure 2-4.

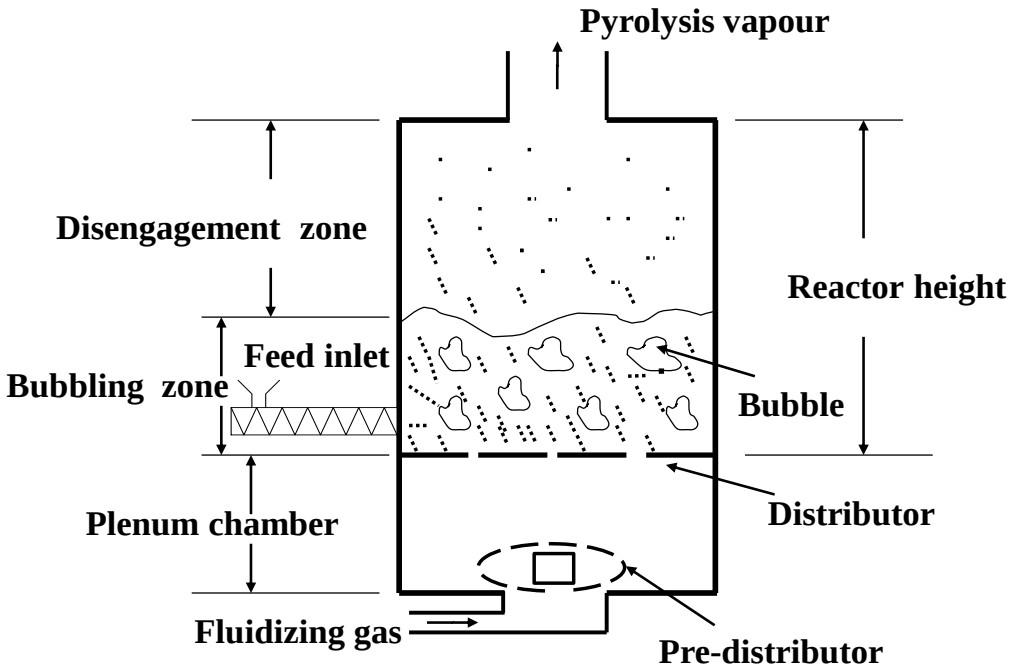

Figure 2-4: Schematic diagram of a bubbling fluidized bed reactor.

A fluidization vessel usually has two zones/phases: a dense bubbling phase having a more or less distinct upper surface separating it from an upper lean or dispersed phase in which the density of solids decreases with height. The section of the vessel between the surface of the dense phase and the exit of the gas stream is called the freeboard and its height is called the freeboard height, H_f (Figure 2-5). Because the density of solids decreases with height in the freeboard, increasing the freeboard decreases the

entrainment from the bed. Eventually, a freeboard height is reached above which entrainment does not change appreciably. This is called the transport disengaging height (TDH) (Figure 2-5). In the disengagement zone, the products, in the vapour phase, leave the bed particles which then fall back in the dense bubbling bed zone.

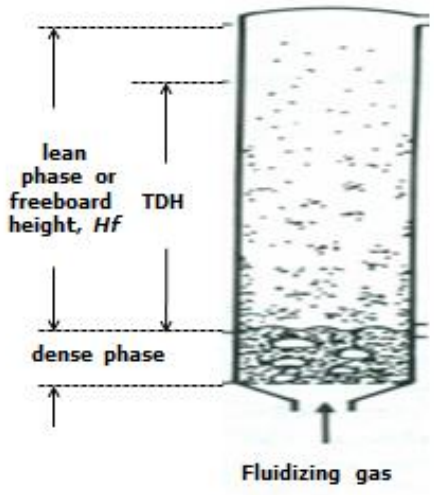

Figure 2-5: The dense phase and lean phase in bubbling fluidized bed (Kunii and Levenspiel, 1991).

In bubbling bed zone, bubbles which form near the distributor plate, rise up the bed, grow and coalesce, producing bigger bubbles which sometimes break up into smaller bubbles. Bubbles eruptively burst, ejecting the particles far from the bed surface making particle circulation in the bed very intensive (shown in Figure 2-6). Every rising bubble has an associated wake (shown in Figure 2-6) of material rising behind it, so particles move upwards behind the bubble and in its trail. Particles move downwards in the emulsion or around the bubbles and between them, and especially near the walls. Bubbles movement thus promotes intensive gas and particle mixing in the fluidized bed.

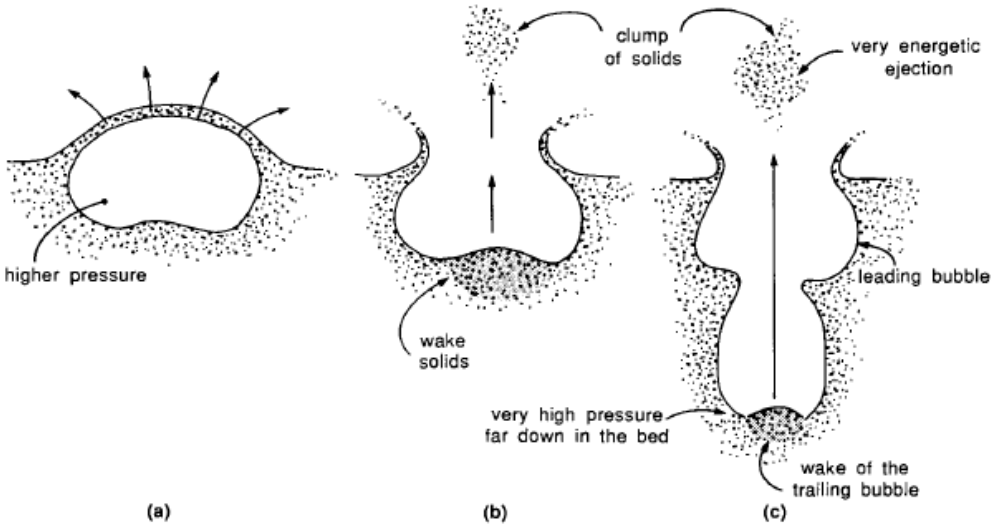

Figure 2-6: Mechanism of ejection of solids from a fluidized bed into the freeboard:(a) from the roof of a bursting bubble; (b) from the bubble wake; (c)from the wake of a trailing bubble just as it coalesces with its leading bubble (Kunii and Levenspiel, 1991).

The bubbles are surrounded and accompanied by a cloud of circulating gas bubble, distinct from the emulsion gas. The rising bubble has an associated wake of material rising behind it (Figure 2-7).

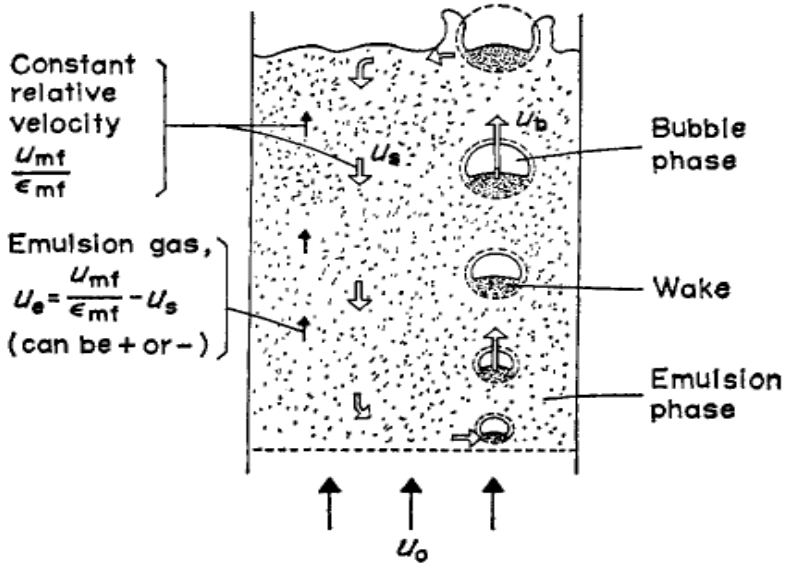

Figure 2-7: Main features of solid movement and gas flow in bubbling fluidized bed (Kunii and Levenspiel, 1968).

There are two types of bubbles formed in fluidization process: fast clouded and slow cloudless bubbles (Figure 2-8, Figure 2-8a and 2-8b show fast and slow bubbles

respectively). The clouded bubbles with their wake drag solids up in the bed and drift down in the emulsion thus a pattern for the flow of solids occurs. Between both phases there is a certain interchange. Since there is low density of solids in the bubble phase and due to its high velocity, reaction takes place in the emulsion phase. There is generally either very little or no gas passing through the bed in bubbles, which takes no part in the chemical reaction, then the gas mixing in the emulsion phase is the most important process concerning the chemical reactions. Fluidized beds with slow bubbles are much more useful for chemical processes, since the bubbles are intensively washed out by the gas from the emulsion phase, so the whole of the gas flow can take part in the reaction. With the fast bubbles, gas passes through the bed without taking part in reactions with the particles (Thermopedia, 2014). So, in a bubbling fluidized bed, the behaviour of bubbles significantly affects the flow or transport phenomena in the bed, including solids mixing, entrainment, and heat and mass transport.

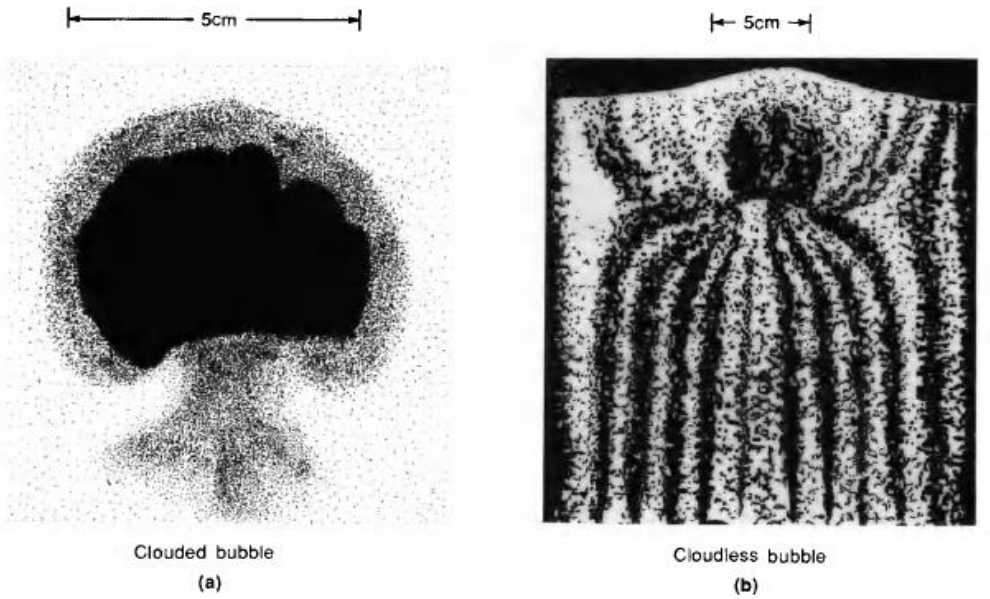

Figure 2-8: Photographs showing the flow pattern of gas around rising bubbles: (a) the cloud surrounding fast-rising bubble; (b) Emulsion gas overtaking the slow-rising bubbles (Kunii and Levenspiel, 1991).

For gas-solid systems, there are at least five distinguishable observable fluidization regimes: (i) fixed bed, (ii) particulate, (iii) bubbling, (iv) slugging and (v) turbulent. The

different regimes for gas-solid fluidization are shown in Figure 2-9 (here is the regimes of fluidization for transporting and non-transporting systems and above is bubble behaviour), Ar in Figure 2-9 is Archimedes number, $Ar = \frac{d_p{}^3 \rho_g (\rho_s - \rho_g) g}{\mu^2}$

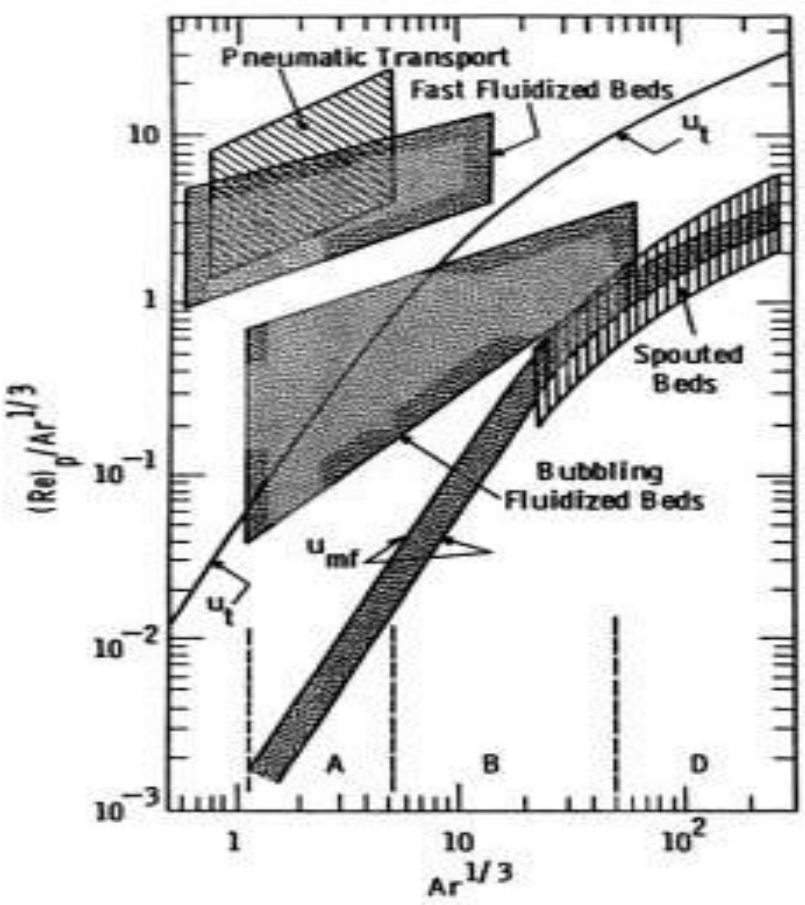

Figure 2-9: Regimes of fluidization for transporting and non-transporting systems (p.61, Yang, 2003).

For Geldart group "B" and group "D" particles, the bed transfers from the fixed bed into a bubbling fluidized bed when the gas velocity is increased beyond the minimum fluidization velocity of the system. However, for group "A" particles (powders), no bubbles form; instead the bed expands homogeneously.

A slugging regimes (a slugging regime is characterized by gas slugs of sizes close to the reactor cross section that rise at regular intervals and divide the main part of the fluidized bed into alternate regions of dense and lean phases) occur in beds - when the ratio of bed height, H to diameter, D (H/D) is larger than about 2, this gives enough time

for bubbles to coalesce into bigger ones. When the bubbles grow to approximately 2/3 of the bed diameter, the bed enters the slugging regime with periodic passing of large bubbles and regular large fluctuation of bed pressure drop corresponding to the bubble frequency (the passage of these gas slugs' produces large pressure fluctuations inside the fluidized bed).

With the continuous increase of the gas velocity, bubbles grow bigger owing to coalescence, and the bubbling bed can transfer into a slugging bed if the bed diameter is small and the particle diameter is large or into a turbulent bed if the bed diameter is large and the particle diameter is small. At higher velocities, beyond the turbulent fluidization velocity, a critical velocity, commonly called the transport velocity, U_{tr}, will be reached where a significant particle entrainment occurs. Beyond this point, continuing operation of the bed will not be possible without recycling of the entrained solids and the bed is now said to be in a fast fluidization regime.

Summary of fast pyrolysis reaction systems for liquids and gas, recently and currently operational worldwide including Malaysia is given in Table 2-2 and according to the information available; it is very clear from this table that the fast pyrolysis systems developed in the past are mostly fluidized bed reactor (FBR 44 out of 87 i.e. 50.57%, Circulating Fluidized Bed, CFB 7 out 87 and Fixed bed 5 out of 87) having the capability to produce liquid by pyrolysis and gas by gasification (Moghadam et al., 2016; Aida et al., 2015; Mazlan et al., 2015; Ahmed et al., 2013; Bridgwater, 2012; Sulaiman, 2012; Sulaiman and Abdullah, 2011; Wan Azlina, 2011; Sukiran et al., 2009; Lam and Zakaria 2008; Abdullah N. and A.V. Bridgwater, 2006; Bridgwater and Peacocke, 2000). In UTP, syngas and hydrogen are produced from the catalytic steam gasification of palm kernel shell (PKS) and polyethylene waste blend in a fluidized-bed with a syngas and hydrogen yield of 422.40 g syngas/kg feedstock and 135.27 g H_2/kg feedstock respectively. In UPM, diesel is produced from the fast pyrolysis of mixed plastic waste in a fluidized-bed reactor with diesel yield of 20ml diesel/15 g feedstock and 35 ml diesel/15 g feedstock

with and without catalyst respectively. In UTP, bio-oil is produced from the pyrolysis of rubber wood sawdust (RWS) and Meranti wood sawdust (MWS) in fixed-bed drop-type pyrolyzer with a yield of 33 wt% from both sources. In UM, bio-oil is produced from the pyrolysis of EFB in fixed-bed pyrolyzer with a yield of 42 wt%. In USM, bio-oil is produced from the pyrolysis of EFB in fluidized-bed pyrolyzer with a yield of 44.7 to 52.5 wt%. In UPM, hydrogen is produced from the gasification Malaysian Agricultural Waste in fluidized-bed gasifier with a yield of 14.08 to 31.04 g H_2/kg biomass, 18.93 to 25.44 g H_2/kg biomass and 11.6 to 23.0 g H_2/kg biomass from Palm Kernel Shell, Coconut shell and Bagasse respectively. The FBR has no moving parts which is also an advantage over the CFB. So we can confidently say that the fluidized bed fast pyrolysis process designed in this research is an attractive choice compared with other design. The rig is supplied with emission sensors to detect hazardous gases and it is designed to be environmentally friendly (low emissions) as the emission from the rig is lowered compared with Malaysian Emission Standards (Table 2-3).

Table 2-3: Comparison of Malaysian emission standard and the syngas composition from the rig

Name of gas	Malaysian Emission Standard*	Exhaust gas released from the rig	Unit
H_2S	5 -6.5 (1-8 hr)	0.5	(vol%)
CO	9-30 (1-8 hr)	6.5	(vol%)
H_2	-	6.5	(vol%)

*Source: Environmental Requirements: A guide for Investors, Eleventh Edition, October 2010, Department of Environment 1996, Environmental Quality (Clean Air) Regulations 1978, Rafia Afroz, et al., 2003.

Table 2-2: Summary of recent and currently operational fast pyrolysis reaction systems for liquids/gas (Bridgwater, 2012).

Fast pyrolysis	**Industrial**	**Units built**	**Max. size (kg/hr)**	**Research**	**Max. size (kg/hr)**
Fluid bed	Agritherm, Canada	2	200	Adelaide U., Australia	1
	Biomass Engineering Ltd, UK	1	200	Aston U., Uk	5
	Dynamotive, Canada	4	80,000	Cirad, France	2
	RTI, Canada	5	20	Cartin U., Australia	2
				ECN, NL	1
				East China U. Science &Tech. Shanghai, China	nk
				Gent U., Belgium	0.3
				Guangzhou Inst., China	10
				Harbin Institute of Technology, China	nk
				Iowa State U., USA	6
				Monash U., Australia	1
				NREL, USA	10
				PNNL, USA	1
				Shandong U. Technology, China	nk
				Shanghai Jiao Tong U., China	1
				Shenyang U., China	1
				South East U., China	1
				Texas A&M U., USA	42
				TNO, Netherlands	10
				U. Basque Country, Spain	nk
				U. Campinas, Brazil	100
				U. Melbourne, Australia	0.1

Fast pyrolysis	**Industrial**	**Units built**	**Max. size (kg/hr)**	**Research**	**Max. size (kg/hr)**
				U. Maine, USA	0.1
				U. Naples, Italy	1
				U. Science & Technology of China	650
				U. Seoul, Korea	not known (nk)
				U. Twente, Netherlands	1
				U. Western Ontario, Canada	nk
				U. Zaragoza, Spain	nk
				USDS, ARS, ERRC, USA	1
				Virginia tech. U., USA	0.1
				VTT, Finland	1
				VTI, Germany	6
				Zhejiang U., China	3
				Zhengzhou U., China	2
				UPM, Serdang, Selangor, Malaysia (Gasification for H_2)	nk
				UPM, Serdang, Selangor, Malaysia (Gasification for H_2)	0.78
				USM, Penang, Malaysia (Liquid Production)	0.15
				SEGi University, Petaling Jaya, Malaysia (Liq. Production)	0.015
				UTM, Johor, Malaysia	nk
				USM, Penang, Malaysia (Liquid Production)	0.15
				UTP, Perak, Malaysia (Co-gasification)	2.0
				UTP, Perak, Malaysia (Co-gasification)	0.3
				USM, Penang, Malaysia (Activated Carbon Production)	nk

Fast pyrolysis	**Industrial**	**Units built**	**Max. size (kg/hr)**	**Research**	**Max. size (kg/hr)**
Spouted fluid bed	Ikerlan, Spain	1	10	Anhui U. Science & technology, China	5
				U. Basque Country, Spain	nk
Transported bed & CFB	Ensyn, Canada	8	4000	CPERI, Greece	1
	Metso/UPM, Finland	1	400	Guangzhou Inst. Energy Conversion, China	nk
				U. Birmingham, UK	Nk
				U. Nottingham, UK	nk
				VTT, Finland	20
Rotating cone Integral catalytic pyrolysis	BTG, Netherlands	4	2000	BTG, Netherlands	10
Rotating cone Integral catalytic pyrolysis	BioEcon, Netherlands+ Kior USA	nk	nk	Battelle Columbus, USA	1
				PNNL, USA	1
				Technical U., of Munich, Germany	nk
				U. Massachusetts-Amherst, USA	nk
				Virginia Tech. U., USA	3?
Vortex centrifuge reactor				TNO, Netherlands	30
				Technical U., Denmark	nk
Ablative	PyTech, Germany	2	250	Aston U., UK	20
				Institute of Engineering Thermophysics, Ukraine	15
Augur or Screw	Abritech, Canada	4	2083	Aubum U., USA	1
	Lurgi LR, Germany	1	500	KIT (FZK), Germany	500
	Renewable Oil Intl, USA	4	200	Mississippi State U., USA	2
				Michigan State U., USA	0.5
				Iowa state U, USA	1.0

Fast pyrolysis	**Industrial**	**Units built**	**Max. size (kg/hr)**	**Research**	**Max. size (kg/hr)**
Radiative-Convective Entrained flow				CNRS-Nancy U., France	nk
				Dalian U. of technology, China	nk
				Institute of Wood Chemistry, Latvia	nk
				Shandong University of technology, China	0.5
Microwave	Carboscape New Zealand & UK	nk	nk	Chinese Academy of Sciences, Dalian 116023, China	nk
	Bioenergy 2020+gmbh, Austria	1	nk	National Inst. Advanced Industrial Sci. & Tech. Japan	<0.1
				Shandong U., China	<0.1
				Technical U. Vienna, Austria	nk
				U. Malaysia Sarawak	<0.1
Microwave				U. Mississippi	nk
				U. Minnesota, USA	10
				U. Nottingham, Uk and China	nk
Moving bed and fixed bed	Anhui Yineng Bio-energy Ltd, China	3	600	Anadolu University, Turkey	nk
				U. Autonoma de Barcelona, Spain	nk
				UTP, Perak, Malaysia (Liquid Production)	0.01
				UM, Kuala Lumpur, Malaysia	0.002
				U. Science & technology of China	~0.5
Ceramic ball downflow				Shandong University of technology, China	110
Unspecified				U. Kentucky, USA	nk
				U. Texas, USA	nk
				Technical U. Compiegne, France	nk
Vacuum	Pyrovac, Canada	1	3500	Not known	

2.3 Design of a bench scale fluidized bed reactor

2.3.1 Design basis and steps

For the present study, a bubbling fluidized bed reactor has been designed. The biomass throughput is taken as 1.0 kg/hr (bone dry basis). The biomass, from the field, has been pre-treated to a moisture content of 10%. Sand bed (with particle size range of 94 to 1180 μm) is considered for better heat and mass transfer in the biomass pyrolysis reactions. Based on literature review, the nominal diameter of the fluidized bed reactor is taken as 3 inches. The column height has been calculated using published design equations and correlations (Yang, 2003; Perry, 1999; Kunii and Levenspiel, 1991; Couper, 2005; Grace, 1982). The total height of the reactor is the sum of the expanded bed and transport disengaging height.

The design calculation involves four steps:

Step-1, selection of bed material and reactor tube (based on 3″ diameter as in the literature review, Table 2-8);

Step-2, calculation of the minimum fluidization velocity, terminal velocity and operation velocity;

Step-3, calculation of the reactor height for (a) sand only as bed material, (b) sand and biomass mixture as bed material and (c) biomass as bed material;

Step-4, design of the gas inlet, plenum and gas distributor. Details of each step are given below.

2.3.1.1 Selection of nominal diameter:

A 3″ ASTM-312 welded austenitic stainless steel pipe type 304 of schedule no 10 which corresponds to 88.90 and 82.80 mm external and internal diameters respectively has been selected as the reactor tube. Sand particle sizes of 94 to 1180 μm are used in design calculation.

2.3.1.2 Calculation of Fluidization velocities

Minimum fluidization velocity:

When the gas is passed upward, with a superficial velocity (U_o), through a packed bed, unrestrained at its upper surface, the pressure drop (ΔP_b) increases with increasing gas velocity until the pressure drop across the bed equals the weight of the bed per unit area (Geldart, 1986; Kunii and Levenspiel, 1991).

The onset of fluidization occurs when, the drag force by upward moving gas equals the weight of the particles, W,

$$W = \Delta P_b A_t = A_t L_{mf}(1-\varepsilon_{mf})[(\rho_p - \rho_f)g] \qquad (2.1)$$

where,

ΔP_b = pressure drop across the fluidized bed (Pa)

A_t = cross-sectional area of tube (m^2)

L_{mf} = height of bed at minimum fluidization (m)

ε_{mf} = bed voidage at minimum fluidization (-)

ρ_p = density of solid (kg/m^3)

ρ_f = density of fluid (kg/m^3)

g = acceleration due to gravity (m/sec^2)

The impact of superficial gas velocity (U_o) on the fluidized bed pressure drop, ΔP_b, (with uniform particle sizes) is illustrated in Figure 2-10. When, U_o increases, ΔP_b increases, reaches a peak, $\Delta P_{bmax,}$ known as maximum pressure drop across the fluidized bed, and then drops off to a constant value, ΔP_{bconst}. As U_o decreases from the ΔP_{bconst}, the pressure drop profile follows a different path without passing through the ΔP_{bmax}.

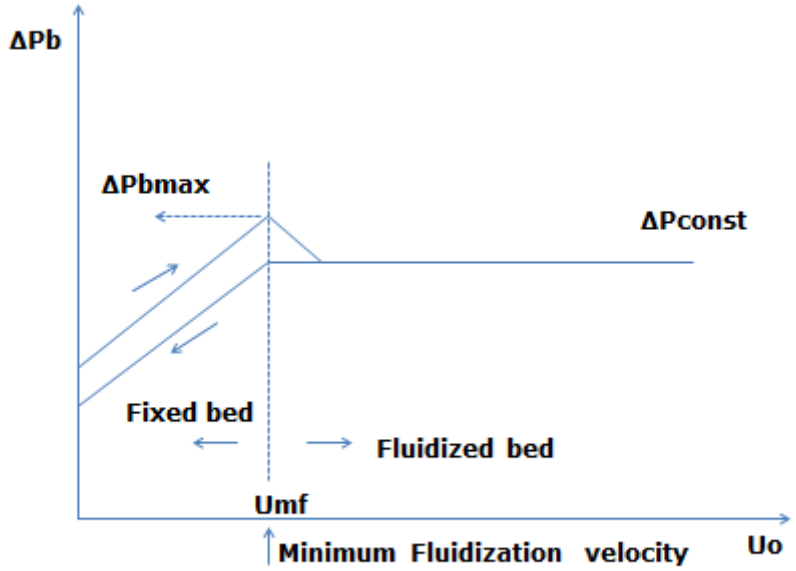

Figure 2-10: Relationship between the pressure drop through the bed and the superficial gas velocity (Fan and Zhu, 2005).

The minimum fluidization velocity, U_{mf} (corresponds to the peak pressure drop, ΔP_{bmax}) is calculated using the following general equation for isotropic-shaped solids (Eqn. 19, Page-69, Kunii and Levenspiel 1991)**:**

$$\frac{1.75}{\varepsilon_{mf}^3 \phi_s} \mathrm{Re}_{p,mf}^2 + \frac{150(1-\varepsilon_{mf})}{\varepsilon_{mf}^3 \phi_s^2} \mathrm{Re}_{p,mf} = Ar \qquad (2.2)$$

where,

$$Ar = \frac{{d_p}^3 \rho_g (\rho_s - \rho_g) g}{\mu^2} \qquad (2.3)$$

and

$$\mathrm{Re}_{p,mf} = \frac{d_p u_{mf} \rho_g}{\mu_g} \qquad (2.4)$$

$Re_{p,mf}$ = particle Reynolds number at minimum fluidization (-)

U_{mf} = minimum fluidization velocity (m/sec)
d_p = diameter of sand particle (μm)
ρ_s = density of sand particle (kg/m^3)
ρ_g = density of fluidizing gas (N_2) (kg/m^3)
μ = viscosity of fluidizing gas (N_2) (kg/m.sec)
g = acceleration due to gravity (m/sec^2)
ε_{mf} = voidage at minimum fluidization (-)
ϕ_s = sphericity of sand particle (-)

Equation 2.2 is a quadratic equation. A standard quadratic equation can be shown as: $ax^2+bx+c = 0$

and its roots are: $x = \frac{-b \pm \sqrt{b^2 - 4ac}}{2a}$.

Comparing equation 2.2 with the standard quadratic equation, the constants are:

$$a = \frac{1.75}{\varepsilon^3_{mf}\phi_s} \qquad b = \frac{150(1-\varepsilon_{mf})}{\varepsilon^3_{mf}\phi_s{}^2} \qquad c = -A_r$$

and the roots are: $\mathrm{Re}_{p,mf} = \frac{-b \pm \sqrt{b^2 - 4ac}}{2a}$ (2.5)

From Equation (2.4), the minimum fluidization velocity, U_{mf} is calculated as follows:

$$U_{mf} = \frac{\mathrm{Re}_{p\,mf} \times \mu_g}{d_p \rho_g} \qquad (2.6)$$

The calculated minimum fluidization velocity, U_{mf}, Archimedes number, Ar and Reynolds number, $Re_{p,\,mf}$ (at minimum fluidization velocity) are shown in Table 2-4. From Table 2-4, it can be observed that the U_{mf}, Ar and $R_{ep,mf}$ values increased as the particles size increased because these values are particle size dependent. So, the smallest particle size resulted the least U_{mf}, Ar and $R_{ep,mf}$ values and the largest particle size resulted the maximum value for the above parameters. It can be seen from Table 2-4 that the U_{mf} values range from 0.001 to 0.649 m/sec for the size range of 31.5 to 1180 μm

calculated for 600°C and vary from 0.001 to 1.087 m/sec for the size range of 31.5 to 1180 µm calculated for 400°C.

The minimum fluidization velocity, U_{mf}, is also calculated using the following equation for Re<20 (Eqn. 21, Page-69, Kunii and Levenspiel 1991) and is shown in Tables 2-5 and 2-6.

$$U_{mf} = \frac{d_p{}^2(\rho_s - \rho_g)g}{150\mu} \frac{\varepsilon^3{}_{mf}\phi_s{}^2}{1-\varepsilon_{mf}} \qquad (2.7)$$

where,

U_{mf} = minimum fluidization velocity (m/sec)
d_p = diameter of sand particle (µm)
ρ_s = density of sand particle (kg/m^3)
ρ_g = density of fluidizing (N_2) gas (kg/m^3)
µ = viscosity of fluidizing (N_2) gas (kg/m.sec)
g = acceleration due to gravity (m/sec^2)
ε_{mf} = voidage at minimum fluidization (-)

From Table 2-5 and Table 2-6, it can be observed that the U_{mf} values increased as the particles size increased because these values are particle size dependent. So, the smallest particle size resulted the least U_{mf} values and the largest particle size resulted the maximum value for the above parameter. It can be seen from Table 2-5 that the U_{mf} values range from 0.001 to 0.731 m/sec for the size range of 31.5 to 1180 µm calculated for 600°C and vary from 0.04 to 3.54 m/sec for the size range of 31.5 to 1180 µm calculated for 400°C. It can be seen from Table 2-6 that the U_{mf} values range from 0.001 to 0.861 m/sec for the size range of 31.5 to 1180 µm calculated for 600°C and vary from 0.04 to 3.16 m/sec for the size range of 31.5 to 1180 µm calculated for 400°C.

Terminal velocity:

The terminal velocity, U_t of a falling object is the velocity of the object when the sum of the drag and buoyancy forces equal the downward force of gravity acting on it. At this condition, the particles experience zero acceleration. The terminal velocity provides information about the upper limit of the gas velocity for the bed. If the bed is operated

below the terminal velocity of a certain particle sizes and densities, then the particles will retain in the bed.

The general equation for terminal velocity is given as below (Eqn. 28-29, page 80, Kunii and Levenspiel, 1991).

$$U_t = \left[\frac{4d_p(\rho_s - \rho_g)g}{3\rho_g C_D}\right]^{\frac{1}{2}} \qquad (2.8)$$

where, d_p is diameter of sand particle, ρ_s and ρ_g are the densities of sand and fluidizing gas (N_2) respectively, g is the acceleration due to gravity and C_D is the drag coefficient. Empirical correlation for C_D is given as (Eqn. 29, page-80, Kunii and Levenspiel 1991).

$$C_D = \frac{24}{\mathrm{Re}_p}\left[1 + \left(8.1716e^{-4.0655\phi_s}\right)\mathrm{Re}_p^{\,0.0964+0.5565\phi_s}\right] + \frac{73.69\left(e^{-5.0748\phi_s}\right)\mathrm{Re}_p}{\mathrm{Re}_p + 5.378e^{6.2122\phi_s}} \qquad (2.9)$$

where,

Re_p = particle Reynolds number (-)

ϕ_s = sphericity of sand particle (-)

The calculated U_t values are shown in Table 2-7. From Table 2-7, it can be observed that the U_t values increased as the particles size increased because these values are particle size dependent. So, the smallest particle size resulted the least U_t values and the largest particle size resulted the maximum value for the above parameter. The U_t values ranges from 0.036 to 7.323 m/sec for the size range of 31.5 to 1180 μm calculated for 600°C and vary from 0.042 to 6.623 m/sec for the size range of 31.5 to 1180 μm calculated for 400°C.

Flow regime diagrams (for locally collected sand particles) have been constructed using the calculated U_{mf} and U_t and are shown in Figures 2-12 and 2-13.

The terminal velocity, U_t, is also calculated using the following equations (Eqn. 31-33, Page-80, Kunii and Levenspiel 1991) for comparison and shown in Tables 2-5 to 2-6.

Terminal velocity, U_t, is calculated by:

$$u_t = u_t * \left[\frac{\mu(\rho_s - \rho_g)g}{\rho_g{}^2} \right]^{\frac{1}{3}} \qquad (2.10)$$

where,

U_t = terminal velocity (m/sec)

U_{t*} = dimensionless gas velocity (-)

ρ_s = density of sand particle (kg/m^3)

ρ_g = density of fluidizing (N_2) gas (kg/m^3)

μ = viscosity of fluidizing (N_2) gas (kg/m^3)

g = acceleration due to gravity (m/sec^2)

Dimensionless gas velocity, U_t*, is calculated using the following expression (valid when $0.5<ø<1$):

$$u_t* = \left[\frac{18}{(d_p*)^2} + \frac{2.335 - 1.744\phi_s}{(d_p*)^{0.5}} \right]^{-1} \qquad (2.11)$$

where,

d_{p*} = dimensionless particle diameter (-)

$ø_s$ = sphericity of sand particle (-)

Dimensionless particle size, d_p*, is calculated using Equation 2.12:

$$d_p^* = d_p \left[\frac{\rho_g(\rho_s - \rho_g)g}{\mu^2} \right]^{\frac{1}{3}} \qquad (2.12)$$

where,

d_{p*} = dimensionless particle diameter (-)

d_p = diameter of sand particle (μm)

ρ_s = density of sand particle (kg/m^3)

ρ_g = density of fluidizing (N_2) gas (kg/m^3)

μ = viscosity of fluidizing (N_2) gas (kg/m.sec)

g = acceleration due to gravity (m/sec^2)

Table 2-4: Estimated values of Archimedes number, Ar, (Eqn. 20, Kunii and Levenspiel, 1991, P. 69), minimum fluidization velocity, U_{mf}, (Eqn. 19, Kunii and Levenspiel, 1991, P. 69), terminal settling velocity, U_t, (Eqn. 31-33, Kunii and Levenspiel, 1991, P. 80), and minimum velocity for complete fluidization, U_{cf} at 400°C and 600°C.

Mean particle diameter, dp (μm)	Ar at 600 °C	Ar at 400°C	$Re_{p,mf}$ at 600 °C	$Re_{p,mf}$ at 600 °C	U_{mf}, m/sec (at 600°C)	U_{mf}, m/sec (at 400°C)	$U_{t(94)}/U_{mf}$ (at 600 °C)	$U_{t(94)}/U_{mf}$ (at 400°C)	U_{cf} at 400°C (m/sec)	U_{cf} at 600°C (m/sec)
31.5	0.23	0.42	0.0002	0.0004	0.001	0.001	500.21	461.76		
94	6.16	11.09	0.0053	0.0095	0.005	0.008	56.17	51.85	0.000050	0.000028
181	43.97	79.18	0.0378	0.0681	0.017	0.031	15.15	13.99	0.000684	0.000380
256	124.41	224.02	0.1069	0.1922	0.034	0.062	7.57	6.99	0.006951	0.003864
362.5	353.23	636.05	0.3024	0.5423	0.069	0.123	3.78	3.49	0.014119	0.007866
512.5	998.18	1797.43	0.8466	1.5073	0.136	0.243	1.89	1.74	0.131455	0.073656
890	5227.55	9413.27	4.1927	7.1985	0.393	0.681	0.63	0.58	0.117583	0.067909
1180	12183.55	21938.97	9.0566	14.9747	0.649	1.087	0.36	0.33	0.034911	0.020855
								$U_{cf} = \sum x_i Umf_i$	0.3058	0.1746

Table 2-5: Estimated fluidizing gas velocities, U_{mf}, U_t, (Eqn. 21 and 31-33 respectively, Kunii and Levenspiel, 1991, P. 69 and 80), minimum velocity for complete fluidization, U_{cf} at 600°C (Eqn. 4.5, Nienow et al., 1997, P. 64) at bed temperature of 600°C for selected sand particles.

Sand particle size (μm)	Mean sand particle size, dpi (μm)	Dimensionless particle size, dp*(Eq. 31)	Dimensionless terminal velocity, u_t* (Eq. 33)	Sand mass (g)	Sand mass fraction, xi	U_{mfi}, (m/sec) eq.21	$x_i.U_{mfi}$ (m/sec)	U_t(m/sec) Eq. 32	$U_{t(31.5)}/U_{mf}$	$U_{t(94)}/U_{mf}$	$(\rho_s-\rho_g)$, kg/m^3
0-63	31.5	0.61	0.02	1	0.002	0.001		0.04	72.01	500.21	2659.61
63-150	94	1.83	0.14	3	0.006	0.005	0.0004	0.26	8.09	56.17	2659.61
150-212	181	3.53	0.37	11	0.022	0.017	0.0039	0.69	2.18	15.15	2659.61
212-300	256	4.99	0.57	56	0.112	0.034	0.0079	1.04	1.09	7.57	2659.61
300-425	362.5	7.07	0.81	57	0.114	0.069	0.0745	1.49	0.54	3.78	2659.61
425-600	512.5	9.99	1.09	269	0.539	0.138	0.0718	2.01	0.27	1.89	2659.61
600-1180	890	17.36	1.61	86	0.172	0.416	0.0235	2.98	0.09	0.63	2659.61
1180+	1180	23.01	1.92	16	0.032	0.731	0.1820	3.54	0.05	0.36	2659.61
$U_{cf} = \sum x_i Umf_i$							0.182				

Table 2-6: Estimated fluidizing gas velocities, U_{mf}, U_t, (Eqn. 21 and 31 to 33 respectively, Kunii and Levenspiel, 1991, P. 69 and 80), minimum velocity for complete fluidization, U_{cf} at 400°C (Eqn. 4.5, Nienow et al., 1997, P. 64) at bed temperature of 400°C for selected sand particles.

Sand particle size (μm)	Mean sand particle size, dpi (μm)	Dimensionless particle size, dp*	Dimensionless terminal velocity, u_t*	Sand mass (g)	Sand mass fraction, xi	U_{mfi}, (m/sec), Eq 21	$x_i.U_{mfi}$ (m/sec)	U_t(m/sec) Eq. 32	$U_{t(31.5)}/U_{mf}$	$U_{t(94)}/U_{mf}$	$(\rho_s-\rho_g)$, kg/m^3
0-63	31.5	0.75	0.03	1	0.002	0.001		0.04	71.27	461.76	2659.49
63-150	94	2.23	0.19	3	0.006	0.005	0.00003	0.28	8.00	51.85	2659.49
150-212	181	4.29	0.48	11	0.022	0.020	0.00045	0.70	2.16	13.99	2659.49
212-300	256	6.07	0.70	56	0.112	0.041	0.00456	1.02	1.08	6.99	2659.49
300-425	362.5	8.60	0.96	57	0.114	0.081	0.00930	1.41	0.54	3.49	2659.49
425-600	512.5	12.16	1.26	269	0.539	0.162	0.08774	1.86	0.27	1.74	2659.49
600-1180	890	21.11	1.82	86	0.172	0.490	0.08459	2.68	0.09	0.58	2659.49
1180+	1180	27.99	2.15	16	0.032	0.861	0.02767	3.16	0.05	0.33	2659.49
$U_{cf} = \sum x_i Umf_i$							0.214				

Table 2-7: Estimated values of Reynolds number, R_{ep}, (Eqn. 19, Kunii and Levenspiel, 1991, P. 69), terminal settling velocity, U_t and drag coefficient, C_D, (Equations 28 and 29 respectively, Kunii and Levenspiel, 1991, P. 80).

Mean particle diameter, dp (μm)	U_t guess (m/sec) values		Reynolds no, R_{ep}		Drag coefficient, C_D		U_t calculated (m/sec)	
	at 600°C	at 400°C	at 600°C	at 400°C	at 600°C	at 400°C	at 600°C	at 400°C
31.5	0.036	0.042	0.012	0.021	2138.040	1222.054	0.036	0.042
94	0.268	0.297	0.266	0.451	116.162	72.858	0.268	0.297
181	0.776	0.830	1.484	2.427	26.622	17.945	0.776	0.830
256	1.297	1.359	3.508	5.620	13.478	9.458	1.297	1.359
362.5	2.097	2.151	8.031	12.596	7.304	5.346	2.097	2.151
512.5	3.253	3.249	17.613	26.898	4.290	3.312	3.253	3.249
890	5.843	5.469	54.938	78.628	2.309	2.030	5.843	5.469
1180	7.323	6.623	91.289	126.246	1.949	1.835	7.323	6.623

Calculations of operating gas velocity:

Operation gas velocity is maintained in between the minimum fluidization velocity and the terminal velocity of particles. To find operation gas velocity, the local sand density and particle sizes are important and hence those properties are determined experimentally.

Sand (bed material) analysis: Sand analysis data is given in Table 2-8.

Table 2-8: Sand (collected from local source) analysis: density and void space.

Weight of empty cylinder (g)	Weight of empty cylinder +200ml of oven dry sand (g)	Weight of 200ml of sand (g)	Bulk density of sand (g/ml)	Water absorbed by 200ml of sand (ml)	Actual volume of sand sample (ml)	Actual density of sand (g/ml)	Sand voidage (static condition), ε
155	453	298	1.49	88	112	2.66	0.44

Estimation of minimum fluidizing velocity, U_{mf}, (Equation 2.2 to 2.6), terminal velocity, U_t (Equation 2.8 to 2.9) and the minimum velocity for complete fluidization, U_{cf} (Equation 2.13): The minimum velocity for complete fluidization is defined as the minimum velocity required to fully support the solids (though not necessarily in a well-mixed state) above the distributor. The minimum velocity for complete fluidization is explained below.

The minimum velocity for complete fluidization, U_{cf}:

When gas is passed upwards through a packed bed unrestrained to its upper surface, the pressure drop increases with gas velocity until, the pressure drop across the bed equals the weight of the bed per unit area. If the bed has been compacted, then an excess pressure is required to free them (points C and C′ in Figure 2-11) and they adopt a higher voidage configuration causing a fall back to the theoretical pressure drop. With group B and D powders a further increase in velocity above the minimum fluidization causes the formation of small bubbles whose size increases with gas velocity. The bed pressure drop begins to fluctuate and if the bed is deep enough (H>2D) the bubbles

occupy a substantial proportion of the cross-sectional area (Nienow et al., 1997; Geldart, 1986). These large bubbles are called slugs and cause the regular piston-like movements of the upper surface of the bed. If the gas velocity is now reduced, depending on the size distribution of the powders, the pressure drop declines along curves 3, 4 or 5 in Figure 2-11. If the particles have a narrow size range, curve 3 is followed; increasing the size distribution (but maintaining the same mean size) results in curves 4 or 5 because the larger particles settle out progressively on the distributor. Points D and E represent the minimum velocity required to fully support the solids (though not necessarily in a well-mixed state) and is called the minimum velocity for complete fluidization, U_{cf}.

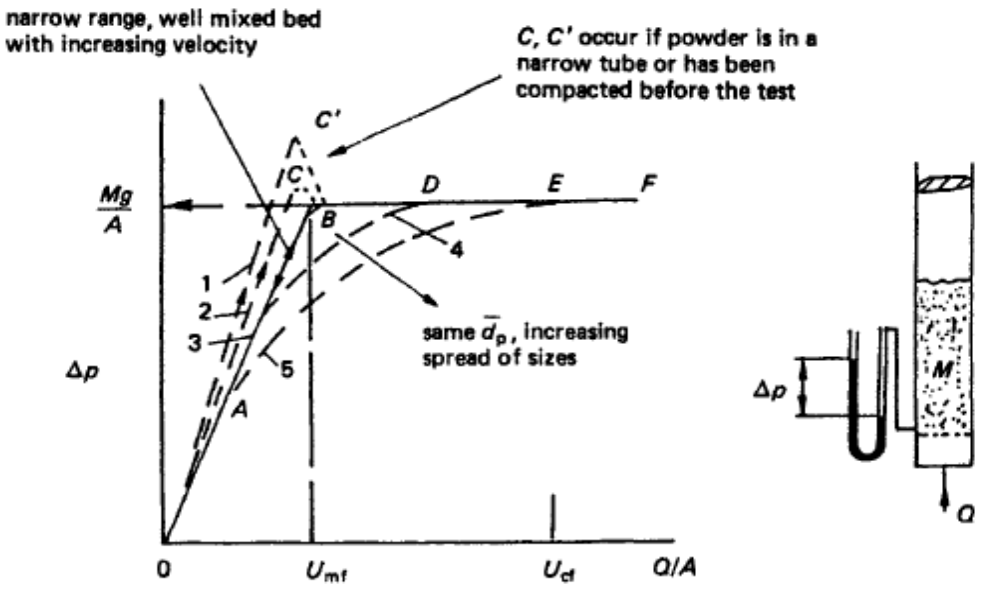

Figure 2-11: Pressure drop across fixed and fluidized bed fro group B and D powders. OAB, fixed bed region; AE partial fluidization for wide size range indicating segregation; EF, fully fluidized region (p.63, Nienow et al., 1997)

The minimum velocity for complete fluidization, U_{cf}, is calculated using Equation 2.13 (Eqn. 4.5, P-64, Nienow et al., 1997) and shown in Tables 2-6 to 2-7.

$$U_{cf} = \sum x_i U_{mfi} \quad \text{... (2.13)}$$

where,

U_{cf} = minimum velocity for complete fluidization (m/sec)

x_i = mass fraction of i size particle (-)

U_{mfi} = minimum fluidization velocity for i size particle (m/sec)

The calculated value of U_{cf}, U_{mf}, U_t were used to draw the flow regime diagram (Figures 2-12, 2-13) to estimate the operation gas velocity for the designed system. So the explanation of Figure 2-11 with respect to current design data is Figures 2-12, 2-13.

Estimation of operating gas velocity

The minimum fluidization velocity, $U_{mf,}$ and terminal velocity, $U_{t,}$ for locally collected sand particles were evaluated at two different operating gas temperatures: 600 and 400^{o}C and were superimposed on fluidization transport regime diagram (Figure 2-9) and shown in Figures 2-12 and 2-13 respectively. In Figure 2-12, the values for the vertices of bubbling fluidized bed are (1, 0.04), (1, 0.7), (50, 1.5) and (50, 4.0). The dimensionless gas velocity u^*_{max}, u^*_{inter} and u^*_{min} (superficial gas velocity extracted from Figure 2-12) for the local sand particles are 3, 1.5 and 0.185 respectively and the terminal velocity ranges from 0.268 to 7.323 (Table 2-7, by using Eqn. 28-29, Kunii and Levenspiel, 1991, P. 80). Now, if the bed is operated with u^*_{min}, all the particle sizes will retain in the bed, but the bed will not be fluidized because the gas velocity is much less than the terminal velocity of the smallest particle size range. If the bed is operated with u^*_{max}, the bed will be fluidized but the particles sizes form 94 to 362.5 μm will not be retained in the bed and the size 512.5 μm may be retained in the bed because the gas velocity is greater than the terminal velocity of the particle size range 94 to 362.5 μm and much less than the terminal velocity of the particle size range above 512.5 μm (Table 2-7 and Table 2-9). The dimensionless gas velocity u^*_{max}, and u^*_{min} (superficial gas velocity extracted from Figure 2-12) for the average local sand particles are 1.90 and 0.295 respectively (Table 2-9). If the bed is operated with u^*_{max} for the average local sand particles, the bed will be fluidized with the particles sizes form 94 to 362.5 μm and the size 512.5 μm may not be fluidized (Table 2-7). If the bed is operated with u^*_{min} for the average local sand particles, the bed will be fluidized only with the particles size 94 μm (Table 2-7). The particle sizes used in the different research labs ranges from 256 to 655 μm (Boateng et al., 2007; Zheng, 2007; Islam et al., 1999 and Wang et al., 2005).

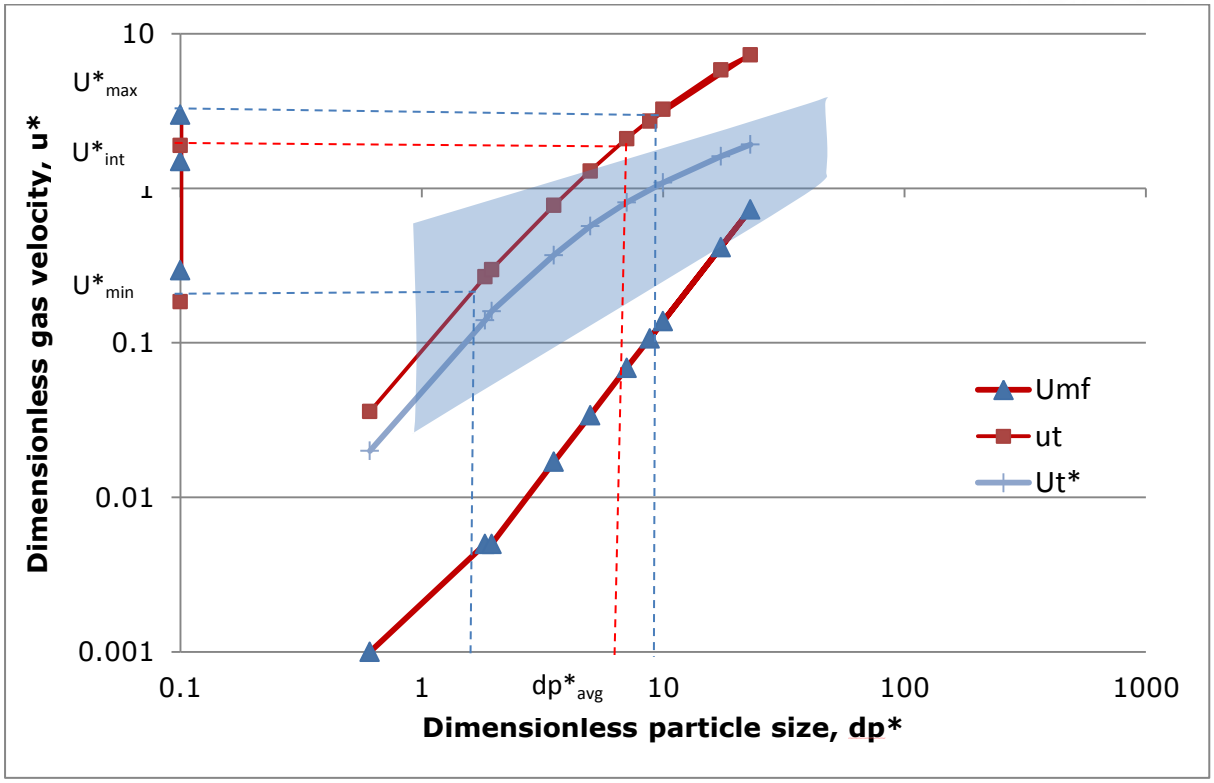

Figure 2-12: Flow regime diagram and operating condition estimation (constructed by using data from Tables 2-7 and 2-9).

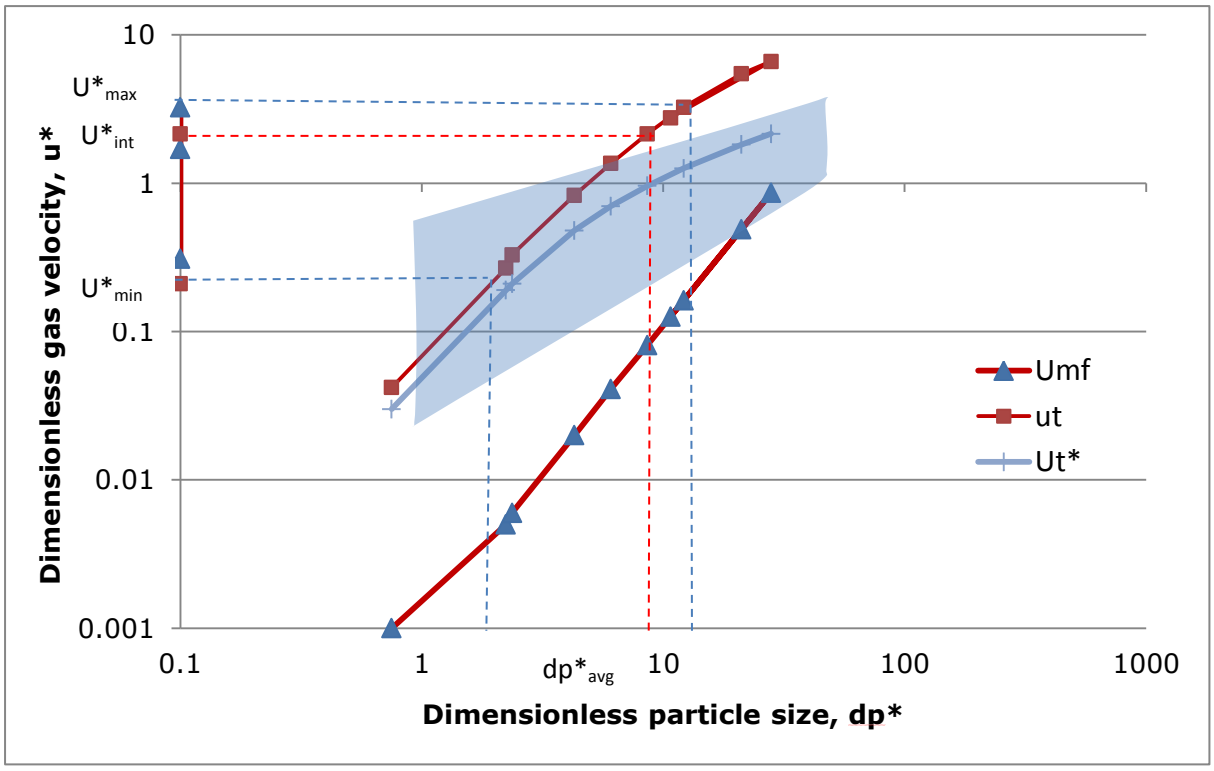

Figure 2-13: Flow regime diagram and operating condition estimation (constructed Using data from Tables 2-7 and 2-9).

The superficial gas velocity (Usc) is estimated using fluidized bed flow regime diagram (Figures 2-12 and 2-13). Four scenarios are selected (superficial gas velocity estimated) i. for $dp_{average}$, and as ii. U_{max}, iii U_{inter} and iv. U_{min}.

Scenario-I: the superficial gas velocity (U_{sc-1}) is estimated as 0.54 m/sec and as 0.46 m/sec at bed temperatures of 600 and 400°C respectively (Figures 2-12 and 2-13). At first, the dimensionless gas velocity is calculated for the local average particle size at 600 and 400°C, and then the superficial gas velocity is calculated for the same size using Equation 2.10.

Scenario-II: the superficial gas velocity (U_{sc-2}) is estimated as 5.54 m/sec at bed temperature of 600°C and 4.77 m/sec at bed temperature of 400°C, the detail estimation method is shown graphically in Figures 2-12 and 2-13 respectively. At first, the dimensionless gas velocity is calculated for the local largest particle size at 600°C and 400°C, and then the superficial gas velocity is calculated for the same size using Equation 2.10.

Scenario-III: the superficial gas velocity (U_{sc-3}) is estimated as 2.77 m/sec at bed temperature of 600°C and 2.50 m/sec at bed temperature of 400°C, the detail estimation method is shown graphically in Figures 2-12 and 2-13 respectively. At first, the dimensionless gas velocity is calculated for the local intermediate particle size at 600°C and 400°C, and then the superficial gas velocity is calculated for the same size using Equation 2.10.

Scenario-IV: the superficial gas velocity (U_{sc-4}) is estimated as 0.34 m/sec at bed temperature of 600°C and 0.31 m/sec at bed temperature of 400°C, the detail estimation method is shown graphically in Figures 2-12 and 2-13. The calculated superficial gas velocity is shown in Table 2-9. At first, the dimensionless gas velocity is calculated for the local minimum particle size at 600°C and 400°C, and then the superficial gas velocity is calculated for the same size using Equation 2.10.

For the present study, the maximum, intermediate and minimum operation gas velocity at 600°C are estimated as 5.54, 2.77 and 0.34 m/sec for the local maximum, intermediate and minimum particle sizes respectively and the estimated terminal velocities at 600°C for the local particle sizes range from 0.036 to 7.323 m/sec. The maximum, intermediate and minimum operation gas velocity at 400°C are estimated as 4.77, 2.50 and 0.31 m/sec for the local maximum, intermediate and minimum particle sizes respectively and the estimated terminal velocities at 400°C for the local particle sizes range from 0.042 to 6.623 m/sec. The terminal velocity is particle size dependent. If the bed is operated above the terminal velocity of a size of particles, that particle size will be entrained from the bed. So, to retain a size of particle within the bed, the bed should be operated under its terminal velocity. For example, at 600°C, if the bed is operated at a superficial velocity of 0.54 m/sec, particles of 94 μm diameter will be entrained as the terminal velocity of this size is 0.27 m/sec, but particles of other sizes above 94 μm will be retained within the bed as their terminal velocity is above 0.54m/sec. So, we can operate the bed with a superficial velocity of 0.54 m/sec with a particle size range of 94 to 1180 μm.

A list of fluidized beds and their operating conditions used in different research laboratories is shown in Table 2-10. The bed operation temperature ranges from 480 to 750°C. Bed diameters of 3.4 to 8.0 cm are mostly used. Most research laboratory used biomass as feed material and sand as bed material. Biomass feed rate ranges from 0.01 to 33.02 kg, and the bed material used by them ranges from 0.03 to 30 kg. Superficial gas velocities used are from 0.004 to 0.71 m/sec. However, most research labs used superficial velocity of 0.40 to 0.70 m/sec. Most laboratories used nitrogen as fluidizing gas and the flow rates range from 0.017 to 3.5 m^3/sec, however most laboratory used fluidizing gas flow rate in the range of 0.017 to 0.17 m^3/sec.

Table 2-9: Estimated fluidizing gas velocities (calculated using data extracted from Figures 2-12 and 2-13)

Operating Temperature (°C)	**Dimensionless gas velocity, U*, extracted from Figures 1-11 & 1-12**			**Calculation of operating velocity U (Eq. 32, Kunii and Levenspiel, 1991, P. 80)**			**Calculation of minimum velocity for complete fluidization U_{cf}, m/s (Eq. 4.5, Nienow et al., 1997, P. 64)**	**Calculation of Reynolds number, Re (Eq.18, Kunii and Levenspiel, 1991, P. 69)**		
	U_{max}*	**U_{inter}***	**U_{min}***	**U_{max} (m/s)**	**U_{inter} (m/s)**	**U_{min} (m/s)**		**Re_{max}**	**Re_{inter}**	**Re_{min}**
600	3.0	1.50	0.185	5.54	2.77	0.34	0.182	45.87	18.39	1.63
400	3.25	1.70	0.21	4.77	2.50	0.31	0.306	60.46	25.35	2.25
Average				5.16	2.64	0.325	0.244			
Calculated from for $dp_{average}$										
600	1.90	-	0.295	3.51	-	0.54	-	16.72	-	2.60
400	2.15	-	0.31	3.16	-	0.46	-	23.01	-	3.32

Table 2-10: Characteristics of fluidized bed used by various researchers.

Bed condition		**Biomass**		**Fluidized bed material**		**Biomass to bed material ratio**	**Fluidizing gas**				**Biomass to fluidizing gas ratio (kg/kg)**	**Bed inner dia. (cm)**	**Superficial velocity used (m/s)**	**Calculated superficial gas velocity at operating condition (T, P) (m/)**	**Reactor height without plenum (cm)**	**Reference**
T (˚C)	**P (atm)**	**Type**	**Feed rate (kg/hr)**	**Type**	**Mass (kg)**	**(kg/hr) /kg**	**Gas type**	**Flow rate X10^{-3} (m^3/s)**	**Condition**							
									T(˚C)	**P(atm)**						
480	1.0	Switch grass	2.22	Silica sand	1.22	1.82	Nitrogen	1.20	20	1.0	0.46	7.8	0.65	0.62	52.0	Boateng et al., 2007
400-550	1.0	Sawdust	0.15	Al_2O_3	1.0	0.15	Nitrogen	0.083	20	1.0	0.91	8.0	0.006	0.004	30.0	Hoe et al., 2010
400-600	1.0	Pine saw dust	0.06	Glass beads	0.0992	0.60	Nitrogen	0.10-0.17	20	1.0	0.14-0.08	3.80	0.50 - 0.60	0.26-0.44	30.0	William et al., 2010
460	1.0	Soft wood	10 g	Quartz sand	30 g	0.33	Nitrogen	0.017	20	1.0	0.14	3.40	-	0.05	7.9	Aho et al., 2008
500	1.0	Lignocellulose	6-10	Sand	9.90	0.60-1.01	Nitrogen	3.5	20	1.0	1.71-2.85	16.2	-	0.45	100.0	Iowa State University

2.3.1.3 Calculation of fluidized bed reactor height (for sand particles only as bed material):

The few steps needed to calculate the height of the fluidized bed reactor is given in detail in the subsection below.

Selection of fluidized bed reactor diameter: (For the present case, a 3 inch nominal diameter ASTM A-312 Welded Austenitic Stainless steel pipe type 304 of Schedule no 10 has been selected. The inner diameter of the pipe is 82.8 mm).

Characterization of bed material (sand) and determination of particle size distribution are given in (Table 2-11).

Table 2-11: Sand (collected from local source) size distribution.

Sand particle size range (μm)	Average of sand particle size (μm)	Mass (g)	Mass fraction (xi)
0-63	31.5	1	0.002
63-150	94	3	0.006
150-212	181	11	0.022
212-300	256	56	0.112
300-425	362.5	57	0.114
425-600	512.5	269	0.540
600-1180	890	86	0.173
1180+	1180	16	0.032
		498	1.000

Determination of terminal velocities for each of the particle size groups by using standard correlations (Equations 2.8 and 2.9).

Construction of a flow regime diagram is done using calculated minimum fluidization and terminal settling velocities for the proposed materials and particle sizes. With the help of flow regime diagram, selection of operating superficial gas velocity for fluidized bed is done as shown in (Figures 2-12 and 2-13).

Calculation of volumetric flowrate is (Equation 2.22 and 2.23) based on estimated superficial operating gas velocity obtained from above at bed operating conditions (pressure and temperature).

Estimation of minimum bubbling bed height is done using standard correlations and

charts (Equation 2.20, Figure A-1 in Appendix -A).

Calculation of expanded bed height is done using standard correlations and charts (Equation 2.19, Figure A-2 in Appendix -A).

Estimation of transport disengaging height used standard correlations (Equation 2.15 to 2.18).

Calculation of total reactor height (Equation 2.14).

Total height of the fluidized bed reactor (Couper, 2005)**:**

The total height (H) of the reactor is the sum of the expanded bed height (L_b) and the transport disengaging height (TDH).

$$H = L_b + TDH \qquad (2.14)$$

There are two methods of calculating TDH: Method-1 and Method-2.

Method-1: George and Grace (1978) suggested a correlation for the TDH of Geldart group B particles as a function of bubble bursting diameter, d_{bo} at the bed surface.

$$TDH = 18.2 d_{bo} \qquad (2.15)$$

where, d_{bo} is calculated from the correlation (Page 130-131, Kunii and Levenspiel, 1991):

$$d_{b0} = \frac{2.78}{g}(U_0 - U_{mf})^2 \qquad (2.16)$$

where,

U_o = superficial gas velocity (m/sec)

U_{mf} = minimum fluidization velocity (m/sec)

g = acceleration due to gravity (m/sec^2)

The correlation (Equation 2.16) is valid when, $d_{bo} > l_{or}$, where, l_{or} is the spacing between adjacent holes in the distributor.

Method-2: The empirical data developed by Zenz and Weil (1958) has been widely used to determine TDH. Some researchers (Horio, 1983) proposed correlations for calculating TDH using superficial gas velocity and bed diameter and others (Amitin, et

al., 1968) used only superficial gas velocity to calculate TDH. The correlations are discussed below:

Horio, correlation:

$$TDH / D = (2.7D^{-0.36} - 0.7)\exp(0.74U_o D^{-0.23}) \qquad (2.17)$$

where,

U_o = superficial gas velocity (m/sec)

D = bed diameter (m)

Amitin correlation:

$$TDH = 1.08U_o{}^{1.2}(6.71 - 1.21gU_o) \qquad (2.18)$$

where, U_o is the superficial gas velocity

The expanded bed height (L_b) is calculated from the following expression (Couper, 2005):

$$L_b = L.r \qquad (2.19)$$

where, L is the minimum bubbling bed height expressed as (Couper, 2005):

$$L = \frac{4m}{\rho_p(1-\varepsilon_{mb})\pi D^2} \qquad (2.20)$$

r is the bed expansion ratio expressed as (Couper, 2005):

$$r = \exp[m'(G_f - G_{mf})/G_{mf}] \qquad (2.21)$$

and ε_{mb} is voidage at minimum bubbling bed condition, expressed as,

The value of ε_{mb} is defined as $\varepsilon_{mb} = \frac{\text{volume of bed - volume of particles}}{\text{volume of bed}}$ (Geldart, 1986)

The parameters and variables in equations 2.19 to 2.21 are defined as,

m = mass of bed material (kg)

D = diameter of the reactor vessel (m)

$m^{/}$ = coefficient of the bed expansion ratio (-) (estimated from Figure A-2 in Appendix –A).

G_f = gas flow rate at superficial velocity (m^3/sec), can be calculated using (Equation 2.22)

G_{mf} = gas flow rate at minimum fluidization velocity (m^3/sec), can be calculated using (Equation 2.23)

G_f /G_{mf} = the ratio of gas flow rate at superficial velocity to minimum fluidization velocity (-).

The gas flow rate at superficial velocity is given by the following:

$$G_f = \frac{\pi}{4} D^2 U_o \qquad (2.22)$$

The gas flow rate at minimum fluidization velocity is given by the following:

$$G_{mf} = \frac{\pi}{4} D^2 U_{mf} \qquad (2.23)$$

The parameter values (from standard tables and charts), calculated gas velocities and reactor height are shown in Table 2-12.

2.3.1.4 Corrections of fluidized bed reactor height when biomass is introduced into the sand bed:

Previously, calculation of the reactor height was done using Equations 2.14 to 2.23 considering the fluidization of sand particles alone. The reactor height calculation when mixture of biomass and sand particles is introduced is given in the subsequent sections.

Density correction for the binary mixture: (sand and biomass) (Ramakers et al., 2004; Chiba et al., 1979):

$$\frac{1}{\rho_m} = \frac{\omega_p}{\rho_p} + \frac{\omega_b}{\rho_b} \qquad (2.24)$$

where,

ρ_m = density of binary mixture (kg/m^3)

ω_p = weight fraction of sand particles (-)

ω_b = weight fraction of biomass particles (-)

ρ_p = density of sand particles (kg/m^3)

ρ_b = density of biomass particles (kg/m^3)

Particle size correction for the binary mixture: (sand and biomass) (Ramakers et al., 2004)**:**

$$\frac{1}{\rho_m d_m} = \frac{\omega_p}{d_p \rho_p} + \frac{\omega_b}{d_b \rho_b} \qquad (2.25)$$

where,

d_m = particle size of the binary mixture (μm)

d_p = sand particles size (μm)

d_b = biomass particles size (μm)

ρ_m = density of binary mixture (kg/m^3)

ω_p = weight fraction of sand particles (-)

ω_b = weight fraction of biomass particles (-)

ρ_p = density of sand particles (kg/m^3)

ρ_b = density of biomass particles (kg/m^3)

Minimum fluidization velocity correction for the binary mixture (sand and biomass):

The minimum fluidization velocity for the binary mixture is calculated using Equations 2.2 to 2.6 with corrected binary mixture particle density (ρ_m) and binary mixture particle size (d_m) values.

Height correction for the fluidized bed pyrolysis reactor for the binary mixture (sand and biomass):

Height of the proposed fluidized bed pyrolysis reactor for binary mixture is calculated using Equation 2.14 with corrected expanded bed height (L_b) and the transport disengaging height (TDH) parameters.

The procedure for reactor height calculation for binary mixture is described earlier in section 2.3.1.3. Table 2-13 shows the calculated reactor height and corrected parameter values for the binary mixture.

Reactor height for biomass alone as bed material was calculated according to the method described above for sand only and is given in Table 2-14.

Calculation details of reactor height for (i) sand only, (ii) binary mixture and (iii) biomass only as bed material will be found in Appendix-B.

2.3.1.5 Estimation of plenum chamber height:

For uniform gas distribution in the fluidized bed, the design and the configuration of the plenum (also known as wind box) and the gas distributor (also known as grid) are critical. Very often the pressure drop across the distributor (ΔP_d) and the fluidized bed (ΔP_b) are measured. If the ratio of the fluidized bed pressure drop to the distributor pressure drop ($\Delta P_b/\Delta P_d$) is high (>10) then the plenum design will probably not be so critical, however if this ratio is low (>3), the plenum design may determine whether the bed will operate satisfactorily (Vakhshouri, 2006; Yang, 2003). The typical plenum design showing various configurations for introducing gas into the plenum are illustrated in Figure 2-14 where certain plenum design can be preferred over the others. If the gas enters the plenum from the bottom, it is preferable that the plenum has a large enough distance between the outlet of the supply pipe and the grid to prevent the gas from preferentially passing through the middle of the grid. When gas enters a plenum from the side, it is preferable to route the gas to the middle of the plenum (Figure 2-14c) rather than have the supply pipe end at the wall of the plenum. In addition, horizontal-to-vertical down gas entry (Figure 2-14c) is preferable over the horizontal-to-vertical up gas entry (Figure 2-14b). It is preferable to have some sort of

Table 2-12: Parameters and velocities used in calculating the reactor height

T(°C)	d_p (μm)	ρ_f (kg/m^3)	μ (Ns/m^2)	D (cm)	G_f (m^3/s)	U_{mf} (m/s)	U_t (m/s)	U_o (m/s)	L (m)	ε_{mb}	m/	r	L_b (m)	TDH (m)	H (m)
600	451.19	0.3927	3.717E-5	8.28	0.00291	0.107	2.782	0.54	0.14	0.50	0.23	1.60	0.22	0.97	1.19
400	451.19	0.5059	3.516E-5	8.28	0.00248	0.126	2.809	0.46	0.14	0.46	0.23	1.36	0.19	0.58	0.77

Table 2-13: Reactor height for binary mixture.

T (°C)	d_p(μm)	d_b(μm)	d_m (μm)	ρ_s (kg/m^3)	ρ_m (kg/m^3)	U_{mf} (m/s)	U_o (m/s)	L_b (m)	TDH (m)	H (m)
600	451.19	2000	1800	2660	192.75	0.12	0.54	0.32	0.93	1.25
400	451.19	2000	1800	2660	192.75	0.13	0.46	0.25	0.55	0.80

Table 2-14: Reactor height for biomass alone as bed material.

T (°C)	d_b(μm)	ρ_b (kg/m^3)	U_{mf} (m/s)	U_o (m/s)	L_b (m)	TDH (m)	H (m)
600	2000	100	0.079	0.54	1.17	1.10	2.27
400	2000	100	0.093	0.46	0.94	0.70	1.64

The parameter, d_p is the average sand particles size, ρ_f and μ_f are the fluidizing gas density and viscosity respectively. D is the fluidized bed reactor diameter. G_f is the volumetric flow rate of gas at the superficial gas velocity U_o, U_{mf} is the minimum fluidizing velocity. U_t is the terminal velocity. L and L_b are the minimum bubbling and expanded bed heights respectively. TDH and H are the transport disengaging and total reactor heights respectively. d_b and d_m are the diameter of biomass and the mixture respectively. ρ_s, ρ_s and ρ_m are the densities of sand, biomass and mixture respectively.

deflection device (Figures 2-14d, e, f) between the outlet of the supply pipe and the grid to prevent the gas from preferentially passing through the middle of the grid. The preferential bypassing causes mal-distribution of the gas. In addition, the configuration in Figures 2-14e and 2-14f are preferable over the configurations in Figures 2-14 (a-d) (Yang, 2003). In Figure 2-14, the plenum configuration chosen for the present design is shown (Figure 2-14 e).

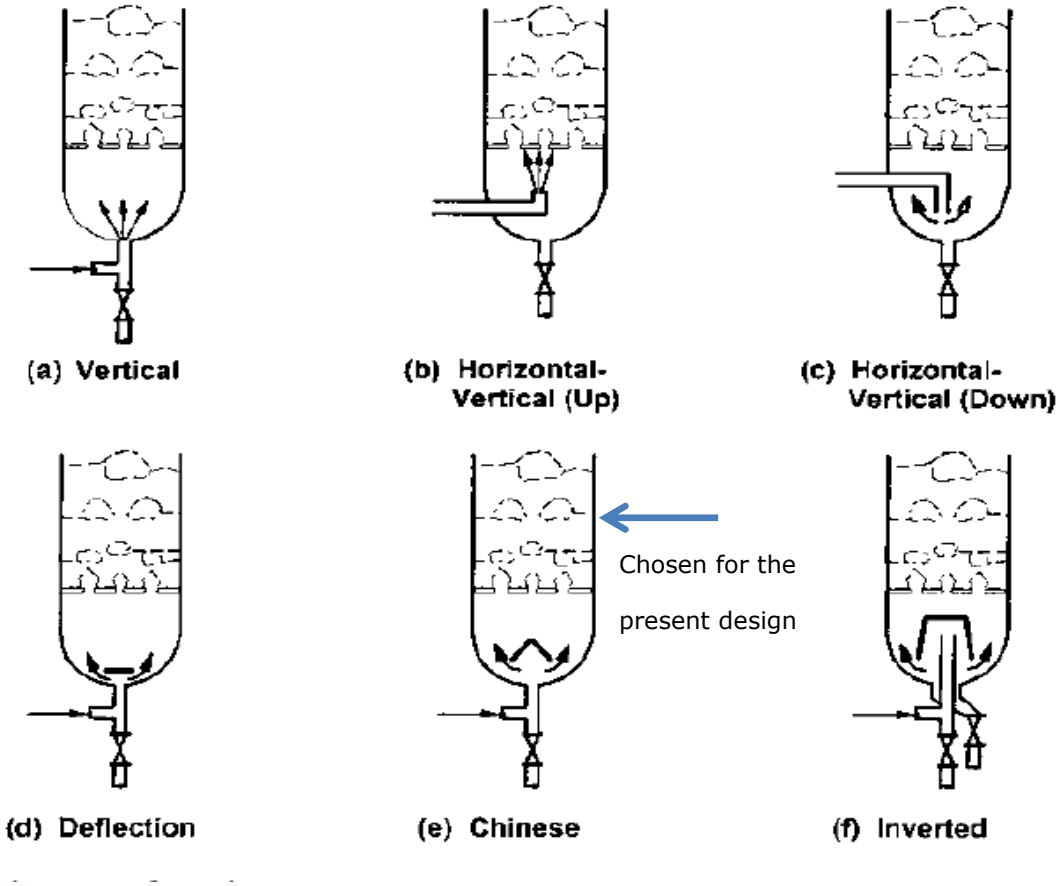

Figure 2-14: Typical plenum configurations (Yang, 2003).

Good design of the gas distribution system is essential to provide uniform gas distribution and thus improve the overall performance of fluidized bed systems. As the height of the plenum chamber is increased, mal-distribution decreases correspondingly.

This happens because, as the height of the plenum chamber increases, the air has sufficient time to develop turbulence free flow, resulting in an increased uniformity (Sachin, et al. 2009). Placement of the gas entrance far enough from the distributor increases the uniformity of flow over the distributor (Mohammadkhah and Mostoufi, 2009). Increasing aspect ratio (plenum height-to-diameter, h/d) improves the flow pattern, and the aspect ratio (h/d) of 1.5 gives the best air distribution (Sachin, et al. 2009). (Hafiz et al., 2013) found that plenum chamber with 350 mm height suffices criteria of high uniformity of gas distribution in the bed.

The ratio of reactor to plenum height used by different researchers is shown in Table 2-15. Most of the researcher used reactor to plenum height ratio of 4 to 6 for laboratory scale units. In the present design study, the ratio is selected to be 4 which lead to the calculated plenum height of 35 cm; however, for the present case moderately higher value has been selected (36 cm) to ensure a uniform gas distribution. Lateral gas entry and the pipe having perforated cap placed vertically at its end inside the plenum is selected for the present case (Figure 2-14e). The photo taken by the infrared camera of the actual behaviour of the fluidizing gas (during operation of the system) inside plenum is recommended as a future work. The plenum configuration and a brief design, for the present case, are shown in Figure 2-15.

Table 2-15: Plenum height used by different researchers for biomass pyrolysis in laboratory environment.

Reactor height (cm)	Reactor dia. (cm)	Plenum height (cm)	Reactor to plenum height ratio	Plenum dia. (cm)	Distributor holes dia. (mm)	Screen holes dia. (mm)	Bed material		Feedstock	Fluidizing gas inlet dia. (cm)	Temperature (˚C)	Reference
							Type	Particle size (μm)				
100.0	16.2	25.6	3.90	16.2	-	-	Sand	735	Lignocellulose	7.3	600	Sadaka, 2006
91.0	10.2	15.0	6.07	15.0	1.0	0.40	Ground concorb	500-600	-	-		Escudero & Heindel, 2011
150.0	30.0	90.0	1.67	30.0	5.0	-	Ballotini	7760	-	-	-	Kumar et al., 2011
110.0	15.0	15.0	7.33	15.0	1.0	-	Glass beads	63-300	-	-	-	Ryu et al., 2011
80.0	15.0	15.0	5.33	15.0	1.0	-	Glass beads	63-300	-	-	-	Ryu et al., 2011
170.0	8.0	30.0	5.66	8.0	-	-	-	-	Coal	-	50-250	Park et al., 2011
0.31	3.81	15.0	2.07	3.81	-	-	Silica sand	520	Cellulose	-	500	Patwardhan et al., 2011
40.0	3.4	15.0	2.67	3.4	-	-	Silica sand	700	Sawdust	-	1000	Salehi et al., 2011
91.0	10.2	15.0	6.07	10.2	-	-	Glass beads, crushed corncob, ground walnut shell	500-600				Drake, 2011
91.0	15.2	15.0	6.07	15.2	-	-	Glass beads, crushed corncob, ground walnut shell	500-600				Drake, 2011

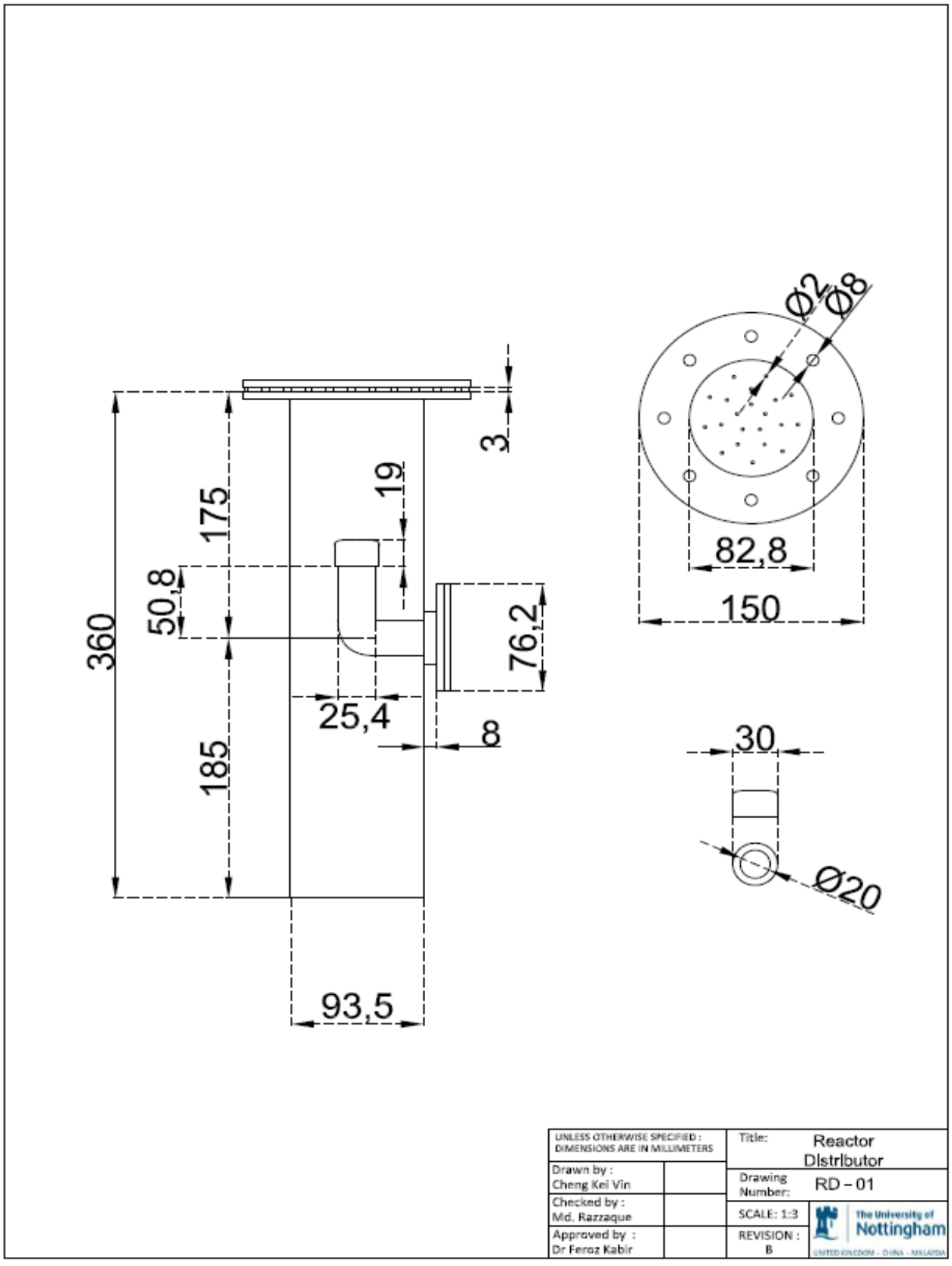

Figure 2-15: Detail diagram of the proposed plenum for the bubbling fluidized bed reactor (Cheng Kei Vin, MEng Internship student).

2.3.1.6 Gas distributor design: Detail of gas distributor design is given in subsection below:

A gas distributor of a fluidized bed provides support to the bed materials, helps uniform gas distribution, promotes particle movement and prevents particle backflow (particles falling from fluidized bed through distributor into the plenum) that may clog gas supply line. During pyrolysis, in a bubbling fluidized bed, the particulate materials circulate within the reactor with the bubbles formed, the particles move upwards behind the bubbles and in its trail. However, the particles near the bed wall and around the bubbles move downwards and tend to fall on the distributor (which can cause variable temperature and rapid de-fluidization of the entire bed).

A properly designed distributor prevents settling of denser particles, on the distributor, demote particle segregation, and avert particle backflow into the gas supply line (to avoid clogging gas supply line), minimize attrition of particles. The distributor will also promote small bubbles formation at the grid, enhance uniform gas distribution within the fluidized bed and reduce pressure drop across the distributor. The parameters that influence the distributor design aspects are: distributor configuration, number of holes, their dimensions and spacing (pitch), and pressure drop ratio (distributor pressure drop ΔP_d, to bed pressure drop ΔP_b, or, $\Delta P_d/\Delta P_b$). Three types of commonly used distributor configurations are shown in Figure 2-16. The simplest configuration is a single perforated plate with holes diameters smaller than the fluidizing particles (Figure 2-16a). For relatively smaller particles double perforated plates with slightly misaligned configuration is used (Figure 2-16b). To prevent any particle backflow, a screen maybe sandwiched between the two perforated plates (Figure 2-16c).

Figure 2-16: Various types of perforated plate distributor configurations: (a) single plate distributor, (b) double plate distributor, (c) screen sandwiched double plate distributor (Kunii and Levenspiel, 1991).

The detail diagram of a proposed single perforated plate is shown in Figure 2-17, and the design calculation details are discussed below.

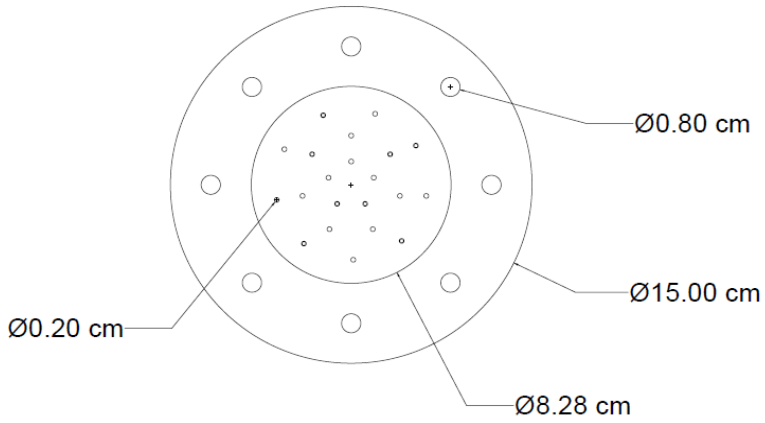

Figure 2-17: Detailed diagram of a single perforated plate distributor (Cheng Kei Vin, MEng Internship student).

Calculation detail of distributor design

Calculation of distributor holes number:

The number of distributor holes required for a single perforated plate is determined by the following correlations (Yang, 2003; Perry, 1999; Kunii and Levenspiel, 1991)**:**

$$N = \frac{4Q}{\pi d_h{}^2 U_h} \qquad (2.26)$$

$$Q = U_o \frac{\pi D^2}{4} \qquad (2.27)$$

$$U_h = C_d \sqrt{\frac{2\Delta P_d}{\rho_f}} \qquad (2.28)$$

where,

N = number of distributor holes (nos.)

Q = volumetric flowrate of gas entering the distributor (m^3/sec)

U_h = velocity of gas through a single distributor hole (m/sec)

d_h = distributor hole diameter (mm)

U_o = superficial gas velocity (m/sec)

D = diameter of fluidized bed (m)

C_d = discharge coefficient (-) (a function of vessel Reynolds number, Page-105, Kunii and Levenspiel, 1991)

Δp_d = pressure drop across the distributor (Pa)

ρ_f = density of gas entering the distributor hole (kg/m^3)

Estimation of distributor pressure drop:

Pressure drop across the dense bed is calculated by the following correlation (Page-68, Kunii and Levenspiel, 1991)**:**

$$\Delta p_b = L_{mf}(1-\varepsilon_{mf})(\rho_p - \rho_f)g \qquad (2.29)$$

where,

Δp_b = pressure drop across the dense bed (Pa)

g = acceleration due to gravity (m/sec^2)

ρ_p = sand particles density (kg/m^3)

ρ_f = fluidizing gas density (kg/m^3)

L_{mf} = bed height at minimum fluidization (m)

ε_{mf} = bed voidage at minimum fluidization (-)

Pressure drop across the distributor is calculated by the following correlation (Page-102, Kunii and Levenspiel, 1991)**:**

$$\Delta P_d = (0.2-0.4)\Delta P_b \qquad (2.30)$$

where,

Δp_d = pressure drop across the grid (Pa)

Δp_b = pressure drop across the dense bed (Pa)

Estimation of distributor holes density and pitch:

The holes density and holes pitch for triangular pitch orientation are calculated by the following correlations (Yang, 2003)**:**

$$N_d = \frac{N}{\frac{\pi}{4}D^2} \qquad (2.31)$$

$$L_h = \frac{1}{\sqrt{N_d \sin 60^\circ}} \qquad (2.32)$$

where, N_d is the holes density (nos./m^2), and L_h is the hole pitch (cm).

Pressure drop across the distributor

Calculation of the distributor pressure drop is necessary to determine the number of grid holes required. Distributors with low pressure drop are known to cause poor fluidization: some parts of the bed receive much less gas than others which may be de-fluidized temporarily or permanently while in other parts channelling may occur which may lead to formation of semi-permanent spouts. On the other hand, the distributors with high pressure drop result in more even gas distribution, however, the power consumption and blower or compressor cost would be high (Kunii and Levenspiel, 1991). For proper distributor design, a pressure drop criterion (a ratio of distributor pressure drop to bed pressure drop, $\Delta p_d/\Delta p_b$) is used. The pressure drop ratio, $\Delta p_d/\Delta p_b$, depends on particle cohesiveness (which is difficult to quantify), bed depth (L_{mf}) and diameter (D). Qureshi and Creasy, (1979) proposed a correlation to estimate the pressure drop required for satisfactory operation as,

$$\frac{\Delta p_d}{\Delta p_b} = 0.01 + 0.2\left\{1 - \exp\left(\frac{-D}{2L_{mf}}\right)\right\} \qquad (2.33)$$

For a properly designed distributor, the $\Delta p_d/\Delta p_b$ is 0.1 to 0.3 or Δpd of 3.4 X 10^3 N/m^2 (0.5 psi), whichever is the greater (Agarwal et al., 1962; Geldart 1986).

Different researchers used different criteria in designing a distributor for stable operations. Hiby (1964) proposed the pressure drop ratio ($\Delta p_d/\Delta p_b$) to be 0.15 when the ratio of superficial gas velocities (U_o/U_{mf}) is between 1 and 2; and $\Delta p_d/\Delta p_b$ to be 0.015 when U_o/U_{mf} is greater than 2. Kunii and Levenspiel (1991) and Geldart (1986) suggested the pressure drop ratios, $\Delta p_d/\Delta p_b$, to be in between 0.2 to 0.4. Vakhshouri (2008) reported the $\Delta p_d/\Delta p_b$ >0.12 and $\Delta p_d/\Delta p_b$ >0.4 for fine and coarse particles respectively. Perry, et al., (1999) recommended the grid pressure drop should be

between ⅓ to ½ of the bed weight for upward flow. For large diameter bed the pressure drop ratio is 0.21 Qureshi and Creasy, (1979), and if the bed solids contain tars or other sticky components, the suggested value may increase to up to 0.3. However, some fluidized beds operate successfully at much lower value of the proposed $\Delta p_d/\Delta p_b$.

Most researchers used $\Delta p_d/\Delta p_b$ of 0.20 to 0.40 (Table 2-16). Industrial applications usually respect this criterion as a minimum rule in order to limit purchase and consumption fan costs (Bonniol et al., 2010). In the present design study, the ratio $\Delta p_d/\Delta p_b$ is selected as 0.45 which is similar to USDA lab (Boateng et. al., 2007). This higher value of $\Delta p_d/\Delta p_b$ is selected to ensure a uniform gas distribution within the fluidized bed reactor. Based on the preselected pressure drop ratio, the number of distributor holes, their sizes and pitches are selected.

Table 2-16: Distributor pressure drop (Δp_d) to bed pressure drop (Δp_b) ratio used by different research groups

$\Delta p_d/\Delta p_b$	Distributor pressure drop (Pa)	Bed pressure drop (Pa)	Method used in calculation
1/3 bed weight	607.67	1823*	Perry, 1999 (1)
1/2 bed weight	911.5	1823*	
0.20 - 0.40	364.6 – 729.2	1823	Kunii, 1991 (2)
≥ 0.30	≥ 546.9	1823	Yang, 2003 (2)
0.10	182.3	1823	Vakhshouri, 2008 (3)
0.015 - 0.4	27.35 – 729.2	1823	Fernandez, 2008 (2)
0.11	200.53	1823	Avery and Tracey, 1968
1.0	1823	1823	Pictor, 1968
0.24	437.52	1823	Agarwal, 1962
0.45	820.35	1823	Boateng, 2007 (Switch grass pyrolysis)
0.37	674.51	1823	Megaritis, 1998 (Coal pyrolysis)

(1)Upward flow; (2) Rules of thumb for distributor; (3) Used in hydrodynamic studies; *Bed weight per unit area.

Distributor pitch selection

It is common to lay out the distributor holes in triangular or square pitch in order to increase the uniformity of fluidization. The relationship between the pitch length (L_h) and

the hole density (N_d) depends on whether the holes are laid out in a triangular or square pitch (Equation 2.31 and 2.32; Yang, 2003). A perforated plate distributor with triangular pitch is chosen because all the holes in a distributor are equidistant with triangular pitch, but this is not the case for a distributor with square pitch. Triangular pitch also results in more holes per unit area allowing more number of small gas bubbles as possible into the bed (Yang, 2003).

To calculate the number of the distributor holes and holes diameter; holes density and pitch standard correlations are followed (Equation 2.26 to 2.30 and 2.31 to 2.32). The calculation steps are: (i) selection of $\Delta p_d/\Delta p_b$ ratio from literature (Table 2-15); (ii) calculation of Δp_d; (Equation 2.30); (iii) estimation of gas velocity through a single distributor hole (Equation 2.28); (iv) determination of volumetric gas flow rate (Equation 2.27); (v) assuming new hole diameter (Equation 2.26) ; (vi) determination of the number of holes required to satisfy the required grid pressure drop using the hole diameter on trial and error basis; (vii) estimation of hole density (Equation. 2.31); (viii) estimation of hole pitch using hole density (Equation. 2.32).

Table 2-17 shows the required number and diameter of distributor holes for the present case. Table 2-18 shows the distributor configurations used by different researchers. The proposed distributor is comparable with the others. The calculation details of gas distributor design will be found in Appendix-B.

Table 2-17: Combinations of N and d_h for the proposed distributor.

Hole dia., d_h (mm)	**Number of grid holes, N**	**Pitch length, L_h (cm)**	**ΔP_d (Pa)**	**ΔP_b (Pa)**
1	84	1.0	820.14	1823
2	21	2.0	820.14	1823
3	9	3.0	820.14	1823
4	5	3.0	820.14	1823

Table 2-18: Distributor configuration used by different researchers

Distributor pressure drop (Pa)	Bed material		Distributor				Application	Reference
	Type	Size (μm)	Configuration	No of holes	Holes dia. (mm)	Screen holes dia. (μm)		
600-2600	FCC particles	70	Double plate with screen	1	12.0	38	Fluidized bed hydrodynamic study	Vakhshouri, 2008
	Glass beads	157	Double plate with screen	1	12.0	38	Fluidized bed hydrodynamic study	Vakhshouri, 2008
300-1600	FCC particles	70	Double plate with screen	33	2.1	38	Fluidized bed hydrodynamic study	Vakhshouri, 2008
	Glass beads	157	Double plate with screen	33	2.1	38	Fluidized bed hydrodynamic study	Vakhshouri, 2008
180-1200	Silica sand	540	Single plate with screen	-	2.0	-	Fluidized bed hydrodynamic study	Fernandez, 2008
	Glass beads	500-600	Single plate with screen	62	1	354	Fluidized bed hydrodynamic study	Escudero and Heindel, 2011
4234	FCC particles	60	Single plate	1824	25.0	-	FCC catalyst bed	Yang, 2003
4575	-	-	Single plate	4200	2.0	-	Commercial fluidized bed reactor	Kunii and Levenspiel, 1991

2.3.2 Feed inlet location, pre-heater and electrical jacket heater

Biomass is fed through an auger into the pyrolysis reactor at a suitable bed height for well mixing and maximum conversion. Usually, the biomass is introduced approximately horizontally into the fluidized bed reactor at a height above the distributor. The feed inlet location used by different research groups are shown in Table 2-19 from which it appears that biomass feed location ranges from 15.6 to 80% of static bed height above the distributor. Most research labs selected the feed location at 30% of the static bed height above the distributor. The feed location for the proposed fluidized bed is selected as 8.5 cm above the distributor which is in the range of 30 to 80% of the static bed height. The detail diagram of feed location is shown in Figure 2-18.

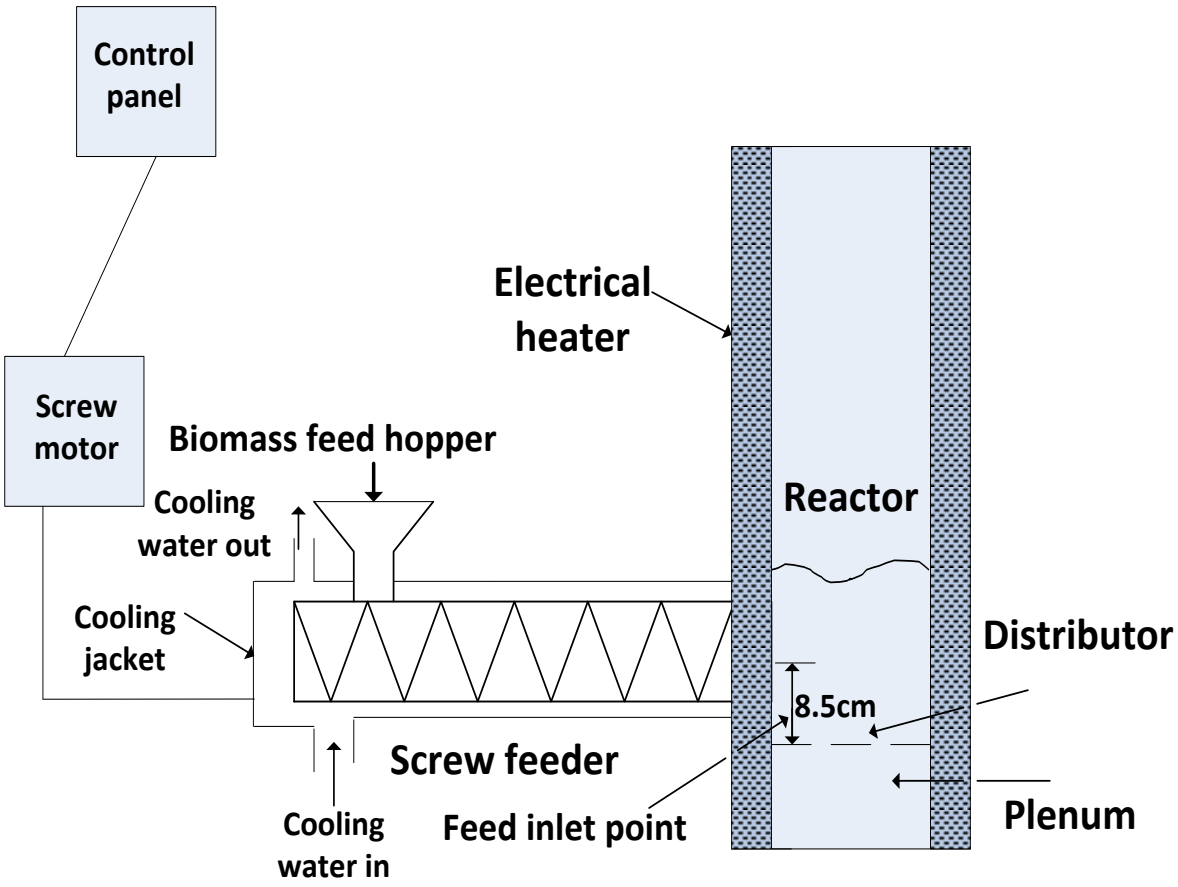

Figure 2-18: The detail of feed inlet connection point

Table 2-19: Feed location of the proposed fluidized bed.

Reactor height (m)	Reactor dia. (cm)	Static bed height (cm)	Feed location above distributor (cm)	Feed location at % of static bed height	Reactor type	Feed material	Bed material	Reference
1.20	15.0	32.0	5.0	15.6	Fluidized bed	Pine saw dust, pine wood chips, cereal straw	Silica sand	Herguido et al., 1992
0.537	5.23	9.20	3.0	32.6	Fluidized bed	Rape-seed	Quartz sand	Predel, 1998
0.770	15.40	20.60	16.50	80.0	Fluidized bed	Rape-seed	Quartz sand	Predel, 1998
0.98	9.36	5.05	1.50	29.7	Fluidized bed	Dried sewage sludge	Ceramsite	Hartman et al., 2005
0.98	9.36	5.23	1.50	28.7	Fluidized bed	Dried sewage sludge	Ceramsite	Hartman et al., 2005
1.30	9.36	10.0	4.0	40.0	Fluidized bed	Blend of coal and PET	Silica sand	Pohorely et al., 2006
1.0	7.50	10.0	-	-	Fluidized bed	Rice husk	Quartz sand	Williams & Nugrand, 2000
0.30	5.0	6.0	-	-	Fluidized bed	Oil palm shell	Silica sand	Islam et al., 1999
2.0	4.30	-	5.0	-	Fluidized bed	Blend of pine chips and coal	-	Pan et al., 2000
4.0	22.0	-	30.0	-	Fluidized bed	Blend of saw dust, rice husk and coal	-	Velez et al., 2009

The fluidizing gas passed through a pre-heater and heat supply to the reactor is done through an electrical jacket heater. The pre-heater and electrical jacket heater dimensions and ratings are given in Table 2-20.

Table 2-20: Dimension and ratings of pre-heater and electrical jacket heater

Name of items	Dimensions (mm)	Rated power (kW)	Voltage (V)	Phase	Frequency (Hz)	Maximum rating temp (°C)
Preheater	390 OD x 1007 length	3.6	240	single	50	1100
Jacket Heater	380Wx380Depthx 1000H	3.6	240	single	50	1100

2.3.3 Conclusion

The design of a bubbling fluidized bed reactor for biomass pyrolysis has been performed for three scenarios. Firstly, the reactor height is estimated considering the fluidization of sand particles alone. Secondly, the reactor height is corrected when biomass is introduced into the sand bed. Thirdly, the reactor height is estimated considering the fluidization of biomass particles alone. For the first case, the diameter of the reactor is selected as 8.28 cm (3″ standard SS304 pipe with schedule no 10) and the total height of the reactor is estimated as 1.19 m. The minimum fluidization and superficial velocities are calculated as 0.107 and 0.54 m/sec respectively. The height and diameter of plenum chamber are assumed 36 cm 93.5 mm respectively. The number and diameter of the holes of the distributor are estimated as 21 and 2 mm respectively. For the second scenario, the reactor height is estimated as 1.40 m and the diameter remains the same. The minimum fluidization velocity is calculated as 0.12 m/sec, whereas the superficial velocity is estimated as 0.54 m/sec. For the third scenario, the reactor diameter is selected as 20.7 cm and the reactor height is estimated as 2.27 m. The minimum fluidization velocity is calculated as 0.079 m/sec, whereas the superficial velocity is estimated as 0.54 m/sec. These data are for the reactor

to be operated at 600°C and for operation at 400°C, data are tabulated earlier. The calculation was done for the two operating temperature to see the difference in sizing of the units. For the three cases, the reactor is designed to operate at 400 to 600°C and 1 atm pressure with a short retention time of 1 to 2 seconds. The fluidized bed systems designed by other researchers are given in Table 2-10 (Page 39). From Table 2-10 it is observed that the operating temperatures ranges from 400 to 600°C and systems operated at 1 atm pressure. The bed diameter used 3.4 to 16.2 cm. The minimum fluidization velocity used 0.13 -0.51 m/sec, the superficial velocity used by them ranges from 0.06 to 0.65 m/sec. So, the design data for the present case is comparable with the literature. The specifications for reactor, heater and screw conveyor are given through Tables 2-21 to 2-23 and Figures 2-19 to 2-21. The Detail Engineering Drawings of the bubbling fluidized bed reactor with detail dimensions are shown in Appendix-B. The detail design of screw conveyor is given in Appendix-B.

Table 2-21: Specification sheet for the bubbling fluidized bed reactor

Reactor temperature 400-600 °C	Minimum fluidization velocity 0.12 m /s
Superficial gas velocity 0.46-0.54 m/s	Reactor inside diameter 8.28 cm
Reactor total height 1.83 m	Static bed height 16 cm
Expanded bed height 32 cm	Plenum height 36 cm
Plenum diameter 9.35 cm	Distributor diameter 8.28 cm
Number of holes in distributor 21	Distributor holes diameter 2 mm

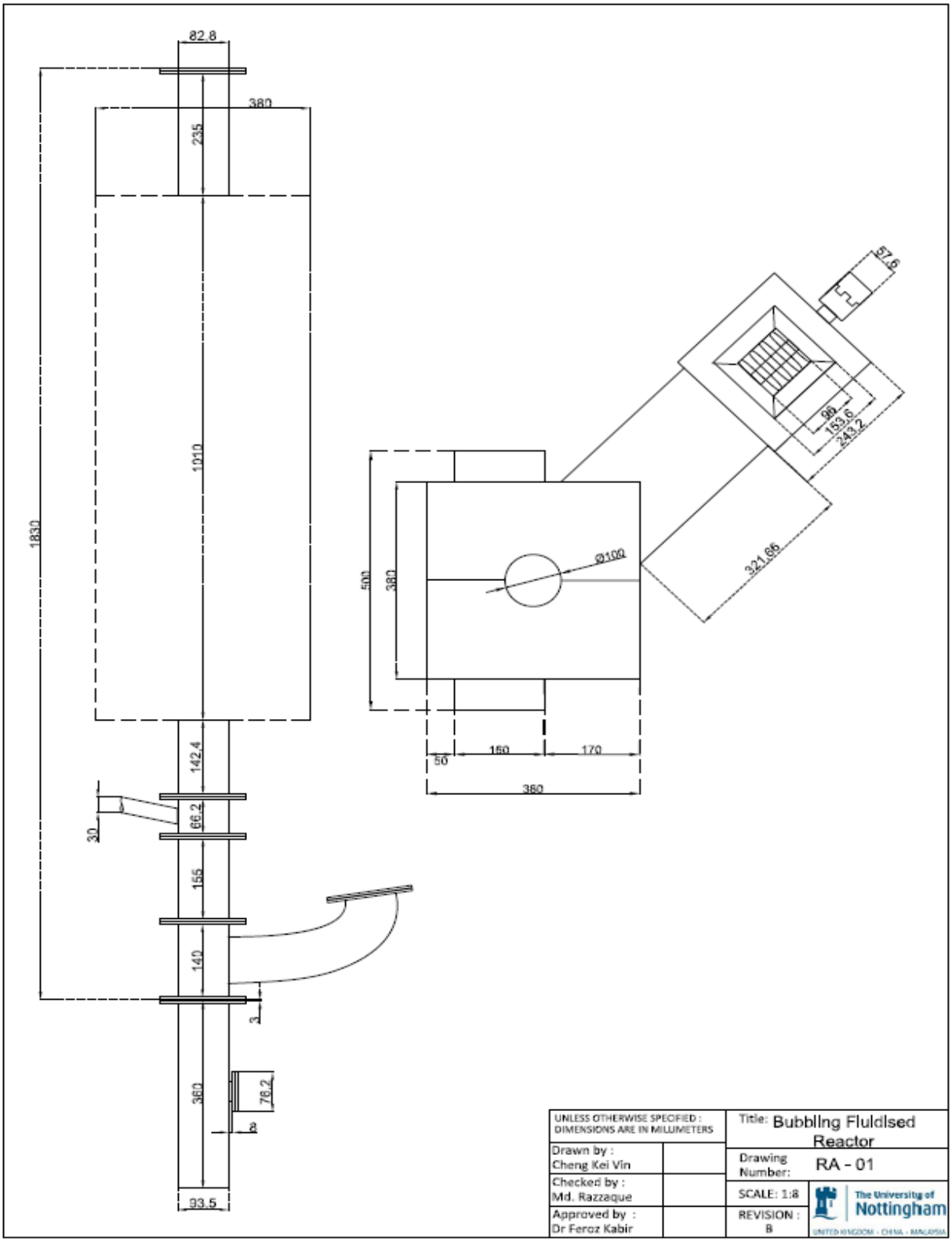

Figure 2-19: Bubbling fluidized bed reactor (Cheng Kei Vin, MEng Internship student)

Table 2-22: Specification sheet for the heater for bubbling fluidized bed reactor

Length of the heater 1000 mm	Width of the heater 380 mm
Depth of the heater 380 mm	No of coils 40 nos.
Diameter of coil 30 mm	Spacing between two coils 20 mm

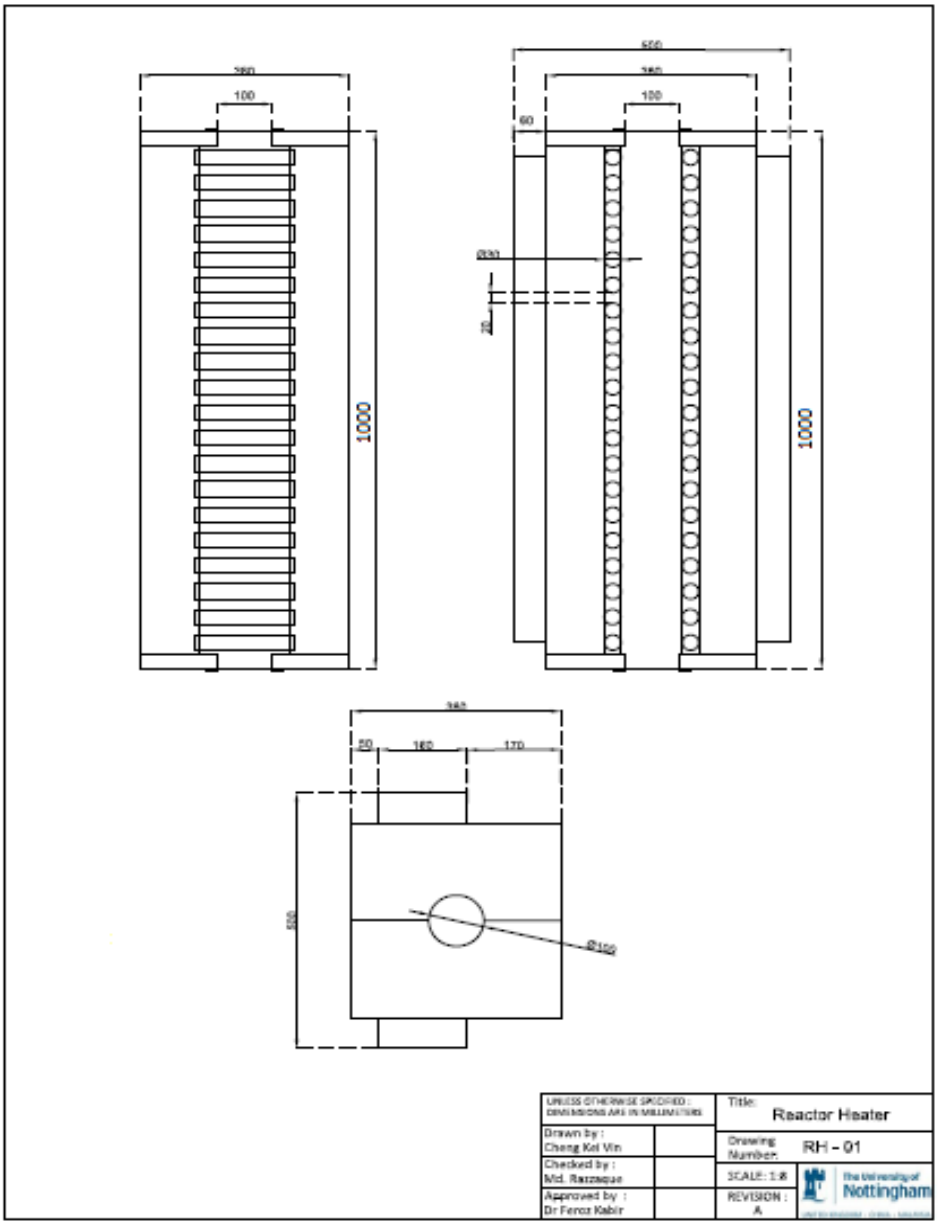

Figure 2-20: Heater for bubbling fluidized bed reactor (Cheng Kei Vin, MEng Internship student).

Table 2-23: Specification sheet for the screw conveyor for bubbling fluidized bed reactor as fabricated.

Length of screw conveyor 440 mm Diameter of the flight 75 mm

Spacing between two flights 20mm Shaft diameter 50 mm

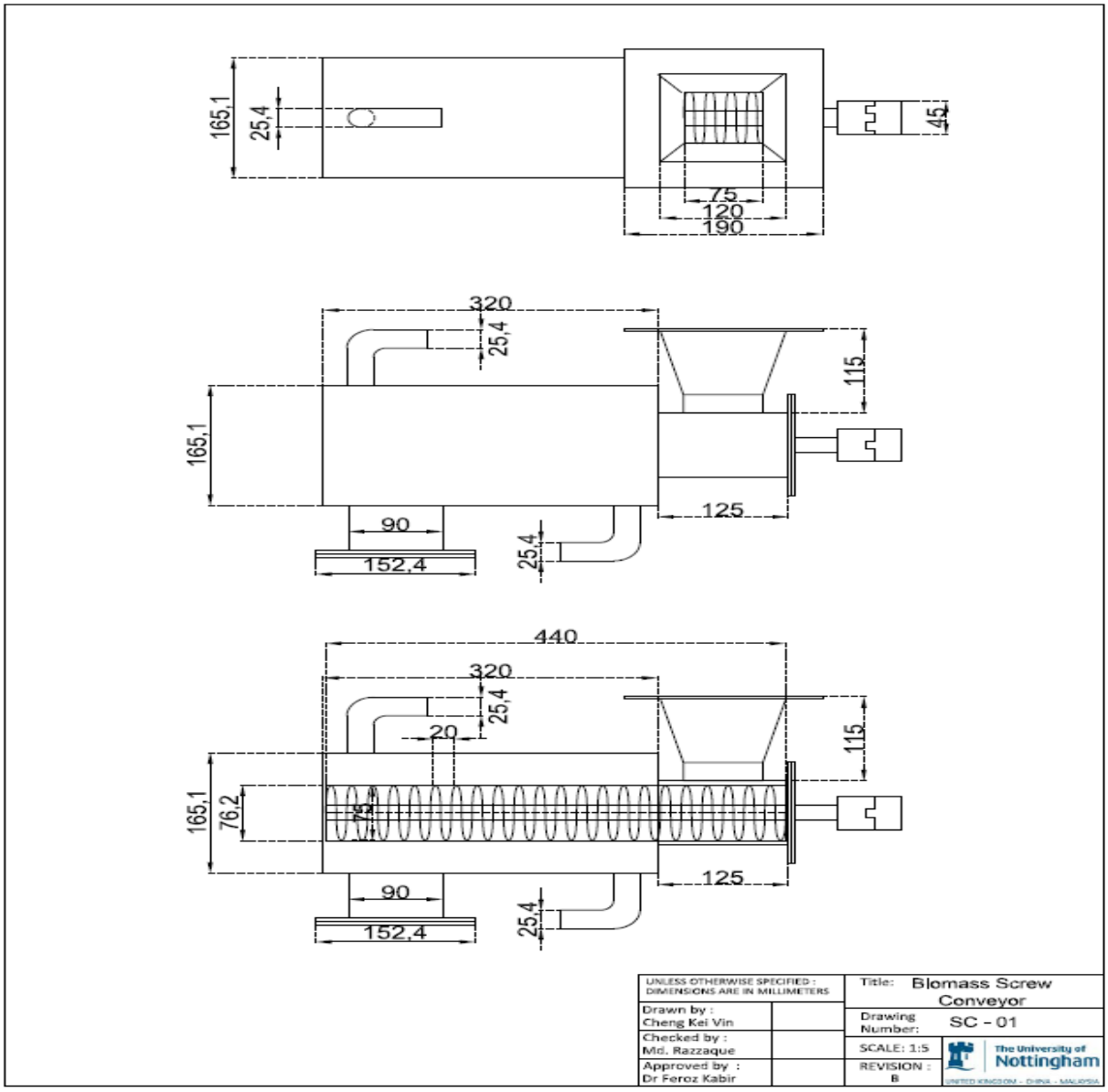

Figure 2-21: Biomass screw conveyor for bubbling fluidized bed reactor (Cheng Kei Vin, MEng Internship student).

CHAPTER 3. DESIGN AND FABRICATION OF UNIT OPERATIONS

3.1 Overview:

Each unit operations and the rig structure of the FBR are fabricated at UNMC workshops. The unit operations are mounted on the rig structure at UNMC. A Solidworks Finite Element Analysis (FEA) structure simulation has been done to assist the rig structure fabrication and the mounting of the unit operations on the rig. The piping and instrumentation of the rig are done at UNMC lab. This chapter describes the details of the fabrication and installation of (i) the biomass pyrolysis rig structure, (ii) the lab scale bubbling fluidized bed reactor and heaters (preheater and jacketed heater), (iii) the cyclone separators with solid collectors, (iv) the vapour condensers with liquid collectors, and (v) the bio-oil upgrading rig. Thirteen temperature sensors are installed at different locations of the rig to measure reaction temperatures, and the hot and cold streams temperatures. Digital control panels are also installed inside the rig.

3.2 Introduction

The major unit operations of the proposed fast pyrolysis rig are feedstock feeder system (auger feeder system including inverter), bubbling fluidized bed reactor, cyclone separators with solid collectors, condenser banks with condensate collectors, electric heaters (preheater and jacketed heater) with temperature controllers, blowers and data acquisition system. These unit operations were designed and fabricated. The fabrication was done at UNMC workshops. SolidWorks software was used to virtually mount all the unit operations with good maintenance accessibility yet compact. The SolidWorks simulation result was used to obtain the rig dimensions and facilitate mounting the unit operations on the rig structure. The simulated rig with fine details is shown in Figure 3-1. The fabrications of all the unit operations are discussed in subsequent sections.

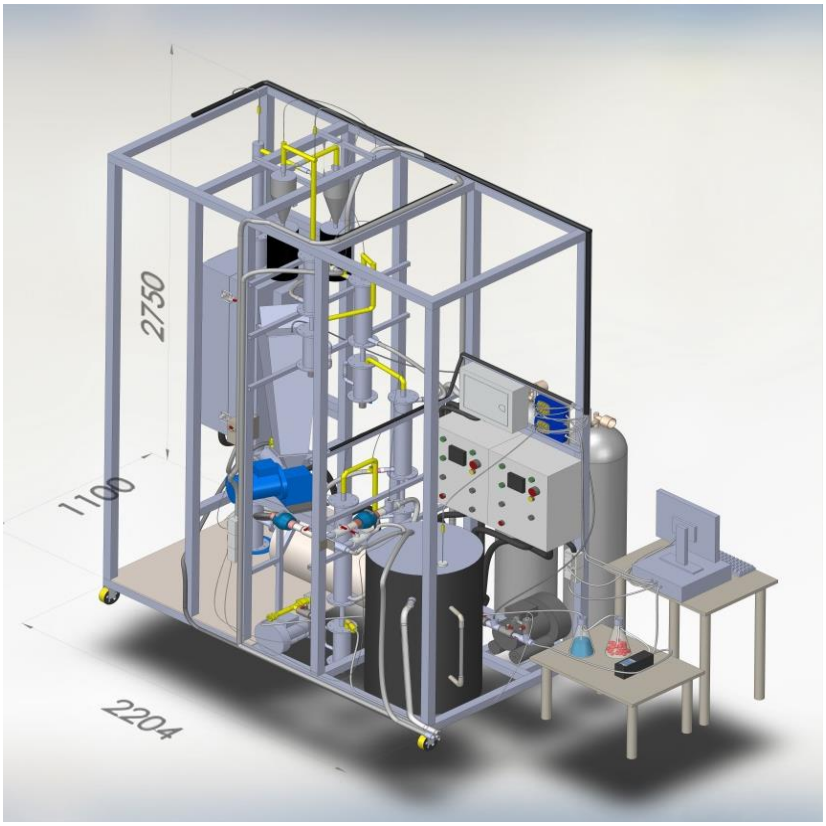

Figure 3-1: The simulated rig with fine details (Cheng Kei Vin, MEng Internship student)

3.3 Design of lab scale 2D2D type cyclone separators

Assumptions made in the design of cyclone separators for the rig of fluidized bed reactor include: the entire cyclone body and the pipe connecting them to the reactor are insulated properly, no temperature loss of the vapour coming out from the reactor and passing through the two cyclones connected in series, the cyclones are of same size, no velocity loss of the exiting vapour which enters the cyclones, the cyclones work adiabatically, particles collection efficiency of the cyclones are about 99%. Based on the above assumptions, a unique and specific type of cyclone that can handle high speed vapour coming out from the reactor is designed and from literature review 2D2D type was chosen as the best choice for this operation. A brief results and drawings of the cyclone separators of pyrolysis rig are presented next.

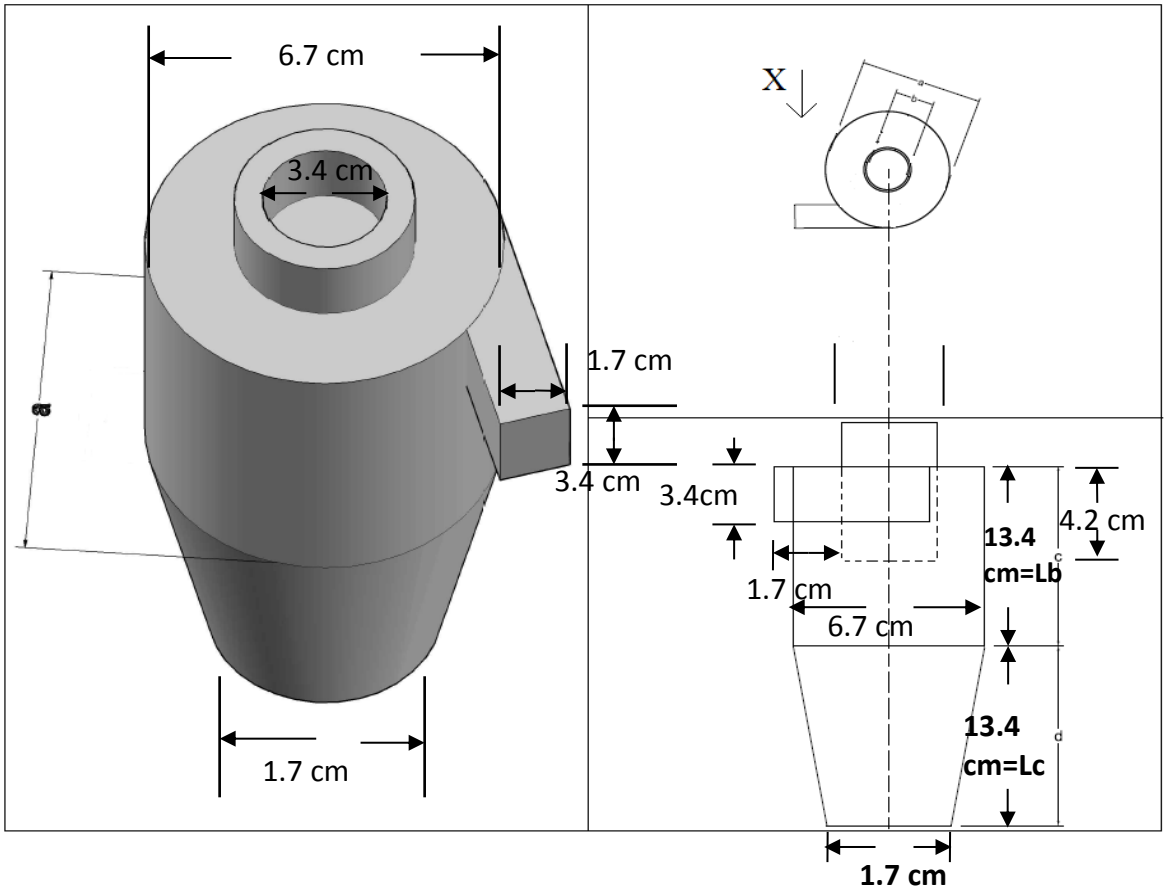

Figure 3-2: Diagram of the proposed 2D2D Cyclone separator ($L_{bc}=L_c=2D_c$)

Table 3-1: Specification of the proposed and fabricated lab scale cyclone separator

Item	**Dimensions of the Calculated cyclone**	**Dimensions of the Fabricated cyclone**	**Unit**
Cyclone body diameter, D_c	6.7	8.28	Cm
Height of inlet, H_c	3.4	4.14	Cm
Length of inlet, W_c	1.7	2.07	Cm
Diameter of vapour exit, D_e	3.4	4.14	Cm
Length of vortex finder, S	4.2	5.18	Cm
Length of body, L_b	13.4	16.56	Cm
Length of cone, L_c	13.4	18.63	Cm
Diameter of solid outlet, D_d	1.7	21.34	Cm
Cone angel, θ	10	10	degree

A 3 inch, SS304, schedule no 10 pipe with 82.80 and 88.90 mm of inner and outer diameters respectively has been selected for the fabrication of the cyclone separator. Therefore, the dimensions of the cyclone for manufacturing are different than the calculated dimensions for practical reasons. The cyclone dimensions of the proposed and manufactured units are given in Table 3-1.

The detail design of the cyclone separators is given in Appendix-C and detailed engineering diagrams of cyclone separator are given in Appendix-D.

3.4 Design of lab scale pyrolysis vapour condensers

Some vapour from fast pyrolysis reactor will be condensed in four condensers connected in series from vapour temperature of nearly 600 to 40°C at nearly atmospheric pressure to selectively condense branched hydrocarbons and alkanes, phenols, aromatics, furans, alcohols, acids, esters and amines. Each of these condensers is designed as single pass shell and tube heat exchangers with three condensing tubes of 3/8″ nominal diameter (SS304, schedule no 40) fitted in a 3″ diameter SS304 pipe of schedule no 10 as shell. The vapour condenses in tube side and the cooling water enters in the shell side.

The detail data specifications for all the four condensers are given in Table 3-2. The calculation details of pyrolysis vapour condensers are given in Appendix-E and detailed engineering drawings of condensers 1 to 4 are given in Appendix-F.

Table 3-2: Data specification of the lab scale condensers

Parameters	Condenser-1	Condenser-2	Condenser-3	Condenser-4
Hot fluid inlet temperature, ^{o}C	600	300	200	125
Hot fluid outlet temperature, ^{o}C	300	200	125	40
Cold fluid inlet temperature	75	60	45	30
Cold fluid outlet temperature	90	75	60	45

Parameters	Condenser-1	Condenser-2	Condenser-3	Condenser-4
Total heat load, Q_{Total} vapour (W)	520	207	116	253
Coolant flow rate (kg/sec)	0.008	0.003	0.0015	0.004
Condensate flow rate (kg/sec)	0.00004	0.00008	0.000009	0.00005
ΔT_{LMTD}, $^{\circ}C$	348.28	179.15	107.22	33.66
U (guess), W/m^2K	500	500	500	500
U (1^{st} iteration), W/m^2K	32.65	22.78	11.83	87.885
U (2^{nd} iteration), W/m^2K	31.66	22.13	16.30	86.49
U (converged), W/m^2K	30.13	22.12	11.57	87.66
Heat transfer area (calculated), m^2	0.047	0.052	0.06	0.087
Heat transfer area (with 20% safety factor), m^2	0.06	0.06	0.08	0.10
Tube length, mm	360	400	500	650
Tube OD, mm	17.15	17.15	17.15	17.15
Tube ID	12.53	12.53	12.53	12.53
Number of tubes, numbers	3	3	3	3
Shell ID (calculated), mm	56.16	56.16	56.47	56.66
Shell ID (with20% safety factor), mm	67.39	67.39	67.77	67.99
Shell ID (for fabrication), mm	82.8	82.8	82.8	82.8
Baffle spacing (calculated), mm	56.27	56.16	56.47	56.66
Baffle spacing (for fabrication), mm	72.14	80.01	71.37	72.14
Tube pitch, mm	triangular	triangular	triangular	triangular
pitch length, mm	21.44	21.44	21.44	21.44
Shell side pressure drop, N/m^2	7.7	0.56	0.29	1.13
Tube side pressure drop, N/m^2	$4x10^{-4}$	0.01	$2.3x10^{-4}$	$1.63x10^{-3}$

3.5 Fabrication of the pyrolysis rig structure and mounting of the unit operations

From the Solidworks simulation, the length, width and height of rig are obtained as 2.2, 1.1 and 2.7 m. The pyrolysis rig is constructed using 50 mm x 50 mm square hollow mild steel pipes with 2 mm thickness. The 6 m long square pipes were cut to sizes and welded to structure at UNMC workshops. The rig structure is sitting on four wheels and four adjustable legs located at the four corners of the rig.

All the unit operations were mounted on the structure following the simulated mounting arrangement including tubing and wiring (Figure 3-3). A 2 mm thick SS304 sheet is used to construct a platform on part of the rig floor on which the electric preheater and the vertically placed fluidized bed reactor are placed. The reactor jacket heater (split type electric heater) is mounted vertically to provide heat to the reactor.

The screw auger assembly, to feed biomass to the reactor, is mounted at elevated location (nearly a meter above the ground). The auger assembly has 5 components, a jacketed screw auger, a gearbox, a hopper, an electric motor and an inverter to control the auger speed.

Figure 3-3: Photograph of the biomass pyrolysis rig.

Two cyclone separators (connected in series) along with their particle collectors are mounted at the top of the rig. The four condensers (connected in series) are mounted at different elevations. The high and low temperature condensers are mounted at the top and at the bottom of the rig respectively, and other two condensers are placed in between. The cooling water reservoir (drum) is installed at the bottom of the rig with water flowmeters on the line coming out of it. Two blowers are placed at the bottom of the rig along with the flow meters to monitor the fluid flow rates. Thirteen thermocouples are installed to monitor reactor temperatures, cooling water inlet, outlet and reservoir temperatures. All the thermocouples are connected to 8 channel data loggers. The data loggers are mounted about one and a half meter above the ground and are connected to a computer to download and monitor the temperatures. Photograph of the pyrolysis rig is shown in Figure 3-3.

3.5.1 Fabrication of screw feeder with biomass hopper

The screw feeder with jacket is fabricated with SS304 stainless steel pipe, plate and rod at UNMC workshop. The screw is fitted in a 3 inch diameter SS304 pipe and the jacket is

Figure 3-4: Picture of the auger feeder with hopper

constructed out of a 6 inch diameter SS304 pipe. The screw is driven by an electric 2 horse power (hp) motor connected with a variable frequency inverter mounted on the rig. Picture of the auger screw feeder is shown in Figure 3-4.

3.5.2 Fabrication of fluidized bed reactor

The fluidized bed reactor is fabricated from 3 inch SS304 stainless steel pipe with schedule no 10 in the UNMC workshop. The reactor is 1.83 m long mounted vertically on the rig. Both ends of the reactor are flanged. The feed inlet port is located 8.5 cm above the distributor plate. The reactor is jacketed with a split type electrical heater. The heater is connected with a digital control panel (80 cmx22 cm x 50 cm, L x W x H) mounted on the

Figure 3-5: Picture of the vertical split jacket heater and reactor tube

rig. Two thermocouples are inserted into the reactor, one at the bed and other at the exit point of the reactor. The electrical jacket heater is installed to provide reactions heat. The jacketed heater dimension is 380 mm in width x 380 mm in depth x 1000 mm in height mounted vertically as shown in Figure 3-5.

A circular preheater is installed horizontally to preheat fluidizing gas from ambient temperature to 450°C. The pre-heater dimension is 390 mm in outer diameter and 1007 mm in length and is shown in Figure 3-6.

Figure 3-6: Picture of preheater

3.5.3 Fabrication of cyclone separators and particle collectors

Two identical 2D2D cyclone separators with solid collectors are fabricated at UNMC workshops. The cyclone separators' (body and cone) are fabricated from a 3 inch stainless steel type 304 schedule no 10 pipe. The cyclone separators' body and cone lengths are 16.56 and 18.63 cm respectively. A flange (150 mm in diameter and 5 mm thick) is welded at the end of each cyclone cone. The particle collectors are 22 cm long and 3 inch diameter fabricated from 3 inch SS304 pipe with schedule no 10. The pipes are cut to size and welded

with flanges at UNMC mechanical workshop. The flanges were fabricated using laser cutter, a total of 55 flanges are made from SS304 plate. The diameter and thickness of the flanges are 150 and 5 mm respectively (two flanges have diameter and thickness of 140 and 3 mm respectively). The particle collectors are joined with cyclone separators with nuts and bolts having gaskets in between two flanges. The cyclone separators with solid collectors are shown in Figure 3-7.

Figure 3-7: Picture of cyclone separators with solid collectors

3.5.4 Fabrication of condensers with liquid collectors

Four shell and tube condensers (single pass) of lengths 410, 450, 550 and 700 mm are fabricated at UNMC workshops. The shells of each condenser are constructed from 3 inch SS304 pipe of schedule no 10. The tubes are constructed from 3/8 inch SS304 pipe of schedule no 40 and are welded to 10 mm thick tube sheet (SS304) with a triangular pitch of 21.44 mm. Each condenser has 3 tubes. The tube length of 1st, 2nd, 3rd and the 4th condensers are 360, 400, 500 and 650 mm respectively.

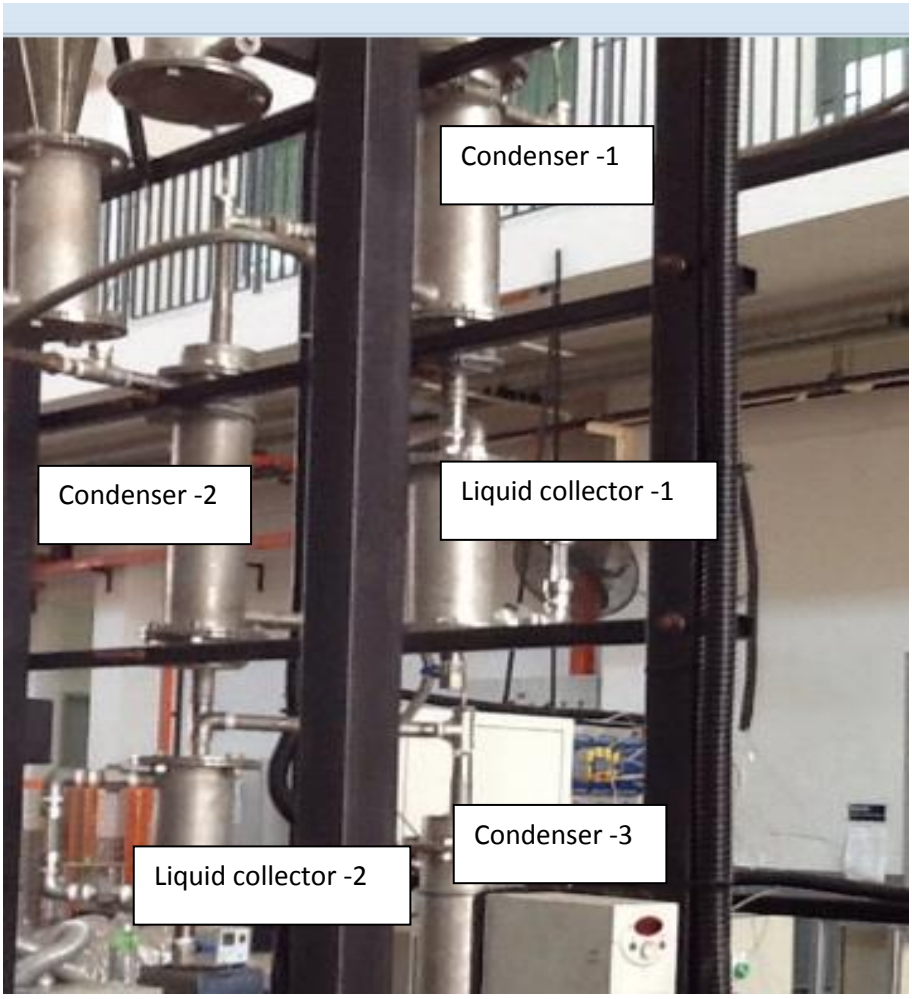

Figure 3-8: Photograph of condenser and condensate collector

The condenser's shells and tubes were cut to size from 6 meter long pipes and fabricated at UNMC workshops. The flanges with outer diameter of 150 mm and thickness of 5 mm were laser cut from SS304 metal sheet. These flanges were welded with the shells and condenser heads. The vapour is condensed in tubes and cooling water is supplied in shell side. Each of the condensers is connected to condensate collectors of 22 cm long. The condensate-collectors are fabricated from 3 inch SS304 pipe of schedule no 10. The condensate collectors are bolted at the bottom of the condensers. Each of the condensate collectors has a liquid drain valve, uncondensed vapour exit lines connected to the next condenser, a liquid level indicator (glass tube) and a thermocouple to measure the condensate temperature. Picture of condenser and condensate-collectors is shown in Figure 3-8.

3.5.5 Cooling water supply reservoir (storage drum) and control panels

A 200 litre PVC drum with a submersible pump has been installed inside the rig to supply cooling water to condensers and auger feeder jacket. The cooling water drum is connected

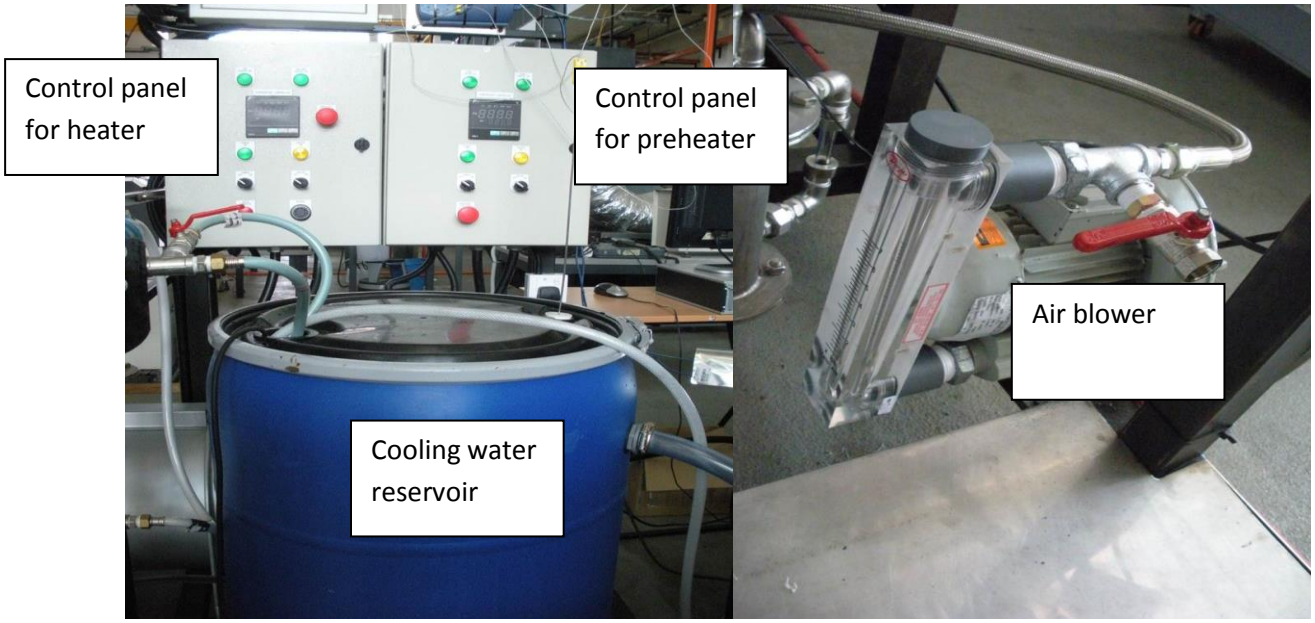

Figure 3-9: Picture of the cooling water supply reservoir, control panel for the heater and air flow meter.

to tap water supply line with 1/2 inch tube, and an overflow line of 1-1/2 inch to avoid any flooding. A thermocouple is installed to measure the supply water temperature. Control panels for the heater and preheater is clamped at the wall along the length of the rig. Air blowers are placed inside the rig. Figure 3-9 shows the picture of the cooling water reservoir, the control panels and one air blower.

3.5.6 Control panels and power supply

Control panels of electric jacket heater and pre-heater are installed inside the rig. The control panels have power switches, temperature controllers, display for instant heater temperatures and emergency shutdown switches (Figure 3-9). A dedicated control panel is installed to control the speed of auger feeder located next to the auger.

The power supply line to the rig is 415 V, 3ø, 50Hz.

3.5.7 Fluidized bed system schematic

Biomass pyrolysis to liquid bio-oil production requires several processing steps. A typical schematic diagram for the fast pyrolysis process has been developed, as part of the research activities, and shown in Figure 3-10. The process has 4 essential processing zones: Area-100, Area-200, Area-300, and Area-400. Area-100 is pyrolysis zone consists of biomass feeder, bubbling fluidized bed reactor (with internal diameter of 82.80 mm and length of 1.83 m), a preheater (3.6 kW, 240V, single phase, 50Hz, temperature rating of 1100°C) and reactor jacket heater (3.6 kW, 240V, single phase, 50Hz, maximum temperature rating of 1100°C). The jacketed heater dimension is 380 mm in width x 380 mm in depth x 1000 mm in height and the pre-heater dimension is 390 mm (outer diameter) and 1007 mm in length. The Area-100 also houses nitrogen gas cylinders to provide inert atmosphere in the reactor.

Area-200 is the solid separation zone where two cyclone separators (an abatement system for particulate control, which provides a method of removing particulate matter from particle-laden gas streams at low cost and low maintenance) with body diameter and total length (body and cone length together) of 82.8 mm and 330 mm respectively are used in series. Each of these cyclones is connected to solid particle collectors (with internal diameter

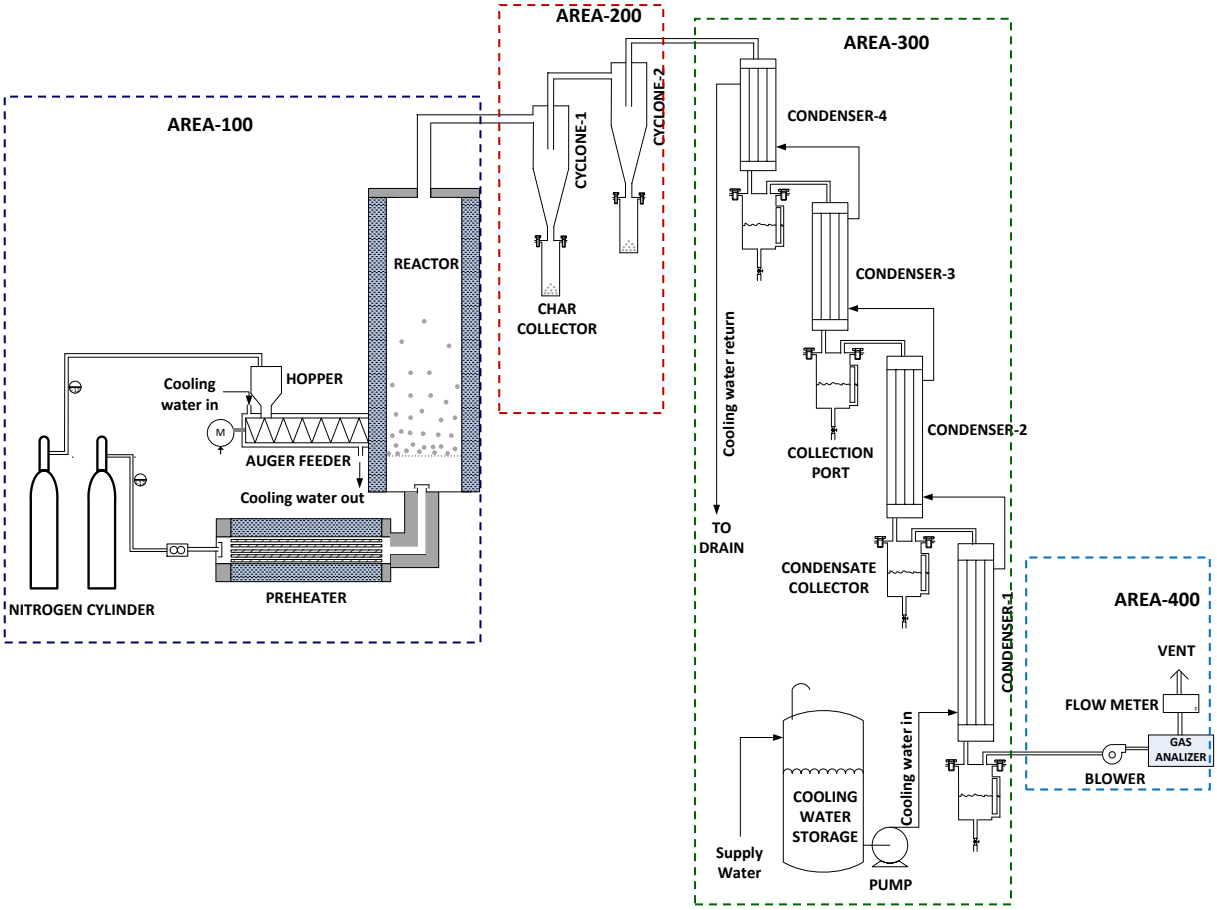

Figure 3-10: Schematic diagram of the UNMC fast pyrolysis process with a bubbling fluidized bed reactor and downstream unit operations.

of 82.80 mm and length of 220 mm). The pyrolysis vapour, from Area-100, may contain particulate matters particularly char, ash and fine sand particles. The particle-laden vapour from fluidized bed is passed through these two cyclones in series to trap the particles as much as possible (up to the smallest particles of 10 μ, Shepherd and Lapple, 1939). The

design efficiency of each of these cyclones is 99% which means theoretically almost all of the particles will be trapped.

In Area-300, pyrolysis vapour is condensed in four condensers connected in series (the internal diameter of each of the condenser shell is 82.80 mm and lengths are 410, 450, 550 and 700 mm respectively). Each of these condensers is connected to liquid collectors with internal diameter and length of 82.80 and 220 mm respectively. The vapour from the fluidized bed reactor contains a mixture of complex molecules that stems from the fast pyrolysis of biomass are rapidly condensed in the condensers to bio-oil. The cooling process effectively minimizes secondary reactions of the vapour products to either non-condensable gases or chars both of which are undesired and reduce the liquid yield. The vapour is selectively condensed in 4 condensers depending on the dew points of the molecules. The condensates (bio-oil fractions) from each condenser will be collected and upgraded with selective catalysts and upgrading conditions.

In Area-400, the non-condensable gases containing N_2, H_2, CO_2, CO, CH_4, C_2H_4, and C_2H_6 (Bridgwater, 2000) is scrubbed to remove greasy and fine particulate matters and water soluble matters, the gas is then dried and analysed by online gas analyser (Drager X-am 5000). A sample from the collected gas in the headspace was then injected into the GC using a 1-mL gas tight syringe injection (SGE Analytical Science Syringe Perfection, Australia). The GC was equipped with a stainless steel column (Porapak R 80/100) and a thermal conductivity detector (TCD) to analyze the CO_2 content of the injected gas. The carrier gas for CO_2 was helium, and the temperatures of the GC were set at 60 °C for the oven, 80 °C for the injector and 200 °C for the TCD.

3.5.8 Fabrication of bio-oil upgrading rig

Bio-oils derived from cellulosic biomass offer the prospect of becoming a major feedstock for production of fuels and chemicals, and lignin is a plentiful, underutilized component of

cellulosic biomass. A central goal of the upgrading is to convert the oxygen-rich, high-molecular-weight lignin into hydrocarbons that are compatible with today's petroleum-derived fuels. Thus, a potentially valuable processing goal is to convert lignin to bio-oils and to subject the bio-oils to hydro deoxygenation (HDO) to remove oxygen primarily in the form of water (Saidi, et al., 2014). Another upgrading technique is cracking by removing oxygen in the form of CO_2. The upgrading rig upgrades the oxygen-rich bio-oil in both ways. The structure of the bench scale bio-oil upgrading rig is fabricated at UNMC workshop from 1 inch square mild steel pipe of thickness 2 mm. The dimension of the rig is 60 cm H x 60

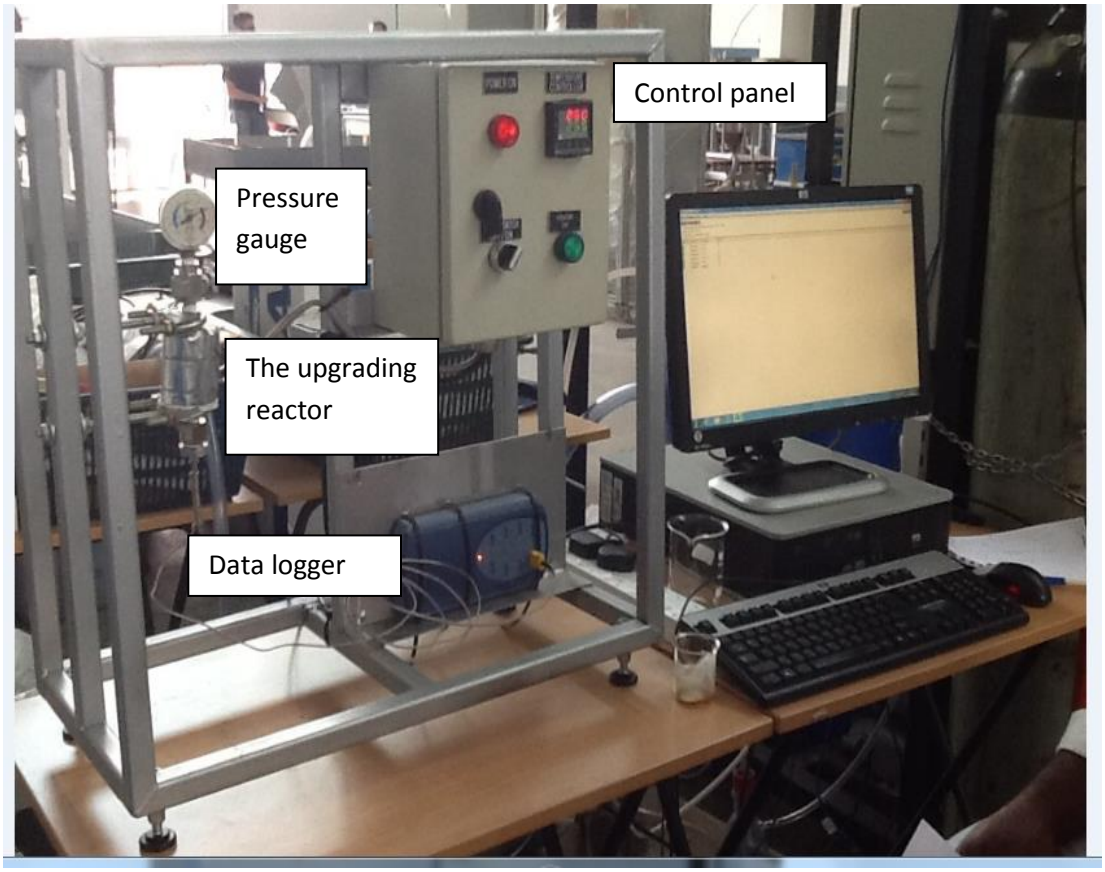

Figure 3-11: Photograph of the bench scale bio-oil upgrading rig

cm W x 30 cm D. The rig houses a batch bio-oil upgrading reactor, a control panel and a data logger. The upgrading reactor volume is 50 ml, heater capacity is 200 to 300°C and

heating rate is 40°C/min. The photograph of the bio-oil upgrading rig is shown in Figure 3-11. The upgrading of bio-oil produced from the pyrolyzer is recommended as future work.

3.6 Conclusion

All the components of the FBR were designed according to the standards. The materials for construction of the units were chosen according to their use and were outsourced from local suppliers/sellers. Then the components were fabricated and assembled at UNMC workshops. The pyrolysis rig fabrication and assemble works were done using the Solidworks FEA structural simulation. The rig stands on wheels at its four corners. The rig also got four adjustable legs at the four corners. The fabricated units are mounted in the pyrolysis rig which is placed in the Engineering Bay in The Engineering Research Building in UNMC. Electrical connections to the rig and water supply have been established. Hydraulic tests have been done for the pyrolysis process. Some modifications in the biomass feeding systems are done to produce bio-oil, bio-char and syngas and the details are being provided in Chapter 4.

CHAPTER 4: COMMISSIONING OF THE FEEDER SYSTEM

4.1 Overview:

The rig was designed to process biomass at a rate of 1kg/hr to produce bio-oil, bio-char and syngas by continuous fast pyrolysis. After completing the design a prototype was built and tested for process optimisation. Some modifications to the initial design of some components were required to solve some minor issues during the initial operation of the reactor. In this chapter some details about these modifications will be discussed.

4.2 Biomass feeding system

Since this is an experimental reactor it is suggested that the feeding system should be modified to allow for continuous operation as well as batch operation. The modification may be on biomass feeder, biomass feeding hoper, biomass supply to auger from feeder, auger design, distributor positioning and biomass charging. Each of the modification was introduced to supply biomass to achieve the target of bio-oil, bio-char and syngas production.

4.2.1 Original design- 1kg/hr continuous fast pyrolysis process: The rig was designed to operate as a continuous process having the capacity of 1kg/hr dry biomass pyrolysis. Initially the biomass was tried to be delivered from a hopper into the reactor with the help of a screw-auger. To avoid the biomass to get stuck inside the feeder, the operational modifications are explained below.

4.2.2 Screw feeder with water jacket: Biomass was fed into the hopper just on top of the screw which was then allowed to be delivered by the auger screw powered by a motor. The screw was kept inside a jacketed feeder where water line was connected to avoid decomposition of biomass before it reaches the reactor. The auger was supposed to

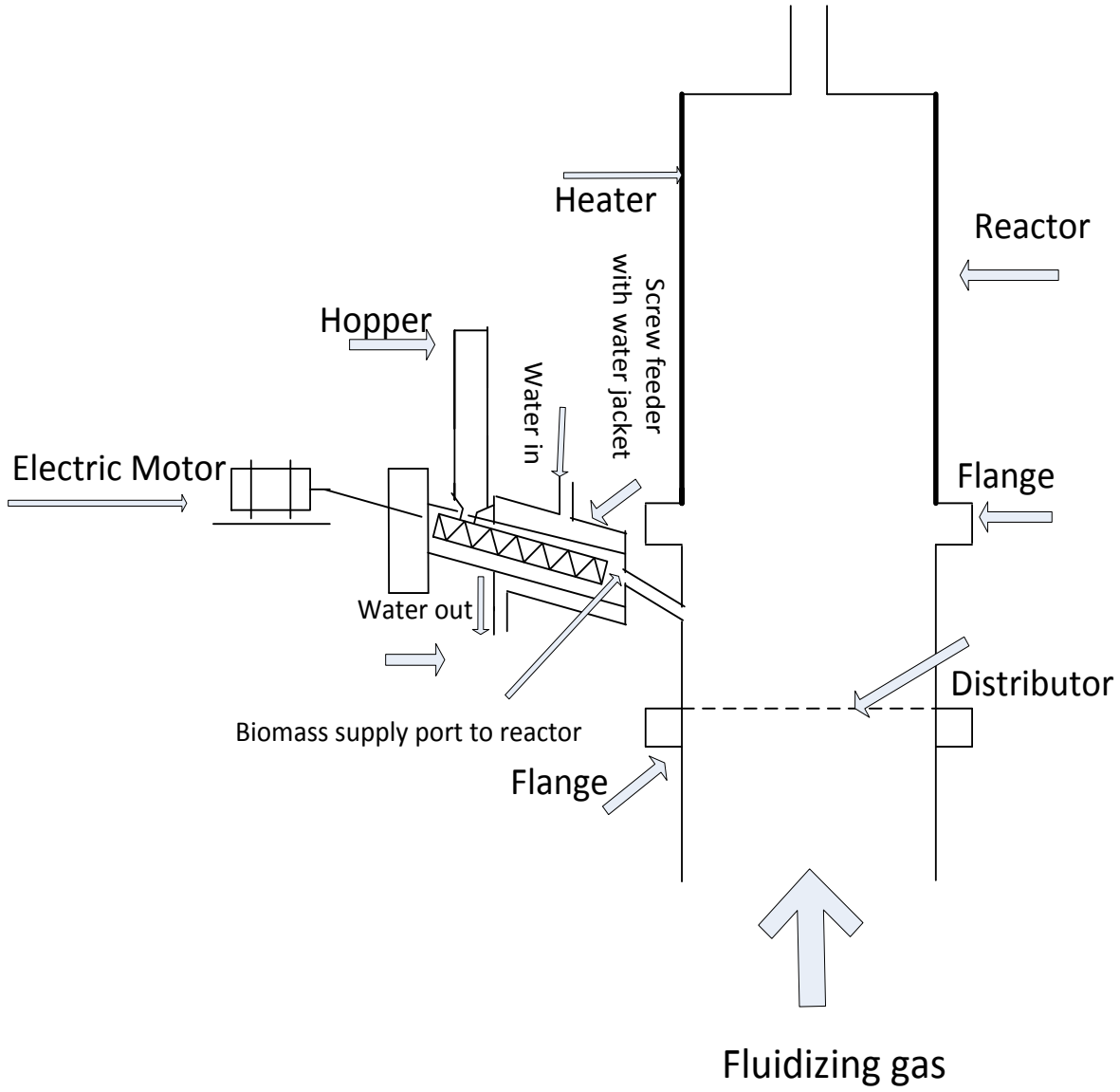

Figure 4-1: Biomass delivery by screw feeder with water jacket

deliver biomass to the reactor through the exit point of the feeder and the pipe connecting the feeder and the reactor. It is shown in Figure 4-1. After a trial operation of the system, the feeder was inspected and for the smooth supply of biomass, a minor change was made in the feeder which is described next.

(i) Screw feeder with water jacket and extension of the feeder: A rearrangement made in the feeder i.e. a hole was made under the feeder just after the intake point of biomass and nitrogen was introduced to push the biomass towards the reactor and one extension more wider than the previous one was connected just after the jacketed feeder for the smooth supply of biomass (Figure 4-2). To prevent the layer of biomass to be formed above the screw, one push system operated by nitrogen supply working in synchronization with the auger rotation was introduced which is described next.

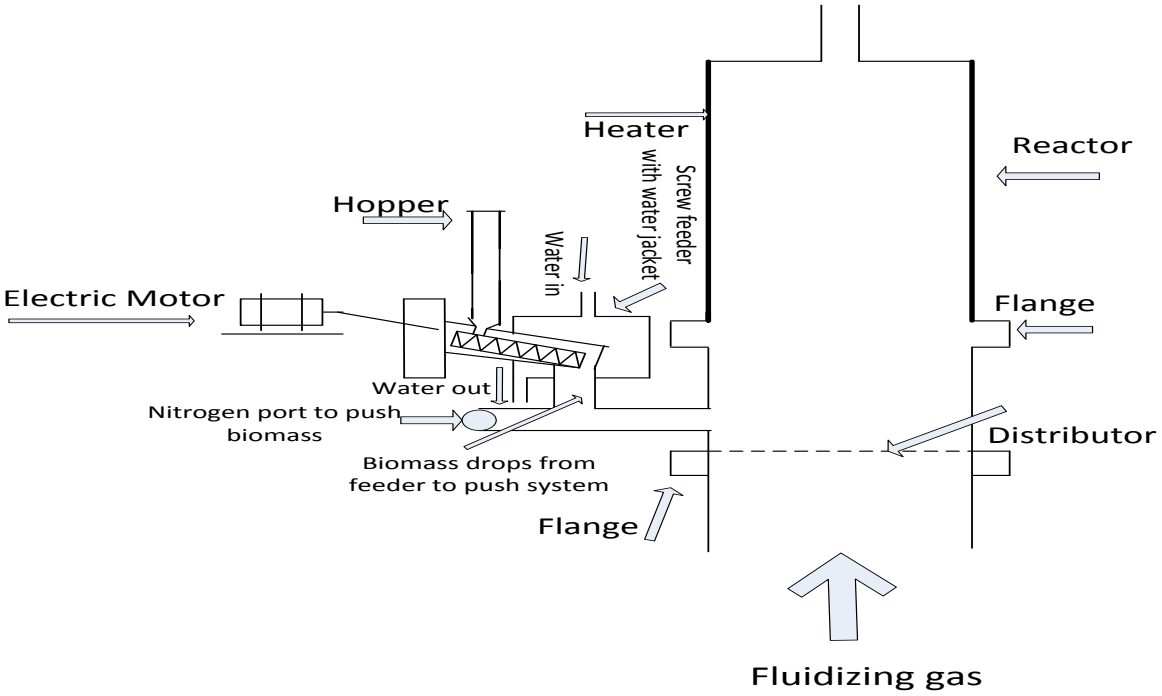

Figure 4-2: Biomass delivery by screw feeder with water jacket and feeder extension

(ii) Screw feeder with water jacket and the push system: A push system was introduced to push the biomass which falls from the hole made under the feeder. The auger delivered the biomass and the push system made the biomass to go further to reach the reactor. The idea was like that the auger should deliver the biomass in one rotation and stops while the push system push the biomass inside the reactor and the process repeats (Figure 4-3). After a trial of this system, further modification was needed to prevent the

accumulation of biomass inside the piston area when it returned back after the delivery. The new screw feeder and hopper system was introduced as the modification which is described next.

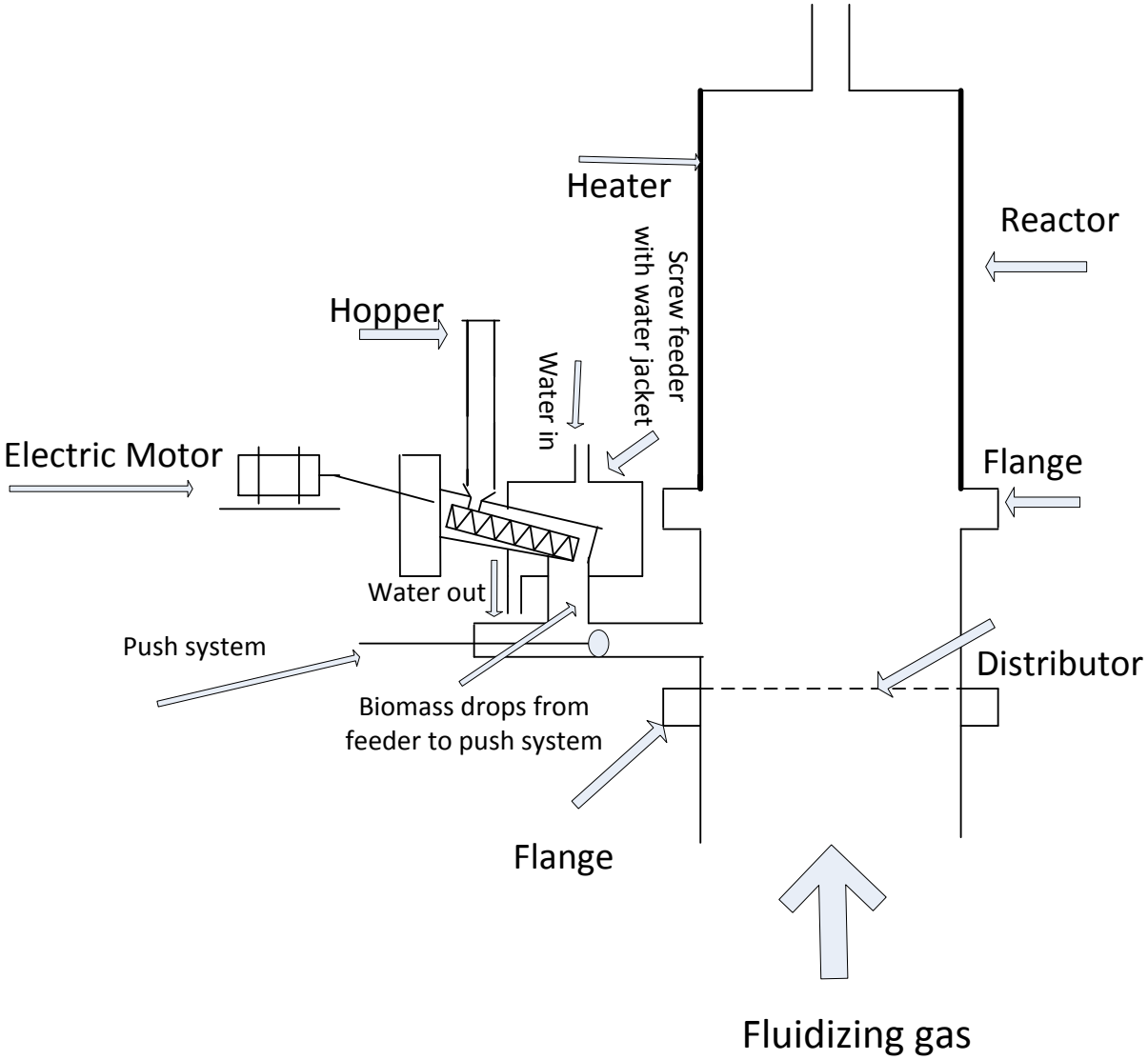

Figure 4-3: Biomass delivery by screw feeder with water jacket and push system

(iii) New screw feeder and hopper: A new screw and hopper was introduced as a modification to deliver biomass. The hopper was redesigned and one screw was hanged inside a pipe with flange at the front end and bearing at the back end of the pipe. The pipe

was then welded at the bottom of the hopper and biomass receiving part of the reactor. While welding the pipe with the hopper and reactor part, a slope was maintained to deliver the biomass which was delivered by the screw powered by a motor. The hopper was filled with biomass and a stirrer was fit to prevent the biomass from clogged (Figure 4-4). Instead of charging biomass directly to the screw, so as a modification, a platform was introduced inside the hopper on which the biomass was charged and it is described next.

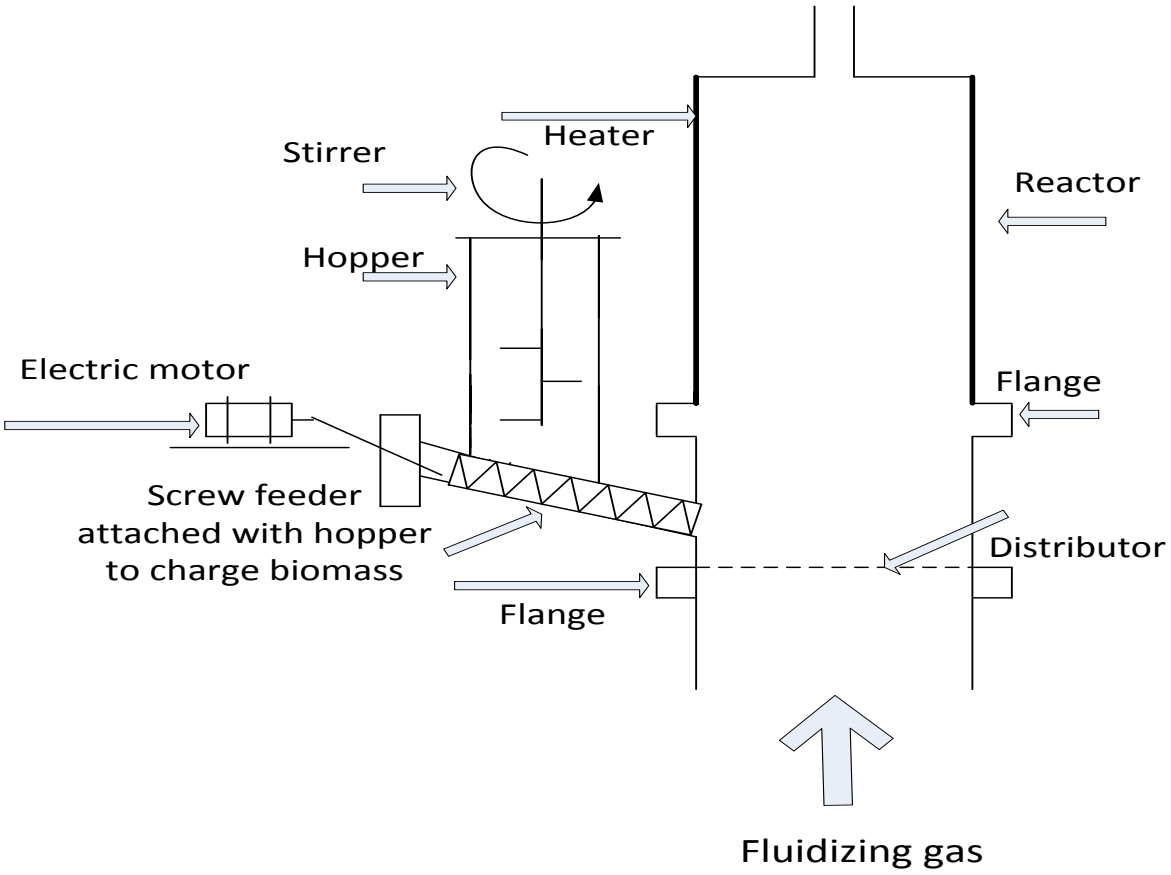

Figure 4-4: Biomass delivery by screw feeder and stirrer system.

(iv) A platform inside the hopper to control biomass charging: An inclined platform was fit inside the hopper on which the biomass was charged and a stirrer was fixed through the top of the hopper to the middle of the platform to send biomass slowly on the screw to

control the flow of biomass to prevent biomass from stuck. This arrangement delivered the biomass as expected (Figure 4-5). To prevent the pipe welded to the hopper and the reactor part from getting overheated, the batch systems were used to produce bio-oil which is described in next two sections.

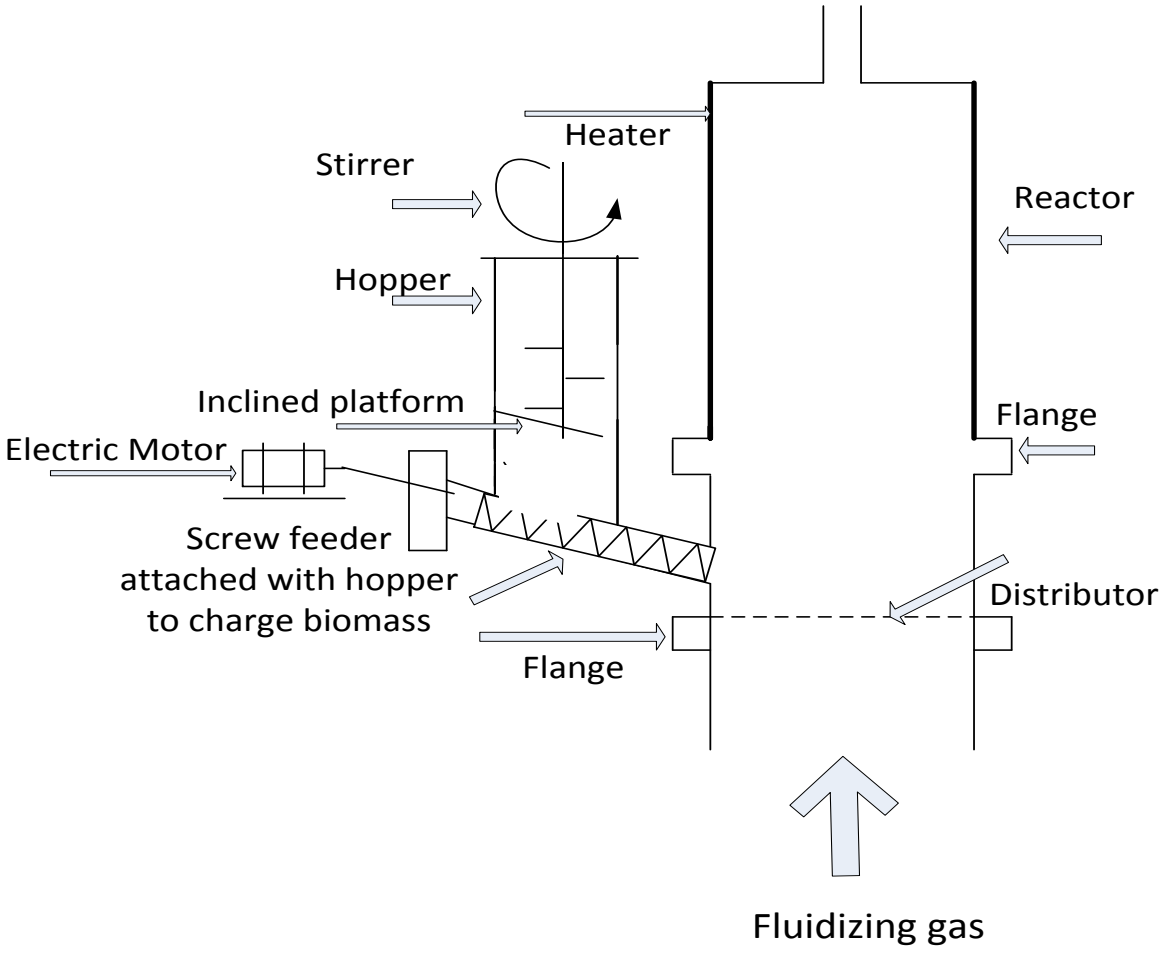

Figure 4-5: Biomass charged on inclined platform and delivered by screw feeder and stirrer system.

(v) The batch process when biomass was supplied through a lateral port:

Biomass was charged on the distributor at a time through a lateral port and fluidizing gas was supplied through preheater to fluidize the biomass (Figure 4-6). The heater was turned

on and the condensers were kept cool by supplying water. The temperatures of the heater, cyclones and condensers were monitored online. To make sure that the biomass gets enough heat for vaporisation, modification was done on the distributor position and biomass charging. The distributor was elevated near to the heating zone of the reactor and biomass was charged through the top of the reactor which is described next.

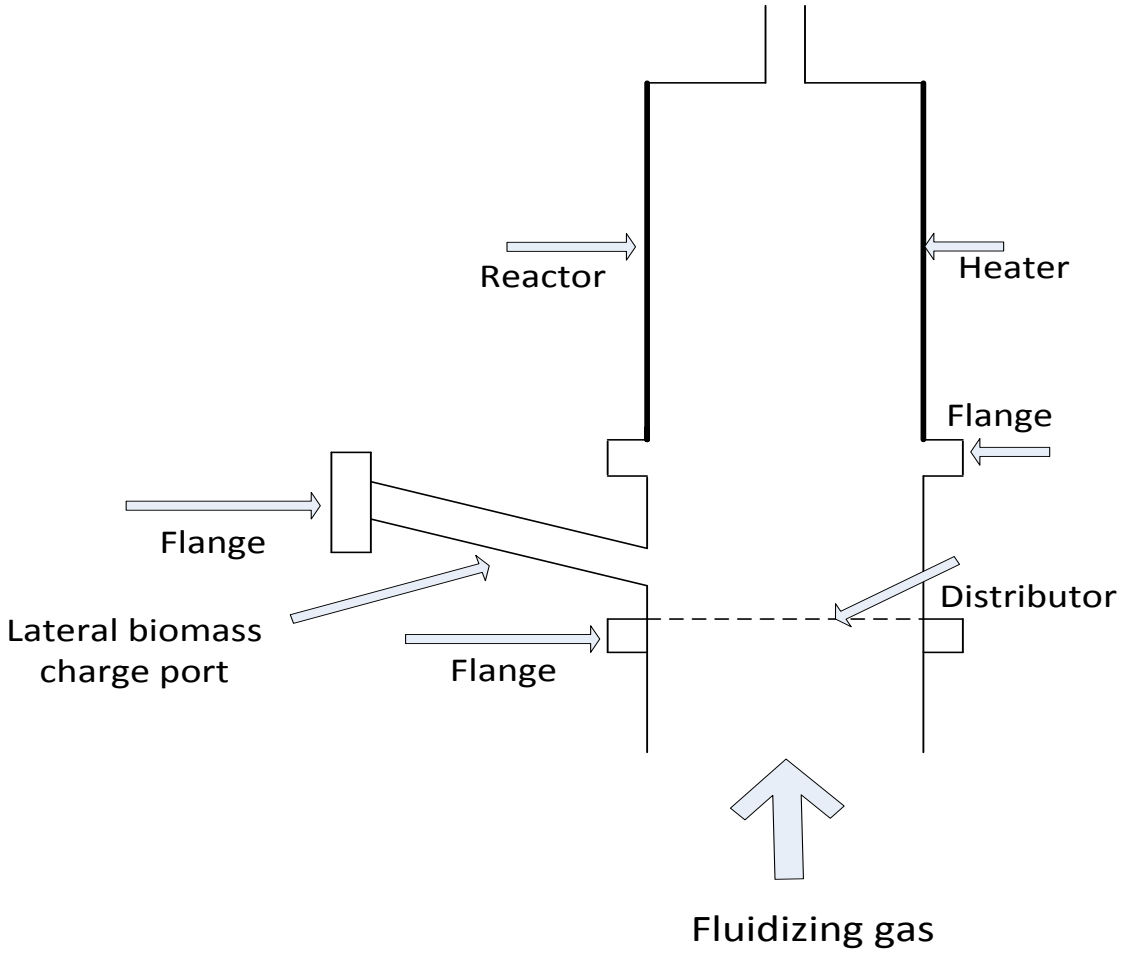

Figure 4-6: Batch process when biomass was charged through a lateral port.

(vi) The batch process when biomass was charged from the top of the reactor:

Biomass was charged at one time on the distributor from the top of the reactor (Figure 4-7) and the fluidizing nitrogen gas was supplied through a preheater which fluidized the

biomass entering the reactor under the distributor. The temperatures of the reactor, two cyclones, and four condensers were monitored online. The water supply was kept running from the beginning of the experiment. The pyrolysis reaction occurred and the vapour started coming out from the reactor which was cleaned in the cyclones and condensed into bio-oil in the condensers and was deposited in the collectors. The non-condensable vapour was allowed to go through a water scrubber first and then through silica gel to absorb the non-condensable as much as possible. After the silica gel absorbent, the exit gas was

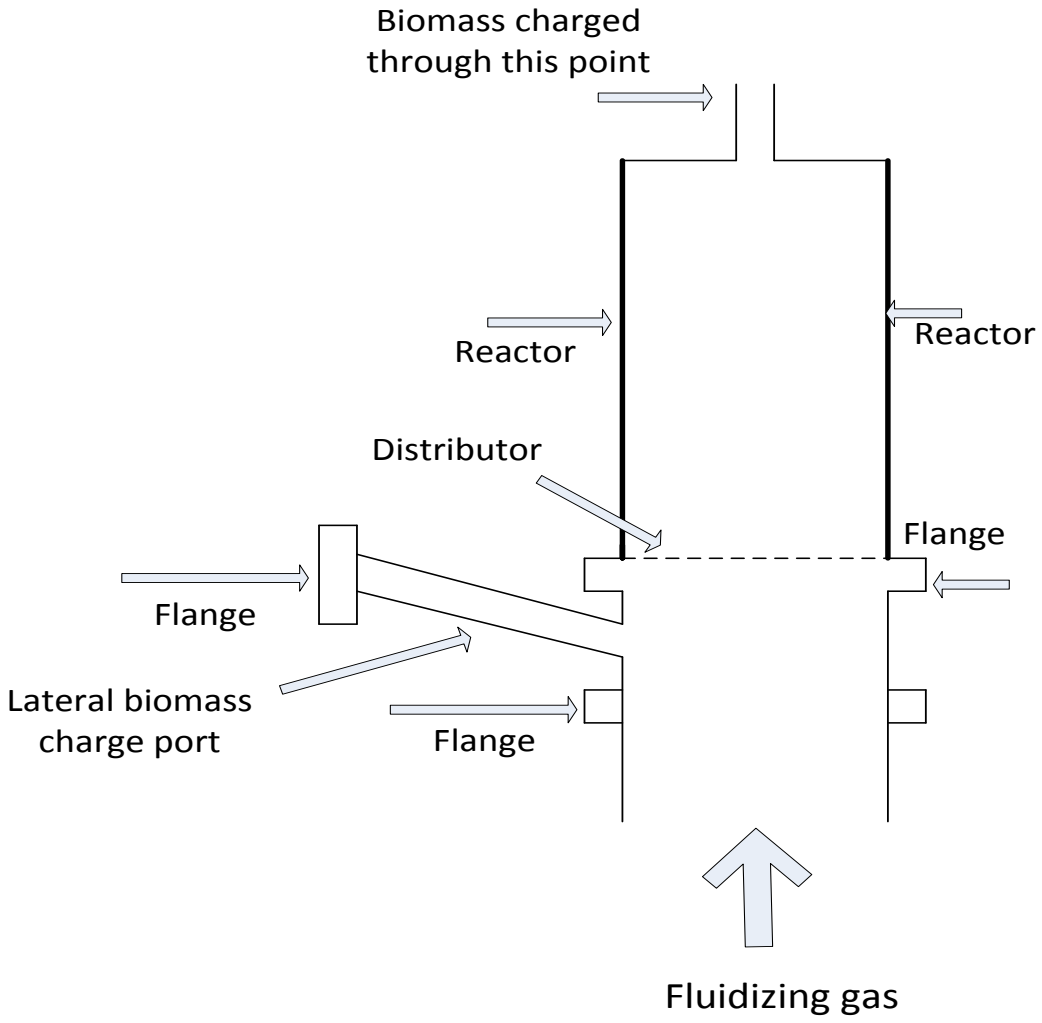

Figure 4-7: Batch process when biomass was charged from the top of the reactor.

allowed to pass through water scrubber again before it was released to the environment. The syngas was analysed with Drager X-am 5000 analyser and the rig was shut down when there was no vapour seen coming out from the exit (no bubble in the water scrubber). The bio-oil was collected from the collectors and was stored for characterization and bio-char was collected from the top of the distributor when the reactor was cooled down to room temperature.

4.3 Recycling the pyrolysis vapour, mass and energy balance and COP of the FBR

The pyrolysis vapour was not recycled for the first few batches rather it was allowed to pass through the multiple scrubbers to be released in the environment which showed low yield of bio-oil (4.92 to 5.06%). But when it was recycled, the yield was higher (20.46 to 21.58%) than before (Table 4-1).

Table 4-1: Mass balance of batch process for bio-oil production

Batch #	Weight of biomass (gm)	Weight of Oil (gm)	Weight of char (gm)	% oil	%char	%NGC (by difference)
1.	534.57	27.07	135.86	5.06	25.41	69.52
2.	557.59	27.44	168.23	4.92	30.17	64.91
3*.	446.93	91.46	60.19	20.46	13.47	66.07
4.*	439.70	94.90	72.73	21.58	16.54	61.87

*the pyrolytic vapour was recycled in batch 3 & 4.

The amount of char reduced in the batches when pyrolytic vapour was recycled, it is because some char was might be driven away by the recycling vapour. The liquid yield is lowered compared to literature (Bridgwater and Gyftopoulou 2013), however it is comparable to others (Imam and Capareda 2012) from lignocellulosic biomass.

Energy balance of the reactor:

For energy computation, energy streams in and out of the pyrolysis system are considered in the control volume illustrated in Figure 4-8. Energy inputs considered are the electrical energy for the reactor and the energy of the biomass. Energy outputs are the energy in the bio-oil, the biochar and the non-condensable gas (NCG). As Figure 4-8 indicates the system boundary is defined at ambient conditions. This eliminates heat transfer as an energy contributor. Other energy sources and outputs are small and considered negligible. These include the energy of ash produced, the energy given up by cooling water in the condensers, the input energy of the nitrogen used as a fluidizing medium and the energy of the water produced.

All material streams are evaluated by their heat of combustion or higher heating value (HHV). Hence, the energy per unit mass is simply assigned the HHV, i.e.,

$$E = HHV \qquad (4.1)$$

From here, efficiency of the system or coefficient of performance (COP) is define as

Energy efficiency= (Energy output)/(Energy input)x100% (4.2)

Both energy input and output were evaluated using appropriate heating values. These represent the energy content for the starting materials and products.

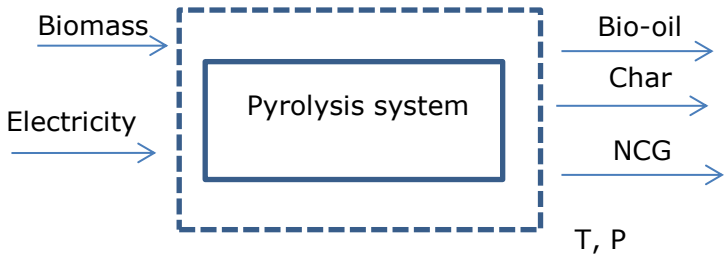

Figure 4-8: Energy flows for the system

Energy analysis results are illustrated in Tables 4-2. As discussed earlier, material energy inputs are evaluated using HHV. Biomass and the reactor electrical energy are inputs and bio-oil (dry), biochar (dry), and NCG are energy outputs. Table 4-2 gives quantitative results for input, output and efficiency. Energy balance is calculated on 0.5 hour operation basis and values are in energy rate (MJ/hr).

Table 4-2: Energy input and output and efficiency of the reactor

Batch #	Energy input (MJ/hr)		Energy output (MJ/hr)		Efficiency (%)
1	Biomass	9.28	Bio-oil	0.81	31.98
	Reactor	6.48	Char	3.87	
	Total	15.76	NCG	0.37	
			Total	5.04	
2	Biomass	9.68	Bio-oil	0.82	36.94
	Reactor	6.48	Char	4.79	
	Total	16.16	NCG	0.36	
			Total	5.97	
3*	Biomass	7.76	Bio-oil	2.74	33.36
	Reactor	6.48	Char	1.71	
	Total	14.24	NCG	0.30	
			Total	4.75	
4*	Biomass	7.63	Bio-oil	2.85	36.78
	Reactor	6.48	Char	2.07	
	Total	14.11	NCG	0.27	
			Total	5.19	

*the pyrolytic vapour was recycled in batch 3 & 4.

The contribution in energy output increased by bio-oil in the recycled batches as bio-oil production increased. But again, the contribution from char in energy output decreased as amount of char dropped as mentioned earlier. So, the overall efficiency did not increase for the recycled batches. The bio-oil yield and energy efficiency of the designed fluidized bed system is low compared to the literature (Boateng et al., 2012) may due to the yield of liquid bio-oil.

Coefficient of performance (COP) of the FBR: The COP of the reactor is calculated by the following expression (Wikipedia, 2016):

Coefficient of performance (COP) = Total cooling demand/Total energy consumption….(4.2).

The total cooling demand is from the four condensers and the total consumption from pump and heater. The COP calculated for the FBR is found to be around 1.0 which is low compared to the literature value (Fei et al., 2011) may be due to assumptions made in the calculation that there will be no heat loss.

4.4 Temperature profile of the fluidized bed reactor operation

The temperature profiles of the designed fluidized bed reactor are shown through Figures 4-9 to 4-10. The temperature profiles for the batch process are shown. Two Picolog Technology TC-08 data loggers each of eight channels are used to record the temperatures online of the whole system through thirteen thermocouples (eight thermocouples connected to one data logger and five to other). Picolog AZ810/278 refers channel-1 to Channel-8 and Picolog AZ810/232 refers to channel 9 to channel 13 (AZ810/232 channel -1 shows temperature recorded by thermocouple no. 9). Channel-1 shows the vapour exit temperature from the reactor of the system. Channel-2 shows the coolant exit temperature from the condenser-2. Channel-3 shows the vapour inlet temperature in condenser-2. Channel-4 shows the vapour exit temperature from cyclone-2. Channel-5 shows the coolant

exit temperature in condenser-3. Channel-6 shows the vapour inlet temperature in condenser-3. Channel-7 shows the vapour inlet temperature in condenser-4. Channel-8 shows the coolant inlet temperature in condenser-4. Channel-9 shows the coolant exit temperature in condenser-1. Channel-10 shows the coolant inlet temperature in condenser-3. Channel-11 shows the vapour inlet temperature in condenser-1. Channel-12 shows the water reservoir temperature and Channel-13 shows the coolant inlet temperature to reservoir.

4.5 The features of the new designed fluidized bed reactor

The designed prototype of the fluidized bed reactor is suitable enough to be operated as batch process to produce bio-oil, bio-char and syngas. The continuous operation of the system to produce bio-oil is recommended as future work where it can be operated for the desired product and product quality by adjusting the operation temperature. The temperature variation can give bio-oil or bio-char as well as syngas as the desired product. For example, reaction temperature less than 425°C favours the char formation while syngas production is increased for reaction temperature above 600°C and bio-oil production yield is maximized temperature around 550°C. The reaction temperature can be controlled easily to produce the targeted product by both batch and continuous operation of the system. The designed system will be able to handle different types and sizes of feedstock material at different flow rates. The pyrolysis was carried out successfully with the designed system for batch process using UTS to produce bio-oil, bio-char and syngas. The rig is designed environmentally friendly (low emissions as the rig has provision of scrubbing exhaust gas) with emission sensors to detect hazardous gases. The improvement of the designed system has been done.

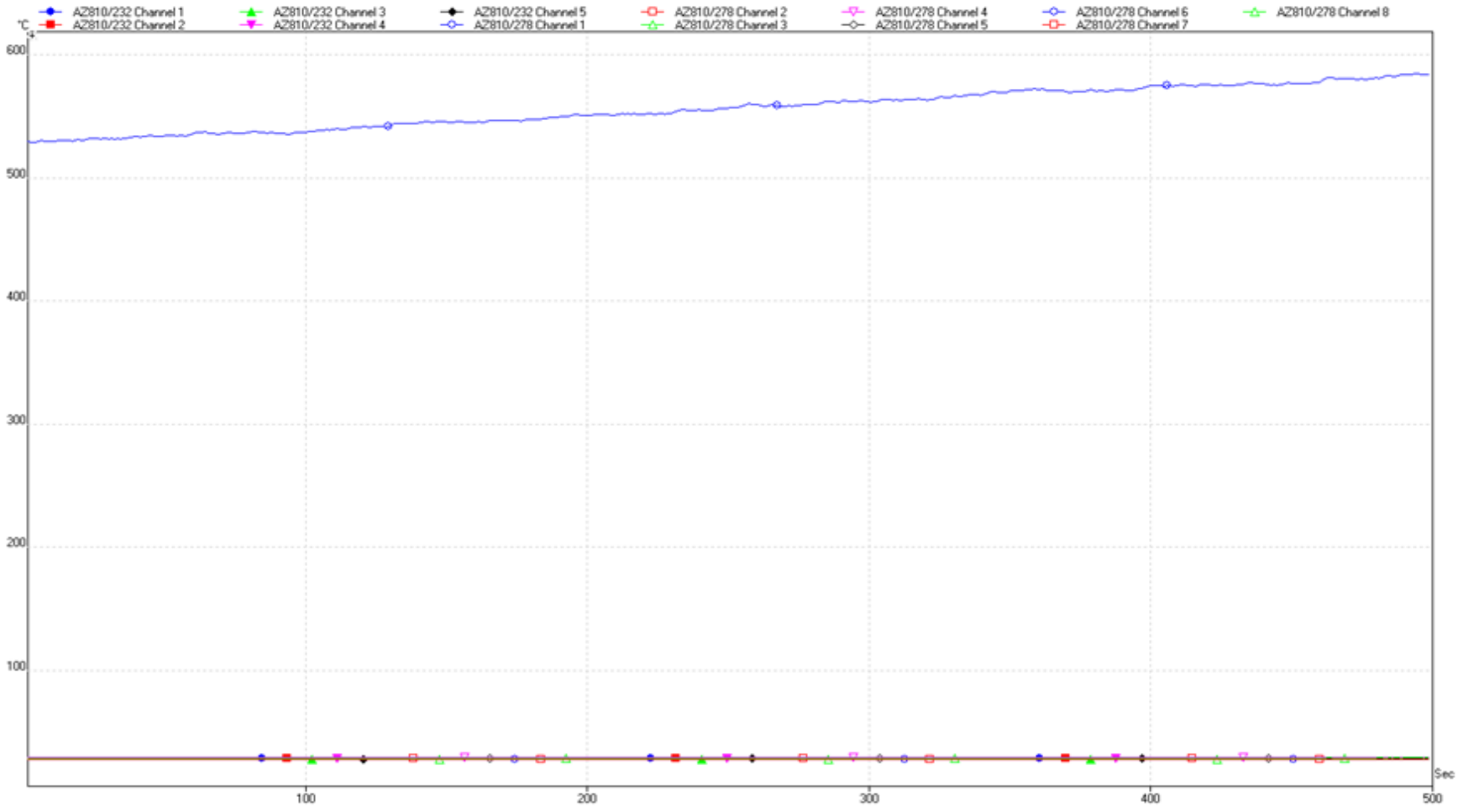

Figure 4-9: Temperature profile of the fluidized bed reactor (Run-1: Batch Process)

Figure 4-10: Temperature profile of the fluidized bed reactor (Run-2: Batch Process).

4.6 Conclusion

Some minor modification was done on the original design of the rig having capacity of 1kg/hr dry biomass supply and bio-oil was produced. The batch process produced bio-oil, char and non-condensable and bio-oil was collected from the collectors attached to the condenser and the char was collected from the top of the distributor which is a new design for char collection. The non-condensable gas was led to the environment after passing through a water scrubber followed by silica gel and was analysed by Drager X-am 5000. Also initial mass balances have been calculated based on this system, yielding useful parameters for future economic and design studies. The energy efficiency of the system was done on the basis of the ratio of products' HHV to raw material and electrical energy input and was found lowered compared to literature may be due to low liquid yield. The COP of the reactor was also found lowered compared to the literature value.

CHAPTER 5: EFFECT OF PRE-TREATMENT ON BIOMASS PYROLYSIS

5.1 Introduction

Optimum operation of the designed pyrolyzer needs the characterization and pre-treatment of biomass with the best operating conditions and optimum nitrogen flowrate and temperature. Biomass usually undergoes pre-treatment when it is used as energy sources (Nor Aishah et al., 2012; Yoo, 2012 and Kumar et al., 2009). This chapter describes (i) the effect of thermal and aqueous pre-treatment with varying liquid-solid ratios, solvent concentrations, reaction times and temperatures on solid extraction from biomass samples, (ii) the effect of solvent concentrations on ash extraction from biomass samples, (iii) the effect of thermal and aqueous pre-treatment on ash content and calorific value of biomass, (iv) the effect of nitrogen gas flow-rates and temperatures on products yield from biomass pyrolysis and (v) results of treated and untreated UTS and Napier Grass pyrolysis and bio-oil characterization.

Four types of biomass namely EFB (cellulose 38.1-42%, hemicellulose 16.8–18.9%, lignin 10.5–14.7%), UTS (cellulose 38-50%, hemicellulose 23-32%, lignin 15-25%), SDS (cellulose 44.75-50%, hemicellulose 16.73-20%, lignin 20-30.72%), SDB (cellulose 45-56%, hemicellulose 10-25%, lignin 18-30%) (Nor Aishah et al., 2012; Forest Bioenergy, 2015; Gu et al., 2013 and Biocyclopedia, 2015) collected from Semenyih area in Selangor, Malaysia, were pre-treated with aqueous acidic (H_2SO_4) and alkaline (NaOH) solutions and UTS was used for producing bio-oil by both tubular furnace and the designed reactor for batch operation as it resulted maximum extraction. The maximum bio-oil yield of 29.5% and 33.3% at nitrogen flow-rate of 30 ml/min and furnace temperature of 600°C and bio-char yield of 33.5 % and 45.5 % for 40 ml/min and 450°C respectively were obtained in tubular furnace. Maximum bio-oil yield of 39.43% and 27.67% and maximum char yield of 38.07% and 30.73% were obtained for raw and pre-treated UTS respectively and maximum

bio-oil yield of 40.13% and 31.53% and maximum char yield of 30.5% and 25.0% were obtained for raw and pre-treated NG respectively at 30 ml/min and 600 °C.

5.2 Background

The physical preparation of the biomass (drying, comminution and screening) and the chemical modification (removal of components) cover pre-treatment. Pre-treatment is defined as the chemical process carried out prior to pyrolysis to modify the biomass lignocellulosic polymers. The components (hemicellulose, ash) from biomass matrix can be removed by pre-treatment. Washing or leaching is engaged in the removal of components prior to pyrolysis has several applications and benefits. Firstly, the number and diversity of biomass chemical pre-cursors entering the reactor is reduced by reducing the number of biomass components and hence the number of chemical products contained in the pyrolysis liquid will be reduced. The removal of one or more biomass components will result in a reduction in total yield. For example, by removing hemicellulose component (approximately 20% of the biomass) of a biomass feedstock would result in 20% less material being fed into the pyrolysis reactor, hence 20% lower yield. However, by removing the hemicellulose component the yield of levoglucasan may be increased by 2 mf wt. % (dry feedstock basis) to 20 mf wt. % (dry feedstock basis) or 16 mf wt. % (dry original starting material basis). Thus the yield of a potentially valuable chemical (levoglucasan) has increased even though the amount of biomass being fed into the reactor has decreased (by removing the hemicellulose). The improved chemical yield from pre-treated feedstock resulted in extraction and purification thus cheaper.

Secondly, the removal of ash will influence the pyrolysis reaction pathways and hence the yields of chemicals because it is known than certain fast pyrolysis pathways are catalysed by the ash component. The ash tends to be incorporated into the char during fast pyrolysis;

also, in the pyrolysis liquid, usually a small amount of char is present. If the pyrolysis liquid is used in a fuel application, fouling and corrosion problems could be caused by the alkali metals contained in the liquid (incorporated into the char).

Thirdly, the odour problems associated with pyrolysis liquid is believed to be due to the presence of certain chemicals from the hemicellulos component (e.g. acetic acid and furfural derived products); hence removal of the hemicellulose component may help to reduce this problem.

The type of pre-treatment to be used depends on the application intended for the product. Low ash content or improved liquid properties can be achieved by reducing downstream problems by pre-treatment when fuel is the primary product. Pre-treatment will be used to either influence the pyrolysis reaction to produce a chemical normally contained in the pyrolysis liquid or to increase the yields of a selected chemical or groups of chemicals in the pyrolysis liquid when the production of chemicals is targeted. Pre-treatment forms an integral part of the process and cannot be avoided for the former case. However, in the latter case, type of pre-treatment to be used depends upon whether it is better to produce a low concentration of a particular chemical in large quantities of pyrolysis liquid or a higher concentration of the chemical contained in a smaller amount of pyrolysis liquid (Hague, 1998).

Biomass pyrolysis often requires some levels of pre-treatments and conditioning to reduce particle sizes, and to control moisture and minerals contents. Desirable particle sizes and moisture contents are 1.5 to 2.0 mm and 3.0 to 10.0% respectively (Bridgwater and Gyftopoulou, 2013; Boateng, 2013; Boateng, 2007; Bridgwater, 1999). However, the moisture content in the freshly harvested biomass is about 50 to 80% (dry basis) which is often required air drying to 25 to 30% in 2 to 4 days. The moisture content is then further

reduced to 2.54 to 4.1% via fast drying methods (typically thermal pre-treatment at 120 to 270°C). The thermal pre-treatment reduces volatile material contents (87 to 56%) which enhances bio-oil yield with low water contents (9 to 10%) (Westover et al., 2013; Delabona et al., 2013; Medic, 2012; Acharjee et al., 2011; Biomass Energy Centre, 2011; Shinners et al., 2007; Yan et al., 2009; Demirbas, 2004). The treatment also helps to reduce size reduction costs. However, pre-treatment at high temperature enhances char production (19 to 28%) and decreases bio-oil production (65 to 51%) (Westover et al., 2013). An optimum thermal pre-treatment condition is reported to be 160 to 180°C for 0.5 to 1.0 hrs (Wang, 2011) that brings moisture contents down to 2.54 from 4.1% (Westover et al., 2013). Moisture content below 12% in the feedstock leads to fire hazard (White, 2013) and higher moisture contents leads to lower energy efficiency (Stuart, 2014; Gebreegziabher et al., 2013; Ringer et al., 2006; Vigouroux, 2001).

Biomass contributes about 1.8% in Malaysian energy mix (Mekhilef et al., 2011). Pyrolysis is the process to maximize the bio-oil yield intended to use biomass efficiently. Table 5-1 below shows the bio-oil productions at different temperature range by various researchers.

Table 5-1: The bio-oil productions at different temperature range by various researchers.

Pyrolysis Temperature (°C)	**Biomass type**	**Bio-oil yield (wt. %)**	**Reference**
500	Wood	60-75	Bridgwater and Peacocke, 2000
469-475	Cassava stalk, cassava rhizome	61.4 - 69.1	Pattiya and Sutibak,,2012
480	Switch grass	60.7	Boateng et al. 2007
460-540	Sugar cane trash	32.5 - 46.2	Treedet and Suntivarakorn 2011
425-550	Sawdust	51 - 62	Salehi et al. 2011
520	Rice husk	46.36	Guo et al. 2011
400-600	Switch grass	22 - 37	Imam and Capareda, 2012
400-600	Palm shell	41 - 58	Islam et al. 1999
350-600	Oil mallee	54 - 63	Garcia-Perez et al., 2008

Pyrolysis Temperature (˚C)	Biomass type	Bio-oil yield (wt. %)	Reference
450-550	Pine, beech, bamboo, demolition wood	65 -67.5	Wang et al., 2005
400-550	Sawdust	46.5 - 58.1	Heo et al., 2010
420-480	Rice husk	53 – 56	Zheng, 2007
500	Rice husk	40	Tsai et al., 2007
400-600	Rice husk	46.5 – 21.5	Wiliams et al 2000
500	Switch grass	60	Mullen and Boateng 2008
500-520	Wood	80	Bridgwater, 1999
510	Wood	60-80	Streff, 2011
500	Non-food biomass	60-75	Ellens, 2010
500	Lignocellulose biomass	65	Sadaka, 2006
500	Wood	75	Bridgwater and Gyftopoulou, 2013

5.3 Materials and method

5.3.1 Feedstock collection

5.3.1.1 Empty fruit bunch (EFB)

EFB was collected from UNMC campus and was chopped by hand saw into small chunks (3 to 4 inch long, 1 inch width and 1 inch breadth). Due to its high moisture content (up to 60%), the EFB chips were dried prior to grinding in the mill since moist biomass causes clog. The EFB was therefore air dried in an air heated oven at 50˚C for 24 hrs prior to grinding in the mill. The air dried small pieces of EFB was allowed to fit through a laboratory scale grinder (Retsch SM 100) fitted with a mesh screen of 4 mm to further reduce the size to 2 to 3 mm. The ground biomass was stored as raw feedstock. The feedstock is kept for storage in a desiccator.

5.3.1.2 Urban tree shavings (UTS)

Urban tree shavings include tree branches, defective logs, broken logs, bark, stumps, injured standing trees were collected from UNMC campus and cut to 1 to 2 inch thick (2 to 3

inch long) by hand and electrical saws. The chips were dried in an oven at 50°C for 24 hrs to a moisture content of 15.36%. The chips were then ground in Retsch SM 100 grinder and passed through a 4 mm screen. The ground biomass was stored in a desiccator as raw feedstock for further processing and analysis.

5.3.1.3 Saw dust (SDB and SDS)

Two types of saw dusts from two different sources were collected from Broga (Saw dust Broga) and Semenyih (saw dust Semenyih). Saw dust Broga (SDB) was obtained from Sh. Direct Sdn Bhd in Ulu Beranang-Broga, Semenyih and saw dust Semenyih (SDS) was obtained from the sawmill in Taman Tasik Semenyih (TTS). Both saw dust types were used as received and no prior preparation was required. The saw dust samples were stored in a desiccator. The samples were prepared following standard procedure (Hames et al., 2008).

5.4 Moisture and ash content analysis

5.4.1 Moisture content analysis:

The moisture content was analysed following ASTM E871 standard (ASTM International, ASTM E871-82(2013)). About 1g of each sample was weighed in a precision digital balance (Sartorius AX224) and placed in a pre-dried and weighed small glass beaker. The beakers containing samples were then placed in an oven at 105°C for 24 hours. The samples were then cooled in a desiccator followed by re-weighing and moisture content was calculated on dry matter basis. The procedure was triplicated for each type biomass samples and the average value was calculated.

5.4.2 Ash content analysis:

The ash content was analysed in accordance with National Renewable Energy Laboratory (NREL) Standard Analysis Method LAP005 (Sluiter et al., 2005). Approximately 2g of each sample was placed in the oven for 24 hrs at 105°C to calculate the moisture content

following ASTM E871. A crucible was pre-heated to 575°C in a muffle furnace for at least 6 hours. The pre-heated crucible was allowed to cool down to room temperature in a desiccator before transferring the oven dried biomass sample in it. The weight of empty crucible and crucible with sample were recorded. The crucible with sample was put in the muffle furnace at 300°C to smoke emitted and when the temperature was raised to 575°C it was observed that no smoke was apparent. Then the crucible with biomass inside the muffle furnace was checked whether any material was left and then the crucible was taken out and kept for cooling. The ash content was calculated on dry basis.

5.5 Feedstock pre-treatment

The four types biomass (EFB, SDB, SDS and UTS) were pre-treated with acidic (H_2SO_4) and alkaline (NaOH) aqueous solutions at different concentrations, liquid-solid ratios, temperatures and retention time. The acid concentrations used were 0% (distilled water, control sample), 0.19%, 0.46%, 0.94%, 1.8%, 4.81% and 9.89% (w/w). The alkali concentrations used were 0.19%, 0.46%, 0.76%, 1.8%, 4.81% and 9.89% (w/w). Liquid to solid ratios used were 2:1, 5:1, 10:1, 15:1, 20:1 and 25:1 by weight. Temperatures of the water bath used were 25 (room temperature), 40, 50, 70 and 90°C. Retention time was also varied from 0, 0.5, 1, 2, 3, 4, 5 and 6 hours. The pre-treated biomass was compared to control sample (untreated biomass) in terms of the calorific value and ash contents. The details of pre-treatment are given below.

5.5.1 Solvent type

Different solvents like dilute aqueous acid (H_2SO_4) and alkali (NaOH), and distilled water were chosen for the pre-treatment study. The measured mass of biomass samples were taken in a 250 ml glass vials and required mass of the acid, alkali and water were added depending on the liquid-solid ratios selected. The details are described below in subsection 4.5.2.

5.5.2 Liquid-Solid ratio

The biomass and solvent were added in a 250 ml glass vials at different proportion to study the effect of liquid to solid ratio in extraction of extractives. The liquid to solid ratios used were 2:1, 5:1, 10:1, 15:1, 20:1 and 25:1 by weight. Approximately 3g of each biomass sample was transferred into a 250 ml glass vial, and 0.94% (w/w) H_2SO_4 or 0.76% (w/w) NaOH solutions was transferred into the vial with different liquid-solid ratios. Water was used to run control samples. The samples were then kept in a water bath (Protech Model-903) with constant speed of 100 rpm. Pre-treatment temperature of 50°C and duration time of 1 hour was fixed for all samples. Upon completion of the pre-treatment reaction, the samples were quenched in ice water before filtration through a Whatman 4 filter paper fitted in a porcelain Buchner funnels under water vacuum. The filter paper was pre-dried in an oven at 105°C for approximately 4 hours and stored in a desiccator before use.

At the beginning of filtration, the pre-dried filter paper was weighed before use. The filtration was carefully conducted to avoid any solid loss. The filtrate was re-filtered if any solid particles were observed. Distilled water was used to wash the biomass while filtering until the p^H of the filtrate was approximately 6 to 8 depending on whether the biomass was pre-treated by acid or alkali. For samples pre-treated with water, no washing was required. A pre-dried, pre-weighed beaker was used to collect the pre-treated and filtered samples together with all the filter papers used for that sample and the beaker was then oven dried at 105°C for 24 hours. Dried samples were then kept in a desiccator for an hour to cool down to room temperature before being weighed. The percentage of solid extracted was then calculated by subtracting the weight of initial pre-dried filter paper(s) and pre-dried empty beaker from the dried sample weight.

5.5.3 Acid/base concentration

Dilute sulphuric acid and alkali were prepared form 98% sulphuric acid having density of 1.84 gm/ml and NaOH pellets having purity of 98 to 100% respectively. H_2SO_4 was supplied by Sigma-Aldrich (M) Sdn Bhd while NaOH was supplied by HmbG Chemical, Malaysia. Different concentration of acid and alkali were used. The aim was to determine the impact of acid concentration of 0.19%, 0.46%, 0.94%, 1.8%, 4.81% and 9.89%.(w/w) and base concentration of 0.19%, 0.46%, 0.76%, 1.8%, 4.81% and 9.89% (w/w) on ash extraction. The liquid to solid ratio used was 20:1.

Approximately 3g of all biomass samples were taken in a 250 ml glass vials and the calculated amount of solution (20:1) of different concentration were added to all biomass samples. The vials were then placed in the hot water bath at 100 rpm agitation speed, extraction temperature 50°C, and reaction time of 1 hour. After completion of the reaction, the samples were quenched followed by vacuum filtration, oven dried at 105°C for 24 hours and sent for ash analysis in a muffle furnace at 575°C.

5.5.4 Temperature

The effect of reaction temperatures on the pre-treatment was studied. The temperatures used include 25, 40, 50, 70 and 90°C. Similar procedure was used as discussed earlier. Approximately 3g of each biomass sample was added in glass vials and the required mass of 4.81% (w/w) acid solution was added (20:1 liquid to solid ratio by weight). The glass vials were kept in water bath at 100 rpm but different temperatures. Contact time was kept constant at 1 hour for all the samples. After completion of the reaction, the samples were quenched followed by vacuum filtration, oven dried at 105°C for 24 hours and sent for ash analysis in a muffle furnace at 575°C.

5.5.5 Retention time

The samples were then subjected to different pre-treatment retention times. The reaction times used were 0, 0.5, 1, 2, 3, 4, 5 and 6 hours. Moreover 17, 24 and 28 hours were also used for EFB samples. Similar procedure was used as discussed earlier. Approximately 3g of each biomass sample was added in glass vials and the required mass of 4.81% (w/w) acid solution was added (20:1 liquid to solid ratio by weight). The glass vials were kept in water bath at 100 rpm, 70°C but removed at different times. After completion of the reaction, the samples were quenched followed by vacuum filtration, oven dried at 105°C for 24 hours and ash analysis in a muffle furnace at 600°C.

5.6 Pyrolysis of UTS and Napier Grass (NG)

The pyrolysis experiments of UTS and NG were carried out in a bench scale tubular furnace under nitrogen atmosphere. The furnace was heated electrically using 220V AC power supply. The temperature of the heater located at the centre of the furnace was measured with the help of thermocouple inserted inside the furnace. The heater temperature was varied from 450 to 800°C which corresponds to calibrated temperature 412.28 to 791.24°C. Nitrogen gas was used as the inert media and the flow-rate of nitrogen was measured by gas flow meter. The vapour produced was made to pass through a nylon tube and was cooled immediately with the help of a copper coil submerged in ice bath and the bio-oil was collected in a conical flask connected to the coil. The non-condensable gas was analysed with a Drager X-am 5000 analyser.

5.7 Design of Experiments

The generation of valid, defensible, and supportable engineering conclusions are ensured by design of experiments (DOE) which is a systematic, rigorous approach to engineering problem-solving that applies principles and techniques at the data collection stage. In

addition, all of this is carried out under the constraint of a minimal expenditure of engineering runs, time, and money. General engineering problem areas in which DOE may be applied include: comparative, screening/characterizing, modelling and optimizing. In the first case, any change in a single factor has in fact resulted in a change/improvement to the process as a whole is assessed by the engineer/researcher. In the second case, the engineer/researcher is interested in "understanding" the process as a whole in the sense that he/she wishes (after design and analysis) to have in hand a ranked list of important through unimportant factors (most important to least important) that affect the process. In the third case, the engineer/researcher is interested in functionally modelling the process with the output being a good-fitting (= high predictive power) mathematical function, and to have well (= maximal accuracy) estimates of the coefficients in that function. In the fourth case, the optimal settings of the process factors are determined by the engineer/researcher (for each factor the level of the factor that optimizes the process response) (NIST, 2015). DOE was used to determine the optimum number of experiments, liquid-solid ratio, solvent concentration and temperature for UTS biomass for extraction of solid for the present study which is given next.

Table 5-2: Input data for DOE

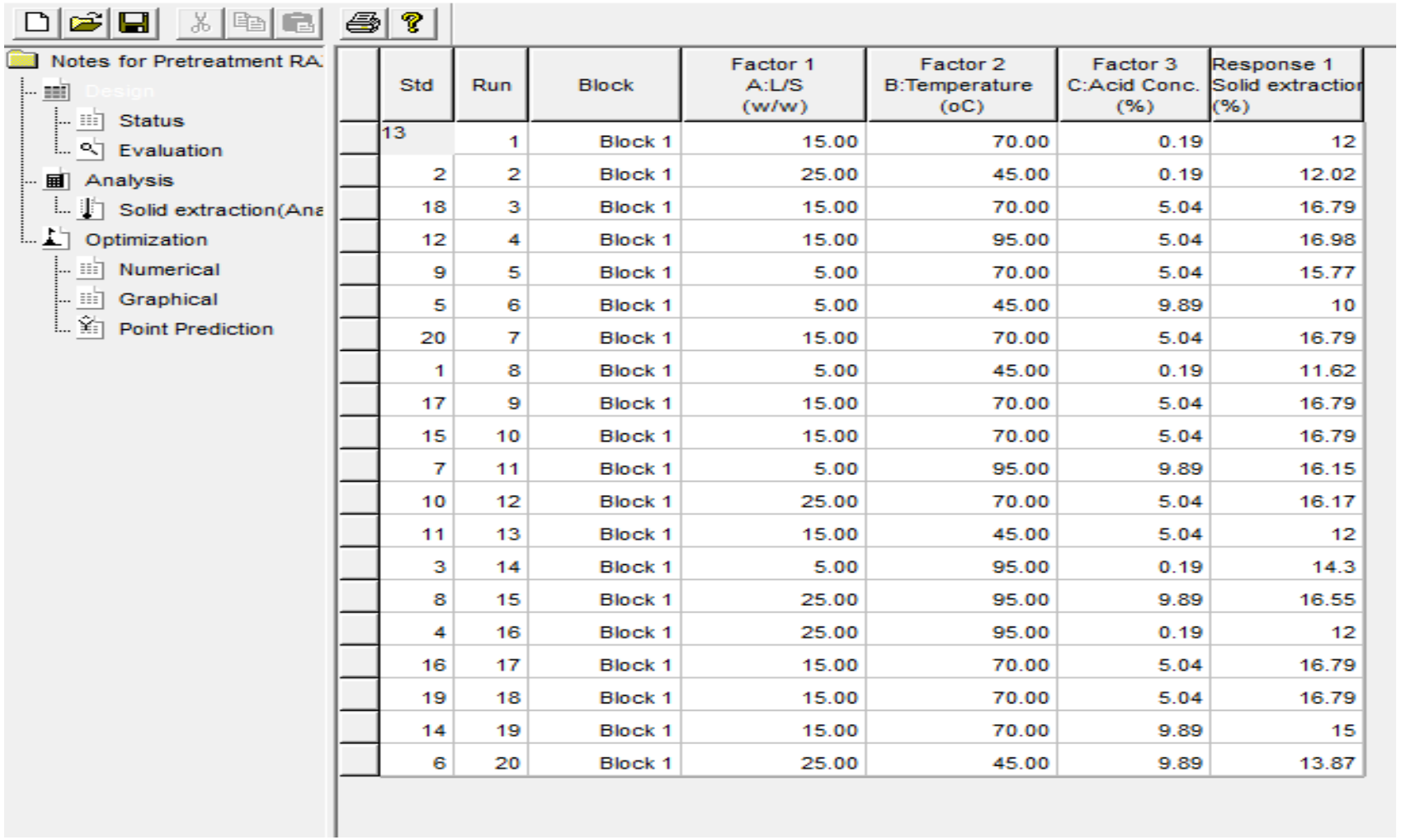

	Std	Run	Block	Factor 1 A:L/S (w/w)	Factor 2 B:Temperature (oC)	Factor 3 C:Acid Conc. (%)	Response 1 Solid extractio (%)
	13	1	Block 1	15.00	70.00	0.19	12
	2	2	Block 1	25.00	45.00	0.19	12.02
	18	3	Block 1	15.00	70.00	5.04	16.79
	12	4	Block 1	15.00	95.00	5.04	16.98
	9	5	Block 1	5.00	70.00	5.04	15.77
	5	6	Block 1	5.00	45.00	9.89	10
	20	7	Block 1	15.00	70.00	5.04	16.79
	1	8	Block 1	5.00	45.00	0.19	11.62
	17	9	Block 1	15.00	70.00	5.04	16.79
	15	10	Block 1	15.00	70.00	5.04	16.79
	7	11	Block 1	5.00	95.00	9.89	16.15
	10	12	Block 1	25.00	70.00	5.04	16.17
	11	13	Block 1	15.00	45.00	5.04	12
	3	14	Block 1	5.00	95.00	0.19	14.3
	8	15	Block 1	25.00	95.00	9.89	16.55
	4	16	Block 1	25.00	95.00	0.19	12
	16	17	Block 1	15.00	70.00	5.04	16.79
	19	18	Block 1	15.00	70.00	5.04	16.79
	14	19	Block 1	15.00	70.00	9.89	15
	6	20	Block 1	25.00	45.00	9.89	13.87

Table 5-3: Anova table for solid extraction from UTS

Response: Solid extraction

ANOVA for Response Surface Quadratic Model

Analysis of variance table [Partial sum of squares]

Source	Sum of Squares	DF	Mean Square	F Value	Prob > F	Remarks
Model	95.39	9	10.60	16.71	< 0.0001	significant
A	0.77	1	0.77	1.21	0.2971	
B	27.13	1	27.13	42.77	< 0.0001	significant
C	9.27	1	9.27	14.62	0.0034	
A^2	0.17	1	0.17	0.26	0.6185	
B^2	4.18	1	4.18	6.59	0.0280	
C^2	13.59	1	13.59	21.43	0.0009	
AB	4.76	1	4.76	7.50	0.0209	
AC	4.76	1	4.76	7.50	0.0209	
BC	4.76	1	4.76	7.50	0.0209	
Residual	6.34	10	0.63			
Lack of Fit	6.34	5	1.27			
Pure Error	0.000	5	0.000			
Cor Total	101.74	19				

Std. Dev.	0.80	R-Squared	0.9377
Mean	14.76	Adj R-Squared	0.8816
C.V.	5.40	Pred R-Squared	0.6372
PRESS	36.91	Adeq Precision	12.445

Final equation in terms of Coded Factors:

$$Solidextraction = +16.36 + 0.28 * A + 1.65 * B + 0.96 * C + 0.25 * A^2 - 1.23 * B^2 - 2.22 * C^2 - 0.77 * A * B + 0.77 * A * C + 0.77 * B * C$$

where *Solid Extraction* is the response, and A, B and C are the coded terms for the three variables that has been selected, i.e. liquid-solid ratio (A), reaction temperature (B) and acid concentration (C). Positive sign in front of each term represent synergistic effect, while antagonistic effect represented by negative sign. Analysis of Variance (ANOVA) was then used to assess the goodness of fit. The significant quadratic model and the corresponding significant model term for the response are tabulated in Table 5-3 for solid extraction. From Table 5-3, the model F-value of 16.71 implies that the model is significant. It was also observed that the linear term of reaction temperature (B) has large significant effect on the

extraction due to the high F-value of 42.77. However, the quadratic terms did not show significant effect on extraction of solid. The relationships between the variables are also shown in Figures 5-1 to 5-3.

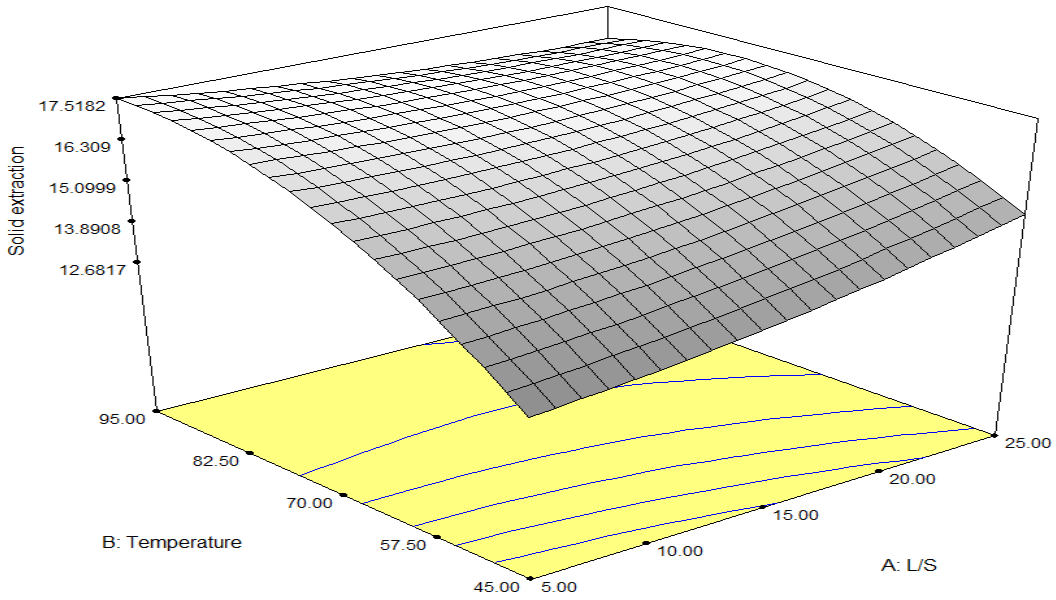

Figure 5-1: Contour plot of solid extraction: Effect of reaction temperature and liquid-solid ratio.

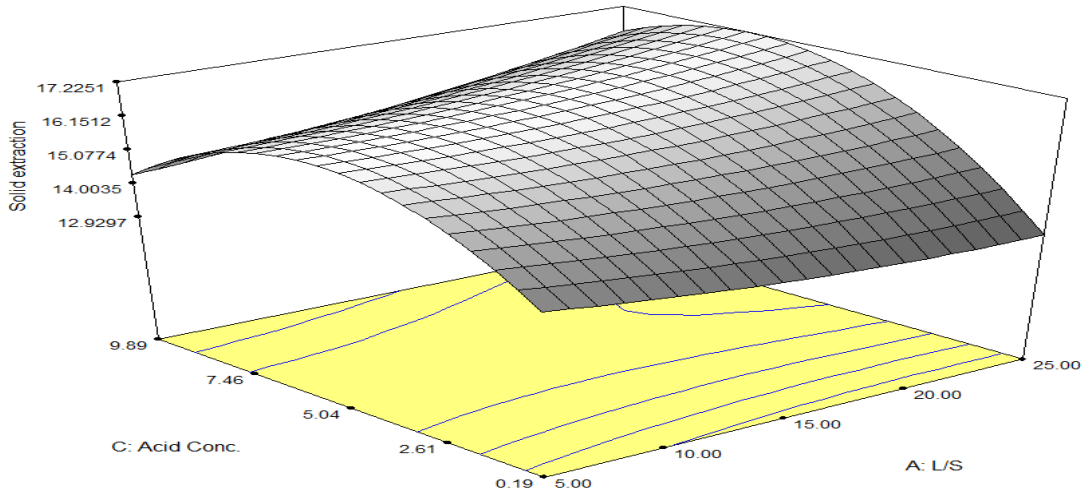

Figure 5-2: Contour plot of solid extraction: Effect of acid concentration and liquid-solid ratio.

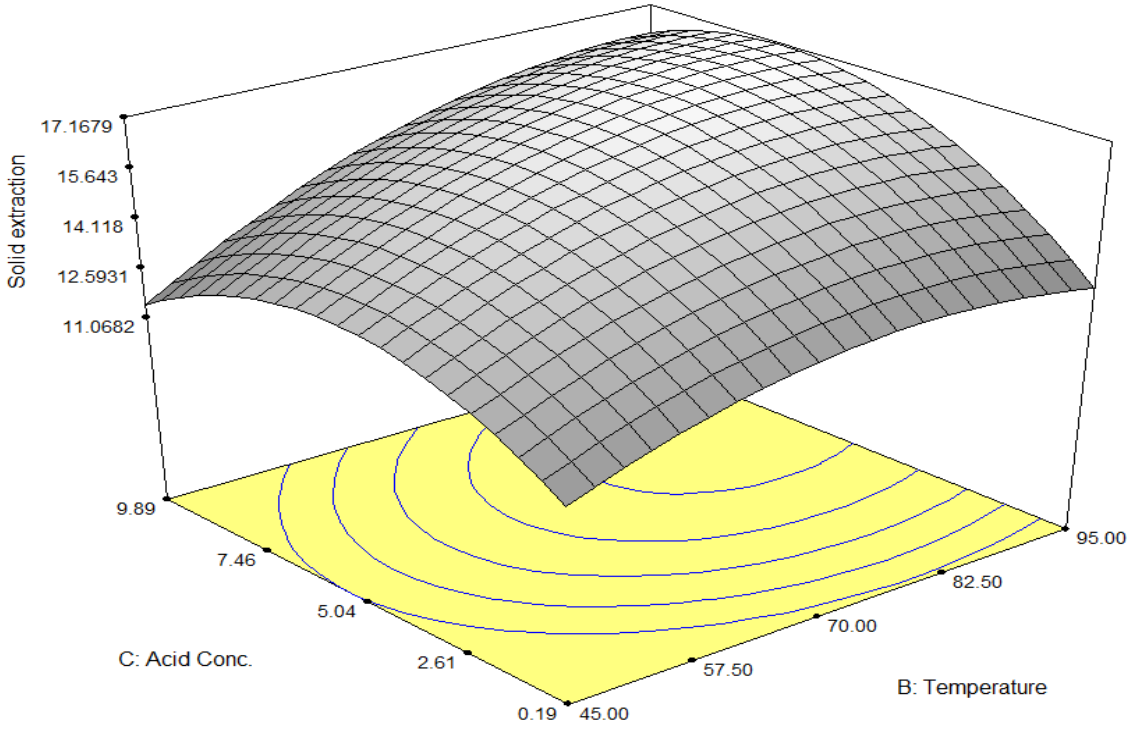

Figure 5-3: Contour plot of solid extraction: Effect of acid concentration and reaction temperature.

In order to test the fit of the model, the regression equation and the determination coefficient (R^2) were evaluated. For the response of extraction of solid, the value of determination coefficient (R^2 = 0.9377) indicates that the sample variation of 93.77% for extraction is attributed to the independent variables and only 6.23% of the total variation could not be explained by the model. The value of adjusted determination coefficient (Adj R^2 = 0.8816) is also very high to advocate for a high significance of the model.

The correlation between experimental values and predicted values of extraction, are shown in Fig. 5-4 and the desirability plot is shown in Figure 5-5. A higher value of the correlation coefficient for all responses justifies an excellent correlation between the independent variables (Jamaluddin et al., 2013; Ghani et al., 2010).

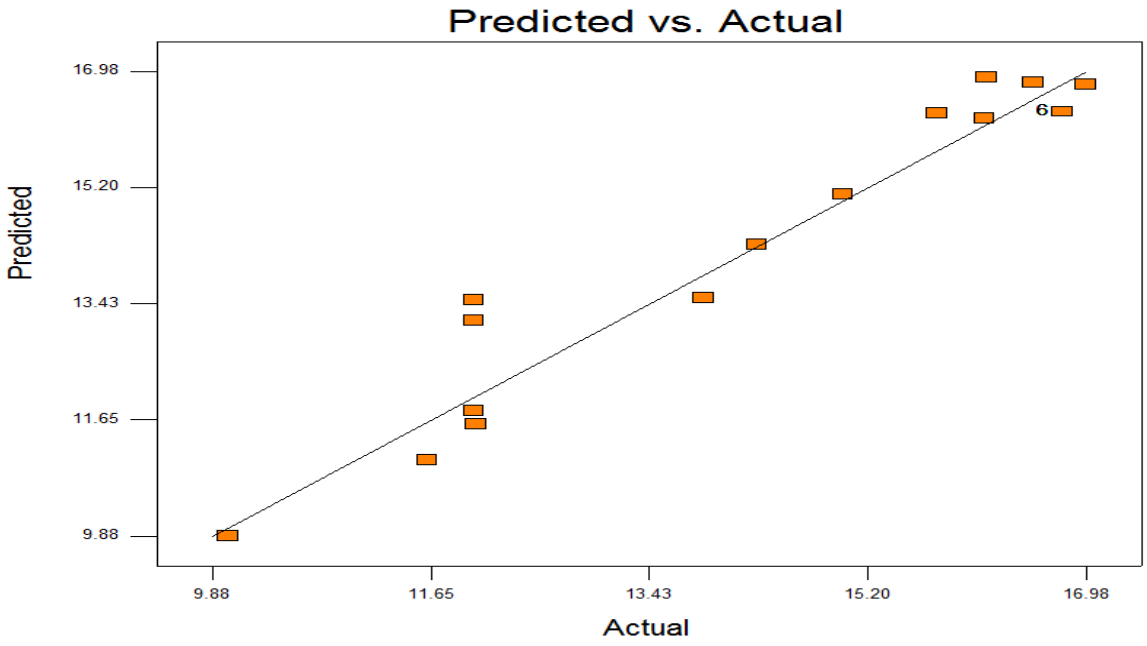

Figure 5-4: Relationship between predicted and actual values of solid extraction.

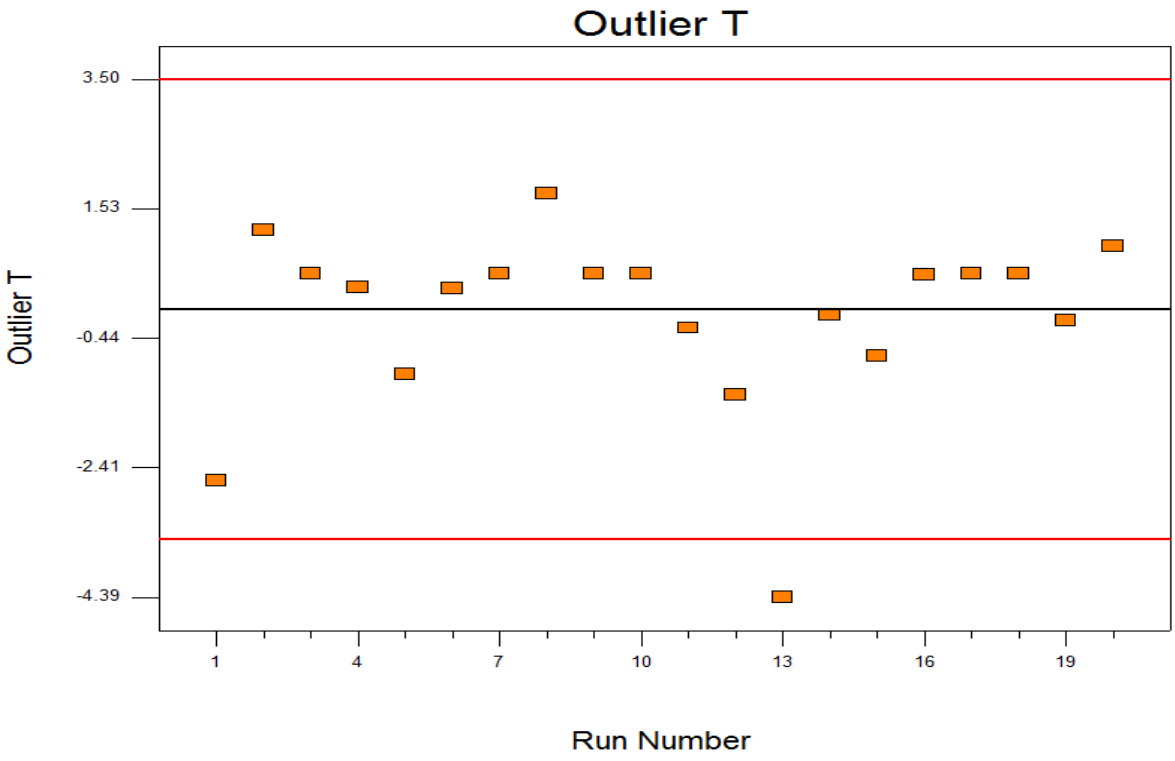

Figure 5-5: Desirability plot

Table 5-4: Optimum condition obtained from the analysis showing the constraint and solutions

Constraints

Name	Goal	Lower Limit	Upper Limit	Lower Weight	Upper Weight	Importance
L/S	is in range	5	25	1	1	3
Temperature	is in range	45	95	1	1	3
Acid Conc.	is target = 4.81	0.19	9.89	1	1	3
Solid extraction	maximize	10	16.98	1	1	5

Solutions

Number	L/S	Temperature	Acid Conc.	Solid extraction	Desirability	
1	8.99	85.11	4.81	17.0603	1.000	Selected
2	9.78	88.36	4.81	17.0674	1.000	
3	8.93	89.85	4.81	17.1306	1.000	
4	8.72	92.53	4.81	17.1451	1.000	
5	25.00	78.46	4.81	16.9426	0.997	
6	25.00	78.71	4.81	16.9425	0.997	
7	25.00	78.93	4.81	16.9423	0.997	

It can be seen from the optimum solution table that the liquid-solid ratio of 8.99 to 25.00 provide almost same percentage of solid extraction. So liquid-solid ration 15:1 was used for the extraction and temperature, acid concentration has been used are 70°C and 4.81% respectively for solid extraction experiment of UTS which also got from the DOE solutions.

5.8 Results and discussion

Moisture and ash contents of the (EFB, SDB, SDS and UTS) biomass samples are given in Tables 5-5 and 5-6 respectively. The properties of UTS are given in Table 5-7.

Table 5-5: Moisture content analysis

Sample	Empty beaker (m_o), g	Beaker + sample (m_1), g	Beaker + sample after 24hrs (m_2), g	Moisture content, %	Average moisture content (%)
EFB-1	32.951	36.2463	35.9517	8.9400	9.1152
EFB-2	32.966	36.7431	36.3974	9.1525	
EFB-3	31.837	37.353	36.8426	9.2531	
SDB-1	43.659	44.84	44.735	8.8908	9.1185
SDB-2	36.63	38.6968	38.5051	9.2752	
SDB-3	32.1008	34.559	34.3331	9.1897	
SDS-1	36.087	38.5896	38.1324	18.2690	18.4043
SDS-2	33.6881	35.9899	35.5658	18.4247	
SDS-3	32.7893	35.0178	34.6051	18.5192	
UTS-1	36.4104	41.6708	40.8601	15.4114	15.3625
UTS-2	33.1846	36.4917	35.9849	15.3246	
UTS-3	33.0458	37.1073	36.4838	15.3515	

Table 5-6: Ash content analysis

Sample	Empty crucible weight (EC),g	Crucible + sample weight, g	Crucible + ash weight(AC),g	Ash weight (AW), g	%Ash	Average %Ash
EFB-1	28.0501	30.395	28.191	0.1409	6.0088	5.974
EFB-2	26.8415	29.4557	27.022	0.1805	6.9046	
EFB-3	27.7265	29.0941	27.795	0.0685	5.0088	
Saw dust Broga-1	31.2643	35.7328	31.3222	0.0579	1.2957	1.366
Saw dust Broga-2	28.0519	32.7739	28.113	0.0611	1.2939	
Saw dust Broga-3	31.2631	32.8731	31.2874	0.0243	1.5093	
Saw dust semenyih-1	26.8405	29.7313	26.847	0.0065	0.2249	0.243
Saw dust semenyih-2	28.014	31.7364	28.0215	0.0075	0.2015	
Saw dust semenyih-3	26.8398	28.2597	26.8441	0.0043	0.3028	
UTS-1	28.012	31.0253	28.1842	0.1722	5.7147	6.151
UTS-2	31.2674	34.8173	31.488	0.2206	6.2143	
UTS-3	28.9742	30.7266	29.0885	0.1143	6.5225	

Ash content in SDS samples is less compared to UTS, may be due to the minerals uptake by the plant and the soil properties and climatic condition of the place where it was grown (Mohammed et al., 2014).

Table 5-7: Properties of the Urban Tree Shavings

Proximate analysis	Composition
Moisture content *	15.36%
Ash*	6.15%
Volatile Matter*	78.79%
Fixed Carbon**	15.06%
Calorific value	17.36 MJ/kg (based on bone dry sample)

* bone-dry basis; **by difference

5.8.1 Effect of solvent types on extraction

Aqueous acid, alkaline and water (as control) were used to extract the biomass extractives. The extraction was most effective when aqueous alkaline was used for extraction**.** The effect was less significant when acid and water were used. This is because alkali is more effective in removing extractives especially lignin compared to acid (Mohammad et al., 2012; Sills and Gossett, 2011; Macintosh and Vancov 2010). Although no specific analysis was made on extractives constituents, the visual observation of the filtrate colour indicated to estimate the amount of extractives extracted.

5.8.2 Effect of liquid-solid ratio on extraction

The effect of liquid-solid ratio was studied by increasing the solvent mass while the amount of solid was kept constant. The ratios were calculated on bone dry biomass weight basis. The percentage of solid extracted, for all samples under same conditions, increased with increase in liquid-solid ratios (Figures 5-6 to 5-9). The liquid-solid ratio of 20:1 was chosen as an optimum ratio.

From Figure 5-6, it is seen that alkali gives more extraction compared to acid from low to high liquid-solid ratio. For EFB, alkali gives the maximum extraction for 25:1 ratio (25.27%) whereas it is 20:1 for acid (16.22%). For 15:1 ratio, alkali gives about 132% more extraction than acid while for 20:1 this value is about 37.5% and for 25:1 ratio, this value is 105.45%. Extraction of solids is more by base compared to acid is also reported in literature (Asli et al., 2013). After 15:1 ratio, the extraction with alkali drops and again goes up for 25:1 ratio, while it drops after 20:1 for acid. A 250 ml vial was used for this experiment. Water shows lower extraction compared to both alkali and acid for all liquid-solid ratios.

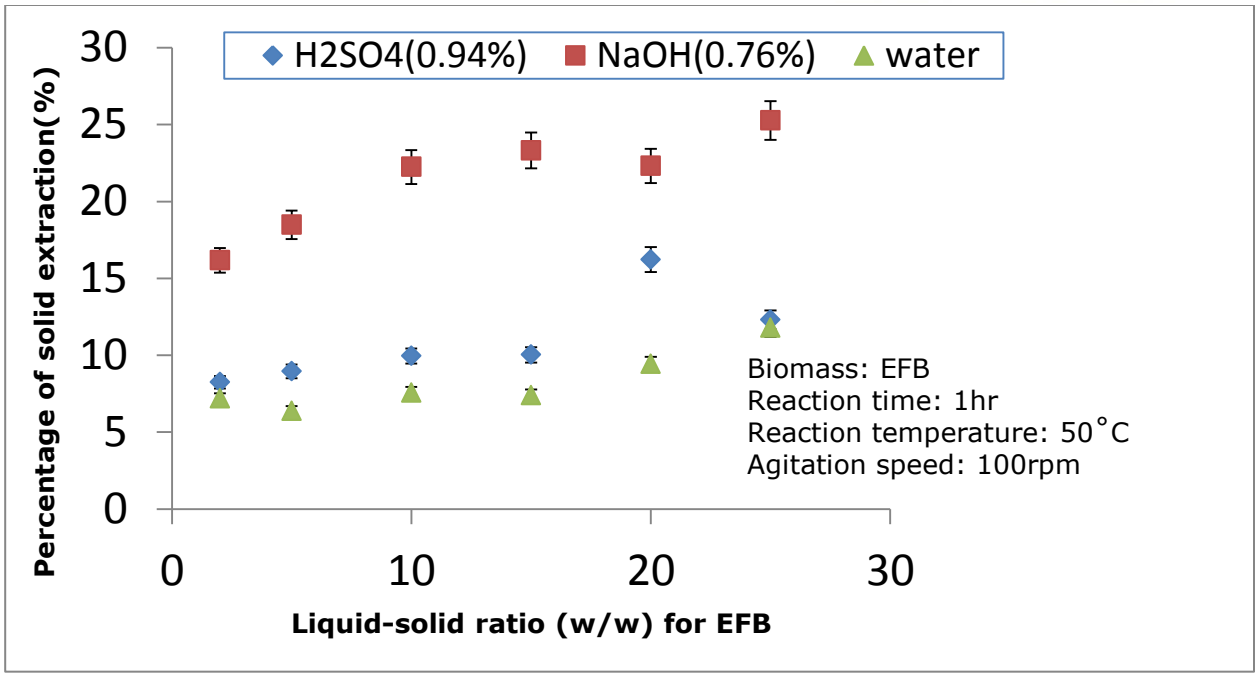

Figure 5-6: Effect of liquid-solid ratio on solid extraction from EFB biomass

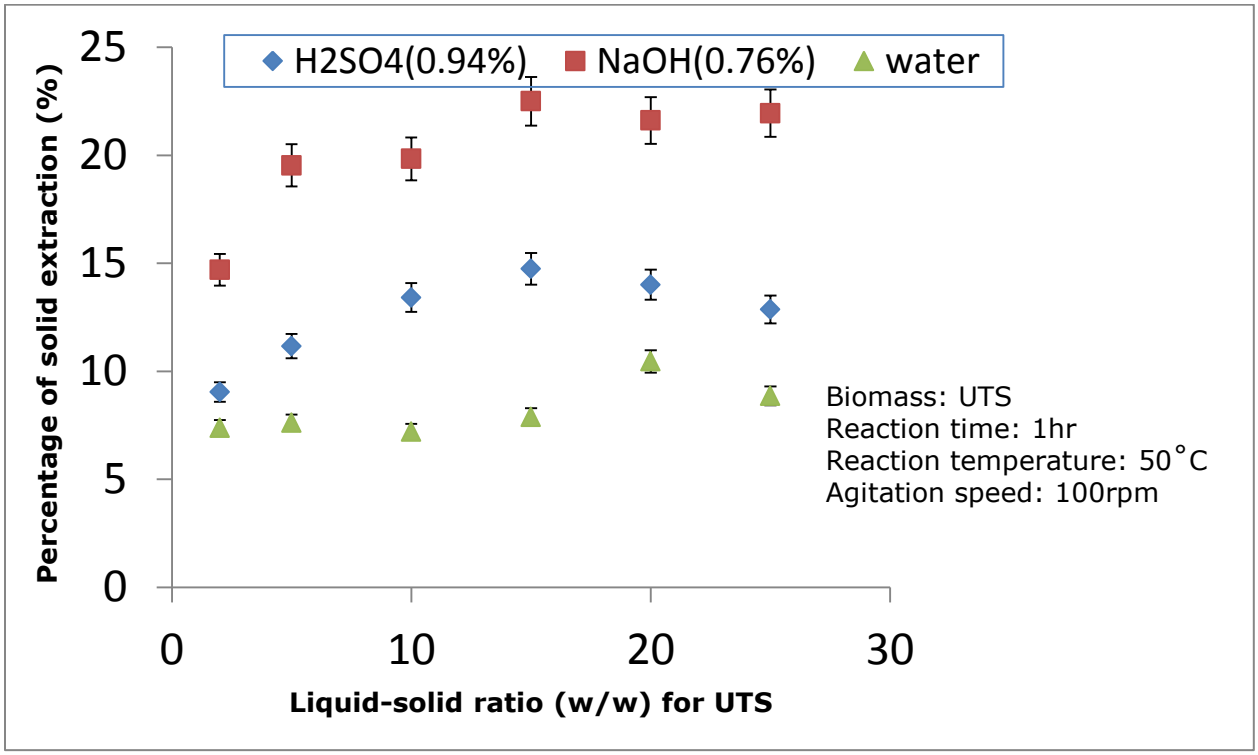

Figure 5-7: Effect of liquid-solid ratio on extraction from UTS biomass

Figure 5-7 shows that alkali resulted in higher extraction percentage compared to the acid from low to high liquid-solid ratio. For UTS, 15:1 ratio gives the maximum extraction for both alkali and acid (22.50 and 14.74% respectively) but alkali gives about 52.65% more extraction than acid. Extraction of solids is more by base compared to acid is also reported in literature (Menon and Rao 2012; Ibrahim et al., 2011; Macintosh and Vancov, 2010). After 15:1 ratio, the extraction with alkali drops and again goes up for 25:1 ratio, while it drops after 15:1 for acid. A 250 ml vial was used for this experiment. Water shows lower extraction compared to both alkali and acid for all liquid-solid ratios.

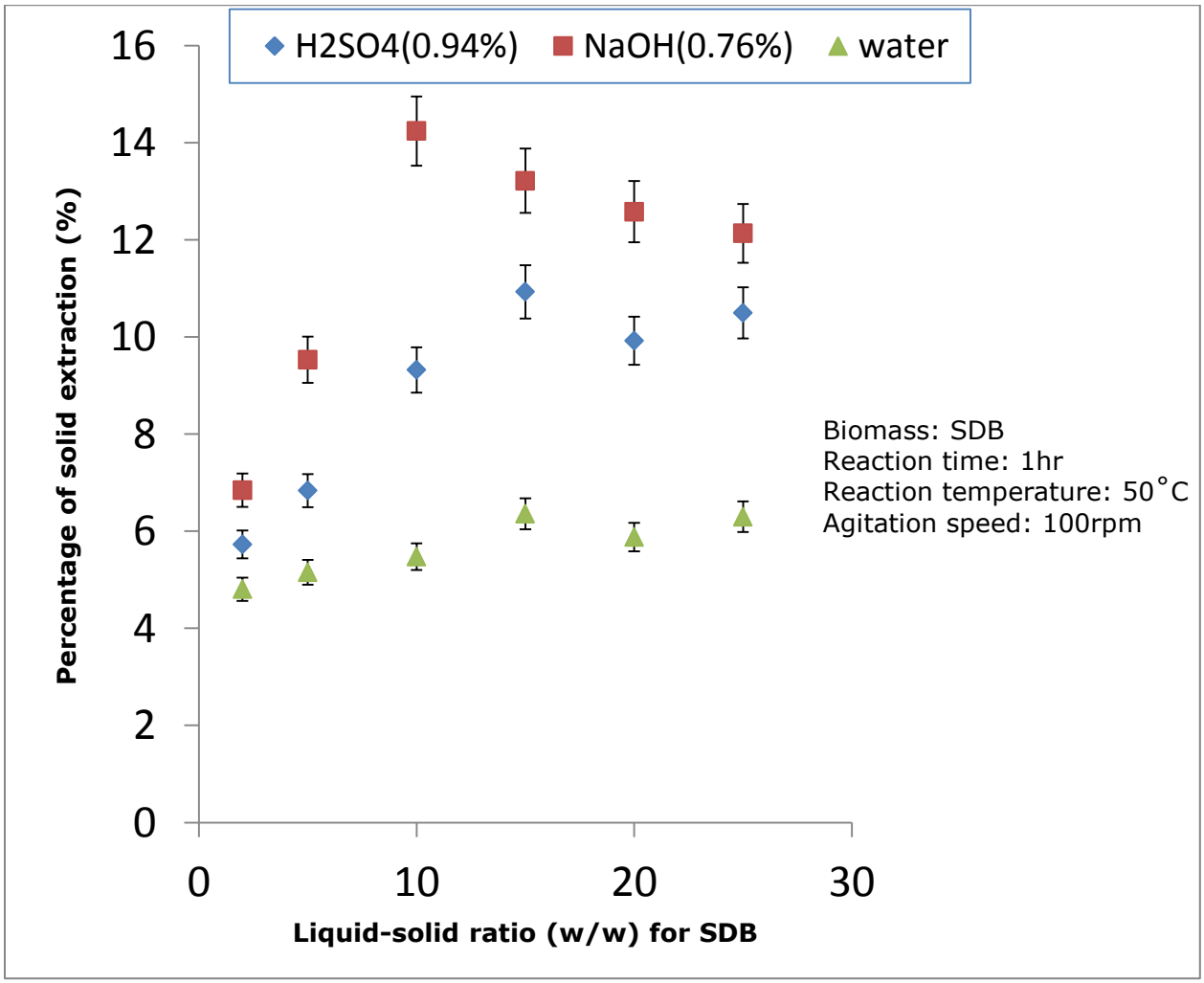

Figure 5-8: Effect of liquid-solid ratio on solid extraction from SDB biomass

From Figure 5-8, it can be seen that alkali gives more percentage of extraction compared to acid from low to high liquid-solid ratio. For alkali, 10:1 ratio gives the maximum extraction (14.24%) whereas it is 15:1 for acid (10.92%). However it is lower compared to EFB and UTS. For 10:1 ratio, alkali gives about 52.79% more extraction than acid while for 20:1 this value is about 26.81%. Extraction of solids is more by base compared to acid is also reported in literature (Menon and Rao 2012; Macintosh and Vancov, 2010). After 10:1 ratio, the extraction with alkali drops and continues this trend up to 25:1 ratio, while it drops after 15:1 for acid and goes up for 25:1. A 250 ml vial was used for this experiment. Water shows lower extraction compared to both alkali and acid for all liquid-solid ratios.

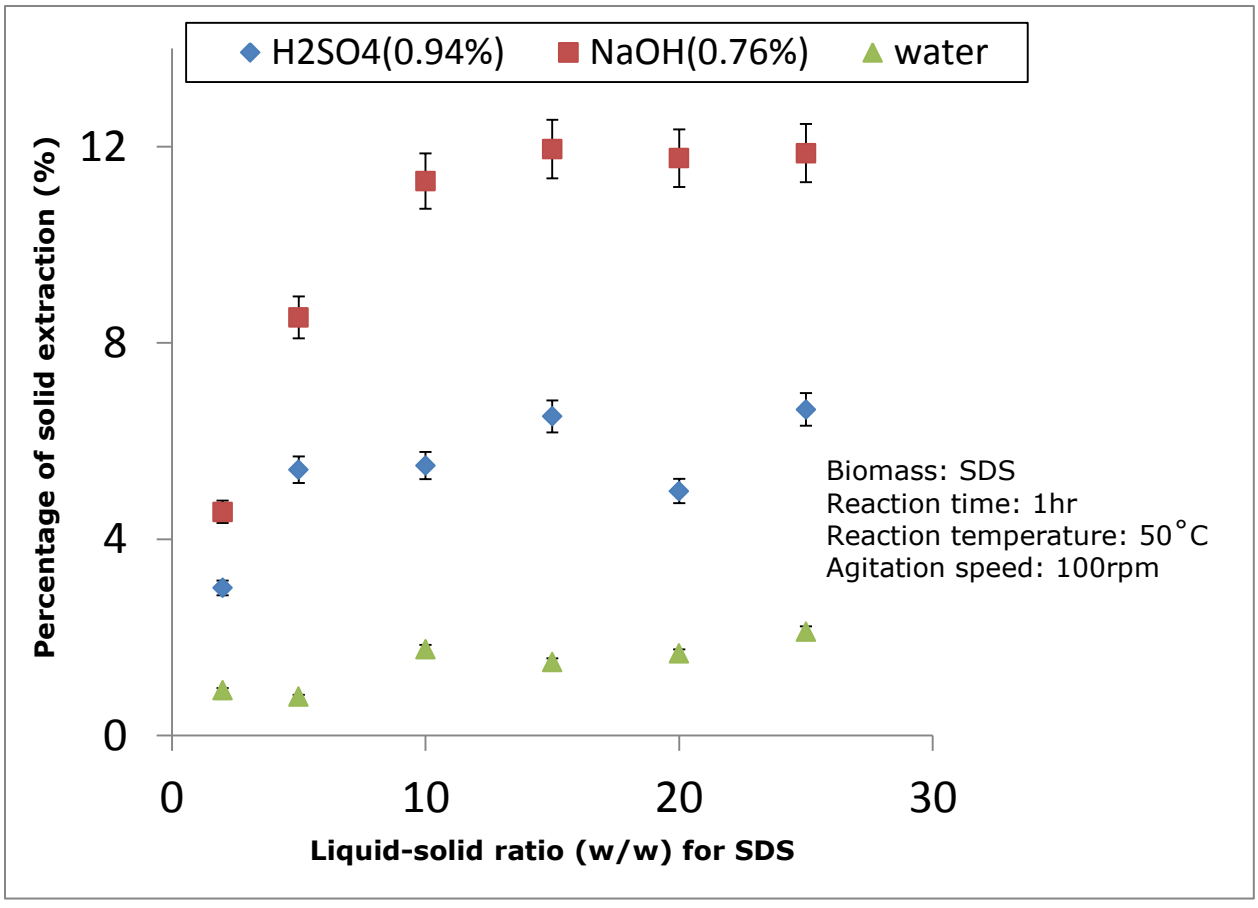

Figure 5-9: Effect of liquid-solid ratio on solid extraction from SDS biomass

From Figure 5-9, it can be concluded that alkali has given more percentage of extraction compared to acid from low to high liquid-solid ratio for SDS. For both alkali and acid, 15:1 ratio gives the maximum extraction (11.95% and 6.5% respectively). However it is the lowest compared to other three types of biomass being used in the extraction experiment. For 15:1 ratio, alkali gives about 83.84% more extraction than acid. Extraction of solids is more by base compared to acid is also reported in literature (Menon and Rao 2012; Ibrahim et al., 2011; Macintosh and Vancov, 2010). After 15:1 ratio, the extraction with alkali drops little and goes up little again for 25:1 ratio, while it drops after 15:1 for acid and goes up for 25:1. A 250 ml vial was used for this experiment. Water shows lower extraction compared to both alkali and acid for all liquid-solid ratios.

The base concentration used was limited to 0.76% (w/w), because more weight loss was recorded for concentration over this limit and it is also reported in literature that base extracts more lignin compared to acid (Macintosh and Vancov, 2010). Among all four types of biomass, UTS gives the maximum extraction for both alkali and acid solvents. Hence, it will be used in bio-oil production for both tubular furnace and the designed reactor.

5.8.3 Effect of acid or base concentration on extraction

The effect of acid and base concentration was studied while keeping the other treatment parameters constant. The concentrations of both acid and base were increased while maintaining the other process parameters constant. The percentage of solid extracted increased with increasing acid and base concentration for all samples (Figures 5-10 to 5-13).

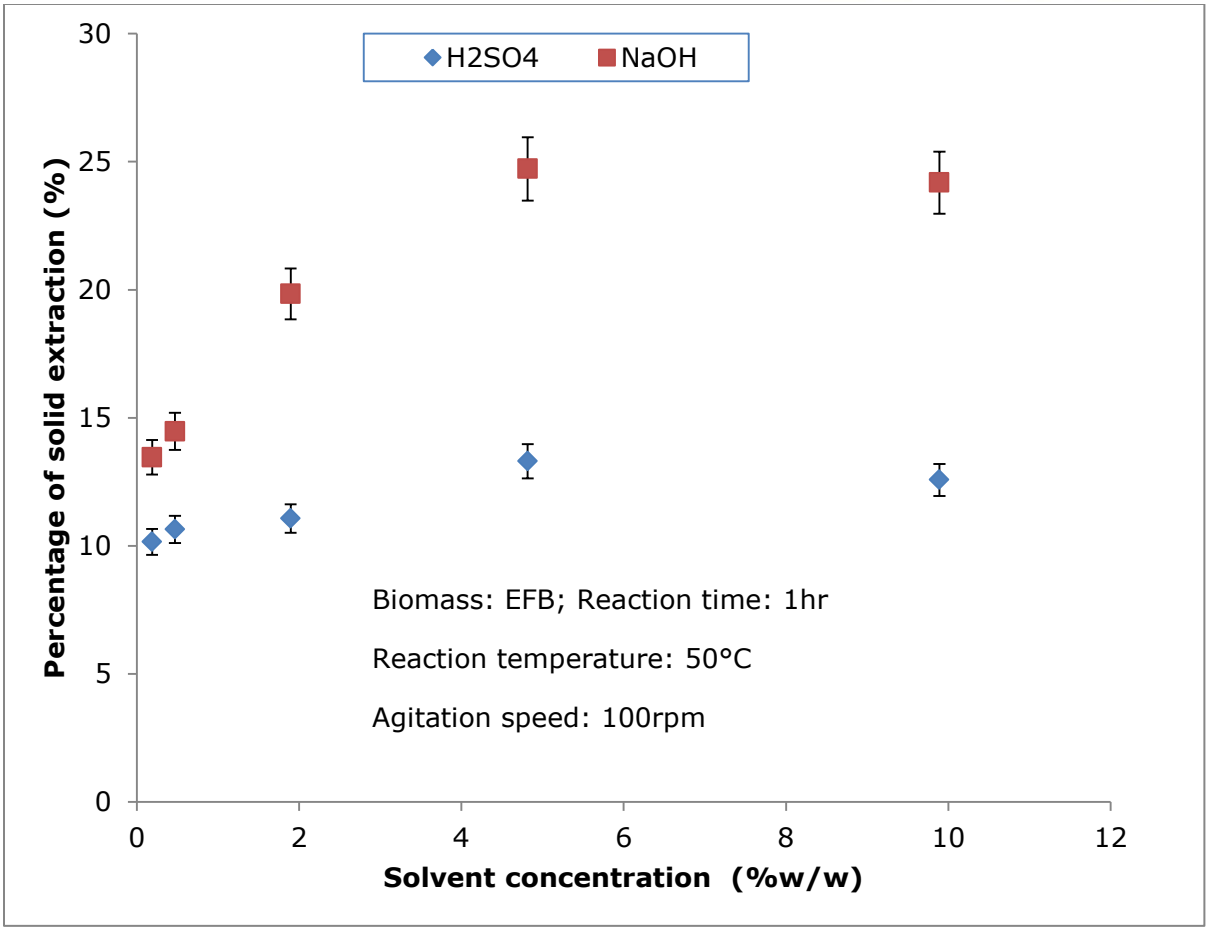

Figure 5-10: Effect of solvent concentration on solid extraction from EFB biomass

From Figure 5-10, it can be seen that extraction increases as concentration of alkali and acid increases, but alkali gives more extraction for EFB compared to acid from low to high concentration. For both alkali and acid, solvent concentration of 4.81% gives the maximum extraction (24.71% and 13.30% respectively), but alkali gives about 85.79% more extraction than acid at this concentration. Extraction of solids is more by base compared to acid is also reported in literature (Asli et al., 2013). After 4.81% solvent concentrations, the extraction for both the solvents drops may be all the extractives solubilized at 4.81% solvent concentration.

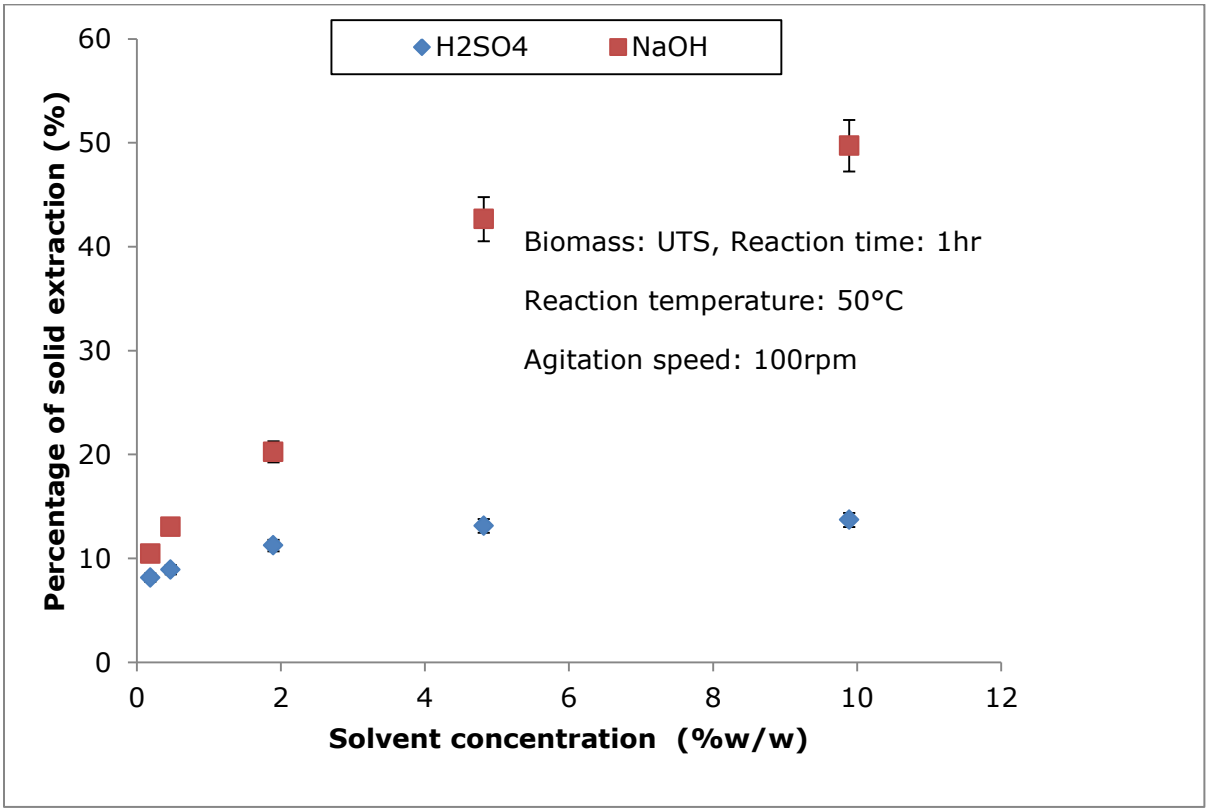

Figure 5-11: Effect of solvent concentration on solid extraction from UTS biomass

Figure 5-11 shows that extraction increases as concentration of alkali and acid increases, but alkali gives higher percentage of extraction for UTS compared to acid from low to high concentration. For both alkali and acid, solvent concentration of 9.89% gives the best extraction (49.71% and 13.70% respectively), but alkali resulted in about 263% more extraction percentage than acid at this concentration. Again at 4.81% solvent concertation, alkali and acid gives 42.65% and 13.11% extraction respectively and alkali extracts 225% more than acid. Extraction of solids is more by base compared to acid is also reported in literature (Menon and Rao 2012; Ibrahim et al., 2011; Macintosh and Vancov, 2010). So 4.81% acid was chosen as the optimum as extraction by acid at 4.81% and 9.89% are very close. As the results showed incremental tendency, the experiment was performed up to 9.89% solvent concentrations.

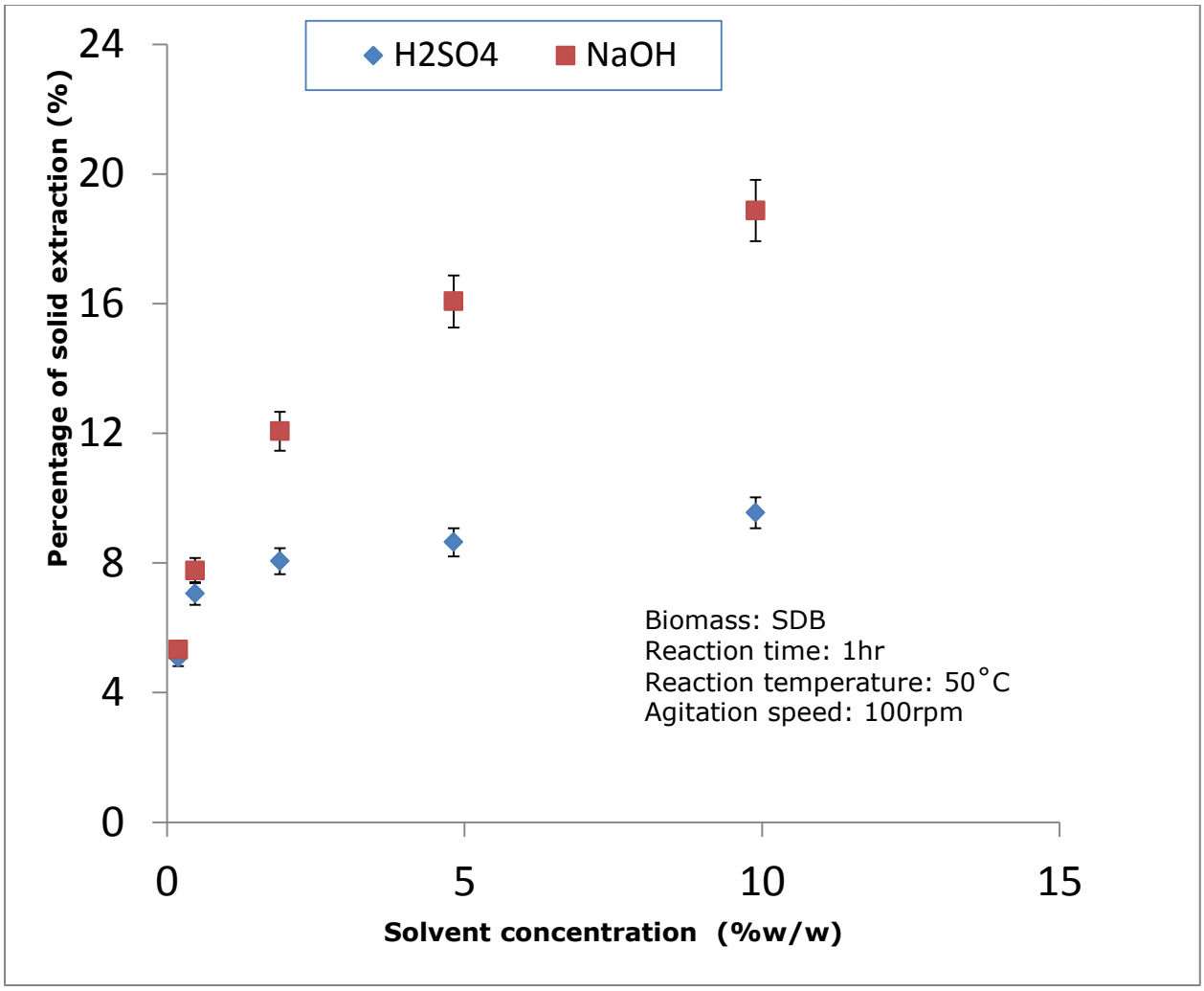

Figure 5-12: Effect of solvent concentration on solid extraction from SDB biomass

From Figure 5-12, it can be said that extraction increases as concentration of alkali and acid increases, but alkali gives more extraction for SDB compared to acid from low to high concentration. For both alkali and acid, solvent concentration of 9.89% gives the best extraction (18.77% and 9.55% respectively), but alkali gives about 97.6% more extraction than acid at this concentration. Extraction of solids is more by base compared to acid is also reported in literature (Menon and Rao 2012; Ibrahim et al., 2011; Macintosh and Vancov, 2010). As the result shows incremental tendency, the experiment was continued up to 9.89% solvent concentrations.

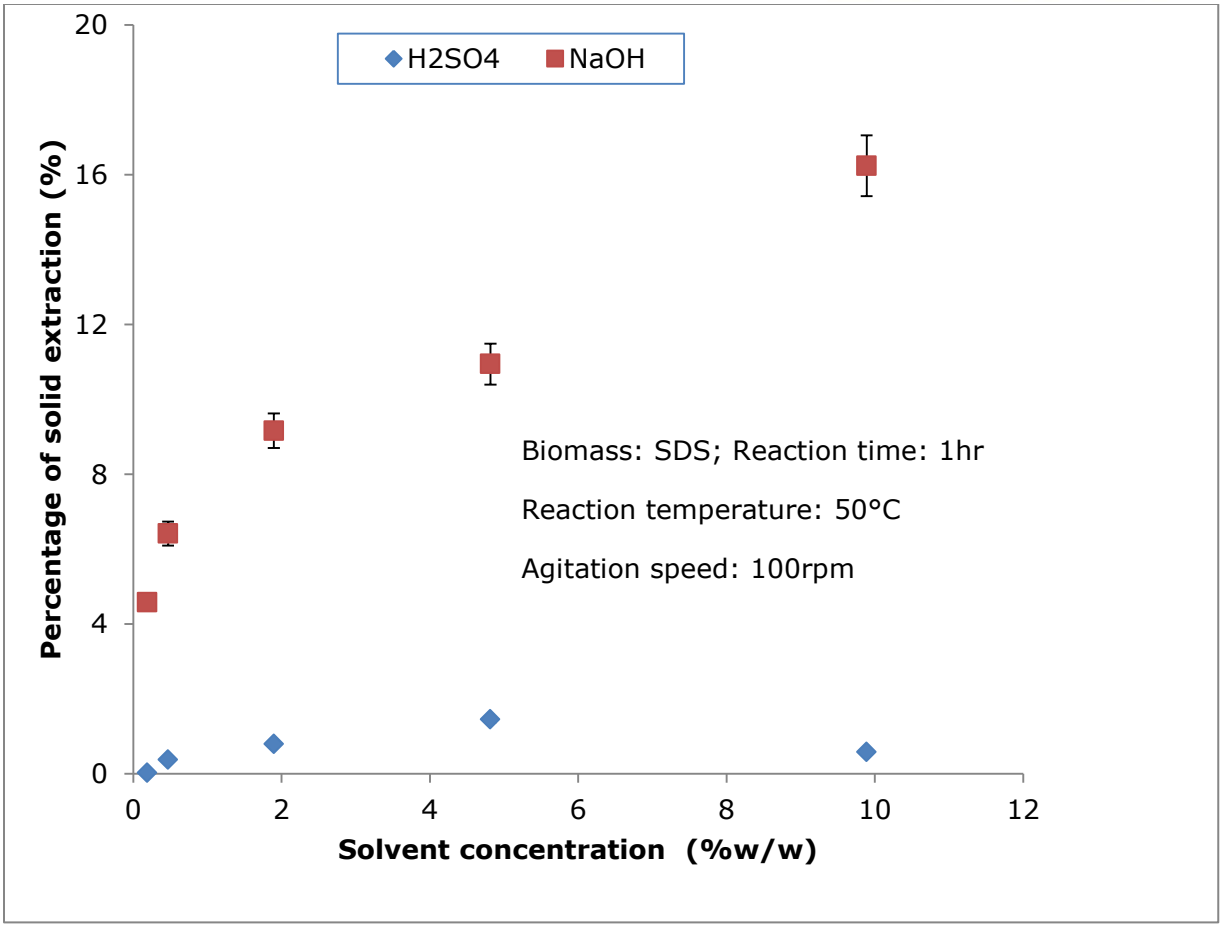

Figure 5-13: Effect of solvent concentration on solid extraction from SDS biomass

From Figure 5-13, it can be seen that extraction increases as concentration of alkali increases, but acid shows very little increase in extraction for SDS from low to high concentration. For alkali, at 9.89% solvent concentration gives the maximum extraction (16.24%) and for acid, at 4.81% solvent concentration gives the maximum extraction (1.45%), but alkali gives about 650% more extraction than acid at its (acid's) maximum extraction concentration level. Extraction of solids is more by base compared to acid is also reported in literature (Menon and Rao 2012; Ibrahim et al., 2011; Macintosh and Vancov, 2010). Extraction increases as alkali concentration increases but for acid it drops after 4.81% solvent concentration may be all the extractives solubilized at this concentration.

For all four types of biomass, UTS gives the maximum extraction and SDS gives the minimum extraction for both alkali and acid solvents this may be due to SDS has more lignin compared to UTS, it gives very less extraction compared to UTS especially by acid solvent. Again UTS is the preferred biomass for producing bio-oil by both tubular furnace and the designed fluidized bed system.

5.8.4 Effect of temperature on extraction

The temperature effect on solid extraction was studied while keeping all other treatment parameters constant. With increasing temperatures, the percentages of solid extraction for all samples were increased. Effect of reaction temperatures on solid extraction from biomass samples are shown in Figure 5-14.

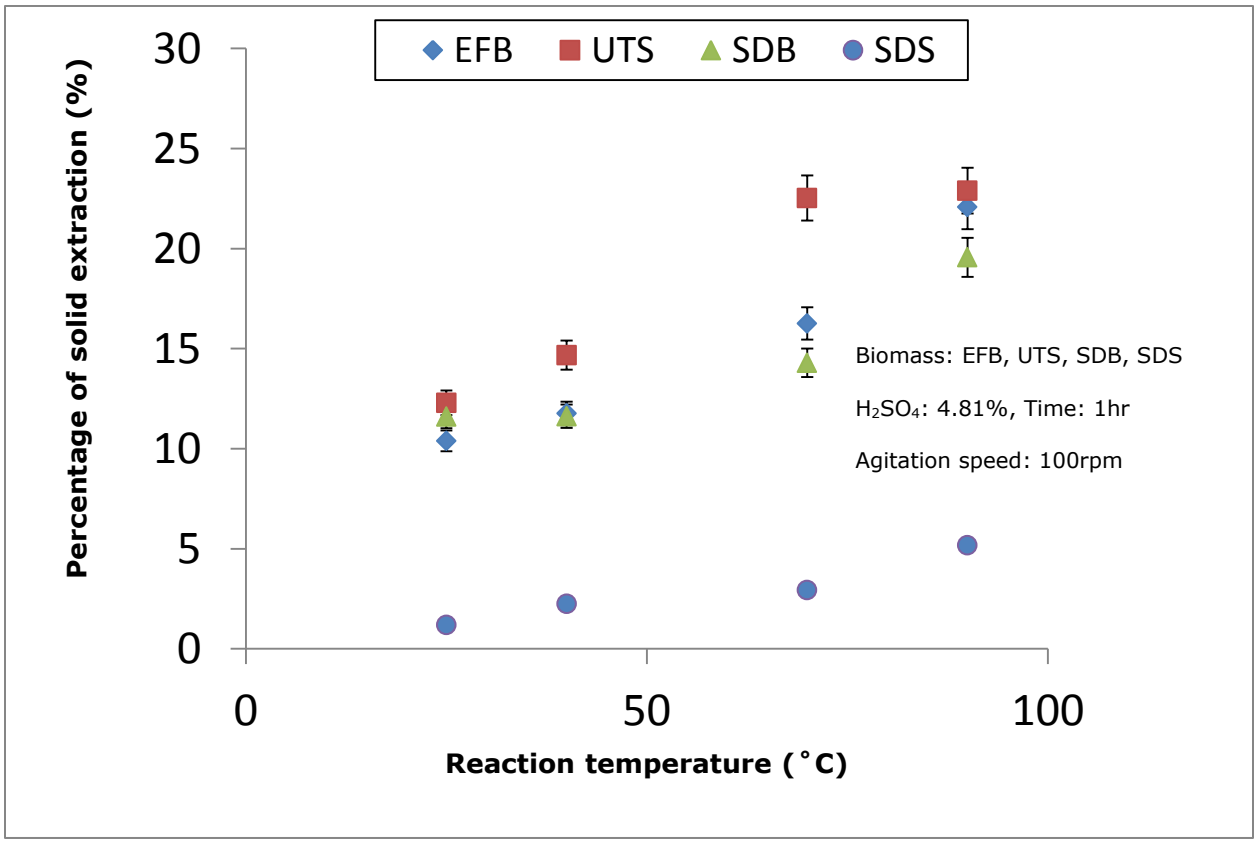

Figure 5-14: Effect of reaction temperatures on solid extraction from biomass samples

From Figure 5-14, it can be seen that extraction increases for all the samples as temperature increases. At 70˚C, UTS, EFB, SDS and SDS show 22.53%, 16.26%, 14.29% and 2.94% extraction respectively and UTS show 38.56% more extraction compared to next highest EFB. Again at 90˚C, UTS, EFB, SDS and SDS show 22.89%, 22.07%, 19.57% and 5.17% extraction respectively and UTS shows 3.72% more extraction compared to next highest EFB. UTS sample shows more extraction than SDS in acid solution because lignin is more in SDS (20-30.72%) compared to UTS (15-25%) and acid can extract less lignin Macintosh and Vancov, 2010). So 70˚C can be the best temperature for UTS extraction experiment and UTS has been chosen for pyrolysis experiment with tubular furnace and the designed reactor.

5.8.5 Effect of retention time on extraction

The extent of contact between biomass substrates and reacting solvent is essential for solid extraction process and hence the length of contact time on solid percentage extraction was studied. A control run at 0 hours of contact time was conducted to study the effect of contact time on solid extraction. For all samples, solid extraction was increased with increasing contact time compared to the control. UTS showed the optimum contact time as 4 hours, followed by SDB, SDS and EFB as 5, 6 and 24 hours respectively (Figures 5-15 to 5-16).

From Figure 5-15 it can be seen that EFB gives maximum extraction (31.66%) at 28 hrs residence time and the closest is 30.77% which is at 24 hrs residence time. EFB gives extraction 29.40% at 17 hrs and 26.52% at 15 hrs. All of these are much long time and it is not a viable option to use EFB as the biomass for pyrolysis.

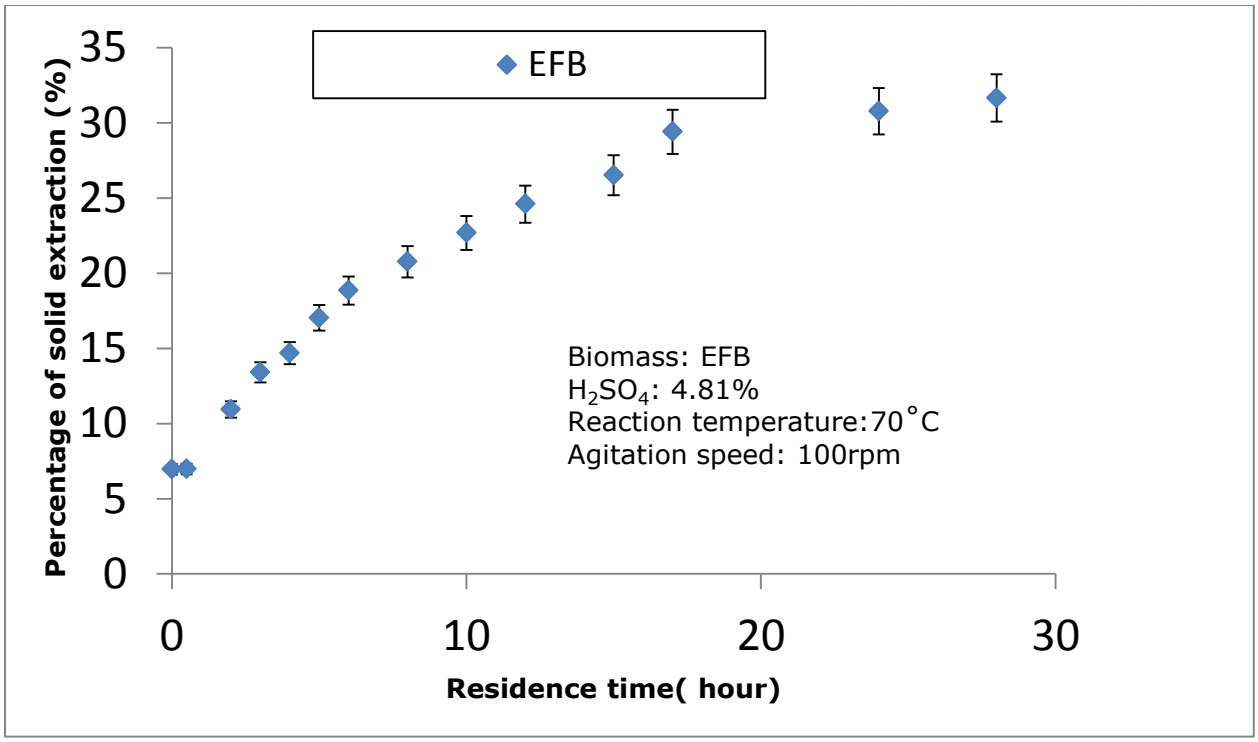

Figure 5-15: Effect of retention time on solid extraction from EFB biomass

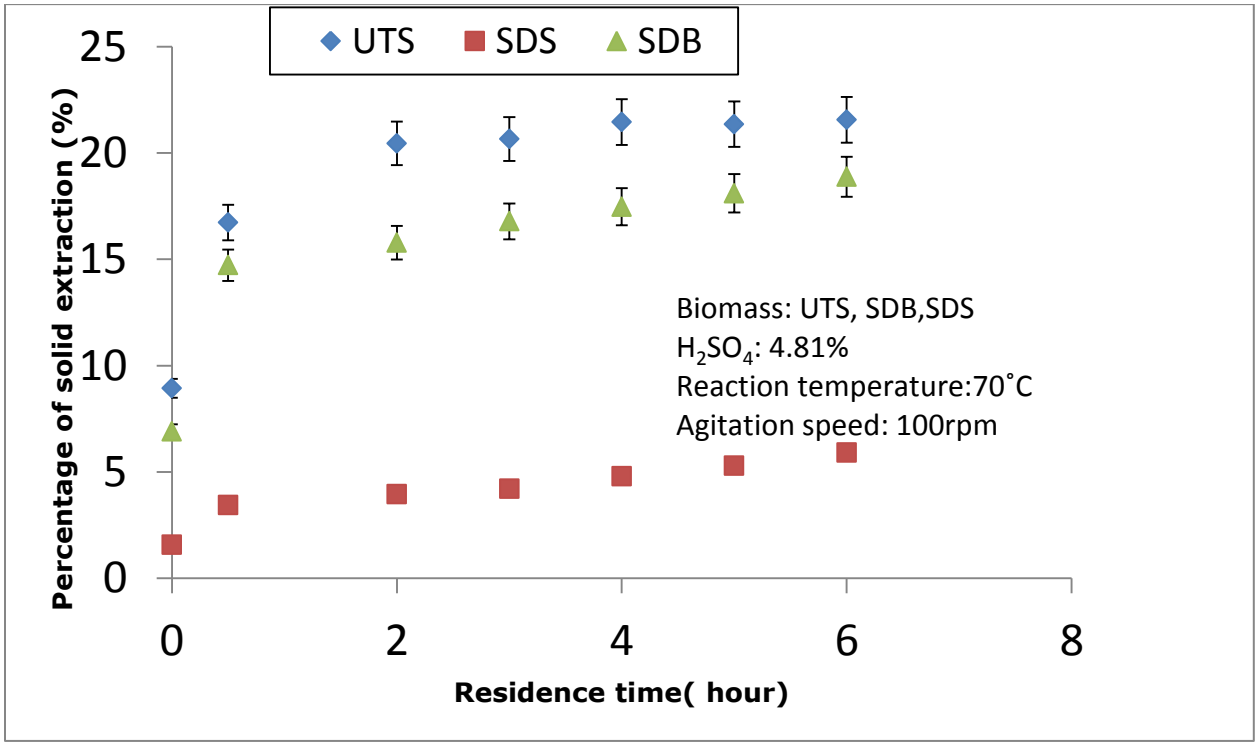

Figure 5-16: Effect of retention time on solid extraction from biomass samples

From Figure 5-16, it can be seen that for UTS the extractions for 4, 5 and 6 hrs are almost same (21.46, 21.36 and 21.55% respectively), so 4 hrs can be chosen as the optimum for UTS. For SDB, the extractions for 4, 5 and 6 hrs are 17.47, 18.11 and 18.88% respectively and the extraction of 5 and 6 hrs are very close. So 5 hrs is chosen optimum for SDB. For SDS, the extractions for 4, 5 and 6 hrs are 4.79, 5.29 and 5.9% respectively and 5 and 6 hrs are very close. So 6 hrs is chosen optimum for SDS. Also UTS gives more extraction (21.46%) than SDB (18.88%) and SDS (5.90%) at lesser time. So, comparing all these, UTS has been chosen as the biomass for pyrolysis. Analyses like effect of retention time and reaction temperatures on solid extraction from biomass using base solution is recommended as future work.

5.8.6 Effect of acid or base concentration on ash extraction

The effect of acid and base concentrations on ash extraction was studied while keeping the pre-treatment parameters constant. The concentrations of both acid and base were increased while maintaining the other process parameters constant. The percentage of ash extraction increased with increasing acid concentrations and decreased with increasing base concentrations for all samples with the exception of SDB with base (Figures 5-17 to 5-19)**.** Ash extraction is more for acid than base because more solid leached as lignin when washed with base (Mohammad et al., 2012 and Misson et al., 2009; Das et al., 2004). Biomass pre-treated with alkali solid loss is reported 13 to 24% more compared to acid (Mohammad et al., 2012). Total solid release/ extraction was maximum when biomass was pre-treated with NaOH represented 4.3 to 5.6 fold higher compared to samples pre-treated in the absence of alkali (Macintosh and Vancov, 2010).

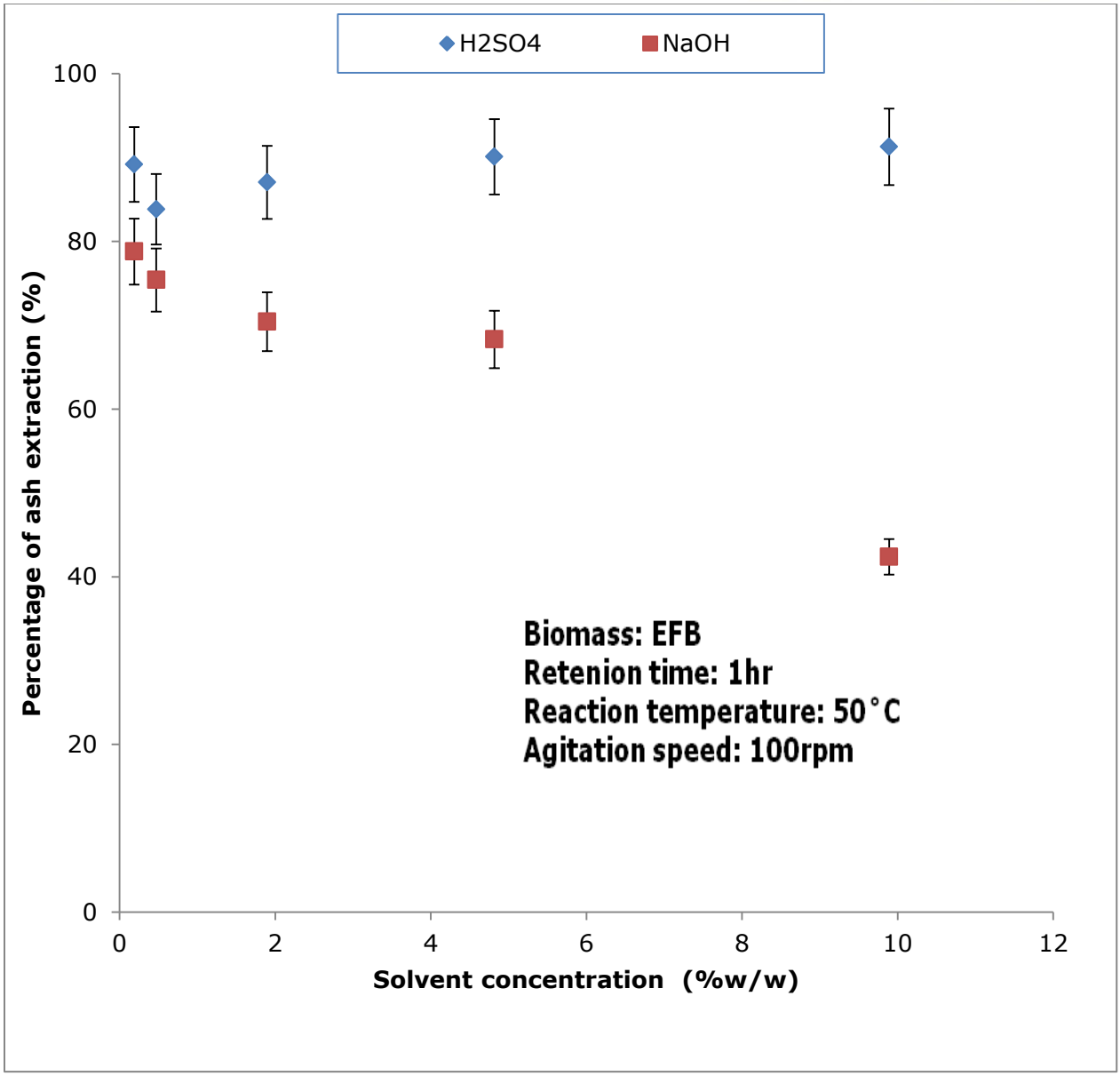

Figure 5-17: Effect of solvent concentration on ash extraction from EFB biomass

From Figure 5-17, it can be concluded that ash extraction increased with increasing acid concentration and the increment is 2.1% (from 89.18% to 91.28%) over the concentration range (from 0.19% to 9.89%) used while it decreased by 36.4 % (from 78.79% to 42.39%) for alkali for the same concertation range for EFB which is comparable with literature (Mohammad et al., 2012 and Misson et al., 2009; Das et al., 2004).

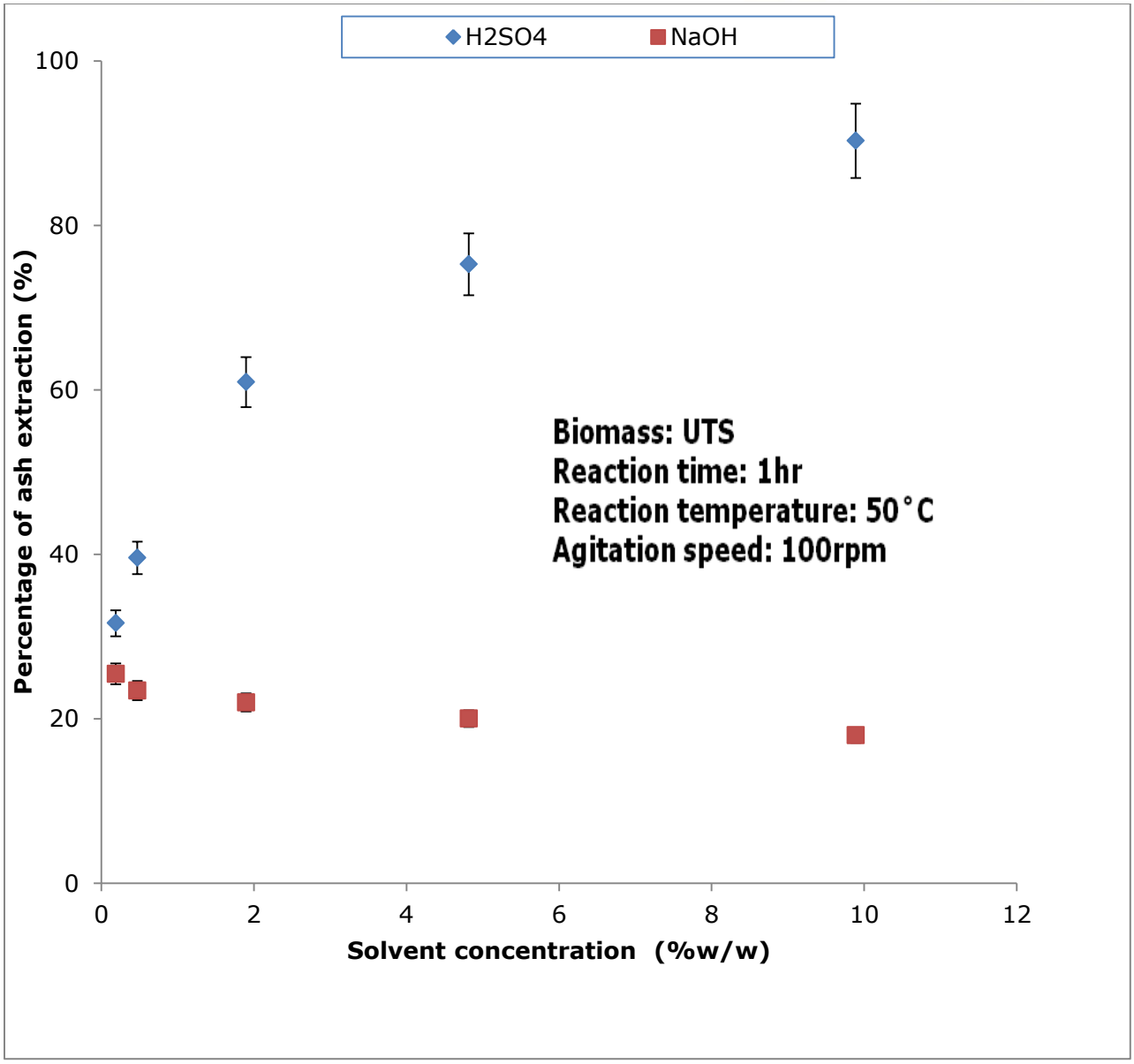

Figure 5-18: Effect of solvent concentration on ash extraction from UTS biomass

From Figure 5-18, it can be concluded that ash extraction increased with increasing acid concentration and the increment is 58.68% (from 31.62% to 90.30%) over the concentration range (from 0.19% to 9.89%) used while it decreased by 7.47% (from 25.46% to 17.99%) for alkali for the same concertation range for UTS which is comparable with literature (Das et al., 2015, Mohammad et al., 2012 and Misson et al., 2009).

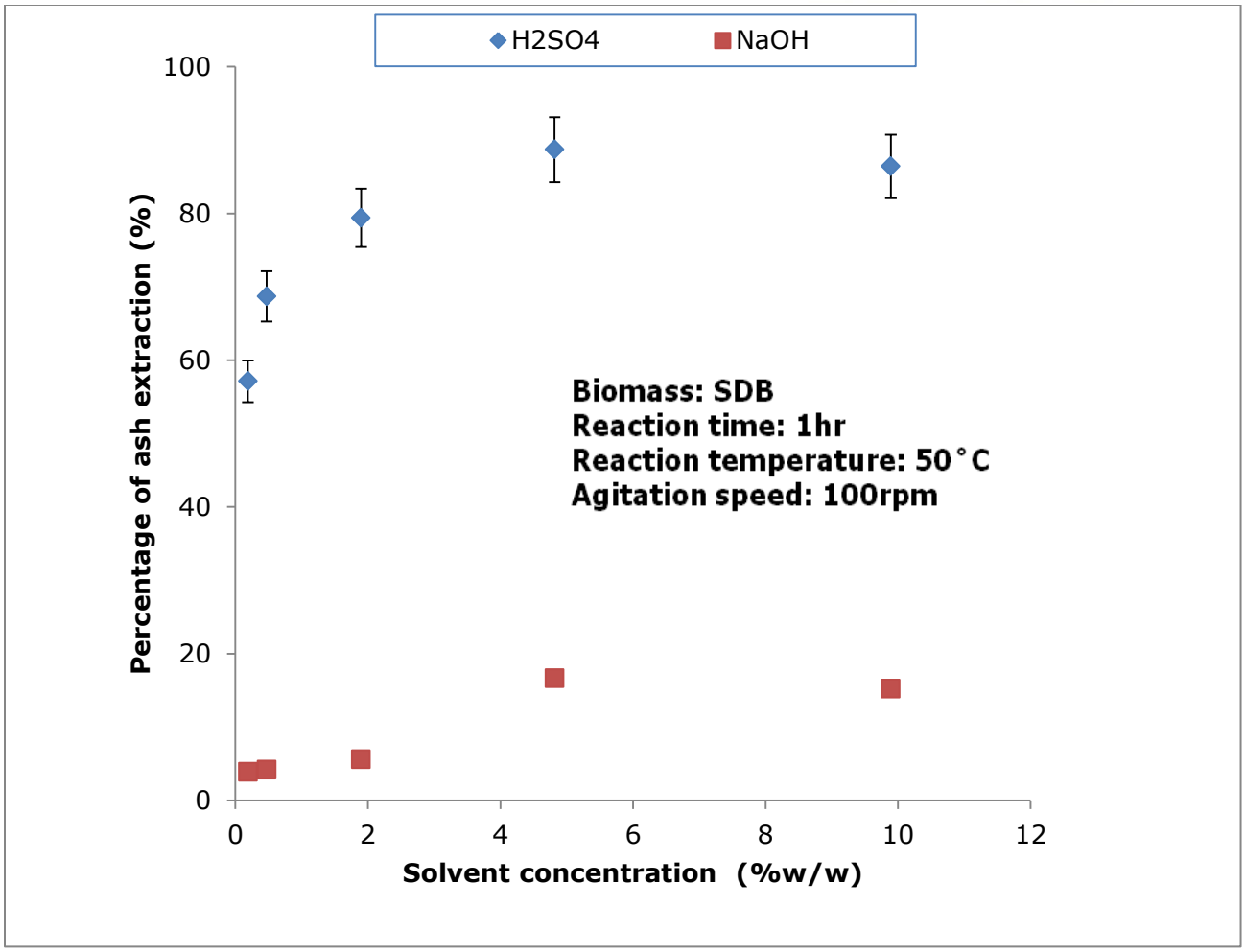

Figure 5-19: Effect of solvent concentration on ash extraction from SDB biomass

From Figure 5-19, it can be concluded that ash extraction from SDB increased with increasing acid and base concentration (from 0.19% to 9.89%) and the increment is 31.57% (from 57.11% to 88.68%) and 12.73% (from 3.88 to 16.66% 57.11%) for acid and alkali respectively which is comparable with literature (Mohammad et al., 2012; Misson et al., 2009; Das et al., 2004).

5.8.7 Effect of pre-treatment on calorific value and ash content of UTS: The calorific value and ash content of not pre-treated and pre-treated UTS samples are shown in Table 5-8 below.

Table 5-8: Comparison of calorific value and ash content of UTS.

Biomass sample	Calorific value (MJ/kg)		Ash content (%)	
	Not pre-treated	Pre-treated	Not pre-treated	Pre-treated
UTS	16.36	18.73	6.15	0.026

5.8.8 Effect of nitrogen gas flow- rate on products yield from UTS pyrolysis

Sweeping the reactor with increasing N_2 flowrates increases the bio-oil yield because increasing flowrates shorten the vapour residence time thus reduce their chances of secondary reactions (thermal cracking, re-polymerization and re-condensation) that lead to char and radical formations. The increase in nitrogen gas flow rate from 10 to 30 ml/min

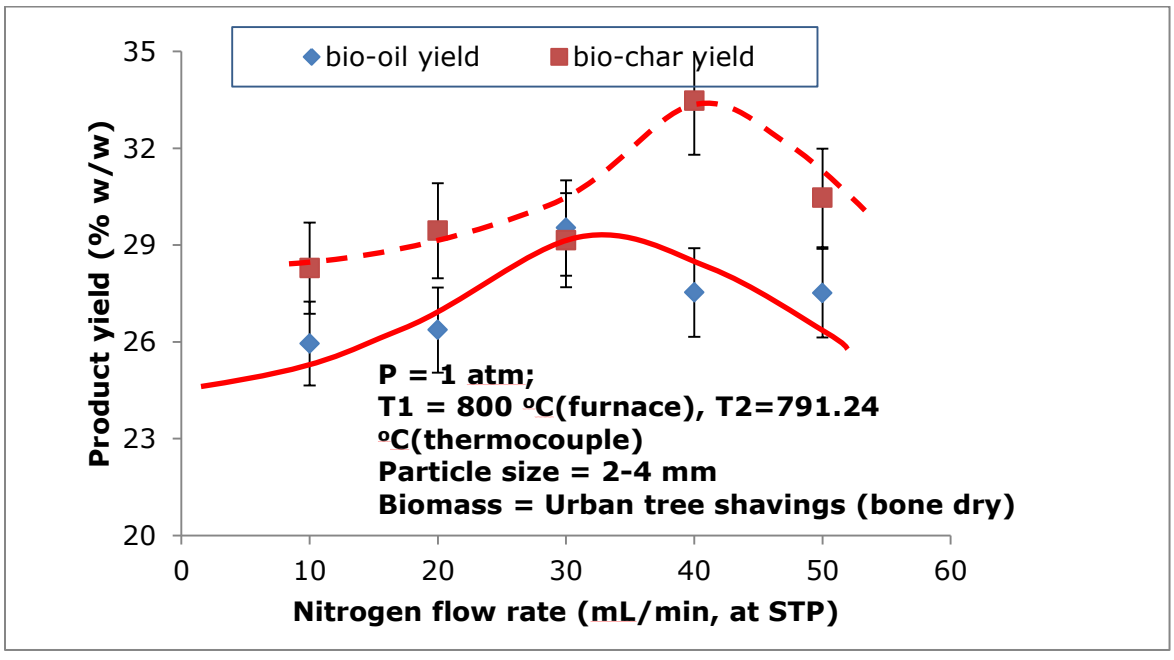

Figure 5-20: Effect of nitrogen flow rate on pyrolysis product yield from urban tree shavings

increased the bio-oil yield from 25.29% to a maximum of 29.52% (Figure 5-20) for untreated UTS pyrolysis. Further increased, from 30 to 50 ml/min, reduced the bio-oil yield

from 29.52% to 27.90% which could be due to shorter residence time of the vapour in the condenser coils which lead to insufficient heat exchange (Soetardji et al., 2014;Treedet and Suntivarakorn, 2011; Keles et al., 2011; Pütün 2010; Uzun et al., 2007).

Figure 5-20 also shows the effect of nitrogen gas flow rate on bio-char yield. The increase in nitrogen gas flow rate from 10 to 40 ml/min increased bio-char yield from 28.28% to 33.47%. The increase in bio-char yield when the flow rate is increased may be due to un-burned UTS in the reactor. Further increased in nitrogen gas flow rate from 40 to 50 ml/min resulted in decreased in bio-char yield from 33.47% to 30.46% and it due to some of the char was driven away.

5.8.9 Effect of pyrolysis temperature on products yield from UTS pyrolysis

Figure 5-21 shows the effect of pyrolysis temperature on bio-oil and bio-char yields from untreated UTS pyrolysis. The increase in pyrolysis temperature from 450 to 600˚C

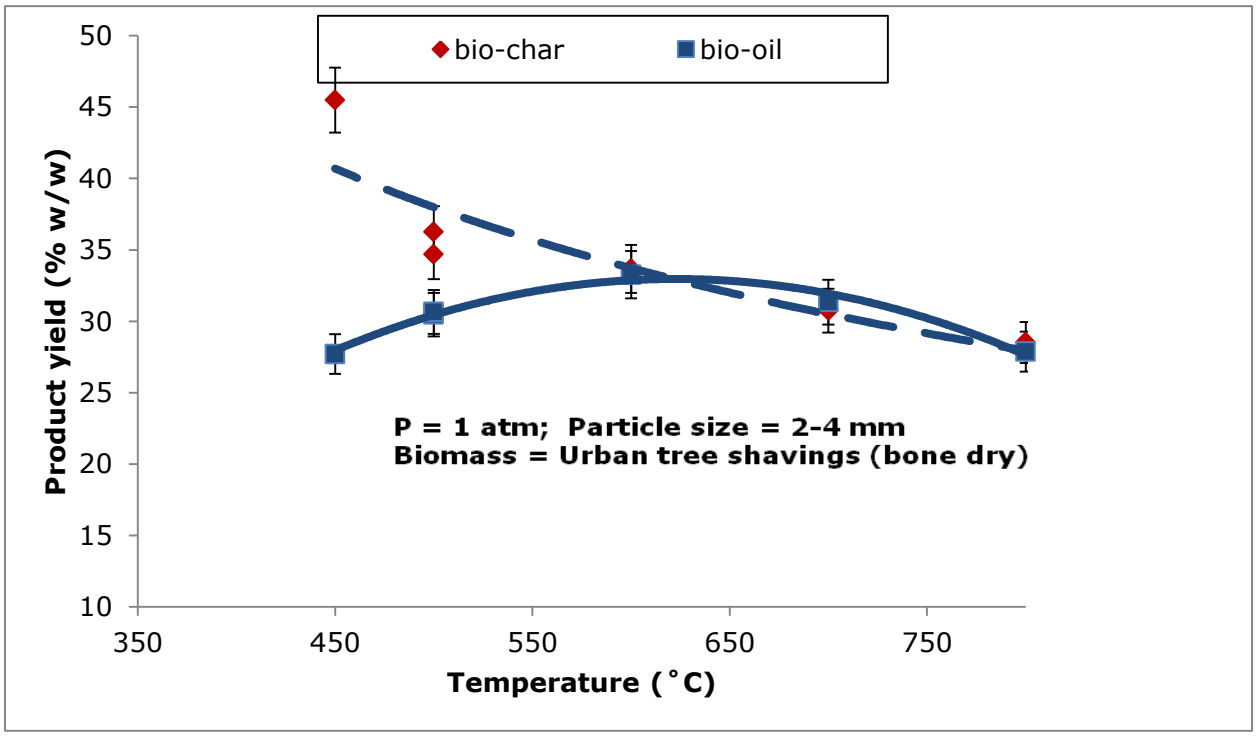

Figure 5-21: Effect of temperature on pyrolysis product yield from urban tree shavings

increased the bio-oil yield from 27.70 to a maximum of 33.26%.This increase in the oil yield may be as a result of degradation of more lignin, which usually occurs at such a high temperature. Further increased in pyrolysis temperature from 600 to 800°C decreased the bio-oil yield from 33.26% to 27.8% which can be attributed to secondary reactions of pyrolysis vapor at elevated temperature (Imam and Capareda 2012; Jung et al., 2008). However, bio-char yield decreased with rise in pyrolysis temperature and reached a minimum value of 28.51% at 800°C. This is not surprising since the devolatilization of organic materials progresses with increasing temperature. More dehydration of hydroxyl groups and decomposition of the lignocellulose structure are expected to increase with rise in temperature (Muradov et al. 2012; Imam and Capareda 2012; Cao and Harris 2010; Demirbas 2004).

Biomass from urban tree savings was selected among the four collected biomass samples (EFB, SDB, SDS and UTS) for the subsequent pyrolysis experiments. The semi-batch pyrolysis results were compared with the continuous process rig operations. The raw and pre-treated UTS were pyrolyzed in a batch tubular furnace at 600°C with nitrogen flowrate of 30 ml/min that resulted in maximum bio-oil yield of 39.43% and 27.67% respectively. Water content and caloric value of bio-oil were measured by Karl Fisher Titrator (ASTM E 203-01) and Bomb Calorimeter respectively. The properties of bio-oil produced from treated and untreated UTS are summarized below in Table 5-9.

Table 5-9: Properties of bio-oil produced from UTS

Type of UTS	**Bio-oil p^H**	**Water content in bio-oil (%)**	**Bio-oil calorific value (MJ/kg)**
Raw	3.62-3.80	39-59	24.2-28.3
Treated (Sample-1)	3.30	42	22.1
Treated (Sample-2)	3.09	45	27.1

5.9 Napier Grass (NG) pyrolysis and bio-oil characterization

Raw and pre-treated (washed with water) Napier grass was pyrolyzed in the tubular furnace at 600°C and at 30 ml/min nitrogen flow-rate. The bio-oil was characterized immediately after production. Bio-oil yield varies from 30.63% to 40.13% for raw Napier Grass and 29.43% to 31.53% for pre-treated (washed with water) Napier grass. Water content and caloric value of bio-oil were measured by Karl Fisher Titrator (ASTM E 203-01) and Bomb Calorimeter respectively. The bio-oil properties are summarized below in Table 5-10.

Table 5-10: Properties of bio-oil produced from NG

Type of NG and severity of pre-treatment used	**Bio-oil P^H**	**Water content in bio-oil (%)**	**Bio-oil calorific value (MJ/kg)**
Raw	2.82-3.18	51-64	23.2-26.3
Treated (0 min, 25 °C)	2.97	49	23.1
Treated (30min, 25 °C)	2.43	42	26.1

It can be seen from the above table that bio-oil water content and p^H decreased and calorific value increases with pre-treatment severity. Increment in calorific value for higher pre-treatment time is because; oil contained less water has high calorific value and vice versa. The designed rig can handle a wide range of biomass for pyrolysis, so NG was used as another source.

The non-condensable from NG pyrolysis was allowed to pass through a water scrubber and then a silica gel scrubber before it passed through a water scrubber for final release to the environment. During pyrolysis operation the non-condensable gas was monitored all the time. Results of non-condensable gas was analysed with Drager X-am 5000 analyser for raw and treated NG pyrolysis are shown below in Table 5-11.

Table 5-11: Non-condensable gas analyses for raw and treated NG pyrolysis.

Type & mass of NG used	Gas analysis temperature(°C)	CH_4 LEL%	H_2 ppm	H_2S ppm	CO Vol%	CO ppm
Raw 30gm	450-500	0	N.D.	21	0.13	1300
	500-550	2	N.D.	24	0.19	1900
	550-600	15	N.D.	36	>>0.2	N.D.
	600-630	49	N.D.	79	>>0.2	N.D.
Raw 50gm	450-500	0	1720	10	0.028	280
	500-550	16	N.D.	N.D.	>>0.2	N.D.
	550-600	64	N.D.	N.D.	>>0.2	N.D.
	600-630	67	N.D.	N.D.	>>0.2	N.D.
Treated(0min, 30gm)	450-500	0	930	9	0.052	520
	500-550	12	N.D.	68	>>0.2	N.D.
	550-600	35	N.D.	103	>>0.2	N.D.
	600-630	60	N.D.	103	>.0.2	N.D.
Treated(30min, 30gm)	450-500	0	1080	12	0.001	10
	500-550	11	N.D.	67	0.097	970
	550-600	16	N.D.	67	>>0.2	N.D.
	600-630	31	N.D.	82	>>0.2	N.D.

N.D =Not Detectable

It can be seen from the above table that gas production increases with increasing mass of raw NG. For instance, CH_4 LEL% increases from 49 to 67% at highest temperature from 30 and 50 gm of raw NG respectively. H_2 is once detectable at low temperature, all other not detectable for 30 and 50 gm of raw NG. H_2S increases from 79 ppm to not detectable level at highest temperature from 30 and 50 gm of raw NG respectively. CO production increases from 1300 ppm to not detectable level at highest temperature from 30 gm of raw NG and from 280 ppm to not detectable level for highest temperature from 50 gm of raw NG. In case of treated NG, production of CH_4, H_2S and CO drops but H_2 production increases significantly with pre-treatment severity. For instance CH_4 LEL% decreases from 60 to 31% at highest temperature from 30 gm of NG treated for 0 and 30 minutes respectively. H_2S decreases from 103 to 82 ppm at highest temperature from 30 gm of NG treated for 0 and 30 minutes respectively. CO production decreases from not detectable level to 970 ppm at 500-550°C temperature from 30 gm of NG treated for 0 and 30 minutes respectively. H_2

production increases from 930 to 1080 ppm at 450-500°C temperature from 30 gm of NG treated for 0 and 30 minutes respectively. H_2 production was beyond the detection limit above 500°C for all types of NG.

5.10 Conclusion

The pre-treatment experiments of biomass ((EFB, UTS, SDB and SDS) have been performed successfully using base and acid solution and pure water and the results of this experiments that affect the performance of the new designed reactor have been analysed depending on the characteristics of the biomass types used. Based on the results of these experiments, the reactor operation was optimized for different feedstock. Comparing all the pre-treatment results, UTS has been chosen as the preferred biomass for producing bio-oil by both tubular furnace and the designed reactor. The bio-oil yield was the maximum at 30 ml/min nitrogen flowrate while bio-char yield was maximum at 40 ml/min nitrogen flowrate and bio-oil yield was maximum at pyrolysis temperature of 600°C in the tubular furnace. Sweeping the reactor with increasing N_2 flowrates increases the bio-oil yield because increasing flowrates shorten the vapour residence time thus reduce their chances of secondary reactions (thermal cracking, re-polymerization and re-condensation) that lead to char and radical formations. The increase in bio-char yield when the flow rate is increased may be due to un-burned UTS in the reactor. The increase in the oil yield may be as a result of degradation of more lignin, which usually occurs at such a high temperature. Pyrolysis of raw UTS and NG in tubular furnace resulted in higher bio-oil and bio-char yield compared to treated samples. So, the objective to define the conditioning and pre-treatment requirements of biomass for the pyrolysis reactions in the new FBR has been achieved.

CHAPTER 6: PYROLYSIS AND PRODUCTS CHARACTERIZATION

6.1 Overview

Bio-oil, syngas and bio-char were produced and characterized from untreated urban tree shavings at 600^0C by pyrolysis. Characterization of the products was performed using various approaches (Karl Fischer water-content tests, Calorimeter Bomb, FTIR, GC-MS, SEM and CHNS/O analyses and Drager X-am 5000). FTIR analysis of bio-oil showed about 9 functional groups of molecules and GC-MS study indicated that the bio-oil contained about 22 compounds. The results also indicated that the bio-oil was acidic and contained high levels of oxygen. Syngas compositional analysis shows the presence of CH_4 as the maximum component (in vol. %). HHV of bio-char was increased compared to biomass. Analysis of elemental composition of bio-char shows increase in carbon and sulphur content, decrease in oxygen and nitrogen content compared to biomass. Before the beginning of the pyrolysis process, the biomass used was identified and its proximate analysis was performed as described in chapter 4. The ultimate analysis of biomass was also performed using Perkin Elmer 2400 Series II CHNS/O analyser.

6.2 Pyrolysis

In order to control the mass fractions, pyrolysis was carried out in the designed reactor in a batch process at a constant temperature of 600^0C. Untreated UTS biomass was charged from the top of the reactor on the distributor. The heater and the preheater were turned on at a time. The water circulation through all four condensers was done by a submersible pump which was kept in a drum continuously filled with water from tap by a long hose. The temperatures of the reactor and preheater were shown on the control panels and also monitored online along with the cyclones and condensers temperatures. When the reactor temperature reached around 400^0C, the fluidizing gas (N_2) supply was started. The fluidizing gas swept the pyrolytic vapour from the reactor as it produced and was cleaned in cyclones

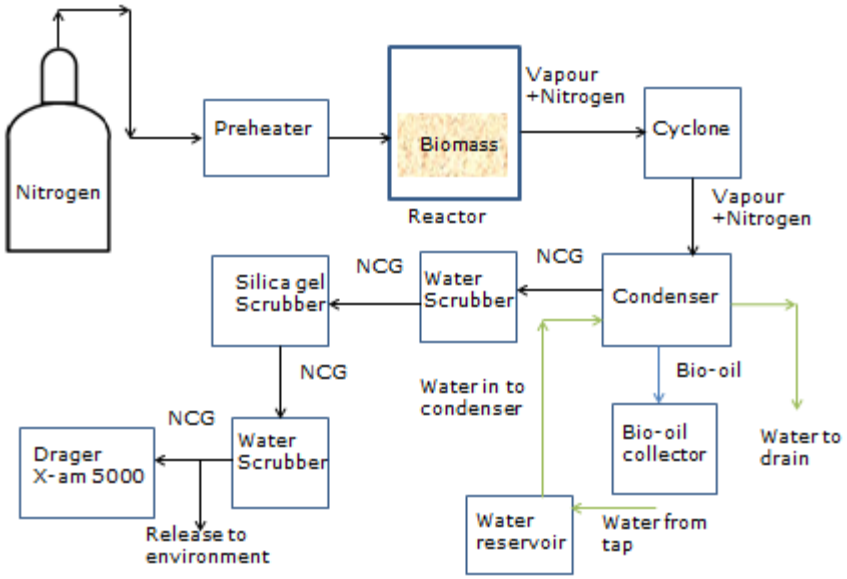

Figure 6-1: Process flow diagram (PFD) of the fluidized bed system to produce bio-oil by pyrolysis.

and the cleaned vapour was condensed into bio-oil in the condensers and was collected from the collector attached under the condensers and was stored for further analysis. Syngas (Non-condensable gas or NCG) was analysed by Drager X-am 5000 analyser. Bio-char was collected from the top of the distributor for mass balance and was further analysed.

6.3 Products characterization: A WalkLAB microcomputer P^H meter TI9000 (Trans Instruments, Singapore) was used to determine the p^H of the bio-oil and water content was determined by Karl Fischer V20 volumetric titrator (Metler Toledo) according to ASTM E203 (2001). The higher heating value was determined using an oxygen bomb calorimeter (Parr 6100), according to ASTM D240 (2009). Ultimate analysis was performed using Perkin

Elmer 2400 Series II CHNS/O analyser. FTIR analysis of bio-oil was performed using FT-IR System purchased from Perkin Elmer, USA, model Spectrum RX1. GC/MS analysis of bio-oil was performed on a Perkin Elmer GCMS- model Clarus SQ 8S. The GC column used was Elite-5MS Capillary Column: Length: 30 m, I.D: 0.25 mm, Film Thickness: 0.25 µm, Temperature Limits: -60 to 325/350°C. The viscosity of bio-oil was detected using DV-E Viscometer, Brookfield, USA, spindle used no. S87. Non-condensable gas was analysed with Drager X-am 5000 analyser. EDX/SEM analysis of bio-char was performed by FESEM: FEI QUANTA 400F, USA. EDX: Oxford-Instruments INCA 400 with X-Max Detector.

6.4 Results and Discussion

6.4.1 Feedstock Characterization. Physical and elemental analyses of the biomass used for pyrolysis are presented in Table 6-1. These data were comparable to those of that in literature (Saidur, 2011; Imam and Capareda, 2012 and Boateng, 2007). Alkali metals contained in ash may act as catalysts for changes in the composition of pyrolysis products (Fahmi et al., 2007). However, such catalytic behaviour was not considered in this case because ash content is only 6.15%, and volatile content is high (78.79%)(Table 6-1).

Table 6-1: Proximate and ultimate analysis of biomass samples used for pyrolysis

Proximate analysis	**(wt. %, db)**	**Ultimate analysis**	**(wt. %, db)**
Moisture	15.36	C	45.34
Ash	6.15	H	6.61
Volatile Matter	78.79	O	41.54
Fixed Carbon*	15.06	N	0.35
Calorific value	17.36 MJ/kg(dry basis)	S	0.01

*by difference

6.4.2 Bio-oil characterization:

Elemental analysis and properties of bio-oil from untreated UTS pyrolysis at 600^0C are presented in Table 6-2.

Table 6-2: Ultimate analysis and physical properties of bio-oil

Ultimate analysis		**Physical properties**	
Element	**(Wt.%, db)**	**Properties**	**Value**
C	49.87	P^H	3.37-3.54
H	8.93	Moisture content (%)	32-46
O	39.19	HHV (MJ/Kg)	27-30
N	1.46	Viscosity, at 25^0C (cp)	2.86-3.97
S	0.55		

The chemical composition, and therefore the properties mentioned above, of bio-oil depend on the feedstock, pyrolysis conditions, and product collection methods. Herein, the chemical compositions of bio-oils produced from the above-mentioned biomass are reported. The P^H of fast pyrolysis bio-oil from untreated biomass is low (2 to 3) (Oasmaa et al. 2010). The bio-oil p^H was measured just after the production and was found to be in the range of 3.37 to 3.54 having about 18.5% higher p^H compared to literature. So, the produced bio-oil is less acidic compared to literature value which is turns is less corrosive. The bio-oil was highly oxygenated (39.19%), which is consistent with results of other studies that show a range of 35 to 40% oxygen in bio-oil (Imam and Capareda, 2012; Sukiran, 2009; Mullen, 2008; Boateng, 2007; Yanik, 2007; Scholze, 2001). Presence of oxygen results in lower energy density (Imam and Capareda, 2012). Moisture content of the bio-oil was 32 to 46%, resulting from the original feedstock moisture and the product of dehydration during pyrolysis reactions (Shihadeh, 2002). Sample of bio-oil produced is shown in Figure 6-2. The higher heating values are comparable to the literature value of between 16 and 36 MJ/Kg (Mortensen et al., 2011; Imam and Capareda 2012, Bridgwater, 2012). However, the value of the bio-oil sample is at higher end may be due to the source of biomass material used for pyrolysis. The viscosity of bio-oil sample is at the lower end of the range compared to literature value may be due to high water content in the sample (Imam and Capareda, 2012 and Boateng, 2007). However, the produced bio-oil can be used as transportation fuel

after upgrading (Augustinova et al., 2013; Imam and Capareda, 2012; Reyhanitash, 2013; Mortensen, 2013; Brown, 2014 and Ciddor et al., 2015).

Figure 6-2: Bio-oil sample kept in vials

6.4.2.1 FTIR analysis of bio-oil sample*:*

Fourier transform infrared (FTIR) spectroscopy is a powerful analytical technique to characterize the functional groups of pyrolysis bio-oil (Lievens et al., 2103). The infrared spectra of the bio-oil sample are shown in Figure 6-2 and the peaks of the functional groups in the bio-oil sample are listed in Table 6-3.

According to Figure 6-3, wavenumbers of substantial functional groups in bio-oil between 2000 and 3500/cm as well as between 625 and 1650/cm, which indicate the existence of O-H bonds, C≡C bonds, C=C bonds, C-H bonds, C-O-C bonds, C-O bonds etc. in bio-oil. These

functional groups demonstrated that there were alcohols, phenols, alkynes, ketones, aldehydes, quinines, alkanes, esters, ethers and hydroxyls in bio-oil. It is well known that

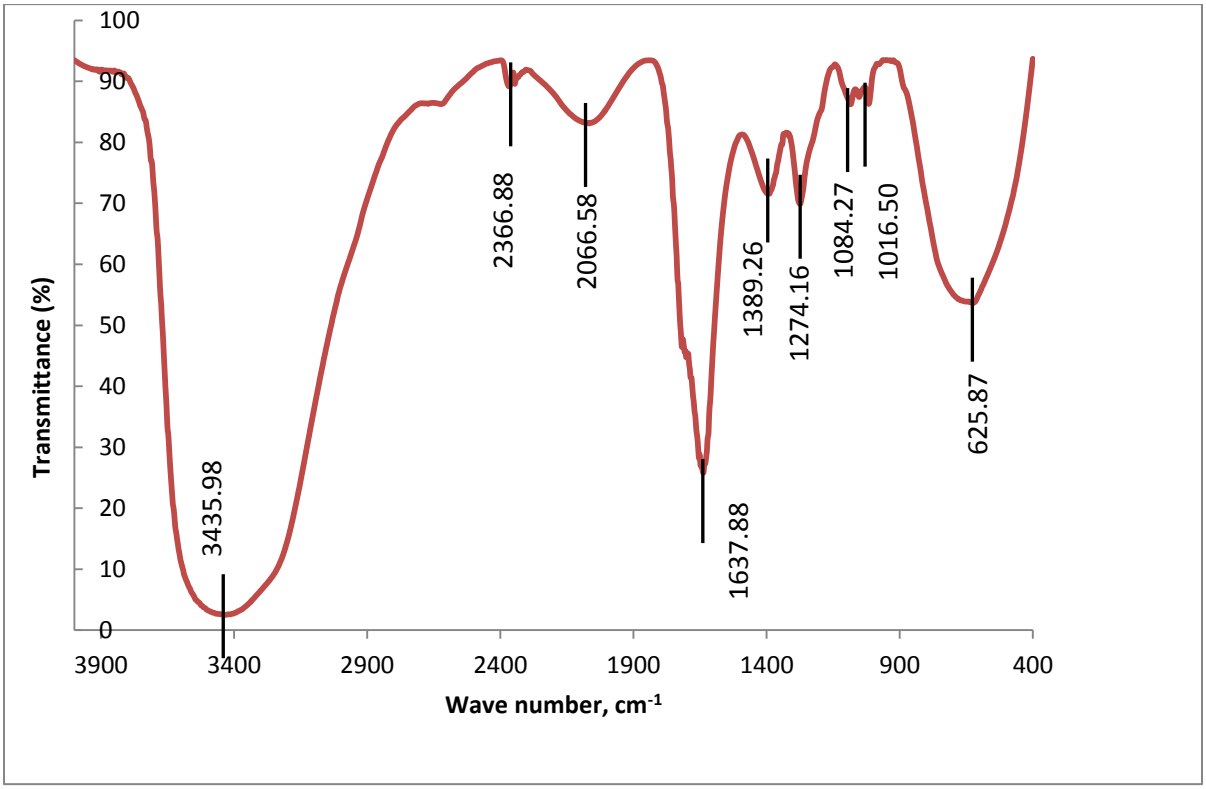

Figure 6-3: FTIR spectra of bio-oil sample

biomass contains cellulose, hemicellulose and lignin, which are totally CHO chemical compounds (Chen et al., 2010). So the FTIR analysis shows the functional groups of compounds having CHO elements.

Table 6-3: FTIR analysis of bio-oil for functional group

Frequency range (cm^{-1})	Group	Class of compound	Ref
3435.98	O-H stretching	Phenols, alcohols	Yang et al., 2014, Ozbay et al., 2006
2366.88	C≡C sharp	Alkynes	Wade, Jr., L.G. 2003

Frequency range (cm^{-1})	Group	Class of compound	Ref
2066.58	Conjugated with C=C, C≡C	Conjugated alkynes	Socrates, G. 2001
1637.58	C=C stretching	Ketones, quinine, aldehydes	Ozbay et al.,2006
1389.26	C-H bending	Alkanes	Ozbay et al., 2006
1274.16	C-O-C stretching	Phenol, esters, ethers	Yang et al., 2014, Ozbay et al., 2006
1084.27	C-O –C stretching	Phenol, esters, ethers	Ozbay et al., 2006
1016.50	C-O stretching	Primary hydroxyl	Valle et al., 2005
625.87	=C-H bending	Alkynes	Stuart, 2004

6.4.2.2 Gas chromatography-mass spectrometry (GC-MS) analysis of bio-oil sample:

The chromatogram of bio-oil sample is shown in Figure 6-4 and compounds detected are given in Table 6-4.

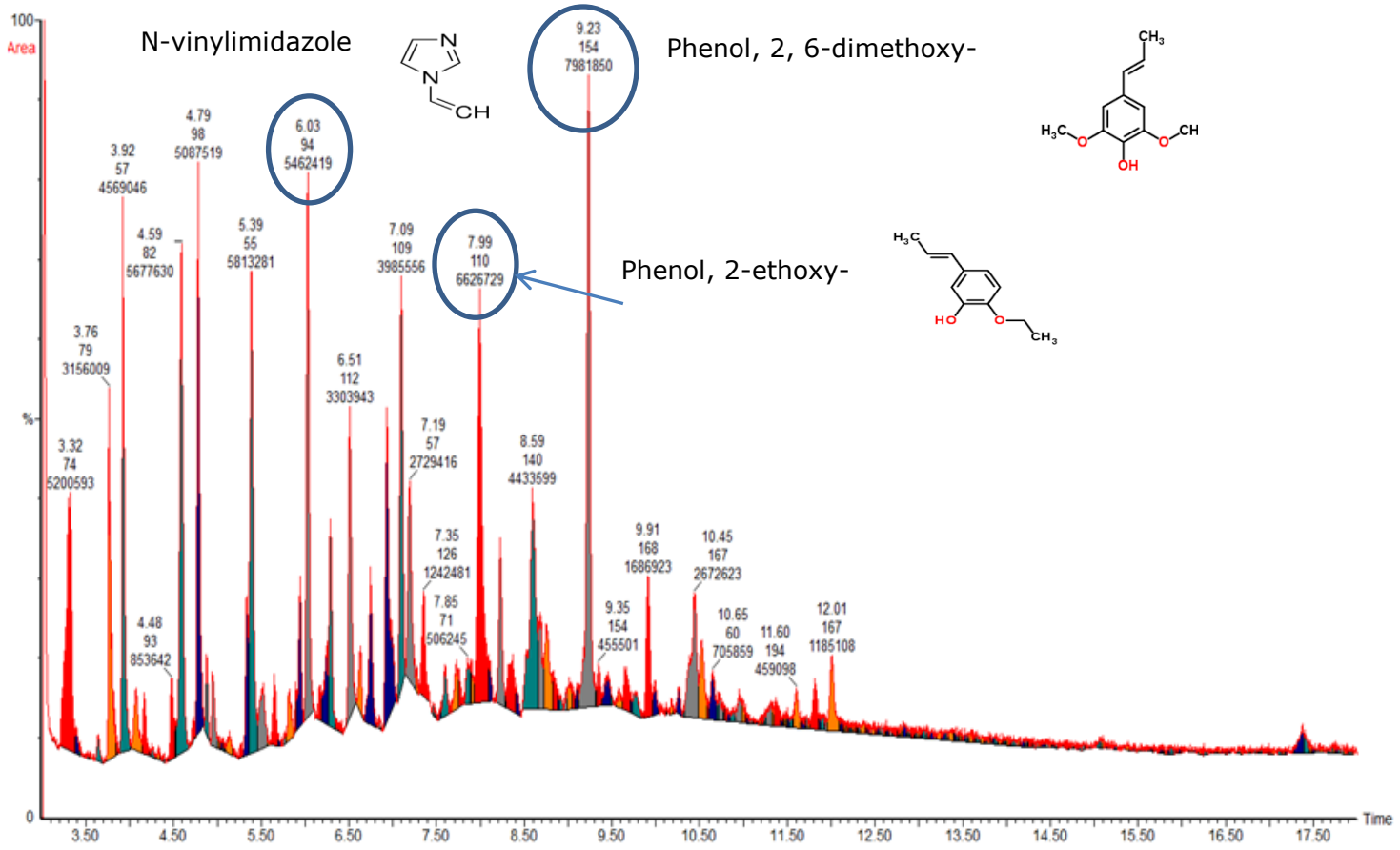

Figure 6-4: Chromatogram of bio-oil sample

Table 6-4: Compounds detected in pyrolysis oil from UTS

ID.	Retention time (sec)	(%) peak area	Compound name	Molecular Weight	Formula
1	3.32	7.047345	benzeneacetic acid, trimethylsilyl ester	208	$C_{11}H16O_2Si$
2	3.76	4.276721	2,4-hexadiyne	78	C_6H_6
3	3.92	6.191533	1,2,4,5-cyclohexanetetrol, (1.alpha.,2.alpha.,4.alpha.,5.beta.)-	148	$C_6H_{12}O_4$
4	4.48	1.156774	pyridine, 2-methyl-	93	C_6H_7N
5	4.59	7.69378	pentadecanal-	226	$C_{15}H_{30}O$
6	4.79	6.894118	but-1-en-3-ynyl methyl sulfide	98	C_5H_6S
7	5.39	7.877601	1,4-di(t-butylthio)but-2-ene	232	$C_{12}H_{24}S_2$
8	**6.03**	**7.402146**	**n-vinylimidazole**	**94**	**$C_5H_6N_2$**
9	6.51	4.477187	1,2-cyclopentanedione, 3-methyl-	112	$C_6H_8O_2$
10	7.09	5.400843	2-cyclopenten-1-one, 3,4,4-trimethyl-	124	$C_8H_{12}O$
11	7.19	3.698643	1,3-heptadiene, 5,5-dimethyl-	124	C_9H_{16}
12	7.35	1.683691	5-acetoxymethyl-2-furaldehyde	168	$C_8H_8O_4$
13	7.85	0.686015	cyclohexanol, 1-methyl-4-(1-methylethenyl)-	154	$C_{10}H_{18}O$
14	**7.99**	**8.979907**	**phenol, 2-ethoxy-**	**138**	**$C_8H_{10}O_2$**
15	8.59	6.007988	1,2-benzenediol, 3-methoxy-	140	$C_7H_8O_3$
16	**9.23**	**10.81624**	**phenol, 2,6-dimethoxy-**	**154**	**$C_8H_{10}O_3$**
17	9.35	0.617251	phenol, 2,6-dimethoxy-, acetate	196	$C_{10}H_{12}O_4$
18	9.91	2.285956	benzenamine, 2-methoxy-5-nitro-	168	$C_7H_8O_3N_2$
19	10.45	3.621682	mandelic acid, 3,4-dimethoxy-, methyl ester	226	$C_{11}H_{14}O_5$
20	10.65	0.956512	d-allose	180	$C_6H_{12}O_6$
21	11.60	0.622126	phenol, 2,6-dimethoxy-4-(2-propenyl)-	194	$C_{11}H_{14}O_3$
22	12.01	1.605945	5-(.beta.-bromoallyl)-5-(1-methylbutyl)barbituric acid	212	$C_{10}H_{12}O_5$

Analysis of the bio-oil produced from pyrolysis of UTS is presented as whole oil, collected from the four condenser canisters. Bio-oil from UTS is composed of a complex mixture of alcohols, long-chain hydrocarbons, sugars, aldehydes, acids, ketones, methyl esters, amines and aromatics which is comparable with the literature (Imam and Capareda, 2012; Mullen, 2008).

6.4.3 The Syngas Characterization

The total gas volume was estimated as 0.48 m^3 (Choren, 2015; Magnus, 2011). The syngas composition is shown in Table 6-5.

Table 6-5: Syngas (non-condensable) composition of UTS pyrolysis (N_2 free basis)

Name of gas	**Composition (volume %)**
CH_4	86.5%
CO	6.5%
H_2S	0.5%
H_2	6.5%

The syngas volumetric composition shows CH_4 as the maximum volume percent in it. Syngas composition shown above is done with the elements the analyser could detect where CO and H_2 shown the maximum level the Drager could detect, but presence of CO_2, C_2H_4, C_2H_2, C_2H_6 and others elements are also reported in literature (Jahirul et al., 2012, Bridgwater, 2000). The flammability of the syngas was performed during the pyrolysis of biomass using a torch with its flame lit by firing it before the syngas was passed over the flame. The Figures (6-5 a, b and c) show the syngas behaviour over flame from the torch. The syngas produced by the reactor from UTS was allowed to pass over the flame of the torch and it was observed that the syngas changed the colour of the flame from yellow to blue which is sign of combustion. So the syngas contains combustible gases. The syngas was passed over the flame from a short distance and also a bit away from the flame and both the times it was burning. Syngas has around half of the energy of natural gas, and can

be combusted to produce thermal energy for use in steam and electricity production (Ecoreps, 2015) and cleaned syngas can be converted into electricity by SOFC (Rabou et al., 2008). Syngas can be converted to liquid transport fuel and valuable chemicals by FT synthesis (Mills, 2015; Fedou, 2015 and Ricci, 2015).

Figure 6-5a: The flame of lighter before the syngas is passed on it

Figure 6-5b: The flame of lighter after the syngas is passed on it (the syngas changes the colour of the flame as it is burning).

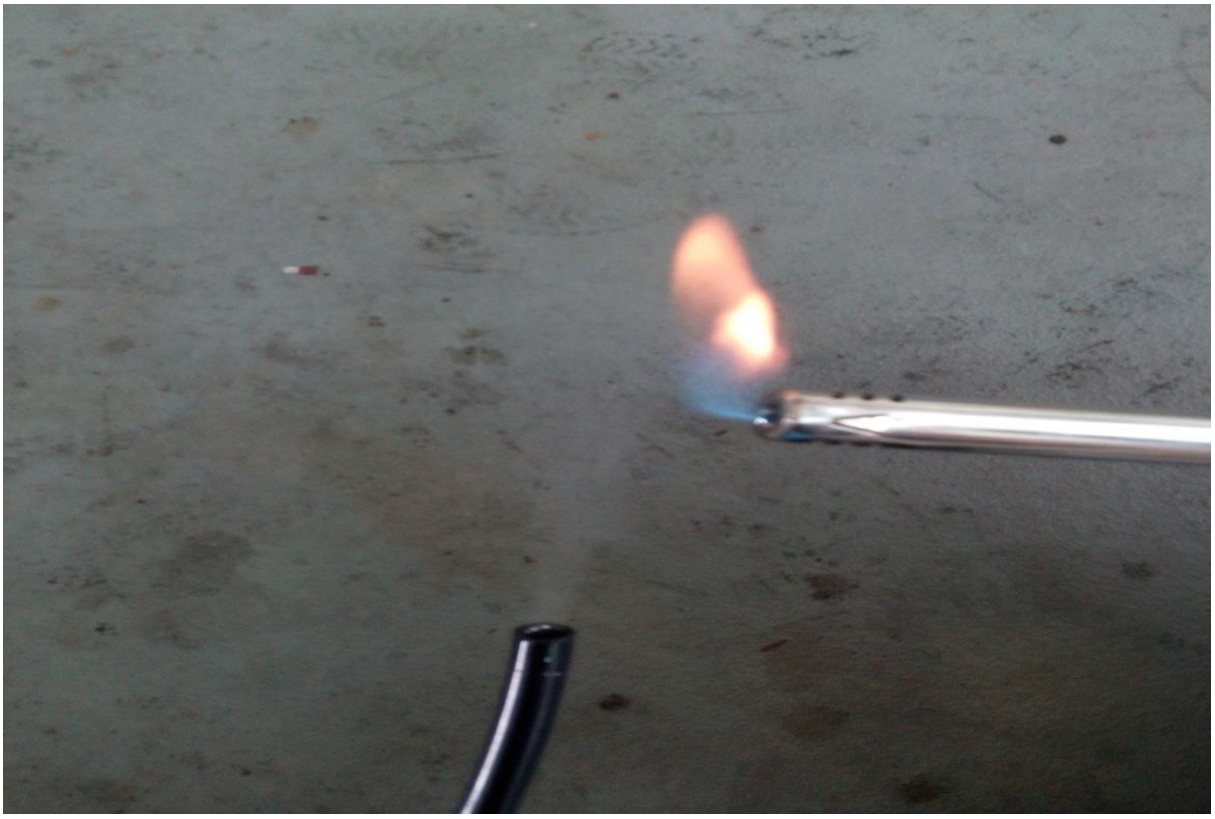

Figure 6-5c: The lighter after the syngas is passed on it (the syngas changes the colour of the flame as it is burning).

6.4.4 Bio-char characterization

Bio-char can be used as soil amendments or in production of porous adsorbents, such as activated carbon. An alternative use for the produced bio-chars is as a renewable solid fuel as the HHV values of bio-char were found between 21.65 and 28.49 MJ/Kg which is comparable to the literature (Abnisa et al., 2013; Brewer, 2012 and Sukiran, 2011). These values are comparable to those of some coals (Bilgen and Kaygusuz, 2008 and Akkaya, 2009). Due to various thermal cracking of organic functional groups on the surface of the mentioned UTS and evolution of volatiles, changes in the elemental composition of the bio-chars are expected. Char elemental analysis (Tables 6-6 a, b, c and d) shows that carbon and sulphur content increased, whereas oxygen contents decreased compared to biomass. A

similar trend was reported in literature (Abnisa, 2013; Onay, 2007). Losses in oxygen are explained by breaking of weaker bonds within bio-char's structure and the bio-char becoming highly carbonaceous at higher pyrolysis temperatures (Onay, 2007, Cai et al., 1996). In Figures 6-6 (a, b, c and d) (electron image of char sample), and 6-7 (a, b, c and d) (spectrum of char sample) are shown.

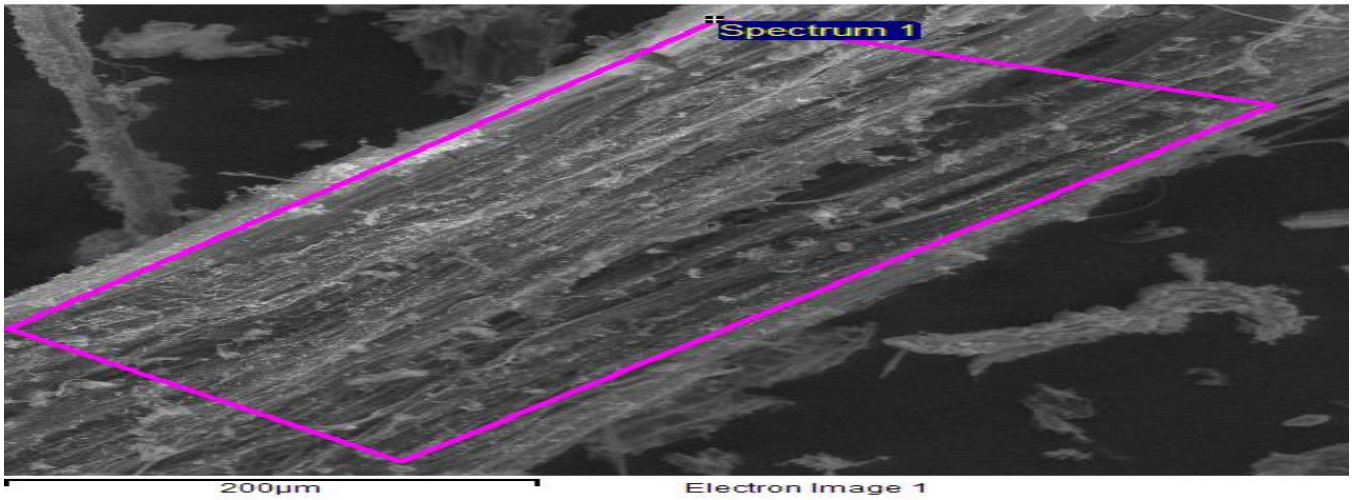

Figure 6-6 a: Electron image of char sample

Table 6-6 a: Char elemental analysis

Element	Weight%	Atomic%
C K	70.58	80.60
O K	17.71	15.18
S K	0.84	0.36
Cl K	1.50	0.58
K K	7.67	2.69
Ca K	1.70	0.58
Totals	100.00	

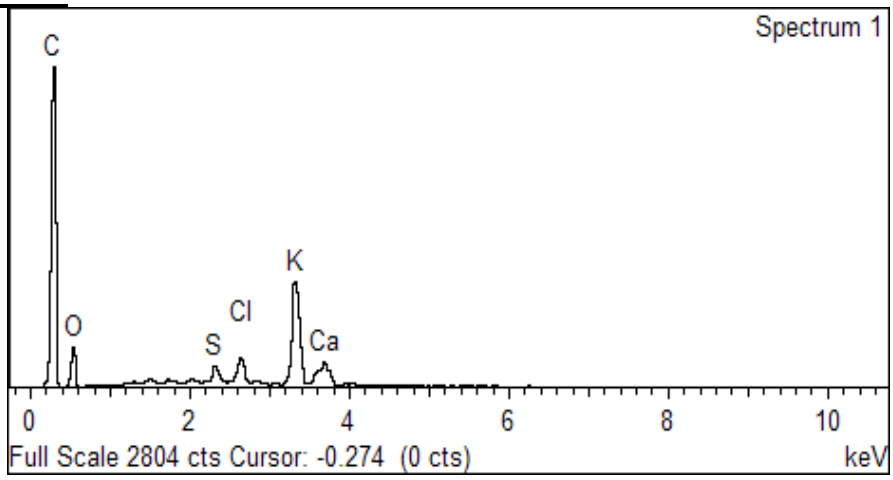

Figure 6-7 a: Spectrum of char sample

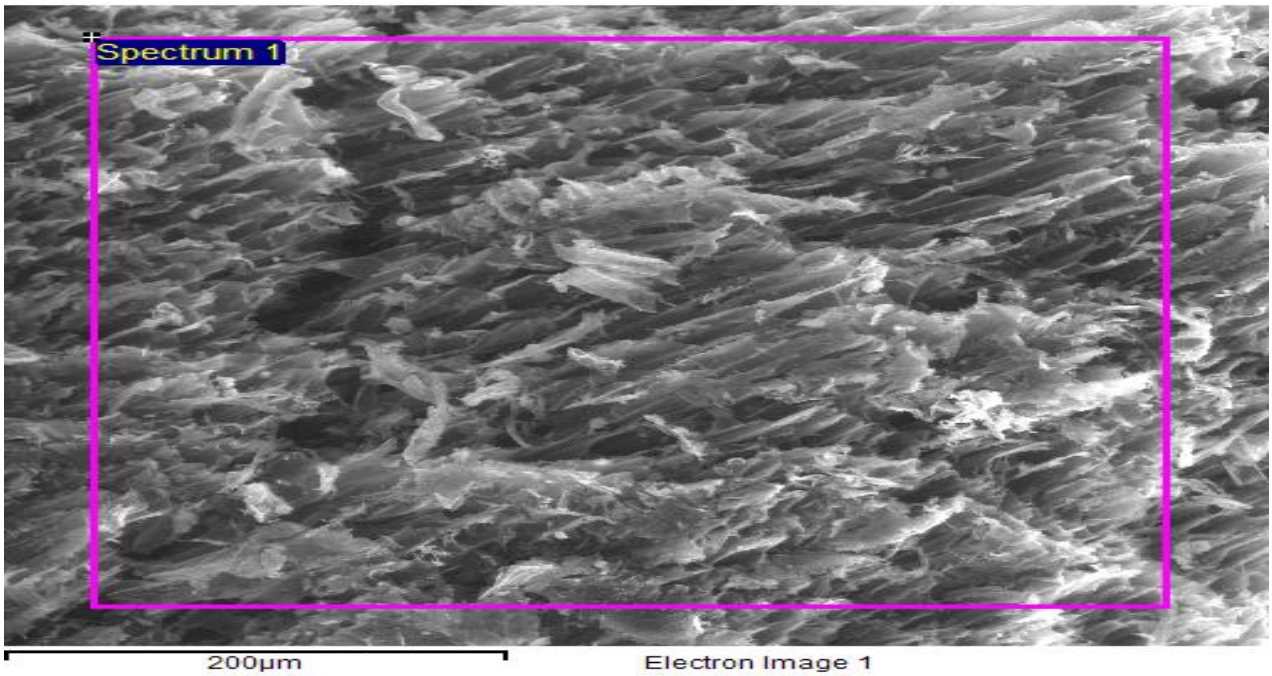

Figure 6-6 b: Electron image of char sample

Table 6-6 b: Char elemental analysis

Element	Weight%	Atomic%
C K	79.31	84.27
O K	18.98	15.14
Al K	0.19	0.09
K K	1.09	0.36
Ca K	0.42	0.13
Totals	100.00	

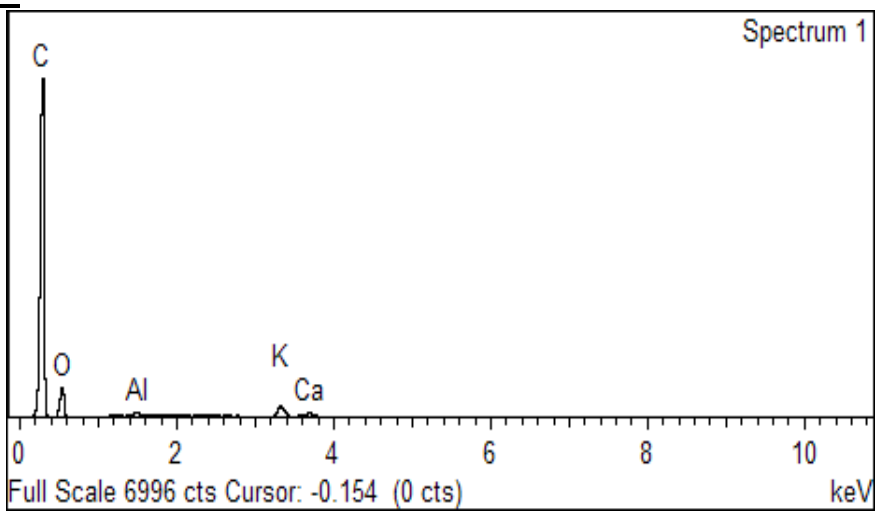

Figure 6-7 b: Spectrum of char sample

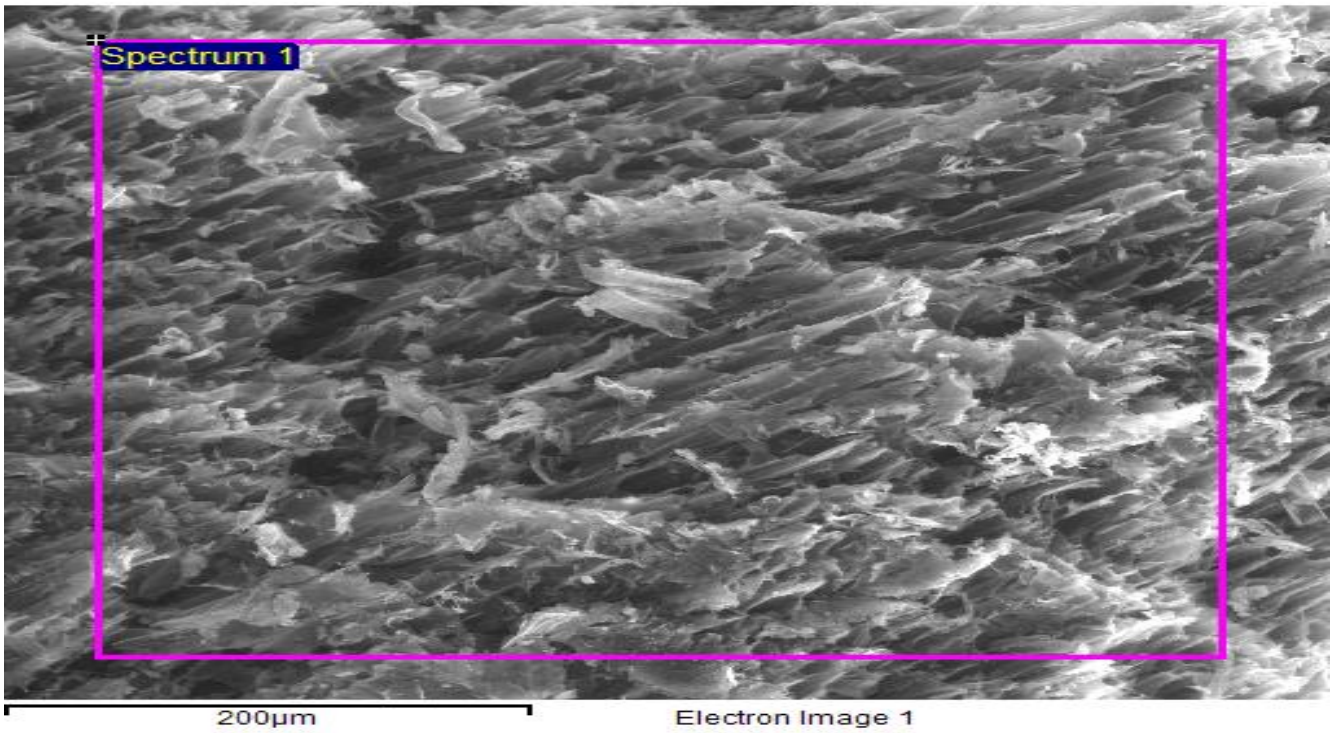

Figure 6-6 c: Electron image of char sample

Table 6-6 c: Char elemental analysis

Element	Weight %	Atomic%
C K	79.31	84.27
O K	18.98	15.14
Al K	0.19	0.09
K K	1.09	0.36
Ca K	0.42	0.13
Totals	100.00	

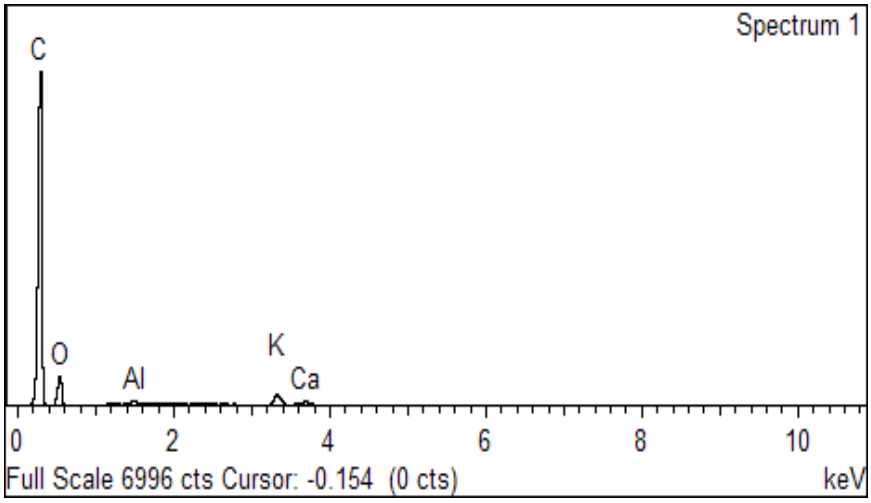

Figure 6-7 c: Spectrum of char sample

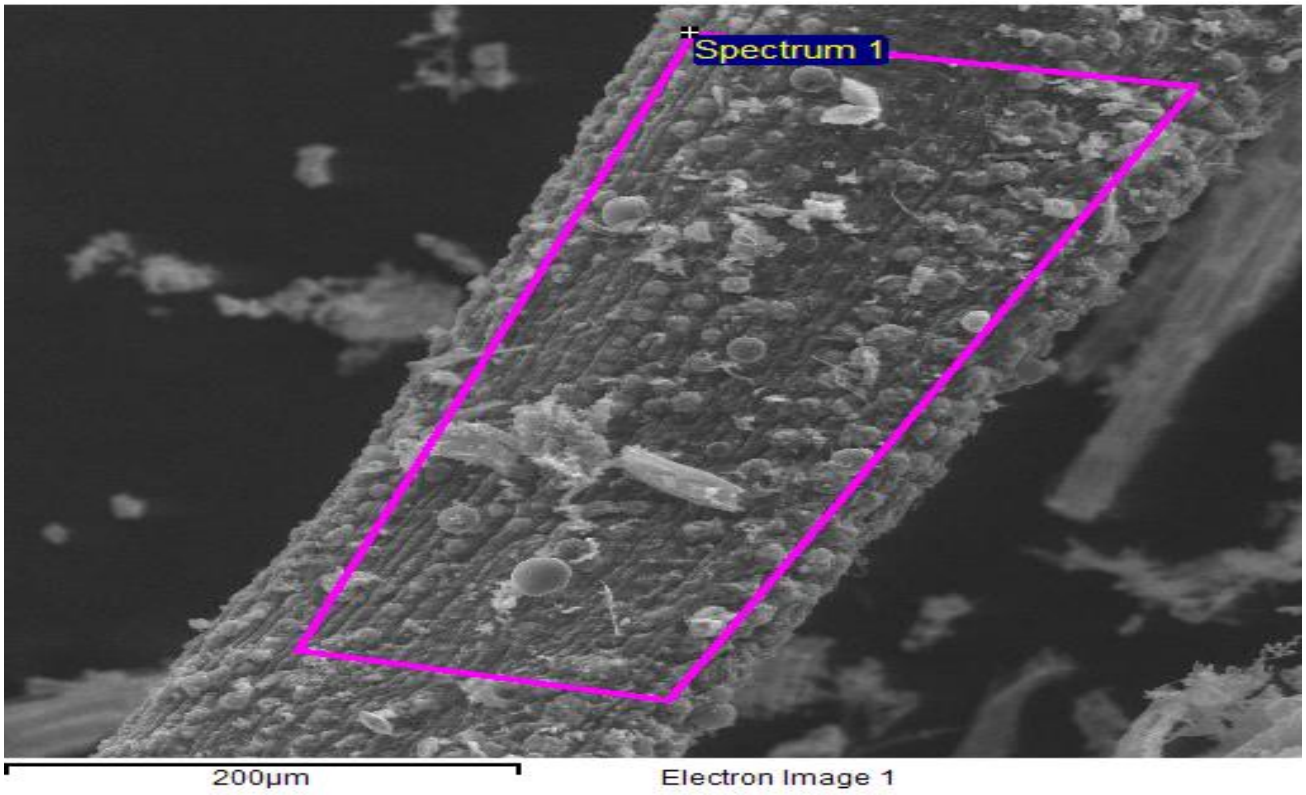

Figure 6-6 d: Electron image of char sample

Table 6-6 d: Char elemental analysis

Element	Weight%	Atomic%
C K	82.68	87.97
O K	12.84	10.25
Si K	2.37	1.08
Cl K	0.24	0.09
K K	1.46	0.48
Ca K	0.42	0.13
Totals	100.00	

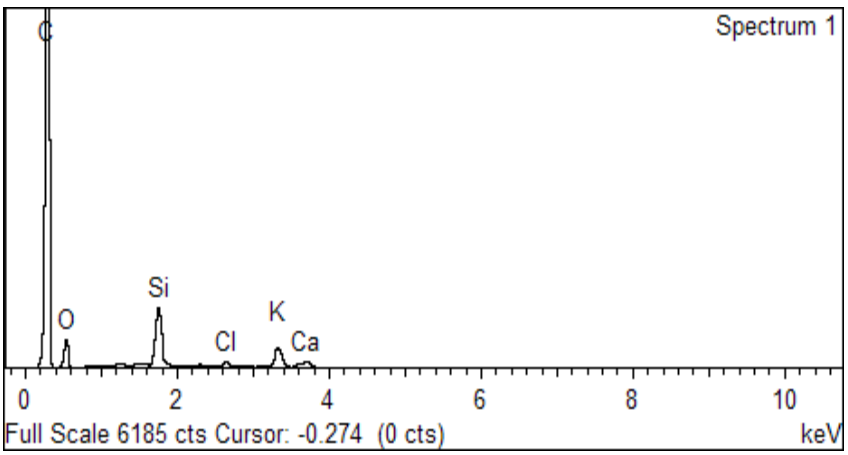

Figure 6-7 d: Spectrum of char sample

Average value of the elements of char is presented in Table 6-7 below:

Table 6-7: Average value of the elements of char

Element	Average (wt. %)
C	77.97
O	17.1275
S	0.84
Si	2.37
Al	0.19
Cl	0.87
K	2.8275
Ca	0.74

The scanning electron microscopy (SEM) images of raw UTS are shown in Figures 6-8a, c, and e and that of bio-char samples are shown in Figures 6-8b, d, and f respectively. [It can be noted that the Forest Shaving (FS) is renamed as UTS]. By comparing of SEM micrographs of the raw biomasses and bio-chars, some conclusions can be drawn about morphological changes. On the surface of the raw UTS, few pores were present. However, some pores are evidenced from the images of the bio-chars of UTS shown in Figures (6-8 b, d and f) and similar results are reported in literature (Abnisa, 2013 and Brewer, 2012). So it can be said that the UTS cell morphological structure originally present was not totally destroyed by the short heating time of the pyrolysis process. More micrographs of scanning electron microscopy for UTS char samples are shown through Figures 6-8 g to 6-8 k.

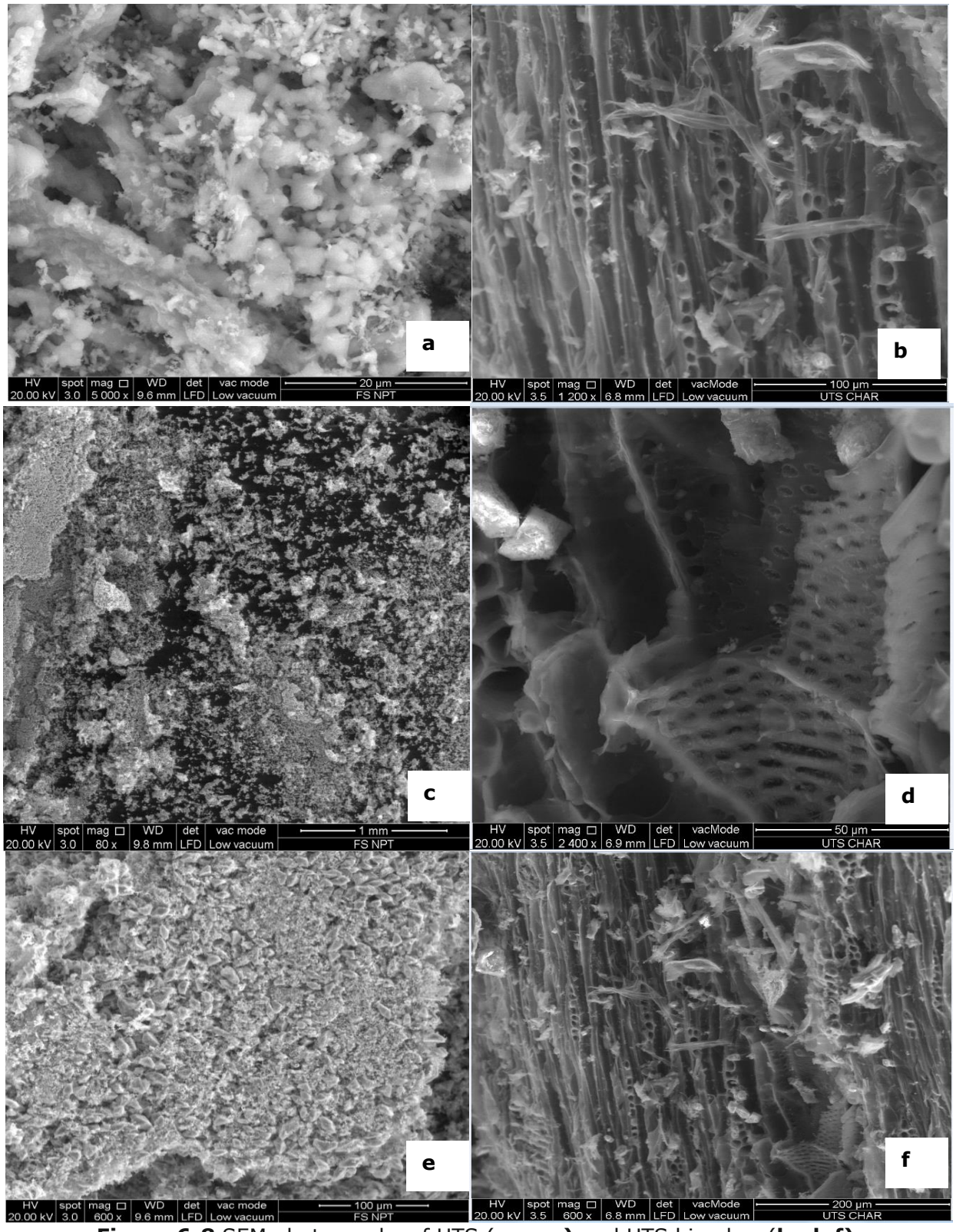

Figure 6-8 SEM photographs of UTS (**a, c, e)** and UTS bio-char (**b**, **d**, **f).**

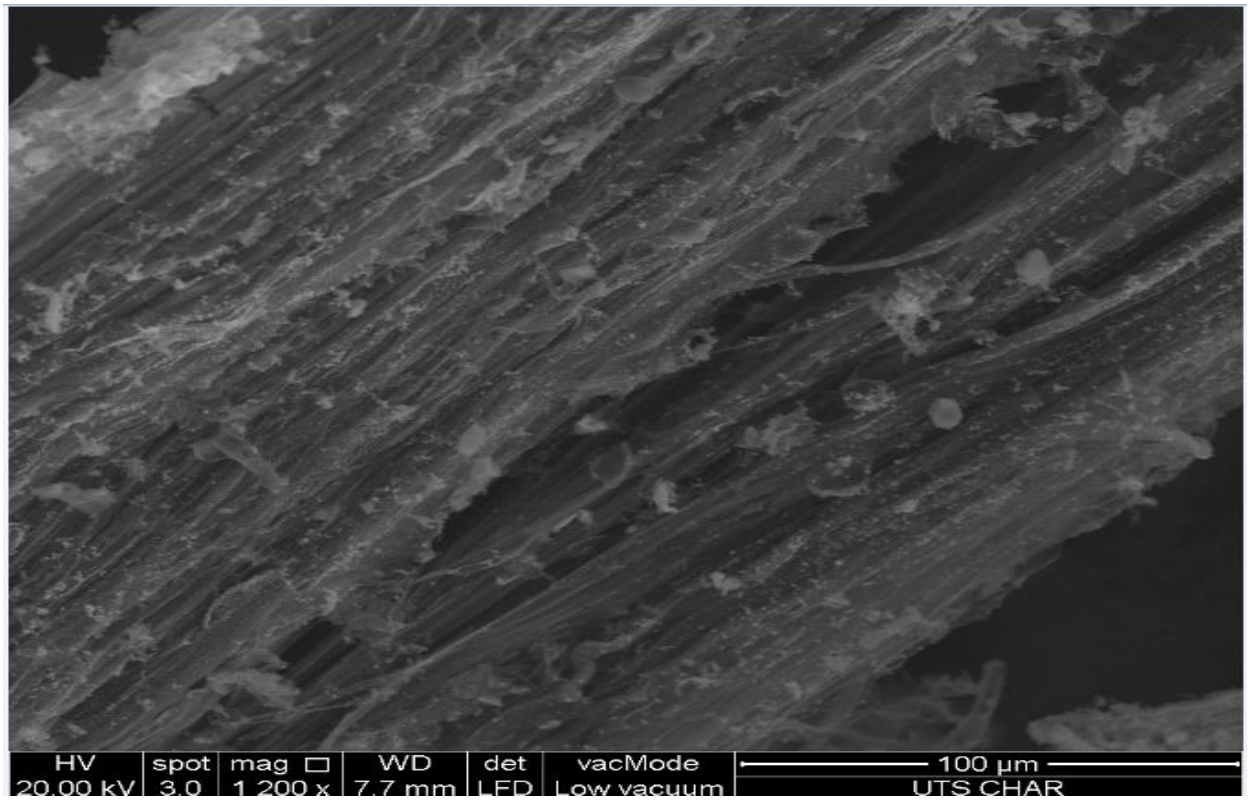

Figure 6-8 (g): SEM photographs for UTS bio-char samples

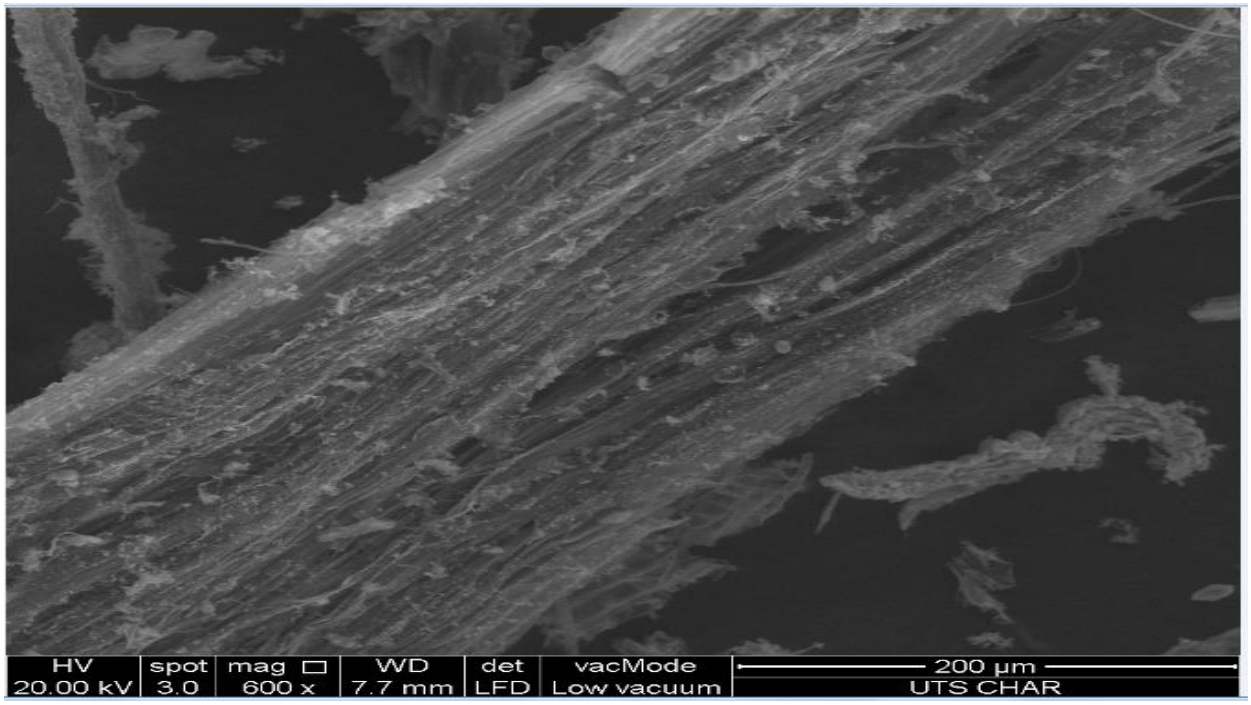

Figure 6-8 (h): SEM photographs for UTS bio-char samples

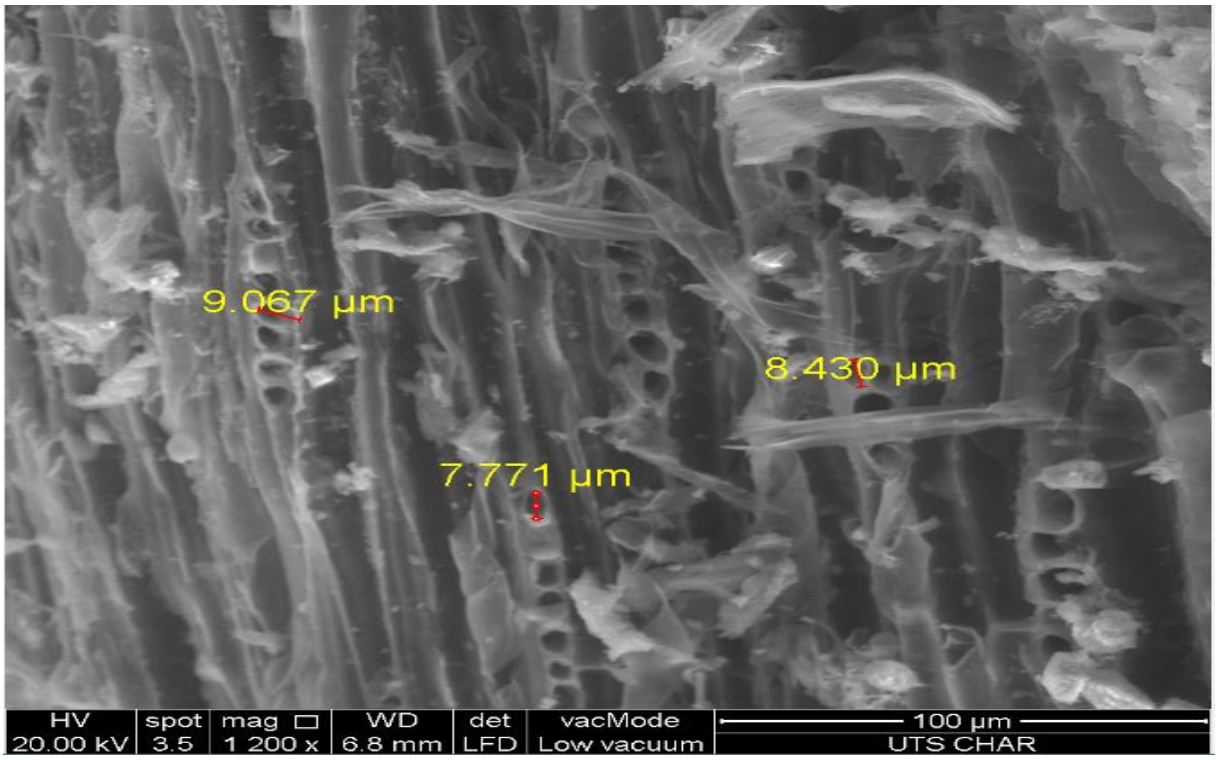

Figure 6-8 (i): SEM photographs for UTS bio-char samples

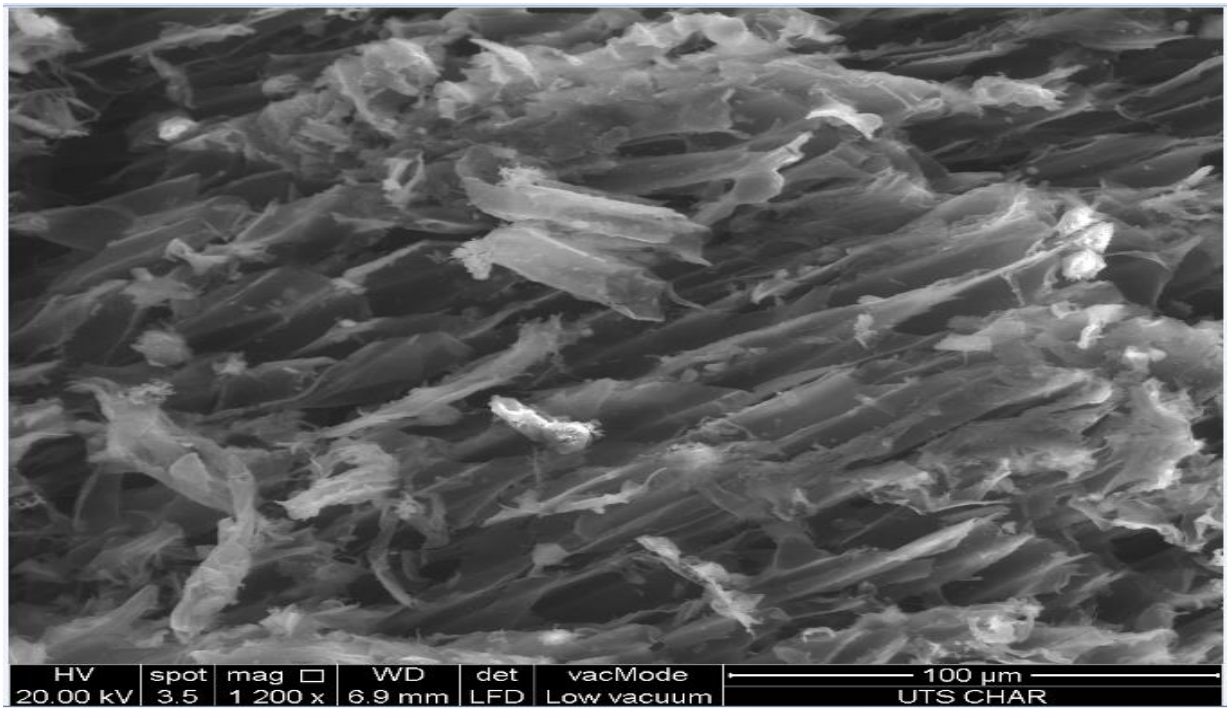

Figure 6-8 (j): SEM photographs for UTS bio-char samples

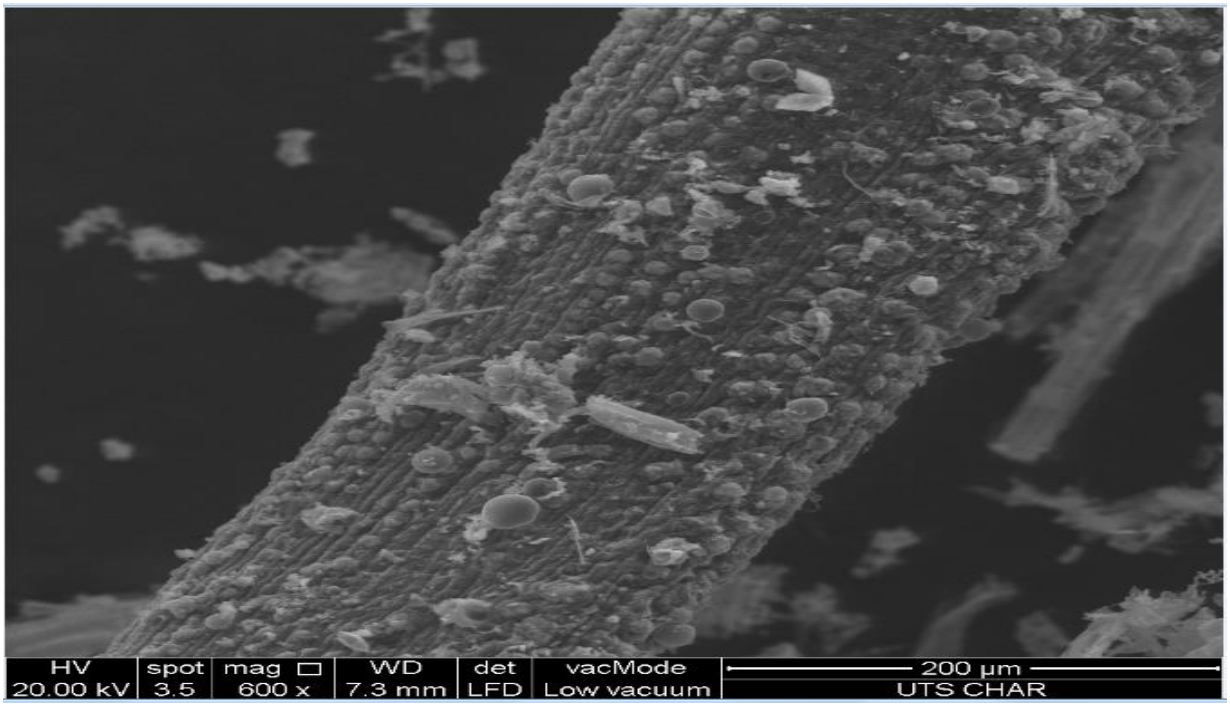

Figure 6-8(k): SEM photographs for UTS bio-char samples

6.5 Conclusion

The rig is flexible enough to produce bio-oil, bio-char and syngas by controlling the parameters for both batch and continuous operation. Bio-oil, syngas and bio-char were produced and characterized from untreated urban tree shavings at 600^0C by pyrolysis. Characterization of the products was performed using various approaches (Karl Fischer water-content tests, Calorimeter Bomb, FTIR, GC-MS, SEM and CHNS/O analyses). FTIR analysis of bio-oil showed about 9 functional groups of molecules and GC-MS study indicated that the bio-oil contained about 22 compounds that can be upgraded to transportation fuel in future research. The results also indicated that the bio-oil was acidic and contained high levels of oxygen. Syngas volumetric compositional analysis shows that CH_4 content is the maximum. Analysis of elemental composition of bio-char shows increase in carbon and sulphur content and decrease in oxygen content compared to biomass. The

syngas was tested for its flammability and was found that it contains combustible gases. These results proved that the designed reactor can be used as pyrolyzer. Based on this experiment, it can be recommended that pyrolysis from the designed reactor is a valid technique that can increase the value of UTS by producing bio-oil, bio-char and syngas. The oil can be used as a fuel in several applications to generate heat energy, and the UTS is a good material for this purpose since it has high calorific value. As a by-product from pyrolysis, the UTS based bio-char has high calorific value and it potentially can be used for any application that uses coal. Syngas can be used as the source of heat generation for electricity production as well as can be converted to liquid transportation fuel. Besides, it also can be noted that the utilization of UTS as bioenergy is able to enhance the energy security.

CHAPTER 7: CONCLUSIONS AND RECOMMNEDATIIONS

The design of a fluidized bed reactor is a complex process where optimum design data are not available in literature and it requires many adjustments to operate the system successfully. In this research work a lab-scale fluidized bed reactor with downstream unit operations like cyclone separators and vapour condensers were designed, fabricated, and installed. The reactor was tested and operated for bio-oil, bio-char and syngas production from UTS biomass pyrolysis. The products were characterized and were found comparable with other researchers using the similar feedstock. Based on the development of the fluidized bed system, experimental testing procedures, and interpretation of the analysed data as discussed, several conclusions can be made along with future recommendations.

7.1 Research conclusions

In conclusion, the important achievements of this research work can be highlighted by the following sentences:

- A Fluidized Bed Reactor with downstream cleaning and condensation unit operations was successfully designed, fabricated and tested
- The new reactor is found to be suitable enough to operate as batch process to produce fuel.
- The feedstock characterization has been done for the optimum operation of the FBR to get best yield out of this system.
- The products (bio-oil, bio-char and syngas) have been characterized following the standard methods and the results were found to be comparable with the published literature.
- The performance of the pyrolysis reactor was assessed and its yield for batch operation was evaluated.
- The energy efficiency of the designed FBR was estimated.

- The prototype was assessed and some modifications were conducted resulting in an improved design.

An operational lab-scale fluidized bed reactor for biomass fast pyrolysis was researched, designed, constructed, demonstrated and tested and the results from this study contribute to the body of knowledge for fast pyrolysis.

Within the fast pyrolysis regime, the engineering design and operational procedures are validated by the product yields and bio-oil yields achieved by the system are comparable with published results from similar lab-scale reactors using similar feedstock. The product compositions of the bio-oil, bio-char and syngas produced were similar to accepted values as reported by published literature.

7.2 Recommendations for future work

As the fluidized bed reactor for this project was operated for batch process only, there are few recommendations to improve the performance and operation of the system. In general, the system can be greatly improved by modifying the design for the biomass supplying system as shown in (Figure G-1, Appendix-G) for continuous pyrolysis process. Rather than using the biomass on top of the distributor at a time, the hopper can be lifted as such that the biomass can be delivered at a an elevated position (near the heating zone of the reactor) directly on the distributor (Figure G-1, Appendix-G). A cooling option can be made to prevent biomass decomposition inside the screw feeder.

The following experiments/analyses can be performed in future for both batch and continuous process:

- the effect of acid and alkali pre-treatment of biomass on the products (yield and quality) of pyrolysis.

-the effect of single/multiple screen used before first and second cyclone as well as before the condensers on the bio-oil quality

-the effect of variation of feed moisture content, size and source, reaction temperature, nitrogen flow rate on the bio-oil, bio-char and syngas yield as well as properties.

-the effect of variation of feed moisture content, size and source, reaction temperature, nitrogen flow rate along with the distributor number and holes diameter on the products of pyrolysis.

- upgrading bio-oil to transportation fuel.

REFERENCES

- Abdelgawad, B., (2013) Design of a gas-solid fluidized bed reactor at high temperature and high pressure, PhD Thesis, University of Montreal.
- Abdullah and Bridgwater A.V. (2006) "Pyrolysis liquid derived from oil palm empty fruit bunches" Journal of Physical Science, Vol. 17(2),117–129.
- Abdullah, N., Sulaiman, F. and Gerhauser, H. (2011) "Characterisation of oil palm empty fruit bunches for fuel application", Journal of Physical Science, 22(1), 1–24.
- Abnisa, F., Arami-Niya, A., Wan Daud, W.M.A. and Sahu, J.N. (2013) "Characterization of Bio-oil and bio-char from pyrolysis of palm oil wastes", Bioenerg. Res. 6:830–840.
- Acharjee, T.C., Coronella, C.J. and Vasquez, V.R. (2011) "Effect of thermal pre-treatment on equilibrium moisture content of lignocellulosic biomass", Bioresource Technology, 102 4849-4854.
- Afroz R., Hassan M.N. and Noor A.I. (2003) "Review of air pollution and health impacts in Malaysia" Environmental Research 92 71–77.
- Agarwal J.C., Davis W.L. and King D.T. (1962) "Fluidized bed coal dryer", Chemical Engineering Progress, 58, 85-90.
- Agbor, V.B., Cicek, N., Sparling, R., Berlin, A. and Levin, D.B. (2011)"Biomass pretreatment: Fundamentals toward application", Biotechnology Advances, 29 675-685.
- Ahmed T.Y., Ahmad M.M., Lam H.L. and Suzana Y. (2013) "Hydrogen from renewable palm kernel shell via enhanced gasification with low carbon dioxide emission", Clean Techn. Environ Policy, 15 513–523.
- Aho, A., Kumar N., Eranen K., Holmbom B., Hupa M., Salmi T. and Murzin, D.Yu. (2008) "Pyrolysis of softwood carbohydrates in a fluidized bed reactor", Int. J. Mol. Sci. 9, 1665-1675.

- Aida I.M.I., Salmiaton A., and Nur Dinie K.B. (2015) "Mixed plastic wastes pyrolysis in a fluidized bed reactor for potential diesel production" International Journal of Environmental Science and Development, Vol. 6, No. 8.
- Akkaya, A.V. (2009) "Proximate analysis based multiple regression models for higher heating value estimation of low rank coals", Fuel Process Technol. 90(2):165–170.
- Amitin, A.V., Matyushin, I.G. and Gurevich, D.A. (1968) Khim. Tekhnol Toplivi Masel, 3, 20.
- Amin, N.A.S., Ya'aini A., Misson, M., Haron, R. and Mohamed, M. (2010) "Enzymed pre-treated empty palm fruit bunch for biofuel production", Journal of Applied Sciences, 10(12):1181-1186.
- Amin, N.A.S. and Asmadi, M. (2011) "Optimization of empty palm fruit bunch pyrolysis over HZSM-5 catalyst for production of bio-oil", http://eprints.utm.my/5125/1/NorAishahSaidinaAmin_OptimizationOfEmptyPalmFruitBunch.pdf accessed 02 November 2011.
- Asli, U. A., Hamid H., Zakaria Z.A., Sadikin A. N., Rasit R. (2013) "Fermentable Sugars from Palm Empty Fruit Bunch Biomass for Bioethanol Production" World Academy of Science, Engineering and Technology, International Journal of Chemical, Molecular, Nuclear, Materials and Metallurgical Engineering 7(12) 960-963.
- Augustinova, J., Cvengrosova, Z., Mikulec, J., Vasilkovova, B., Cvengros, J. (2013) "Upgrading of bio-oil from fast pyrolysis", 46th International Conference on Petroleum Processing, June 7, Bratislava, Slovak Republic.
- Avery, D.A. and Tracey, D.H. (1968),"The application of fluidized beds of activated carbon to solvent recovery from air or gas streams", IChemE. Symp. Series (Fluidization), 30, 28-33.

- Bensah, E.C. and Mensah, M. (2013) "Chemical Pretreatment Methods for the Production of Cellulosic Ethanol: Technologies and Innovations", International J. of Chemical Engineering, Article ID 719607, 21pages.
- Bharadwaj, A., Wang Y., Sridhar S. and Arunachalam V.S. (2004), "Pyrolysis of rice husk", Research communications, Current Science, 87(7): 981-986.
- Bilgen, S., Kaygusuz, K. (2008) "The calculation of the chemical exergies of coal-based fuels by using the higher heating values", Applied Energy 85(8):776–785.
- Biocyclopeida, http://www.biocyclopedia.com/index/biotechnology/biotechnology_and_environment/biomass_a_renewable_source_of_energy/biotech_biomass_composition_of_biomass.php accessed on Jan 13, 16
- Boateng, A.A. and Mullen C.A. (2013) "Fast pyrolysis of biomass thermally pre-treated by torrefaction", Journal of Analytical and Applied Pyrolysis 100 95–102.
- Boateng A. A., Mullen C. A., Osgood-Jacobs L., Carlson P., Macken N.(2012) "Mass Balance, Energy, and Exergy Analysis of Bio-Oil Production by Fast Pyrolysis", Journal of Energy Resources Technology Vol. 134 / 042001-9.
- Boateng, A.A., Daugaard, D.E., Goldberg, N.M. and Hicks, K.B. (2007) "Bench-scale fluidized bed pyrolysis of switch grass for bio-oil production," Ind. Eng. Chem. Res., 46 1891-1897.
- Bonniol, F., Sierra, C., Occelli, R. and Tadrist, L. (2010) "Experimental study of the interaction of a dense gas–solid fluidized bed with its air-plenum" Powder Technology 202 118–129.
- Brewer, C.E. (2012) "Bio-char characterization and engineering", PhD Thesis, Iowa State University, Ames, Iowa, USA.
- Bridgwater, T. and Gyftopoulou, E. (2013) "Fast pyrolysis of biomass: Technology and applications", Aston University Bio-energy research Group, Birmingham, UK.

- Bridgwater, A.V. (2012) "A review of fast pyrolysis of biomass and product upgrading", Biomass and Bioenergy, 38, 68-94.
- Bridgwater, A.V. (2007) **"**The production of biofuels and renewable chemicals by fast pyrolysis of biomass", International J. Global Energy Issues**,** 27, (2), 160-203.
- Bridgwater, A.V. and Peacocke, G.V.C. (2000) "Fast pyrolysis processes for biomass", Renewable Sustainable Energy Review, 4(1), 1-73.
- Bridgwater, A.V. (1999) "Principles and practice of biomass fast pyrolysis process for liquids", Journal of Analytical and Applied Pyrolysis, 51 3-22.
- Bridgwater, A.V. (1999) An introduction to fast pyrolysis of biomass for fuels and chemicals. In Fast Pyrolysis of Biomass: A Handbook Volume 1, Bridgwater, A. V., Ed. CPL Press: Newbury, UK, Vol. 1.
- Bridgwater, A.V. and Grassi. G. (1991) Biomass pyrolysis liquids upgrading and utilisation, 1st edition, Elsevier Science Publishers Ltd Crown House, Linton Road, Barking, Essex IGll SJU, England.
- Brown, R.C. (2014) "Thermal de-polymerization of biomass to monosaccharides and phenolic monomers" Department of Mechanical Engineering, Bioeconomy Institute, centre for Sustainable Environmental Technologies, Iowa State University, Ames, IA.
- Brown, R.C. (2014a) Thermochemical Processing of Biomass: Conversion into Fuels, Chemicals and Powder, John Wiley & Sons.
- Brown, R.C. and Holmgren, J. (2014) Fast Pyrolysis and Bio-Oil Upgrading, http://www.ars.usda.gov/sp2UserFiles/Program/307/biomasstoDiesel/RobertBrown&JenniferHolmgrenpresentationslides.pdf, accessed on April 11, 2014.
- Brown, R.C. (2007) "Hybrid thermochemical/biological processing of biomass", Applied Biochemistry and Biochemistry, 137-140, 947-956.
- Bulk Density and Specific Gravity chart,

http://www.asiinstr.com/technical/Material_Bulk_Density_Chart_S.htm accessed 01 November 2011

- Cai, H.Y., Guell, A.J., Chatzakis, I.N., Lim, J-Y., Dugwell, D.R. and Kandiyoti, R. (1996) "Combustion reactivity and morphological change in coal chars: effect of pyrolysis temperature, heating rate and pressure", Fuel 75, 15-24.
- Cao, X., and Harris, W. (2010) "Properties of dairy-manure-derived biochar pertinent to its potential use in remediation" Bioresour. Technol. 101(14), 5222-5228.
- Chen, T., Deng, C. and Liu, R. (2010) "Effect of selective condensation on the characterization of bio-oil from pine sawdust fast pyrolysis using a fluidized-bed reactor", Energy Fuels, 24, 6616–6623.
- Chiba, S., Chiba, T., Nienow, A.W., Kobayashi, H. (1979) "The minimum fluidization velocity, bed expansion and pressure-drop profile of binary particle mixtures", Powder Technology, 22, pp. 255-269.
- Choren (2015) Information on gasification and FT production, http://www.choren.de/?LC=en. Accessed on July 01, 2015.
- Chemspider, The free chemical database, webpage www.chemspider.com/Chemical-Structure, accessed on 01 September, 2012
- Ciddor, L., Bennett, J.A., Hunns, J.A., Wilson, K. and Lee, A.F. (2015)"Catalytic upgrading of bio-oils by esterification", J Chem Technol Biotechnol 90: 780–795
- Colburn, A.P. and Edison, A.G. (1934) "Design of cooler condenser for mixtures of vapours with non-condensing gases," Ind. Eng. Chem. 26 1178.
- Cooper, C.C., and Alley, G.C. (2011) Air Pollution Control; A Design Approach. Long Grove, Illinois: Waveland Press, Inc.
- Couper, J.R., Penney, W.R., Fair, J.R., and Walas, S.M. (2005) Chemical Process Equipment: Selection and Design, Second Edition, Gulf Professional Publishing, 30 Corporate Drive, Suite 400, Burlington, MA, USA.

- Cui, H., Grace, J. R. (2007). "Fluidization of biomass particles: A review of experimental multiphase flow aspects." Chem. Eng. Sci., 62(1-2), 45-55.
- Cuthbert, R. (2011) Cyclone design, https://www.scribd.com/doc/37853568/CYCLONESver2, accessed on December 21, 2011
- Das P., Ganesh A. and Wangikar P. (2004) "Influence of pre-treatment for deashing of sugarcane bagasse on pyrolysis products" Biomass and Bioenergy 27 445-457.
- Davasgaium, M.M. and Boodoo, A.A. (1997) "Litter management: Use of bagasse as a potential source of litter material for broiler production", Agricultural Research and Extension Unit http://www.gov.mu/portal/sites/ncb/moa/farc/amas97/pdf/areu22.pdf, accessed 01 November 2011.
- Daugaard, D.E.; Brown, R.C. (2003) "Enthalpy for pyrolysis for several types of biomass", Energy & Fuels**,** 17, 934-939.
- Escudero, D. and Heindel, T.J. (2011) "Bed height and material density effects on fluidized bed hydrodynamics", Chemical Engineering Science 66 3648–3655.
- Van de Velden, M., Baeyens J. and Boukis, I. (2007) "Operating parameters for the circulating fluidized bed (CFB) pyrolysis of biomass, The residence time distribution of the gas phase in circulating fluidized beds (CFB)", Proceedings of European Congress of Chemical Engineering (ECCE-6), Copenhagen, 16-20 September.
- Delabona, Das P., Pirota, R.D.P.B., Codima, C.A., Tremacoldi, C.R., Rodrigues, A., Farinas, C.S. (2013) "Effect of initial moisture content on two Amazon rainforest Aspergillus strains cultivated on agro-industrial residues: Biomass-degrading enzymes production and characterization", Industrial Crops and Products 42 236–242.

- Demirbas, A. (2004) "Effects of temperature and particle size on bio-char yield from pyrolysis of agricultural residues", Journal of Analytical and Applied Pyrolysis, 72 (2): 243-248.
- Demirbas, A. (2000) "Mechanisms of liquefaction and pyrolysis reactions of biomass" Energy Conversion & Management 41 633-646.
- Diebold, J.P.; Bridgwater, A.V., Overview of fast pyrolysis of biomass for the production of liquid fuels. In *Fast* Pyrolysis of Biomass: A Handbook Volume 1, Bridgwater, A. V., Ed CPL Press: Newbury, UK, 1999; Vol. 1
- Dobele, G., Rossinskaja, G., Dizhbite, T., Telysheva, G., Meier, D. and Faix, O. (2005) "Application of catalysts for obtaining 1, 6-anhydrosaccharides from cellulose and wood by fast pyrolysis", J. Anal. Appl. Pyrolysis 74 401–405.
- Ecoreps, Environmental sustainability, http://www.ecoreps.com.au/syngas.html, accessed on September, 03, 2015
- Edye, L.A., Richards, G.N. and Zheng, G. (2014) "Transition metals as catalysts for pyrolysis and gasification of biomass" Wood Chemistry Laboratory, University of Montana, Missoula, MT 59812.
- Ellens, C. (2010) "Biomass to bio-char and fast pyrolysis oil fractions" Avello Bioenergy, Inc., Illinois Sustainable Technology centre, Bio-char: Production, Properties & Agricultural use, September 1, 2010.
- Emmons, H.W. and Atreya, A. (1982) The Science of Wood Combustion. Proc. Indian Academy of Sciences 5: 259-268.
- Estela, A. (2011) "Rice husk– an alternative fuel in Peru", Director of Biomass and Coal Research Programme, at the Pontificia Universidad Catolica del Peru; Av. Universitaria cuadra 18 Lima 32 Peru

- Fahmi, R., Bridgewater, A.V., Darvell, L. I. Jones, J.M., Yates, N., Thain, S. and Donnison, I.S (2007) "The effect of alkali metals on combustion and pyrolysis of Lolium and Festuca grasses, switch grass and willow", Fuel 86 1560-1569.
- Fan, L-S and Zhu, Chao (2005) Principles of gas-solid flows, Cambridge University Press.
- Faulkner, W.B., Shaw, B.W. (2006) "Efficiency and pressure drop of cyclones across a range of inlet velocities" Applied Engineering in Agriculture, American Society of Agricultural and Biological Engineers ISSN 0883−8542, Vol. 22(1): 155-161.
- Fedou, S., Eric Caprani, Douziech, D. and Axens, S.B. (2015) Conversion of syngas to diesel

  http://www.google.com/url?sa=t&rct=j&q=&esrc=s&source=web&cd=3&cad=rja&uact=8&ved=0CC8QFjACahUKEwiOme7Es9zHAhUEnJQKHSZ6DoY&url=http%3A%2F%2Fwww.axens.net%2Fdocument%2F19%2Fconversion-of-syngas-to-diesel---article-ptq%2Fenglish.html&usg=AFQjCNGE-xG-iXeMo4AqGjjVraLaIq3oFw,
  accessed on September 04, 2015

- Fei X., Li W., Xian-fang Y. (2011) "Exergy Analysis and Experimental Study of a Vehicle-Mounted Heat Pump–Assisted Fluidization Drying System Driven by a Diesel Generator", Drying Technology, Volume 29, Number 11, pp.1313-1324(12).
- Fernandez, C.S. (2008) Experimental study of a bubbling fluidized bed with a rotating distributor, PhD thesis, Leganes, Madrid, June 2008.
- Forest Bioenrgy http://www.bioenergyconsult.com/tag/pretreatment-of-biomass/accessed on jan 13, 16
- Fu, Q., Argyropolous, D.S., Lucia, L.A., Tilotta, D.C., Lebow, S.T. (2009) "Chemical yields from low-temperature pyrolysis of CCA-treated wood", Research Paper FPL-RP-652. Madison, WI: U.S. Department of Agriculture, Forest Service, Forest Products Laboratory. 18 p.

- Garcia-Perez, M., Wang, X.S., Shen, J., Rhodes, M.J., Tian, F., Lee, W.J., Wu, H. and Li, C. Z. (2008) "Fast pyrolysis of oil mallee woody biomass: Effect of temperature on the yield and quality of pyrolysis products", Ind. Eng. Chem. Res. 47 1846-1854.
- Gebreegziabher, T., Oyedun, A.O. and Hui, C.W. (2013) "Optimum biomass drying for combustion-A modeling approach", Energy 53 67-73.
- Geldart, D. (1986) Gas Fluidization Technology, pp. 65, John Willey & Sons, Great Britain.
- Geldart, D. (1973) "Types of Gas Fluidization", Powder Technology, 7 285-292.
- George, S.E. and Grace, J.R. (1978) "Entrainment of particles from aggregative fluidized beds" AIChE Symp. Ser. 74:67-74.
- Ghani Z.A., Ishak M.A.M., Ismail K. (2010) "Direct liquefaction of Mukah Balingian lowrank Malaysian coal: optimization using response surface methodology", Asia Pacific Journal of Chemical Engineering; 6(4):581-588.
- GlobalSpec Inc, 30 Tech Valley Dr Suite 102, East Greenbush, NY, 12061, http://www.globalspec.com/learnmore/manufacturing_process_equipment/air_quality/cyclone_separators, accessed on April 18, 2013
- Goodfrey, B (2004) Renewable Energy, Power for a Sustainable Future. 2nd ed.; Oxford University Press: New York, NY.
- Grace, J.R. (1982) Fluidized-Bed Hydrodynamics. In Handbook of Multiphase Systems, Hetsroni, G., Ed. Hemisphere: Washington, pp. 5-64.
- Graham, L.J., Taillon, R., Mullin, J., Wigle, T. (2010) "Pharmaceutical process/equipment design methodology case study: Cyclone design to optimize spray-dried-particle collection efficiency" Computers and Chemical Engineering 34 1041–1048.

- Gronli, M.; Antal, M.J.; Schenkel, Y.; Crehay, R. (2005) The science and technology of charcoal production. In Fast Pyrolysis of Biomass: A Handbook Volume 3, Bridgwater, A. V., Ed, CPL Press: Newbury, UK, 2005; Vol. 3.
- Gu X., Maa X., Li L., Cheng L., Cheng K., Li Z. (2013) "Pyrolysis of poplar wood sawdust by TG-FTIR and Py–GC/MS", Journal of Analytical and Applied Pyrolysis 102 16–23.
- Guo, X.; Wang, S.; Wang, Qi; Guo, Z. and Luo, Z. (2011) "Properties of bio-oil from fast pyrolysis of rice husk," Biotechnology and Bioengineering, Chinese journal of Chemical Engineering, 19(1) 116-121.
- Gupta, A.K. (1984) Swirl Flows, Techonomic Publishing Co., 851 New Holland Ave., P.O. Box 3535, Lancaster, PA 17604, USA.
- Hafiz, M.A., Batchaa M.F.M. and Asmuin, N. (2013) "Effect of plenum chamber depth in a swirling fluidized bed" 2nd International Conference on Mechanical Engineering Research (ICMER 2013) IOP Publishing, IOP Conf. Series: Materials Science and Engineering 50, 012 021.
- Hague, R.A. (1998) "The pre-treatment and pyrolysis of biomass for the production of liquid for fuels and speciality chemicals", PhD thesis, Aston University, UK.
- Hames, B., Ruiz, R., Scarlata, C., Sluiter, A., Sluiter, J. and Templeton, D. (2008) "Preparation of samples for compositional analysis", Laboratory Analytical Procedure (LAP)
- Hasan, M.F.B. (2009) "Physical and combustion characteristics of densified palm biomass", Faculty of Mechanical Engineering, University of Teknoloy, Malaysia.
- Hartman, M., Svoboda, K., Pohorely, M. and Tranka, O. (2005) "Combustion of dried sewage sludge in a fluidized-bed reactor" Ind. Eng. Chem. Res., 44, 3432-3441.

- Harmsen, P., Lips, S. and Bakker, R. (2013) Pretreatment of lignocellulose for biotechnological production of lactic acid, Research review, Wageningen UR Food & Biobased Research,P.O. Box 17, NL-6700 AA Wageningen.
- Hendriks, A.T.W.M. and Zeeman, G. (2009) "Pre-treatments to enhance the digestibility of lignocellulosic biomass", Bioresource Technology 100 10–18.
- Hoffman, A.C., de Groot, M., Peng, W., Dries, H.W.A. and Kater, J. (2001) "Advantages and risks in increasing cyclone separator length" AIChE, J 47(11) 2452-2460.
- Horio, M., Shibata, T. and Muchi, I. (1983) Symp. Of 4th Int. Conf. on Fluidization, Kashikojima, Japan
- Heo, H.S., Park, H.J., Park, Y.K., Ryu, C., Suh, D.J., Suh, Y.W., Yim, J.H., Kim, S.S. (2010) "Bio-oil production from fast pyrolysis of waste furniture sawdust in a fluidized bed", Bioresource Technology, 101, S91–S96.
- Herguido, J., Corella, J. and Gonzalez-Saiz, J. (1992) "Steam gasification of lignocellulosic residues in a fluidized bed at a small pilot scale. Effect of the type of feedstock", Ind. Eng. Chem. Res. 31, 1274-1282.
- Hiby, J.W. (1964) "Critical minimum pressure drop of the gas distribution plate in fluidized bed units", Chemical Engineering & Technology, 36, 228.
- Hoekstra, E., Van Swaaij, W.P.M., Kersten, S.R.A. and Hogendoorn, K.J.A. (2014) "Fast pyrolysis in a novel wire-mesh reactor: Decomposition reactions of pine wood and model compounds", University of Twente, Faculty of Science and Technology, P.O. Box 217, 7500 AE Enschede, The Netherlands.
- Ibrahim M.M, El-Zawawy W.K., Abdel-Fattah Y.R., Nadia A.S. and Agblevor F.A. (2011) "Comparison of alkaline pulping with steam explosion for glucose production from rice straw", Carbohydrate Polymers 83 720–726.

- Imam, T. and Capareda, S. (2012) "Characterization of bio-oil, syn gas and bio-char from switch grass pyrolysis at various temperatures", J. Anal. Appl. Pyrolysis 93 170-177.
- Islam, M.R., Islam, M.N and Nabi, M.N. (2004) "Design, fabrication and performance study of a biomass solid waste pyrolysis system for alternative liquid fuel production", Journal of Energy & Environment 3 103 – 117.
- Islam, M.R., Islam, M.N. and Islam, Md.N. (2003) "Fixed bed pyrolysis of sugarcane bagasse for liquid fuel production", Proceedings of the International Conference on Mechanical Engineering 2003 http://www.buet.ac.bd/me/icme/icme2003/Proceedings/PDF/ICME03-TH-16.pdf accessed 02 November 2011.
- Islam, M.N., Zailani, R. and Ani, F.N. (1999) "Pyrolytic oil from fluidised bed pyrolysis of oil palm shell and its characterisation", Renewable Energy, 17, 73-84.
- Jahirul, M.I., Rasul, M.G., Chowdhury, A.A. and Ashwath, N. (2012) Biofuels Production through Biomass Pyrolysis —A Technological Review Energies 2012, 5, 4952-5001.
- Jakobsen, H.A. (2008) Chemical Reactor Modeling, Multiphase Reactive Flows, Springer-Verlag Berlin Heidelberg.
- Jamaluddin M.A., Ismail K., Mohd Azlan M.I, Ghani Z.A ,Abdullah M.F., Safian M.T, Siti S.I. Tahiruddin S., Mohammed Faisal M.Y., Noor Irma Nazashida M.H. (2013) "Microwave-assisted pyrolysis of palm kernel shell: Optimization using response surface methodology (RSM)", Renewable Energy 55 357-365.
- Jared, N.B. (2009) "Development of a lab-scale auger reactor for biomass fast pyrolysis and process optimization using response surface methodology" A thesis submitted to the graduate faculty in partial fulfilment for the requirements for the degree of M.Sc., Iowa State University, Ames, Iowa.

- Jha, S.K. and Singh, A. (2007) "Physical and thermal properties of untreated and chemically treated rice husk", Journal of Agricultural Engineering, 44 (4): 48- 53.
- Drake, J.B. (2011) Hydrodynamic characterization of 3D fluidized beds using noninvasive techniques, Iowa State University Ames, Iowa.
- Keles, S., Kaygusuz, K., and Akgün, M. (2011) "Pyrolysis of woody biomass for sustainable bio-oil," Energy Sources Part A 33, 879-889.
- Kim, S.B., Lee, S.J., Lee, J.H., Jung, Y.R., Thapa, L.P., Kim, J.S., Um, Y., Park, C. and Kim, S.W.(2013) "Pre-treatment of rice straw with combined process using dilute sulphuric acid and aqueous ammonia", Biotechnology for Biofuels, 6 109
- Kumar P., Barrett D.M., Delwiche M.J., and Stroeve P. (2009) "Methods for Pre-treatment of Lignocellulosic Biomass for Efficient Hydrolysis and Biofuel Production" Ind. Eng. Chem. Res., Article ASAP • DOI: 10.1021/ie801542g • Publication Date (Web): 20 March.
- Kumar, V.V., Batcha, M.F. and Raghavan, V.R. (2011) "Study of the fluid dynamic performance of distributor type in torbed type reactors" Engineering e-Transaction (ISSN 1823-6379) 6(1) 70-75.
- Kunii, D. and Levenspiel, O. (1991) Fluidization Engineering, 2nd Ed. pp. 67-68, 80, 95-96, 102, 131, 165, Newton: Butterworth-Heinemen.
- Kunii, D. and Levenspiel, O. (1968) "Bubbling bed model for kinetic process in fluidized beds", I & EC Process Design and Development, 7(4) 481-492.
- Kuo, K.Y. and Tsai, C.J (2001) "On the theory of particle cut-off diameter and collection efficiency of cyclones" Aerosol and Air Quality Research, 1(1) 47-56Lapple, C.E. (1951) "Processes use many collectors types," Chemical Engineering, 58(5) 144-151.
- Lam M.K., Ridzuan Z. (2008) "Production of activated carbon from sawdust using fluidized bed reactor" International Conference on Environment (ICENV 2008).

- Lappas, A.A., Samolada, M.C., Iatridis, D.K., Voutetakis, S.S. and Vasalos, I.A. (2002) "Biomass pyrolysis in a circulating fluid bed reactor for the production of fuels and chemicals", Fuel 81 2087–2095.
- Lapple, C.E. (1951) "Processes use many collectors types", Chemical Engineering, 58(5) 144-151.
- Lee, K.H., Kang, B.S., Park, Y.K. and Kim, J.S. (2005) "Influence of reaction temperature, pre-treatment and a char removal system on the production of bio-oil from rice straw by fast pyrolysis using a fluidized bed", Energy Fuels, 19(5), 2179-2184
- Leva, M. (1959) Fluidization, pp.105, McGraw-Hill, New York.
- Lewnard, J.J., Herb, B.E., Tsao, T.R. and Zenz, J.A. (1993) Effect of design and operation parameters on cyclone performance for circulating fluidized bed boilers. In: Avidan AA, ed. Circulating Fluidized Bed Technology IV. NY, AIChE, pp 525-531
- Lievens, C., Mourant, D., Gunawan, R., Li,X. and Li, C.-Z.(2013) "FT-IR carbonyl bands of bio-oils: importance of water", Fuel 112, 596.
- Lievens, C., Mourant, D., He, M., Gunawan, R., Li, X. and Li C-Z. (2011) "An FT-IR spectroscopic study of carbonyl functionalities in bio-oils", Fuel 90, 3417.
- Lin, T.Y. and Kuo, C.P. (2012) "Study of products yield of bagasse and sawdust via slow pyrolysis and iron-catalyse" Journal of Analytical and Applied Pyrolysis, 96 203–209.
- LookChem™Look for Chemicals, webpage http://www.lookchem.com/ accessed on 02 September, 2012.
- Lou, R., Wu, S., Lv, G. and Zhang, A. (2013) "Factors related to minerals and ingredients influencing the distribution of pyrolysates derived from herbaceous biomass, fast pyrolysis factors for gases", Bio Resource 8(1) 1345-1360.

- Ludwig, E. E. (1999) Applied Process Design for Chemical and Petrochemical Plants, Volume 1, Third Ed, Gulf Publishing Company, Houston, TX.
- McIntosh S. and Vancov T. (2010) "Enhanced enzyme saccharification of Sorghum bicolor straw using dilute alkali pre-treatment" Bioresource Technology 101 6718–6727.
- Magnus, G. (2015), Bio-fuel production in Iceland, Gasification experiments: Evaluation of syngas production from different raw materials and calculation on quantity of fuels. (1 version). Available at http://www.lifeldsneyti.is/resources/Files/Lifeldsneyti/Lifeldsneyti---Arskyrsla-2011/Fylgiskjal_6.pdf accessed on July 01, 2015
- Mansaray, G. and Ghalya. E. (1997) "Physical and thermochemical properties of rice husk", Energy sources, 19(9) 989-1004.
- Martin Screw Conveyor and Elevator - Scribd http://www.scribd.com/doc/67126144/Martin-Screw-Conveyor-and-Elevator#scribd, accessed on October 16, 2011.
- Masia, A.A.T., Buhre, B.J.P., Gupta, R.P. and Wall, T.F. (2007) "Characterising ash of biomass and waste", Fuel Processing Technology 88 1071-1081.
- Material Safety data Sheets (MSDS), webpage, www.msds.com, accessed on 25 July 2012.
- Mazlan M.A.F., Uemura Y., Noridah B.O, Suzana Y. (2015) "Fast pyrolysis of hardwood residues using a fixed bed drop-type pyrolyzer" Energy Conversion and Management 98 208–214.
- Medic, D. (2012) "Investigation of torrefaction process parameters and characterization of torrefied biomass" Graduate Theses and Dissertations Paper 12403, Iowa State University, Ames, Iowa.

- Megaritis, A., Zhuo, Y., Messenbock, R., Dugwell, D.R. and Kandiyoti, R. (1998) "Pyrolysis and gasification in a bench-scale high-pressure fluidized-bed reactor" Energy & Fuels, 12 144-151.
- Mekhilef, S., Saidur, R., Safari, A., Mustafa, W.E.S.B. (2011) "Biomass energy in Malaysia: Current state and prospects," Renewable and Sustainable Energy Reviews, 15(7) 3360-3370.
- Menon V., Rao M. (2012) "Trends in bioconversion of lignocellulose: Biofuels, platform chemicals & biorefinery concept" Progress in Energy and Combustion Science 38 522-550.
- Miller, S.F. and Miller, B.G. (2007) "The occurrence of inorganic elements in various biofuels and its effect on ash chemistry and behaviour and use in combustion products" Fuel Processing Technology, 88 1155–1164.
- Mohamed, A.B. and Ghanem, G.H.A. (2011) "Modifying a thresher for ensiling the green rice straw by shredding", Misr J. Ag. Eng., 27(2): 482 – 500.
- Mohammadkhah, A. and Mostoufi, N. (2009) "Effect of geometry of the plenum chamber on gas distribution in a fluidized bed", Ind. Eng. Chem. Res. 48, 7624–7630.
- Michael, E., Ronald, C.H., Vincent, J.S., Joseph, D.M., Richard, P., Dennis, C.D. (1982) "Evaluation of a cyclone dust collector for high-temperature, high-pressure particulate control," Ind. Eng. Chem. Process Des. Dev., 21 (1) 158–161.
- Mills, G.A. (2015) Liquid fuels from syngas - progress report, Department of Chemical Engineering, University of Delaware, Newark, DE 19716 https://web.anl.gov/PCS/acsfuel/preprint%20archive/Files/37_1_SAN%20FRANCISCO_04-92_0116.pdf, accessed on September 04, 2015

- Mishra, P., Chakraverty, A. and Banerjee, H.D. (1986) "Studies on physical and thermal properties of rice husk related to its industrial application" , Journal of Materials Science, 21(6) 2129-2132.
- Misson, M., Haron, R., Kamaroddin, M.F.A. and Amin, N.A.S. (2009) "Pre-treatment of empty palm fruit bunch for production of chemicals via catalytic pyrolysis" BioResource Technology, 100 2867–2873.
- Misson M., Haron R., Kamaroddin M.F.A. and Nor Aishah S.A. (2009) "Pre-treatment of empty palm fruit bunch for Lignin degradation" Jurnal Teknologi, 50(f) 89–98.
- Moe, S.T. (2014) Pretreatment and hydrolysis of lignocellulosic biomass for bio-refinery processes, NTNU, Department of Chemical Engineering.
- Mohamad S.E., Idi A.,. Salleh M.M, Ibrahim Z. (2012) Pre-treatment of Cocoa Waste for Bioethanol Production Using Ionic Liquid Jurnal Teknologi (Sciences & Engineering) 59 Suppl. 1, 49–56.
- Mohammed, I.Y., Kazi, F.K., Yusup, S., Alshareef I. and Chi S.A. (2014) "Higher heating value prediction model from biomass proximate analysis data", ICCE 2014 Proceedings: October 20-22, Quebec, Canada.
- Moghadam R.A., Suzana Y., Uemura Y., Chin B.L.F., Lam H.L., Shoaibi A.A. (2016) "Syngas production from palm kernel shell and polyethylene waste blend in fluidized bed catalytic steam co-gasification process" Energy (Aticle in Press).
- Mortensen, P.M. (2013) Catalytic conversion of bio-oil to fuel for transportation, PhD Thesis, Combustion and Harmful Emission Control, Department of Chemical and Biochemical Engineering, Technical University of Denmark.
- Mortensen, P.M., Grunwaldt, J.D., Jensen, P.A., Knudsen, K.G. and Jensen, A.D. (2011) "A review of catalytic upgrading of bio-oil to engine fuels", Applied Catalysis A: General 407 (1-2) 1-19.

- Mullen, C.A. and Boateng, A.A. (2008) "Chemical composition of bio-oils produced by fats pyrolysis of two energy crops" Energy & Fuels, 22 2104-2109.
- Muradov, N., Fidalgo, B., Gujar, A. C., Garceau, N., and T-Raissi, A. (2012). "Production and characterization of Lemna minor bio-char and its catalytic application for biogas reforming," Biomass Bioenergy 42, 123-131.
- Nag, A.; Manchikanti, P. (2008) Photosynthetic plants as renewable energy sources. In Biofuels Refining and Performance, Nag, A., Ed. McGraw-Hill: New York, NY.
- Natarajan, E. and Ganapathy, S.E. (2009) "Pyrolysis of rice husk in a fixed bed reactor", World Academy of Science, Engineering and Technology, 56.
- National Biomass Strategy 2020: New wealth creation for Malaysia's palm oil industry, 2011, available at : https://www.google.com/search?q=National+biomass+strategy+2020&formbutton1=GoogleSearch#q=National+biomass+strategy+2020%3A+New+wealth+creation+for+Malaysia's+oil+palm+industry%2C+2011+(ebook) accessed on January 22, 2014.
- National Institute of Standards and technology (NIST), 2011 by the U.S. Secretary of Commerce on behalf of the United States of America, Webpage http://webbook.nist.gov/cgi/cbook.cgi?ID=C1333740&Type=JANAFG&Plot=on, accessed on 02 September, 2012.
- Ndoke, P.N. (2011) "Performance of palm kernel shells as a partial replacement for coarse aggregate in asphalt concrete", Department of Civil Engineering, Federal University of Technology, Minna, http://lejpt.academicdirect.org/A09/145_152.htm accessed 01 November 2011.
- Nienow, A.W., Harnby, N. and Edwards, M.F. (1997) Mixing in the Process Industries, Second Edition, Butterworth-Heinemann.

- Nor Aishah S.A., Misson M., Haron R., Mohd Fadhzir A.K., Wan Nor Nadyaini W.O., Haw K-G (2012) "Bio-oils and diesel fuel derived from alkaline Treated empty fruit bunch (efb)" International Journal of biomass & renewables 1 6–14.
- NIST, Sematech, Engineering Statistics Handbook, web address http://Www.Itl.Nist.Gov/Div898/Handbook/Pmd/Section3/Pmd31.Htm, accessed on 01 September, 2015.
- Nusselt, W. (1916) "Die oberflachenkondensation des wasserdampfes," Z. Ver. Duet. Ing. 60 541.
- Oasmaa, A., Elliot, D.C. and Korhonen, J. (2010)"Acidity of biomass fast pyrolysis bio-oils", Energy & Fuels, 24 6548-6554.
- O'Connor, M. (2010) "The density of rice husk" ehowfood http://www.ehow.com/facts7625366density-rice-husk.html accessed 06 November 2011.
- Onay, O. (2007) "Influence of pyrolysis temperature and heating rate on the production of bio-oil and char from sunflower seed by pyrolysis, using a well-swept fixed-bed reactor" Fuel Processing Technology, 88 523–531.
- Ozbay, N., Putun, A.E. and Putun, E. (2006) "Bio-oil production from rapid pyrolysis of cottonseed cake: product yields and compositions" Int. J. Energy Res., 30 501–510.
- Pan, Y.G., Velo, E., Roca, X., Manya, J.J., Puigjaner, L. (2000) "Fluidized-bed co-gasification of residual biomass/poor coal blends for fuel gas production" Fuel, 79, 1317–1326.
- Parnell, C.B.Jr. (1996) "Cyclone design for air pollution abatement associated with agricultural operations," In Proc. 1996 Beltwide Cotton Production Conferences. Nashville, Tenn.: National Cotton Council.

- Parnell, C.B. Jr. and Davis, D.D. (1979) "Predicted effects of the use of new cyclone designs on agricultural processing particle emissions", ASAE Paper No. SWR-79-040, Presented at 1979 Southwest Region Meeting of the ASAE, Hot Springs, Ark.
- Park, J., Shun, D., Bae, D-H, Lee, S., Seo, J.H., Park, J.H. (2011) "The effect of gas temperature and velocity on coal drying in fluidized bed dryer", 2010 ECI Conference on the 13th International Conference on Fluidization - New Paradigm in Fluidization Engineering http://services.bepress.com/eci/uidization xiii/101.
- Pattiya, A., and Suttibak, S. (2012) "Production of bio-oil via fast pyrolysis of agricultural residues from cassava plantations in a fluidized bed reactor with a hot vapour filtration unit," Journal of Analytical and Applied Pyrolysis, 95 227-235.
- Patwardhan, P.R., Dalluge, D.L., Shanks, B.H. and Brown, R.C. (2011) "Distinguishing primary and secondary reactions of cellulose pyrolysis", Bioresource Technology, 102 5265–5269.
- Patwardhan, P.R., Satrio, J.A., Brown, R.C. and Shanks, B.H. (2010) "Influence of inorganic salts on the primary pyrolysis products of cellulose", Bioresource Technology, 101 4646–4655.
- Pena, J. and Pascual. A. (2011), "Bubbling Fluidized Bed (BFB), When to use this technology", Industrial Fluidization SA, pp. 1-12.
- Perry. C. (1999) Perry's Chemical Engineers' Handbook, 7th Ed. Mc-Graw Hill Book Companies Inc. NY.
- Peter, T., Bryan, M. J., Charles, E.L. and Sidsel, G. (2006) "Compositional constraints on slag formation and potassium volatilization from rice straw blended wood fuel", Fuel Processing Technology, 87(5) 383-408.

- Philip, C.B. and Peter, F. (2006) "Use of mobile fast pyrolysis plants to densify biomass and reduce biomass handling costs- A preliminary assessment", Biomass and Bioenergy, 30 321-325.
- Pictor, J.W.D. and Robinson, L.W.J. (1968) Inst. Chem. Eng. Symp. Ser., (27) 166.
- Pittman, C.U.Jr., Mohan, D., Eseyin, A., Li, Qi., Ingram, L., Hassan, El-B.M., Mitchell, B., Guo, H. and Steele, P.H. (2012) "Characterization of bio-oils produced from fast pyrolysis of corn stalks in an auger reactor" Energy Fuels, 26 3816−3825.
- Piyarat, W., Chaiyot, T. and Mallee, T. (2010) "Comparison of pyrolysis kinetic models for thermos-gravimetric analysis of biomass", Suranaree J. Sci. Technol., 17(4) 387-400.
- Qureshi, A.E. and Creasy, D.E. (1979) Powder Technol., 22 113.
- Pohorely, M., Vosecky, M., Hejdova, P., Puncocha, M., Skoblja, S., Staf, M., Vosta, J., Koutsky, B. and Svoboda, K. (2006) "Gasification of coal and PET in fluidized bed reactor" Fuel, 85 2458–2468.
- Pütün, E. (2010). "Catalytic pyrolysis of biomass: Effects of pyrolysis temperature, sweeping gas flow rate and MgO catalyst," Energy 35(7), 2761-2766.
- Predel, M. and Kaminsky, W. (1998) "Pyrolysis of rape-seed in a fluidized bed reactor", Bioresource Technology, 66 113-117.
- Rabou, L.P.L.M., van Leijenhorst, R.J.C. and Hazewinkel, J.H.O. (2008) "High efficiency power production from biomass and waste", Energy Research Centre for the Netherlands. Ragland, K.W., Aerts, D.J. and Baker, A.J. (1991) "Properties of wood for combustion analysis", Bioresource Technology, 37 161-168.
- Rajeev, J. and Anil, K.R. (1997) "Sugarcane leaf-bagasse gasifiers for industrial heating applications", Biomass and Bioenergy, 13 (3) 141-146.

- Ramakers, B.J., Ridder, R. de. and Kerkhof, P.J.A.M. (2004) "Fluidization behaviour of wood/sand mixtures", Maderas. Ciencia y tecnología, 6(2) 145-153.
- Ravi, M.R. (2004) "Development of a semi-empirical model for pyrolysis of an annular sawdust bed", J. Anal. Appl. Pyrolysis, 71 353–374.
- Razuan, R., Finney, K.N., Chen, Q., Sharifi, V.N. and Swithenbank, J. (2011) " Pelletized fuel production from palm kernel cake", Fuel Processing Technology, 92 (3) 609-615.
- Razuan, R., Chen, Q., Zhang, X., Sharifi, V.N. and Swithenbank, J. (2010) "Pyrolysis and combustion of oil palm stone and palm kernel cake in fixed-bed reactors", Bioresource Technology, 101 (12) 4622-4629.
- Reyhanitash, E. (2013) Upgrading Pyrolysis Oil to Produce Liquid Transportation Fuels, Master thesis, The University of Western Ontario.
- Rice Knowledge Bank (2011)http://www.knowledgebank.irri.org/rkb/index.php/rice-milling/byproducts-and-their-utilization/rice-husk accessed 06 November 2011.
- Ricci, M. and Perego, C. (2015) "From syngas to fuels and chemicals: Chemical and biotechnological routes http://www.eurobioref.org/Summer_School/Lectures_Slides/day6/L17_M.Ricci.pdf accessed on September 04, 2015
- Ringer, M., Putsche, V. and Scahill, J. (2006) "Large-scale pyrolysis oil production: A technology assessment and economic analysis", Technical report, NREL/TP-510-37779, November, 2006.
- Rolando, Z., Krister, S. and Emilia, B. (1995) "Rapid pyrolysis of bagasse at high temperature" Orally presented at the Third Asia-Pacific International Symposium on Combustion and Energy Utilization", Hong Kong 11-15 December 1995. Proceeding of the symposium, Vol 1, 211-215, http://hem.fyristorg.com/zanzi/paper/apisceu95.pdf accessed 01 November 2011.

- Ryu, H-J., Park, J., Shun, D. and Lee, S.-Y. (2011) "Novel two-interconnected fluidized bed system for selective solid circulation", 2010 ECI Conference on the 13th International Conference on Fluidization - New Paradigm in Fluidization Engineering, Vol. RP6, Article 63, http://services.bepress.com/eci/fluidization_xiii/63.
- Sachin, V. J., Arun, S.M. and Bhaskar, N.T. (2009) "Design of an efficient gas distribution system for a fluidized bed dryer", Drying Technology, 27 1217–1228.
- Sadaka, S. (2006) "Fast pyrolysis and its applications" Centre for sustainable environmental technologies, Biomass working groups, Iowa State University, August 17.
- Sadaka, S. (2014) "Pyrolysis", Centre for Sustainable Environmental Technologies Adjunct Assistant Professor, Department of Agricultural and Bio-systems Engineering, Iowa State University 1521 West F. Ave. Nevada, IA 50201.
- Sadaka, S. and Boateng, A.A. (2011),"Pyrolysis and bio-Oil", Agriculture and Natural Resources, University of Arkansas, United States Department of Agriculture, and County Governments Cooperating , http://www.uaex.edu, accessed 01 November 2011.
- Saidi, M., Samimi, F., Karimipourfard, D., Nimanwudipong, T., Gates, B.C. and Reza, M.R. (2014) "Upgrading of ligin-derived bio-oils by catalytic hydrodeoxygenation", Energy Environ. Sci., 7 103.
- Saidur, R., Abdelaziz, E.A., Demirbas, A., Hossain, M.S. and Mekhilef, S. (2011) "A review on biomass as a fuel for boilers" Renewable and Sustainable Energy Reviews 15 2262–2289.
- Salehi E., Abedi, J. and Harding, T. (2011) "Bio-oil from sawdust: Effect of operating parameters on the yield and quality of pyrolysis products" Energy & Fuels, 25 4145-4154.

- Scholze, B. and Meier, D. (2001) "Characterization of the water-insoluble fraction from pyrolysis oil (pyrolytic lignin). Part I. PY–GC/MS, FTIR and functional groups" Journal of Analytical and Applied Pyrolysis, 60 41–54.
- Scott, D.S., Paterson, L., Piskorz, J. and Radlein, D. (2000) "Pretreatment of poplar wood for fast pyrolysis: rate of cation removal", Journal of Analytical and Applied Pyrolysis, 57 169 – 176.
- Sills D.L., Gossett J.M. (2011) "Assessment of commercial hemicelluloses for scarification of alkaline pre-treated perennial biomass" Bioresource Technology 102(2) 1389–1398.
- SIMetric, density of materials, http://www.simetric.co.uk/si_materials.htm, accessed on December, 04, 2011.
- Sinnott, R.K. (2005) Coulson & Richardson's Chemical Engineering, Chemical Engineering Design, Volume 6, Fourth Edition, Elsevier Butterworth-Heinemann, Linacre House, Jordan Hill, Oxford OX2 8DP, 30 Corporate Drive, MA 01803.
- Shepherd, C.B., and Lapple, C.E. (1939) "Flow pattern and pressure drop in cyclone dust collectors," Industrial and Engineering Chemistry, 31(8) 972-984.
- Shepherd, C.B., and Lapple, C.E. (1940) "Flow pattern and pressure drop in cyclone dust collectors," Industrial and Engineering Chemistry, 32(9).
- Shinners, K.J., Binversie, B.N., Muck, R.E. and Weimer, P.J. (2007) "Comparison of wet and dry corn stover harvest and storage", Biomass and Bioenergy, 31 211–221.
- Stairmand, C.J. (1951) "The design and performance of cyclone separators," Transactions of Industrial Chemical Engineers, 29(1) 356-373.
- Shihadeh, A. and Hochgreb, S. (2002) "Impact of biomass pyrolysis oil process conditions on ignition delay in compression ignition engines" Energy & Fuels, 16 552-561.

- Sluiter, A., Hames, B., Ruiz, R., Scarlata, C., Sluiter, J. and Templeton, D. (2005) "Determination of ash content in biomass", Laboratory Analytical Procedure (LAP).
- Soetardji, J. P., Widjaja, C., Djojorahardjo, Y., Soetaredjo, F. E., Ismadjia, S. (2014). "Bio-oil from jackfruit peel waste," Procedia Chemistry 9, 158–164.
- Socrates, G. (2001) Infrared and Raman characteristic group frequencies: tables and charts, 3rd ed. John Wiley & Sons Ltd, Baffins Lane, Chichester, West Sussex PO19 IUD, England.
- Somrat, K. and Krongkaew, L. (2011) "Renewable energy from palm oil empty fruit bunch", Department of Mechanical and Aerospace Engineering, King Mongkut's University of Technology, North Bangkok, Thailand, http://www.intechopen.com/source/pdfs/22681/InTech-Renewable energy from palm oil empty fruit bunch.pdf accessed 02 November 2011
- Song, B.H., Jang, Y.W., Kim, S.D. and Kang, S.K. (2001) "Gas yields from coal devolatilization in a bench-scale fluidized bed reactor", Korean J. Chem. Eng., 18(5) 770-774.
- Standard auger sizes and capacities: Auger manufacturing specialists, http://www.augermfgspec.com/standard.html, accessed on 21 October 2011.
- Stuart, B (2004) Infrared Spectroscopy: Fundamentals and Applications, John Wiley & Sons, Ltd.
- Stuart, P.R. and El-Halwagi, M.M. (2014) "Integrated Bio-refineries: Design, Analysis, and Optimization", CRC Press.
- Subbu, M. (2011) Chemical engineering learning resources, Fluidization, http://www.msubbu.in/ln/fm/Unit-IV/Fluidization.htm, accessed on April 19, 2014.
- Sukiran, M.A, Chin, C.M and Abu Bakar N.K. (2009) "Bio-oils from pyrolysis of oil palm empty fruit bunches" American Journal of Applied Sciences 6 (5) 869-875.

- Sukiran, M.A, Abu Bakar N.K. and Chin, C.M. (2009) "Optimization of pyrolysis of oil palm empty fruit bunches" Journal of Oil palm Research 21 653-658.
- Sukiran, M.A., Kheang, L.S., Abu Bakar, N. and May, C.Y. (2011) "Production and Characterization of Bio-Char from the Pyrolysis of Empty Fruit Bunches", American Journal of Applied Sciences, 8(10) 984-988
- Sulaiman F. and Abdullah N. (2011) "Optimum conditions for maximising pyrolysis liquids of oil palm empty fruit bunches" Energy, Volume 36, Issue 5, 2352–2359.
- Sulaiman, W. (2012)" Pyrolysis of eucalyptus wood in a fluidized-bed reactor", Research on Chemical Intermediates. pp. 1-15. ISSN 0922-6168.
- Swift, P. (1969) "Dust control in industry," Steam Heating Engineering, 38.
- Theodore, L., and DePaola, V. (1980) "Predicting cyclone efficiency," Journal of the Air Pollution Control Association, 31(10).
- Thermopedia (2014), Fluidized bed, http://www.thermopedia.com/content/46/, accessed on March 30, 2014.
- Tisa, F., Abdul Aziz, A.R., and Wan Mohd. Ashri, W.D. (2014) "Basic Design of a Fluidized Bed Reactor for Wastewater Treatment Using Fenton Oxidation", International Journal of Innovation, Management and Technology, Vol. 5, No. 2, 93-98.
- Treedet, W. and Suntivarakorn, R. (2011) "Sugar cane trash pyrolysis for bio-oil production in a fluidized bed reactor", Bioenergy Technology, World Renewable Energy Congress 2011- Sweden, 8-13 May, Linkoping, Sweden.
- Tsai, W.T., Lee, M. K. and Chang, Y.M. (2007) "Fast pyrolysis of rice husk: Product yields and compositions" Bio Resource Technology, 98 22-28.
- Utikar, R., Darmawan, N., Tade, M., Li, Q, Evans, G., Glenny, M. and Pareek, V. (2010) Hydrodynamic Simulation of Cyclone Separators. In: Computational Fluid

Dynamics, Edited by: Hyoung Woo OH, ISBN 978-953-7619-59-6, pp. 420, January, INTECH, Croatia.

- Uzun, B. B., Pütün, A. E., and Pütün, E. (2007). "Rapid pyrolysis of olive residue. 1.Effect of heat and mass transfer limitations on product yields and bio-oil compositions," Energy & Fuel 21(3), 1768-1776.
- Valle, C.J. Duran, Corzo, M.G. Villegas, J.P. and Serrano, V.G. (2005) "Study of cherry stones as raw material in preparation of carbonaceous adsorbents" J. Anal. Appl. Pyrolysis, 73 9–67.
- Vakhshouri, K. (2008) "Influence of the distributor and the plenum chamber volume on fluidized bed hydrodynamics", Master of Applied Science Thesis, The Faculty of Graduate Studies (Chemical Engineering), The University of British Columbia (Vancouver).
- Varhegyi, G., Antal, Jr. M.J., Szekely, T., Till, F. and Jakab, E. (1988) "Simultaneous thermogravimetric-mass spectrometric studies of the thermal decomposition of biopolymers. 1. Avicel Cellulose in the Presence and Absence of Catalysts", Energy & Fuels, 2 267-272.
- Vassilev, S.V., Baxter, D., Andersen, L.K. and Vassileva, C.G. (2010) "An overview of the chemical composition of biomass", Fuel, 89 913–933.
- Velez, J.F., Chejne, F., Valdes, F.C., Emery, E.J. and London, C.A. (2009) "Co-gasification of Colombian coal and biomass in fluidized bed: An experimental study", Fuel, 88 424-430.
- Vigouroux, R.Z. (2001) Pyrolysis of biomass, Rapid pyrolysis at high temperature, Slow pyrolysis for active carbon preparation, Dissertation, Department of Chemical Engineering and Technology, Royal Institute of Technology, Stockholm, Sweden.
- Wade, Jr., L.G. Organic Chemistry, 5th ed. Pearson Education Inc., 2003.

- Wan Azlina Wan Ab Karim Ghani, Reza A. Moghadam and Mohamad Amran Mohd Salleh (2011). Air Gasification of Malaysia Agricultural Waste in a Fluidized Bed Gasifier: Hydrogen Production Performance, Sustainable Growth and Applications in Renewable Energy Sources, Dr. Majid Nayeripour (Ed.), ISBN: 978-953-307-408-5, InTech, Available from: http://www.intechopen.com/books/sustainable-growth-andapplications-in-renewable-energy-sources/air-gasification-of-malaysia-gricultural-waste-in-a-fluidized-bedgasifier-hydrogen-production-perf, accessed on January 12, 2016.

- Wang, L.G. (2011) Different Pre-treatments to Enhance Biogas Production-A comparison of thermal, chemical and ultrasound methods, Halmstad University, Master Thesis in Applied Environmental Science.
- Wang, L., Parnell, C.B., Shaw, B.W., Lacey, R.E. (2006) "A theoretical approach for predicting number of turns and cyclone pressure drop" Transactions of the ASABE, American Society of Agricultural and Biological Engineers ISSN 0001−2351, 49(2) 491−503.
- Wang, X., Kersten, S.R.A., Prins, W. and van Swajj, W.P.M. (2005) "Biomass pyrolysis in a fluidised bed reactor. Part 2: Experimental validation of model results" Ind. Eng. Chem. Res., 44 8786-8795.
- Wang, L., Parnell, C.B.Jr. and Shaw. B.W. (2002) "Performance characteristics of cyclones in cotton-gin dust removal." Agricultural Engineering International: the CIGR Journal of Scientific Research and Development. Manuscript BC 02 001. Vol IV.
- Wang, L., (2004) "Theoretical study of cyclone design," A dissertation submitted to the graduate studies of Texas A&M University in partial fulfilment of the requirements for the degree of Doctor of Philosophy.

- Wang, L., Parnell, C.B. and Shaw, B.W. (2000) "1D2D, 1D3D, 2D2D cyclone fractional efficiency curves for fine dust", In Proc. 2000 Beltwide Cotton Production Conferences. San Antonio, Tex.: National Cotton Council.
- Wyman, C.E., Dale, B.E., Elander, R.T., Holtzapple, M., Ladisch, M.R. and Lee, Y.Y. (2005) "Coordinated development of leading biomass pre-treatment technologies", Bioresource Technology, 96 1959–1966.
- Westover, T., Phanphanich, M., Clark, M.L., Rowe, S.R., Egan, S.E., Zacher, A.H. and Santosa, D. (2013) "Impact of thermal pre-treatment on the fast pyrolysis conversion of southern pine", Biofuels, 4(1) 45-61.
- White, B. (2013) "More than meets the eye: meeting biomass handling challenges", North American Clean Energy, http://www.seps.sk/zp/fond/dieret/biomass.html, accessed on July 14, 2013.
- White, F.M. (1991) Heat and Mass Transfer, Addison-Wesley Publishing Company Inc. USA.
- William, J.D., Nathan, Hill. II., Sedat, H.B., Saikrishna, M., Jincy, J., Cirila, B., Ta-Hsuan, O., Elizabeth, A.S., Clayton, M.W., Brian, G.F. and Adriaan, van H. (2010) "Fast pyrolysis of pine sawdust in a fluidized-bed reactor", Energy & Fuels, 24 2642–2651.
- Williams, P.T., Nugranad, N. (2000) "Comparison of products from the pyrolysis and catalytic pyrolysis of rice husks" Energy, 25 493–513.
- Willem, H., Bryan, J. and Matt, S. (2005) "Storage systems for rice straw in California", Department of Biological and Agricultural Engineering, University of California, Davis. http://www.fte.wur.nl/NR/rdonlyres/3B4A9556-8AE9-44B3-97BD-D9317266E63F/40598/StoragesystemsforricestrawinCalifornia1.pdf accessed 01 November 2011

- Wikipedia, the free encyclopaedia, webpage en.wikipedia.org/wiki, accessed on 30 August, 2012.
- Yang, X., Lyu, H., Chen, K., Zhu, X., Zhang, S. and Chen, J. (2014) "Selective extraction of bio-oil from hydrothermal liquefaction of salix psammophila by organic solvents with different polarities through multi-steps extraction separations", BioResources, 9(3) 5219-5233.
- Yang, W.C. (2003) Handbook of fluidization and fluid-particle systems, Marcel Dekker, Inc. 270 Madison Avenue, New York, NY 10016.
- Yanik, J., Kornmayer, C., Saglam, M. and Yuksel, M. (2007) "Fast pyrolysis of agricultural wastes: Characterization of pyrolysis products" Fuel Processing Technology, 88 942–947.
- Yan, Wei., Acharjee, T.C., Coronella, C.J. and Victor R. Va´ squez (2009) "Thermal pre-treatment of lignocellulosic biomass", Environmental Progress & Sustainable Energy, 28(3) 435-440.
- Yoo, C.G. (2012) "Pre-treatment and fractionation of lignocellulosic biomass for production of biofuel and value-added products" Graduate Theses and Dissertations, Iowa State University, Paper 12700.
- Zenz, F.A. and Weil, N.A. (1958) AIChE, J. 4, 472.
- Zheng, Ji-lu. (2007) "Bio-oil from fast pyrolysis of rice husk: Yields and related properties and improvement of the pyrolysis system", J. Anal. Appl. Pyrolysis, 80 30–35.